UNIVERSITÀ DEGLI STUDI FIRENZE

DOTTORATO DI RICERCA IN
SCIENZE CHIMICHE

CICLO XXVII

COORDINATORE Prof. Andrea Goti

Synthesis of functionalized polymeric materials from natural raw materials

Settore Scientifico Disciplinare CHIM/04

Dottorando
Dott. *Oliva Rosangela*

_____
(firma)

Tutore
Prof. Salvini Antonella

_____
(firma)

Coordinatore
Prof. *Goti Andrea*

_____
(firma)

Anni 2012/2014

1 INTRODUCTION

1.1 Sustainability and green chemistry

In recent years, thanks to the raise of public attention towards the environment, there has been a strong push towards the development of technological solutions with reduced environmental impact, for a sustainable development.

The reasons for this new trend reside in the awareness of the negative effects that, in the long term, human activities can have on the environment and humans, such as climate change, pollution on a large scale and the subsequent spread of diseases. In the past, the main focus in the development of new industrial processes has been on the achievement of high efficiency in synthetic procedures and excellent earnings. Consequently, economic considerations have played the main role in the design of synthesis paying less attention to safety and environmental aspects. In particular, the industrial development that started in the 50s in the Western world Countries and in parallel with the economic recovery after the II World War, was characterized by attention focused on the improvement of the economic conditions of the population and the quality of life linked to the availability of artifacts and new materials. The drive towards high productivity has therefore resulted in a limited attention to the impact of production processes. In the following years, the situation has not improved, because of the growth in size of industrial plants and their concentration in certain areas, which led to an increase of the critical issues.

In the chemical industry the search for high productivity, involving processes with high yields and reduced reaction times, determined the choice of drastic conditions such as high temperatures, high pressures and high concentrations of acids or bases, with high energy consumption and with use of special equipments. Under these reaction conditions, processes did not often show high selectivity, consequently producing by-products that formed waste materials.

The lack of attention to the environment and human health and the lack of restrictive laws and regulations aimed at the control of chemical plants, have contributed in the past years to a negative image of the chemical industry. The correlation between the activities of the chemical industry and the increase in environmental pollution became increasingly clear, while increasing accidents with serious consequences occurred both in productive factories and at the extraction of raw materials. Bhopal, (December 3, 1984), is remembered as one of the serious accidents, when an explosion at the plant of Union Carbide caused the loss of 20 to 40 tons of methyl isocyanate, a very toxic gas, causing the death of over 2,000 people and injuring 100,000, covering

an area of over 40 km^2. Methyl isocyanate was the intermediate product used in the production of the insecticide carbaryl (Sevin commercial name) in Bhopal plant. In the U.S. phosgene was used to obtain carbaryl (Figure 1).

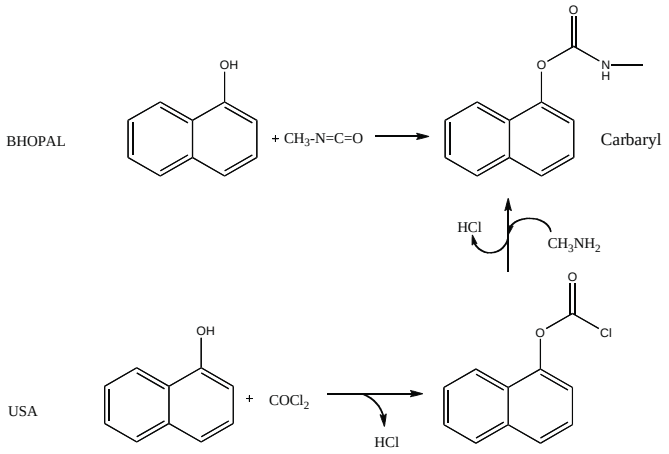

Figure 1: production of Carbaryl

The hypothesis concerning the cause of the accident has been attributed to the penetration of water in the tanks containing methyl isocyanate, which caused an exothermic reaction with a strong development of heat and increased pressure within the tank, due to production of methylamine and carbon dioxide. This accident could have caused far less damage, if more precautions had been taken; in fact, deficiencies resulted in the security system of the plant, as well as the lack of an emergency plan and the houses were too close to the plant (Figure 2)

Figure 2: Remains of the factory in Bhopal

Another major disaster occurred in Germany in a BASF plant, where a leak of dioxins on a production line of trichlorophenol occurred in 1953. A similar accident occurred few years later, in

1976 in Seveso, in the ICMESA plant, where TCDD (tetrachloro-p-dibenzodioxin) was dispersed in the environment due to the explosion of a reactor.

Another striking example is what happened in Porto Marghera, where the various factories (EniChem Agriculture Agrimont, Montefibre, Montedison), poured VCM (vinyl chloride monomer), chlorinated hydrocarbons and heavy metals in the lagoon and in the surrounding environment. The damage to the environment and many serious diseases among the inhabitants of the surrounding areas were traced to manufacturing processes in Porto Marghera. Following these episodes the Montedison management was accused of having deliberately underestimated the toxic effects of the VCM, although these had already been determined and made known to the company since 1972. In addition, insufficient resources were assigned for the protection of health workers, the population outside the plant and the environment.

The environmental damages that has contributed to create a negative image of chemistry did not concern only the production stage, but also the exploitation and transportation of raw materials: a serious accident involving the spill of crude oil from a tanker (Exxon Valdez) took place in 1989 in Alaska (Prince William), causing critical problems to the marine ecosystem for many years. In 2010, the oil rig Deepwater Horizon BP caused a disaster 10 times more severe in the waters of the Gulf of Mexico due to an explosion that caused a fire on the rig with the emission of large amounts of hydrocarbons and thus determining the worst environmental disaster in American history (Figure 3).

Figure 3: oil spill in Alaska (Prince William) on the left and fire on the oil rig Deepwater Horizon (Gulf of Mexico)

The awareness of the need to maintain active the industrial development achieved but also the contemporary need to safeguard the environment and human health have spawned the desire to review the priorities in the development of the manufacturing procedures. Environmental disasters, social diseases and fatalities have given way to the development of several chemical researches in order to recover a positive image of the chemistry but above all for a sustainable

development of industrial processes. The fragility of the climate balance and deficiencies in the availability of some raw materials have shown that the environment is a critical resource, rare and precious, which not to be exploited indiscriminately. In recent years, in both academic and industrial research there has been a strong awareness to issues more directly involved in sustainability, such as population growth, the availability of food for nutrition, energy issues, the destruction of natural resources, global climate change, the use of water resources, the generation and dissemination of toxic substances and waste.

In order to be able to pursue sustainability, the development of new technologies is required to combine economic growth with social and environmental responsibility.

Over the past twenty years, an aid for sustainable development has been given by **Green Chemistry**, born in the '90s thanks to EPA (Environmental Protection Agency), with the help of OPPT (Office of Pollution Preventing & Toxics) that had already worked on research projects with the aim to reduce the environmental impact of products and processes in the chemical industry.

In 1992, OPPT has created a program of aid for research and for the first time has provided financial support for the projects regarding pollution prevention in the synthesis of organic products. In 1995, following the support of the American administration to the new environmental policy, a consortium of recognition for companies and factories, that have achieved important successes in the field of Green Chemistry, has been established; then a center has been created, the Green Chemistry Institute, where the experiences and scientific initiatives worldwide are collected.

In the wake of the American experience, in the last decade, also in Europe Green Chemistry has reached a huge development, both in academic and industrial research.

Green Chemistry is based on very simple concepts, that have to be implemented in an economic-productive system that in the past was based primarily on the goal of economic development at any cost. The definition given by its founder, Paul Anastas, is as follows: "**Green Chemistry** is the utilization of a set of principles that reduces or eliminates the use or generation of hazardous substances in the design, manufacture and applications of chemical products."

Anastas and Warner[1] have developed 12 principles to assess how much and what a process is "green":

1) It is better to prevent waste than to treat or clean up waste after it is formed.
2) Synthetic methods should be designed to maximize the incorporation of all materials used in the process into the final product.
3) Wherever practicable, synthetic methodologies should be designed to use and generate substances that possess little or no toxicity to human health and the environment.

4) Chemical products should be designed to preserve efficacy of function while reducing toxicity.
5) The use of auxiliary substances (e.g. solvents, separation agents, etc.) should be made unnecessary wherever possible, and innocuous when used.
6) Energy requirements should be recognized for their environmental and economic impacts and should be minimized. Synthetic methods should be conducted at ambient temperature and pressure.
7) A raw material of feedstock should be renewable rather than depleting wherever technically and economically practicable.
8) Unnecessary derivatization should be avoided whenever possible
9) Catalytic reagents (as selective as possible) are superior to stoichiometric reagents.
10) Chemical products should be designed so that at the end of their function they do not persist in the environment and break down into innocuous degradation products.
11) Analytical methodologies need to be further developed to allow for real-time, in-process monitoring and control prior to the formation of hazardous substances.
12) Substances and the form of a substance used in a chemical process should be chosen so as to minimize the potential for chemical accidents, including releases, explosions, and fires.

It is important to point out that sustainable chemistry is not synonymous with Green Chemistry, but this latter is one of the tools to be used to achieve a sustainable industry. Indeed, main objective of **sustainable chemistry** must be the prosecution of a productive development respecting the environment and human health, while ***green chemistry*** focuses on the design, manufacture and use of chemicals and chemical processes with little or no potential pollution or environmental risk, economically and technologically feasible.

Following the principles of green chemistry, many fields of science have tried to adapt to the new criteria for a more sustainable development. The implementation of new and more sustainable processes in fact requires the integration of different disciplines with a focus on environment and safety. The concept of green chemistry has to be integrated with a green engineering and with the concept of "industrial ecology", obviously taking into account the production of energy from renewable sources. This new approach has led to a growing interest in new and more efficient catalytic processes, in the process intensification and a greater focus on waste management. The study of more selective processes is of great importance for this latter aspect, as well as the assessment of the environmental impact of waste (E-factor) and also the search for new

production systems that can use as raw material the waste materials produced by food farming industries and forestry machining. Even in the field of polymers, together with improving the performance of production processes, the researchers have tried to reduce the environmental impact of the materials throughout the life cycle "cradle to grave", i.e. from production to the disposal, which today is evaluated through the Life Cycle Assessment (LCA)[2]

This method evaluates the interactions that a product has in its entire life cycle with the environment, from pre-production, production, distribution, use, recycling and final disposal (Figure 4). The procedure for evaluating the LCA is now internationally standardized and the standards to which it refers are the ISO 14040 and ISO 14044, which take into account the environmental impact of the product examined in respect of human health, the quality of the ecosystem and of resource depletion, also considering the impact of economic, financial and social aspects.

Figure 4: phases of LCA cycles

1.2 Renewable sources and Biorefineries

In recent years, the growing interest in the optimal exploitation of renewable sources has led to the development of the concept of biorefinery defined as an integrated set of transformation and separation systems of the main components of "biomass" with the goal of producing energy, fuels, chemicals, solvents, plastics and food.

The term "biomass" identifies any organic matter available on a renewable basis, excluding the old wood and including productions of crops and trees dedicated to energy, food farming

products, feed from crop residues, aquatic plants, wood and wood waste, animal waste and other waste materials, usable for industrial purposes.

Biomass has a complex composition and it is therefore necessary to achieve a preliminary separation of the constituent materials prior to further processing into products of different interest. The production of industrial products from renewable sources still needs the search for new systems of chemical or enzymatic transformation to optimize conversions and selectivities.

There are several definitions of biorefinery[3]: the first on the "**Green Biorafinery**" was described in 1997 as "a complex (to fully integrated) system of sustainable, environmentally and resource-friendly technologies for the comprehensive (holistic) material and energetic utilization as well as exploitation of biological raw material in form of green and residue biomass from a targeted sustainable regional land utilization".

The US Department of Energy (DOE), today uses the following definition: "A biorefinery is an overall concept of a processing plant where biomass feedstocks are converted and extracted into a spectrum of valuable products". On the basis of this definition a biorefinery plays a role similar to that of a petrochemical refinery.

Finally, the American National Renewable Energy Laboratory (NREL), has published the following definition: "a biorefinery is a facility that integrates biomass conversion processes and equipment to produce fuels, power and chemicals from biomass. The biorefinery concept is analogous to today's petroleum refinery, which produce multiple fuels and product from petroleum. Industrial biorefineries have been identified as the most promising route to the creation of new domestic biobased industry".

The development of biorefineries is supported by political and economic reasons with an interest in improving the quality of the environment from the local level up to the global level, trying to recover waste materials and to combat the critical issues related to a lower availability of fossil fuels in the future years.

Three types of biorefinery can be identified: those of the ***first generation*** in which, for example, the production of ethanol is obtained by fermentation, those of the ***second generation***, in which different types of products can be produced, suitable to the market needs, such as ethanol, starch, fructose syrups, corn oil, gluten and flour and the ***third generation***, not yet fully developed, that uses forestry and agricultural biomass or organic waste, respecting the biodiversity of the territories, for the production of many products with high added value (such as chemicals and bioplastics). This last type of biorefinery resembles the oil refineries in complexity and flexibility. The importance of the new biorefinery relies on the use of waste materials for the

production of raw materials without affecting the availability of food, an ethical problem that has slowed so far an intensive development of these materials.
In Italy there is a type of II generation biorefinery, developed in Crescentino (VC) for the production of biofuels that will produce, at operating speed, 75 million liters per year of bioethanol, using agricultural residual, i.e. non-food biomass.
The new model of biorefinery offers a great opportunity to convert abandoned industrial sites and at the same time strengthen the leadership of the Italian and European industries in the field of biomaterials. Novamont, with Mossi & Ghisolfi and Eni-Versalis (through a joint venture called Matrica), is implementing the conversion of the petrochemical plant at Porto Torres in a third generation integrated biorefinery that, starting from the use of agricultural raw materials and vegetable waste will produce a range of chemicals (biochemicals, bio-intermediates, bio-lubricants bases and bio-additives for tires) through innovative processes and low-impact.

1.3 Biopolymers

The term "**biopolymer**" has been used, in recent years, both in the scientific field and in common speech even though its use is not univocally defined. Often this term identifies all those polymers and/or polymeric materials with reduced environmental impact compared to conventional polymers, defined as polymers derived from oil and non-biodegradable and/or non-compostable.

The definitions of biodegradability and compostability are often confused with each other, while indicating different things; a biodegradable material is consumed by microorganisms to return to naturally occurring compounds, which can also be toxic, while a compostable object degrades in the conditions of a composting plant in the time and manner prescribed by the regulations. In this sense, there are differences between the American and European regulations (UNI EN and ASTM).
For the ASTM standards a compostable material "decomposes biologically in a compost site so that the material is not visually distinguishable and breaks down into CO_2, water, inorganic compounds, and biomass at a speed adapted to that of the known compostable materials" (ASTM D 6002).
For the UNI EN 13432 a material, to be called compostable, must:
• degrade at least 90% in 6 months if subjected to an environment rich in carbon dioxide; these values should be tested with the standard method EN 14046 (also known as ISO 14855);

• in contact with organic materials for a period of 3 months, the mass of the material must be made up at least 90% of fragments of size less than 2 mm; these values should be tested with the standard method EN 14045;

• the material must not have negative effects on the composting process;

• the concentration of heavy metals with additives to the material should be low;

• the values of pH, salt content, the concentration of solids, nitrogen, phosphorus, magnesium and potassium should be within established limits.

Biodegradability is therefore an intrinsic property of the material, while the compostability requires that the degradation products are not toxic and depends on the shape of the object; objects with a high volume/surface ratio (for example a log of wood) are not compostable because it would take too long to degrade in composting plants, but if the volume/surface ratio is lowered, they become compostable (e.g. sawdust wood).

Because of all these definitions, the term "biopolymer" becomes generic and often misleading; in fact, recycled polymers (which have a lower environmental impact than virgin polymers) or polymers containing additives that make them oxodegradable[4] (like many of the shoppers used today) can take the connotation of biopolymers.

This confusion has imposed the need to attain to a single definition of the term "biopolymer". In this work, the definition of biopolymer as indicated by the UNI/CEN TR 15932 of 2010 will be used, which coincides with the definition given by European Bioplastics, the association of European producers of bioplastics.

According to this rule, the first major distinction must be drawn between ***natural biopolymers*** and those resulting ***from synthesis***.

According to the UNI/CEN TR 15932, the natural biopolymers are those polymers that are naturally produced by living organisms, while synthetic biopolymers are those polymers that "are derived from renewable sources and/or are biodegradable."

As it can be seen, at schematic level (Figure 5) the definition of biopolymer therefore includes "three families":

1) Polymers not derived from renewable sources but biodegradable;
2) Polymers derived from renewable sources but not biodegradable;
3) Polymers derived from renewable sources and biodegradable.

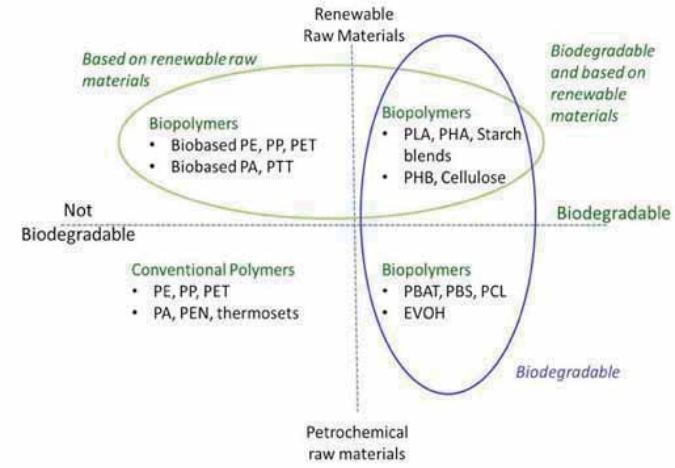

Figure 5: diagram on families of biopolymers

1.3.1 Natural biopolymers and their derivatives

Natural biopolymers are those polymers that are naturally produced by living organisms. In other words, they are polymeric biomolecules. They are divided into different classes on the basis of their chemical composition and the main ones are[5]:

- The polynucleotides (such as DNA and RNA) that are long polymers with 13 or more nucleotide monomers.
- The polypeptides, which are short polymers derived from amino acids polycondensation.
- The polysaccharides which are linear or branched chains based on monosaccharide units.
- Other compounds, including lignins and polyphenols, terpene resins

Natural biopolymers are generally biodegradable and represent the class of polymers most widespread on Earth.

Cellulose (Figure 6), a polysaccharide, is the most common organic compound on Earth and represents approximately 33% of the total mass of plants. Cellulose content is equal to 90% in cotton and 40-50% in wood, considering its dry weight[6]. It is a linear polymer of high molecular weight (degree of polymerization between 5,000 and 10,000), consisting of glucose monomers joined together by β-1,4-glycosidic bonds. Cellulose can be hydrolyzed under acidic conditions until its disaccharide constituent, the cellobiose and subsequently to glucose. It is a polymer insoluble in water and in most organic solvents, because of its supramolecular structure, a characteristic that limits its use in various fields, not allowing the production of formulations in solution. However, the reactions with the cellulose can be performed at a solid state, in

heterogeneous phase ("swollen-state" reactions) or in the homogeneous phase in non-classical solvents obtaining various cellulose derivatives usable in many application fields[7].

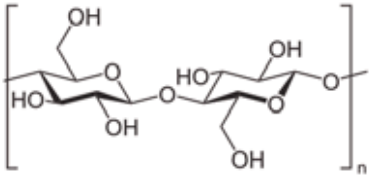

Figure 6: repeat unit of cellulose

Derivatives of cellulose

Cellulose is an important resource, almost inexhaustible, for the production of biocompatible compounds (Figure 7) with low environmental impact.

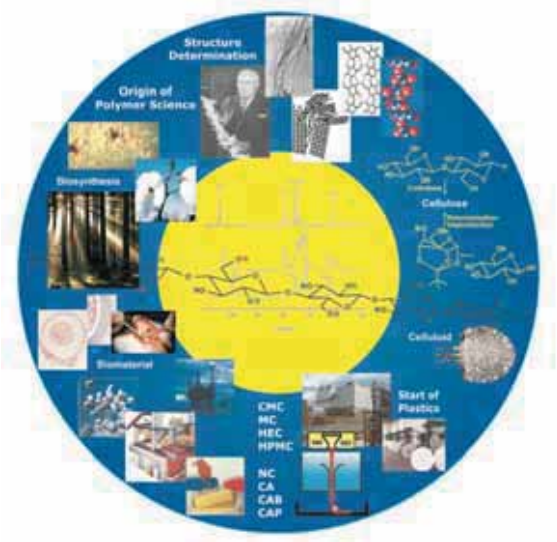

Figure 7: Cellulose derivatives

It is used, after appropriate processing, for the production of many types of polymers, the first of which was a thermoplastic polymer synthesized in 1860, the **celluloid**. This reaction and others like it, have hinted that various chemical modifications of cellulose on an industrial scale were possible, with the possibility of formation of plastics with different characteristics. Today, among the most important derivatives of cellulose there are cellulose acetate, carboxymethyl cellulose, ethyl cellulose and the hydroxyethyl cellulose. In addition to the type of the substituent, the composition of the cellulose derivatives is determined by the degree of substitution (DS).

Cellulose acetate is obtained by acetylation of cellulose with a mixture of acetic acid and acetic anhydride, in the presence of sulfuric acid as catalyst. It is a polymer soluble in many solvents, which is used as thermoplastic material for the production of very light objects, lacquers, varnishes and for the production of artificial silk. It has also found wide use in the production of photographic and cinematographic film, as insulating material for electrical engineering (eg. computer tapes), in the production of glasses and, in the form of fiber, to obtain the filters of cigarettes and the common playing cards. The cellulose acetate is not biodegradabile[8].

Carboxymethyl cellulose (CMC), is produced industrially by alkali cellulose and sodium chloroacetate; in relation to its degree of substitution it can be dissolved or can swell in water.

For its hydrophilicity, for the adhesive properties and high viscosity of its solutions, it is used in the finishing of the fabrics together with starch, in the paper industry, in the preparation of adhesives, protective colloids and emulsifiers; it is also a food additive (E466) used in particular as thickener agent[9].

Ethyl cellulose (EC) is a polymer soluble in many common solvents (DS> 1.5) and in water (DS = 0.7- 1.7) and is capable of producing thin films with good resistance to weathering. For this reason it is often used in the preparation of paints. It is also used as a plastics molding and for the production of adhesives[9].

Finally, **hydroxyethyl cellulose (HEC)** is produced by reaction of alkali cellulose with ethylene oxide in a slurry process. To disperse it, acetone, isopropyl alcohol, 1,2-dimethoxyethane or mixtures of short hydrocarbons with alcohols are used. On the market it is available with different degrees of viscosity (from 10 to 100000 mPa*s). Its solutions are compatible with many water-soluble polymers, such as EC and other cellulosic ethers, but are incompatible with tannins, phenols and some special complex salts, with which it forms insoluble complexes. HEC can be attacked by some enzymes and it is protected only if it has a high and uniform degree of substitution. It is used as an additive (thickener, binder, stabilizer and protective colloid) in cosmetics and in paints, adhesives, inks, and it is also used in the paper industry[9].

Cellulose derivatives have also been studied as consolidating for the waterlogged archaeological wood showing however limitations and problems related to the type of cellulose derivatives studied and to their molecular weight[10]. Despite the problems recognized in the past, the possibility of using materials similar to the components of the artefacts to be consolidated is an aspect of particular importance. Starting from these considerations, in recent years a research project has been developed at the Department of Chemistry, Università degli Studi di Firenze, for the synthesis of biopolymers, for their use as new materials for applications in the field of cultural

heritage. In recent years, various cellulosic ethers have been synthesized to evaluate their ability to penetrate finds of waterlogged archaeological wood. Reactions were carried out either in heterogeneous or in homogeneous phase; however, the best results were obtained in the second case, with the use of a solution of LiCl in DMAc (6% w/w)[11]. This solvent system gave good results for the solubilization of cellulose and it has allowed to solve the problems encountered in the reactions in heterogeneous phase, such as poor uniformity of substitution, unfavorable reaction kinetics, low yields and formation of by-products.

Productions of the alkali cellulose necessary for subsequent etherification reactions were performed in homogeneous phase. The purpose was to get to water soluble products containing reactive groups that could produce cross-linking after application. The reactive groups introduced in the cellulosic "frame" were allyl groups, for their ability to give cross-linking once applied inside the wood.

3 types of ether cellulosic derivatives were synthesized[11]:

1) allyl cellulose

2) allylcarboxymethyl cellulose

3) allylhydroxypropyl cellulose.

Allyl cellulose was obtained with a DS equal to 3, therefore completely allylate and showed solubility in chloroform and dimethylsulfoxide, but not in water.

The second derivative synthesized was a derivative of carboxymethyl cellulose, a polymer which shows a good solubility in water when it has a DS> 3. The allylcarboxymethyl cellulose with DS_{allyl}= 1 and $DS_{carboxymethyl}$= 1 had reactive groups for cross-linking reactions and gave a stable colloidal system in cold water.

The third product synthesized was a derivative of the hydroxypropyl cellulose. 2-hydroxypropyl ether is a commercial product widely used in the cosmetic and food industry (as the hydroxyethyl cellulose) obtained industrially by reaction of the alkali cellulose with propylene oxide. However, due to problems of toxicity and hazard of propylene oxide, allyl 1-hydroxypropyl cellulose was synthesized using 3-bromo-1-propanol, which is less toxic and less reactive . In fact, another reason for which propylene oxide was not used in allyl 1-hydroxypropyl cellulose is due to its high reactivity towards the hydroxyl groups of the cellulose, which could lead to a degree of substitution not controlled and too high. The final product had a DS equal to 0.8 (DS_{allyl}= 0.2, $DS_{n\text{-}hydroxypropyl}$= 0.6) and showed a partial water solubility.

These products, made from a cellulose partially hydrolyzed to reduce its molecular weight, were used as consolidant for wood, but in the application study several problems were observed due to

the high molecular weights, which led to a poor penetration ability. It was also demonstrated that they undergo a fast deterioration due to biotic agents.

Hemicelluloses are heteropolysaccharides containing different monosaccharides according to the origin (softwood or hardwood trees). In dry wood their percent content is between 20 and 30% w/w. Like cellulose, they have a support function in the cell walls but have lower molecular weight. They are linear or branched and some are water soluble. They are easily hydrolyzed in the constituent monosaccharides: D-glucose, D-mannose, D-xylose, L-arabinose and small amounts of D-glucuronic and D-galacturonic.

Another biopolymer widely distributed on Earth, constituting 15-35% of the dry weight of the wood is **lignin**, a polymer with a complex cross-linked structure.

Its characteristics are completely different from those of cellulose; it is in fact a three-dimensional polymer, with molecular weight between 4000 and 12000 Da, insoluble in all solvents, if not previously subjected to chemical reactions that break the molecule into smaller fragments, by modifying its structure; these fragments are made from aromatic phenyl propene monomers, among which the main ones are three alcohols: coniferyl alcohol, coumaryl alcohol and sinapyl alcohol[6].

Lignin structure has not yet been clearly defined and the type of the monomers varies depending on the type of wood.

Another natural biopolymer that has enormous importance and diffusion is **chitin** (Figure 8), the polymer of N-acetylglucosamine; it is the main component of the exoskeleton of insects and crustaceans, it is located in the cell walls of fungi and the internal shells of cephalopods[12–14].

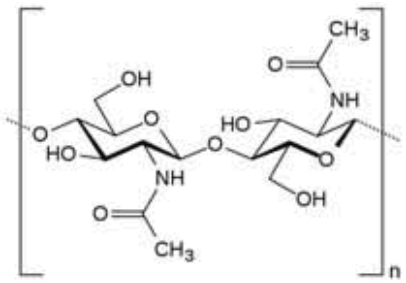

Figure 8: repeat unit of chitin

In general, natural biopolymers can find not only technologically advanced applications of great interest (wood as construction material has been known for a few million years), but also

represent a convenient and easily accessible source of raw material to obtain derivatives with properties and uses very varied.

Derivatives of chitin

Chitosan is produced industrially by de-acetylation, partial or total, of chitin with NaOH in aqueous solution; this polymer has found many applications in agriculture, as a defense for plants and to increase the yield of cultivated land because it is a natural biopesticide, in water treatment as part of the filtration process, in biomedical industry, where it is an excellent hemostatic agent and in pharmaceutical applications for its biodegradability, biocompatibility and non-toxicity, and in many other possible applications. Furthermore, the amino group on the chitosan, makes it more easily chemically modifiable in comparison to cellulose and chitin[12–14]. It can be obtained with different molecular weight, based on various factors, such as time, temperature, concentration of reactants and pressure of the deacetylation reaction.

Unfortunately, in some cases, the applications of these polysaccharides are limited because of their low solubility in water.

1.3.2 Synthetic biopolymers

According to the UNI/CEN TR 15932, synthetic biopolymers can be defined as polymers that "are derived from renewable sources and/or are biodegradable."

As previously described in the diagram in Figure 5 synthetic biopolymers can differentiate into three families based on their origin and biodegradability:

1) **Polymers not derived from renewable sources but biodegradable**: these polymers are obtained from monomers derived from petroleum, but can then be degraded biologically. Many polymers known for decades, such as **polyvinyl alcohol (PVA)** obtained from vinyl acetate polymers, **polycaprolactone (PCL)** obtained from caprolactone and the **polyethylene glycol (PEG)** resulting from the polymerization of ethylene oxide, belong to this family. They are widely used in printing processes, in the production of films (eg. packaging for detergents of washing machine), but also in the biomedical field, where they are used as carriers of drugs and formulations. Another example is **Ecoflex® BASF**, a polymer used for films and bags.

2) **Polymers derived from renewable sources but not biodegradable**: polymers that can be produced from renewable sources, such as vegetal oil, wheat, sugar, maize, but which are not biodegradable, belong to this family. Examples of this type of materials are many polyamides such as **PA11**, whose monomer aminoundecanoic acid, is obtained from castor oil. Another polyamide on the market, **PA10,10** (derives from sebacic acid) that is another derivative of castor oil: this polyamide is produced by Evonik, trademark VESTAMID® using 100% bio-based monomers.
Also the so-called **bioPE**, **bioPP** and **bioPET**, produced from bioethanol, belong to this category.

3) **Polymers derived from renewable sources and biodegradable**: in this category polymers derived from starch can be found, such as **Mater-Bi Novamont**, commonly used for disposable food shoppers, some polyesters such as **polylactic acid (PLA)**, derived from wheat or sugar, and **polyhydroxyalkanoates (PHA)** obtained by bacterial fermentation of sugar or lipids[8].

The market for this type of polymers is rapidly expanding; according to data of the European Bioplastics in 2008-2011 the production of biopolymers has increased from 180,000 tons to 1,160,000 tons and is expected to arrive at 1.71 million tons in 2015 and about 5.8 million tons in 2016 (Figure 9, Figure 10).
The graphs relating to the global production capacity for bioplastics show that in the next years Asia and South America will focus on building new plants (Figure 9). On the contrary, Europe and North America will have a strategic importance in the field of research and development.

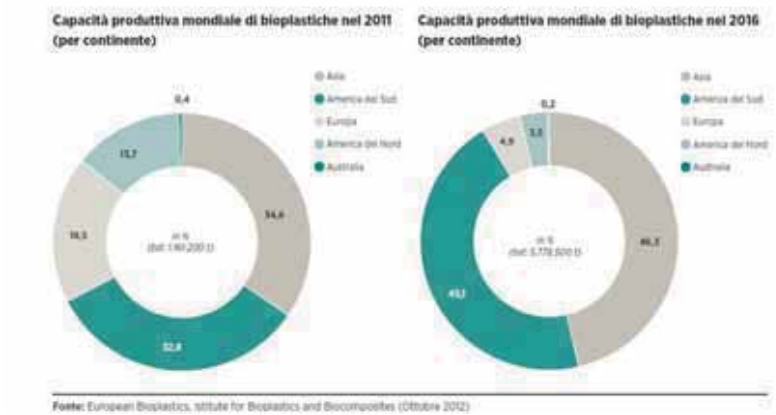

Figure 9: graphics relating to the production capacity of bioplastics in 2011 (left) and 2016 (right) by continent

It should be emphasized that these biopolymers, at present, are generally not economically competitive with "classic" plastics, but their price in the last years has decreased and could

become competitive when the cost of the "bio" monomers will be comparable to that of the monomers derived from non-renewable sources.

However, statistics of the past years have underestimated the growth of this industry; they imagined in fact a more modest growth or at least, more progressive and slower, compared to the reality. Instead, many companies are looking to invest in the field of biopolymers, especially with regard to the supply of vegetable raw materials and the registration of new patents, to try to have future market advantages.

This sudden development can be attributed mainly to the feared "oil crisis", as it is expected that in the next few years the oil availability will be much more reduced for both the depletion of deposits more easily exploited and for the political problems of some geographical areas, with a consequent increase in the prices of raw materials derived from it.

Another important fact that emerges from the data of the European Bioplastics is related to the types of biopolymers that will be greatly produced and placed on the market. Both for 2015 and 2016 a greater production of biobased polymers not biodegradable is in fact expected, since the market requires a greater amount of long-lasting products.

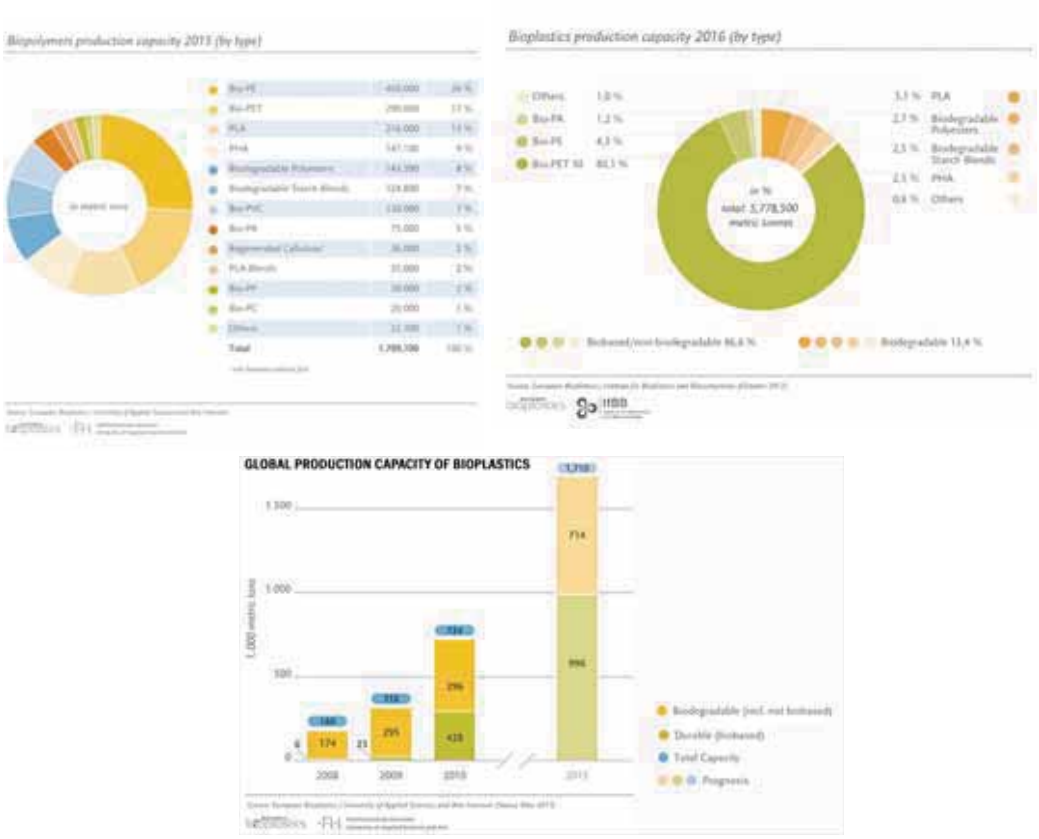

Figure 10: graphs relating to the productive capacity of bioplastics relating to the materials produced

1.4 Polyamides

As above reported, some industrial polyamides belong to the class of biopolymers. In this area they represent a family of polymers extremely promising and for this reason they are intensively studied at both academic and industrial level.

More generally, the interest for polyamides derives from the fact that these polymers are very versatile, and their applications vary from the textile field to the field of plastic materials of various kinds.

Polyamides are obtained by polycondensation reaction of monomers containing acid and/or amino groups; using differently functionalized monomers and different reaction conditions it is possible to obtain a large variety of products with different molecular weight and with different chemical-physical characteristics.

Commercial polyamides containing aliphatic amines are indicated with the term Nylon while those containing aromatic amines, such as Kevlar® and Nomex®, are called polyaramids.

The first synthesis of a polyamide dates back to 1935 and was carried out by Wallace Carothers (DuPont) that, starting from adipic acid and hexamethylenediamine synthesized the polyexamethylene adipamide (nylon 6,6); this product was patented in 1937[15] and marketed in 1938, having good characteristics for use as a textile fiber. In 1938 polycaprolactam (nylon 6) was synthesized, and subsequently patented in 1941[16].

At the industrial level polyamides are synthesized directly from an amino acid, or a dicarboxylic acid and a diamine or lactams.

Regardless of the choice of monomers, polyamides have some common features[17]:

- They are partially crystalline thermoplastic polymers (up to 60% of crystallinity) and have high hygroscopicity. The crystallinity is due to the numerous intra- and intermolecular hydrogen bonds due to amide groups, which give rise to intense forces of cohesion, but also to the regularity of the polyamide chains.
- The mechanical characteristics are variable and depend on the structure of the monomeric units of the polymer, the quantity of water absorbed and the crystallinity.

  In general it can be stated that, thanks to the polar amide groups, the products obtained show a good impact resistance; this is possible because the absorbed water molecules act as a plasticizer, increasing the toughness; they also have good tensile strength and wear.
- They are resistant to aromatic, aliphatic and chlorinated hydrocarbons, gasoline, oil, grease, some alcohols, esters, ketones, ethers and weak alkaline solutions; also have good stability in aging.

• They are not resistant to mineral acids, strong alkaline solutions, solutions of oxidizing agents, formic acid, phenols, cresols, glycols and chloroform.

As already mentioned, there are polyamides entirely derived from renewable sources, such as **PA11** and **PA10,10** that show excellent properties as materials engineering, and there are also polyamides, such as **PA6,10** or **PA4,10** that have a "partial" derivation from renewable sources, because only one of the two starting monomers derives from a product of natural origin (sebacic acid, derived from castor oil). Another polyamide which today can be produced entirely from natural origin is **PA6,6**; in fact, by treatment with dilute sulfuric acid of simple sugars, furfural can be produced from monosaccharides pentoses (xylose), while the 5-hydroxymethylfurfural from hexoses (glucose, fructose). From furfural it is possible to produce in a few steps both the hexamethylenediamine and the adipic acid, monomers required for the synthesis of nylon 6,6 (Figure 11).

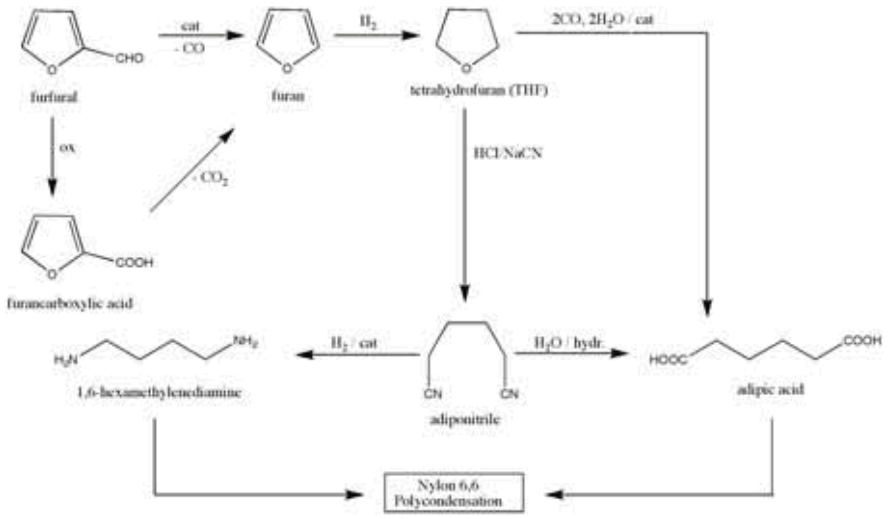

Figure 11: furfural- based Nylon 6,6 process

Beyond the examples mentioned, many types of polyamides can be derived from renewable sources and, through appropriate choice of the starting monomers and the molecular weight of the polymer obtained, they may also be biodegradable.

1.4.1 Functionalized polyamides

In recent years, polyamides based on hydroxylated monomers from aldaric acid (Figure 12) suitably modified have been developed; these hydroxylated monomers show stereoregularity and

for this reason it is very important to control the configuration, in order to obtain the stereoregular polymers.

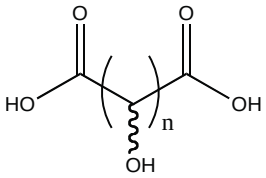

Figure 12: aldaric acids

Hydroxylated polyamides may be important in the biomedical field because non-toxic and often biodegradable[18,19], but also as fibers, adhesives[20] and plastics. These products show a high solubility in water, and so they have also been used as additives in water-based formulations, for example, as curing agents for epoxy resins[21].

The syntheses of many hydroxylated nylons, obtained by polycondensation reaction between aldaric acid derivatives and diamines, have been reported in literature.

Ogata in the 70s studied the influence of the ester derivatives of hydroxylated carboxylic acids, demonstrating that the hydroxyl groups, in α or β position with respect to the ester group, have greater reactivity than the corresponding non-hydroxylated monomers in polycondensation reactions with polar solvents. This effect has been attributed to the formation, in an intermediate stage of the reaction, of the hydrogen bonds between the hydroxyl groups of the diester and those of the $-NH_2$ of the diamine. Ogata synthesized the poly-L-tartaramides and poligalactaramides (Figure 13) respectively from ester derivatives of L-tartaric acid and galactaric acid with examethylenediamine[22–25].

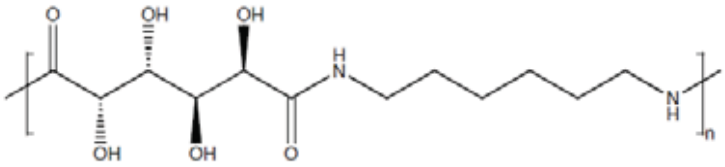

Figure 13: Polyexamethylenegalactaramide

The mechanism of aminolysis of various galactaric and xilaric esters in the reactions of polycondensation were studied by Hoagland[26,27], showing two successive steps in the reaction, the base catalyzed lactonization of diester and then the aminolysis reaction of the lactone.

These studies showed that the activation of aldaric diesters with 5 and 6 carbon atoms is due to the formation of the respective aldarolactones which possess high reactivity.

Subsequently Kiely[28–30], using a similar procedure, carried out the synthesis of polialdaramides based on D-glucaric acid.

Minoura[31] developed politartaramides synthesis starting from the salt of tartaric acid with various diamines whereas Muñoz-Guerra synthesized a series of stereoregular polyamides [32].

Recently, some types of functionalized polyamides partially derived from natural sources, were synthesized at the Department of Chemistry, Università degli Studi di Firenze with the aim of using them as consolidating the waterlogged archaeological wood. The interest in these compounds is related to the fact that their structure is similar to that of the components of the wood and that it is possible to modulate the chemical-physical characteristics based on the initial choice of the monomers (diacids, diamines, and amino acids). The synthesis through polycondensation reactions also allows to control the degree of polymerization, obtaining compounds with different molecular weight.

Due to their possible use as consolidant for archaeological wood, the choice of the polyamides was determined on the base of their versatility and high chemical resistance, basic features for a consolidant.

Initially, the use of glucose as starting monomer and the insertion in its structure of carboxylic and amine groups (with consequent protections), were evaluated. Unfortunately, due to the instability of the molecule in the deprotected form and its incompatibility with the methods of polycondensation used, it was not possible to obtain the desired polyamide.

Subsequently polyamides were synthesized between polyhydroxylated diacids or carbohydrate-derived diacids and aliphatic diamines, to obtain a series of oligo- or polyamide compounds type (m, n). Polytartaramides (polyethylene-L-tartaramide and polyhexamethylene-L-tartarammide), a polyglucaramide (polyethylene-D-glucaramide) and a politrehaluronamide (poliethylene- α,α'-trealuronamide) were in fact designed and synthesized[33].

In addition to the preliminary study of these polyamides for their use as a consolidant other possible fields of application of these products have been analyzed, in view of their structure similar to polar matrices and their water solubility. Consequently a new interest has grown toward the synthesis of a library of oligoamides with different structural characteristics. Keeping constant the diacid, it is in fact possible to synthesize polyamides having different molecular weights according to the nature of the diamines involved in polycondensation and to the synthetic conditions.

2 AIM OF THESIS

2.1 Biobased polyamides

The goal of this research project was the study of polymers and oligomers containing polar functional groups able to facilitate secondary interactions with natural or synthetic matrices having structural polar features. The interest for this type of products is determined by the possibility to use them in different polymeric formulations for several application fields (paper, wood and textile fibres).

Possible applications for such formulations can include both “everyday” products and more ”technological” fields such as the preservation of materials having historical and artistic interest. In this latter field, the design of new materials based on precursors of natural origin, gives the possibility to have compounds similar to the natural materials that constitute the artefacts and ensures the maintenance of their chemical, physical and mechanical properties.

Besides this aspect, the use of raw materials of natural origin matches with the growing interest towards the use of renewable sources, recoverable mainly from waste materials of agricultural production and forestry, fully integrating with the possible future development of third-generation biorefineries.

As a matter of facts, in XXI century chemical industry, a basic requirement for the search of new formulations and new synthetic methodologies is the use of reagents and methods with reduced environmental impact, identifying formulations in accordance with the principles of Green Chemistry.For this reason it is interesting to use, as starting materials, substances of natural origin, mainly monosaccharides, oligosaccharides, polysaccharides and amino acids to be used as such or after suitable transformations.

This work is part of a research project that is being performed in the Department of Chemistry, of Univeristà degli Studi di Firenze[33,34], based on the synthesis of hydroxylated oligoamides and their derivatives, with the aim of expanding the library of water soluble compounds, with high affinity for polar materials such as wood, paper and natural fibres. Parallel researches have been carried out including the synthesis of new oligoamides and the use of new monomers of natural origin with suitable structural characteristics. At the end, new methods for the synthesis of nanocomposites and their possible applications were deepened.

To obtain a progressive and regular chain growth in the step-growth polymerization, it is necessary to use stoichiometric amounts of the two monomers: generally in industrial processes

this is accomplished working in bulk starting from the salt between the diamine and diacid. However, the sensitivity of the monomers to high temperatures makes it is difficult the use of this method of activation of the hydroxylated diacid. Therefore in our syntheses the dimethyl esters of diacids were used, in order to work with low temperature (80°C) to avoid alteration of the carbohydrate portions.

In the first part of this project, structural changes for some oligotartaramides, produced in the past in our laboratory, have been studied. In fact, after the positive evaluation of their use as consolidating agent for the archaeological wood, the need for an industrial scale-up had emerged, to encourage the introduction in the market. The first research carried out in collaboration with a leader company in the field of polyamides synthesis showed, in the scale-up from laboratory to pilot plant, the need to provide some structural changes to make the material more suitable for the production scheme of commercial polyamides. The main problem is due to the more drastic reaction conditions used on an industrial level. In fact, under these reaction conditions, the high amount of hydroxyl groups in the polymer chain, obtained with dimethyl L-tartrate, causes a partial crosslinking and promotes other structural transformations that lead to intense color variations.

For this reason it was decided to continue the study, planning the synthesis of new oligoamides derivative that could be more suitable for an industrial scale production, always maintaining structural features similar to those of the oligotartaramides. To solve the problems observed in the scale-up, the "density" of hydroxyl groups in the chain was reduced, using units deriving from not-hydroxylated diacids together with monomeric units derived from dimethyl L-tartrate. In particular, dimethyl adipate, a diester synthesised from adipic acid was used.

The insertion of a monomer in the chain having a different reactivity from the one of L-tartaric acid, due to the lack of hydroxyl groups in α position to the carboxyl group, required appropriate modifications of the synthesis procedure previously developed for oligotartaramides.

The industrial scale-up of a synthetic process requires the identification of suitable application fields, that can promote the development of a commercial product. For this reason it is important to evaluate other possible application fields for the products synthesized or for their derivatives. This consideration led to a further development of this project, involving the use of polidiethylenamino-L-tartaramides derivatives in the oil industry, as kinetic hydrate inhibitors (KHI_S). In fact, in the literature it is well known that water-soluble polymers with structures similar to the one of oligoamides allow the delay in the formation of gas hydrates in oil drilling operations by acting on slowing down the kinetics nucleation of the process.

Products having amide groups which can inhibit the growth of gas hydrates are found among the most known KHIs; analysing the structure of the products giving the best results, it resulted essential to develop proper structural modifications on oligotartaramides in order to make these oligoamides suitable as KHIs. For this purpose, new oligoamides containing hydrophobic groups bonded with the nitrogen atoms were synthesized and subsequently oxidation of tertiary amine has been studied.

These studies were conducted in collaboration with the Norwegian University of Stavanger, and in the next months measures to assess the suitability of the structural features introduced will be carried out, matching them with the application requirements as KHIs.

In a second part of the project, the optimization of synthetic pathways involving only the use of reagents having natural origin in the synthesis of oligoamides was studied, in order to obtain fully bio-based products.

The syntheses have been developed starting from the experiences derived from the studies made in the past in our laboratory on the synthesis of oligoamides, considering the possibility of replacing the synthetic diamines with other resulting from natural products. The fundamental requirement for their choice is the presence of two terminal amino groups; among the most suitable natural molecules there are, for example, some amino acids, such as lysine, histidine and arginine. These molecules have functional groups that promote water solubility of the product as well as of their derivatives. Another solution regarding the choice of diamines obtained from biomass could be found with the use of hexamethylenediamine (HMDA) derived from transformation of furfural, a product resulting from biomass, but the oligoamides obtained using HMDA have been studied[35] and did not show the desired water solubility.

In this study L-lysine, a basic amino acid which is industrially produced by fermentation technologies, was used. L-lysine was used together with L-tartaric acid for the synthesis of oligoamides and two different synthetic methods were explored.

Finally, nanocomposites with core-shell structure were synthesized, promoting the growth of oligomers on the functionalized nanoparticles, to obtain polymeric films having a homogeneous distribution of the nanoparticles.

In particular, the project was focused on the use of TiO_2 (anatase form) nanoparticles , because this mineral, thanks to its antimicrobial activity, has great importance in many application areas, including wood preservation, application for which the functionalized oligoamides showed excellent qualities. Therefore, a system for the synthesis of core-shell nanocomposites, formed by TiO_2 nanoparticles linked to oligoamides obtained by in-situ polymerization process, has been developed. Nanoparticles were first subjected to a process of activation, followed by

functionalization with two coupling agents; then the oligoamides synthesis was conducted in order to promote their growth on functionalized nanoparticles, comparing two synthetic methodologies.

2.2 Choice of monomers

1. **Tartaric acid** is a white crystalline diprotic acid. This aldaric acid occurs naturally in many plants, particularly grapes, bananas and tamarinds (as well as in other fruits) and it is commonly combined with baking soda to function as a leavening agent in recipes. It is one of the main acids found in wine.

   The "traditional" production method is the extraction from by-products of the wine industry. However new methodologies, such as the production for oxidation of some carbon hydrates, or the treatment with nitric acid of glucose, lactose or starch, are under development. A very interesting alternative method is the oxidation of glucose in presence of oxidase and peroxidase (45% conversion) or the electrolysis of saccharic acid in an acid solution or with H_2O_2. Another method is the oxidation with bromine or chlorine from fumaric or maleic acid.

In our study tartaric acid was chosen as one of the monomers for the production of polyamides because it has two hydroxyl groups in the molecule, a structural feature similar, at least partially, to the one of a sugar in the open form; these structural characteristics make the final product affine to polar materials such as wood.

2. **α,α'-trehaluronic acid** was obtained from α,α'-trehalose, which derives from renewable sources. The peculiar characteristics of α,α-trehaluronic acid make this molecule an appealing candidate to be used as a reactant for the synthesis of the oligoamides through polycondensation reaction: in particular, the presence in the chemical structure of two D-(+)-glucose moieties, joined together by their anomeric positions, is responsible for good thermal stability and excellent chemical resistance in a large pH range. The absence of free anomeric positions does not allow reactions with amino compounds such as aminoacids or proteins (Maillard reaction). Given these particular characteristics, α,α'-trehaluronic acid is largely studied as building block in the industrial field.

   α,α'-trehalose is a sugar widely found in nature and it is one of the most important sources of energy in many living organisms including bacteria, fungi, insects, plants and invertebrates.

It also protects organisms from various stresses, such as drought, freezing or pressure changes and stabilizes membranes and other macromolecular complexes in extreme environmental conditions.

In the past, the low production volumes of this sugar have limited its use: in fact, the traditional method for the production of α, α'-trehalose is the extraction from yeasts, a process with low yield and high cost.

In 1994 an enzyme system capable of producing trehalose was developed, allowing an easier industrial-scale production that resulted in the reduction of its production cost.

The bacterial strain, from which the enzyme (Arthrobacter sp. Q36) was originally extracted , was isolated from soil.

The system consists of two new enzymes, maltooligosyl trehalose synthase (MTSase) and maltooligosyl trehalose trehalohydrolase (MTHase). In the first strep MTSase catalyzes the intramolecular transglycosylation of glucose residues from malt-oligosaccharide having a α-1,4 bond to malt oligotrehalose having a α-1,1 bond, which contains residues of trehalose at the end of the saccharide chain. Trehalose is released thanks to the second enzyme, MTHase. The yield of the process is higher than 80%[36].

Higashiyama et al. have studied this mechanism and were able to produce large quantities of α, α'-trehalose from starch[37].

In the polyamides synthesis the choice of using α,α'-trehaluronic acid was also determined by its stability and by other positive properties of the sugar precursor. In fact the use of α, α'-trehalose as a starting monomer allows to insert in the structure of the resulting polymer a derivative of a natural product that is biocompatible and biodegradable and, as previously mentioned, possesses high stability and has a relatively low cost.

In particular, the development of its large-scale production process makes α,α-trehalose one of the most appealing reagents used in polymer synthesis that should employ non-toxic and biodegradable raw materials from renewable resources.

3. **L-Lysine** (Figure 14) is an essential amino acid, with chiral polar structure:

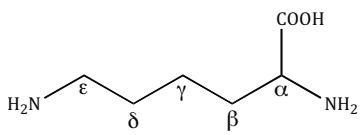

Figure 14: L-lysine

The R group is constituted by an aliphatic chain that terminates with an amino group (pKa = 10,54), therefore L-Lysine is a basic amino acids and acts as a base in enzymatic reactions.

In human diet it is obtained through meat, blue fish, soy, cheese and vegetables, and its deficiency can cause various diseases, even pellagra.

The discovery of lysine[38] dates back to 1873, when Hlasiwete and Habermann showed that proteins could be advantageously hydrolyzed by means of hydrochloric acid in the presence of tin. They discovered that the decomposition took place smoothly and that the products were leucine, tyrosine, glutamic and aspartic acids and ammonia, with only *a* small residue of unknown material. Schutzenberger in 1879 decomposed proteins by heating them at 150°C with barium hydroxide and likewise obtained aspartic and glutamic acids, tyrosine, and leucine, and in addition, a series of substances that he regarded as homologues of leucine. Other substances were found in small amounts but these seemed to be the main products.

Drechsel in 1889, carrying out studies on the hydrolysis of the protein chains, crystallized lysine for the first time and he identified its empirical formula.

Drechsel's paper contains the suggestion that lysine is a derivative of pentamethylenediamine; this hypothesis was demonstrated in 1899**,** when Ellinger showed that pentamethylenediamine could be obtained from lysine by anaerobic putrefaction.

The synthesis of lysine was developed and optimized by Fischer and Weigert from 7-cyanopropylmalonic ester by treatment with nitrous acid followed by reduction. Other syntheses have been described since then, by Sorensen and by von Braun.

Lysine comes from an intermediate of the Krebs cycle (such as ornithine) but it is industrially produced by fermentation technologies, using *Corynebacterium glutamicum*; lysine production exceeds 600,000 tons/year[39].

This molecule is totally derived by natural source and presents a double amino termination and it was chosen as the natural diamine to be used in the polycondensation process with diesters to obtain a totally bio-based polyamide.

4. **Adipic acid**: it is an important chemical intermediate, as well as being the diacid used for the synthesis of Nylon 6,6. For this reason it was chosen for the synthesis of the copolymers together with tartaric and ethylenediamine.

   There are several methods to produce adipic acid production on an industrial level[40] (Figure 15):the main production process is based on the oxidation of a mixture of cyclohexanol and cyclohexanone, the so-called KA Oil (ketone/ alcohol oil or Ol/One), or of cyclohexanol. These

compounds can be produced by different methods, the principal one being the oxidation of cyclohexane with air.

Cyclohexane is obtained either by the hydrogenation of benzene, or from naphtha fraction in small amounts. This process was first industrialized by DuPont in the early 1940s. Oxidation is catalyzed by Co or Mn organic salts (e.g., naphthenate), conducted between 150 and 180°C and 10–20 atm. Indeed, this reaction is a two-step process (an oxidation and a deperoxidation step), and two variants are currently in use. The oxidation step can be performed with or without a catalyst. The deperoxidation step always uses a catalyst (Co(II) or NaOH).

Two variants are currently employed for the synthesis of Ol/One:

1) the hydrogenation of phenol to cyclohexanol and cyclohexanone.

2) the hydration of cyclohexene to cyclohexanol; cyclohexene is synthesized thanks to selective hydrogenation of benzene. Cyclohexanol is then oxidized to adipic acid using the same process as that employed for the nitric acid oxidation of KA Oil.

Hydrogenation of phenol has been adopted by Solutia and Radici. This process has some advantages, particularly for smaller scale manufacturers and for companies that are large-scale manufacturers of phenol. The equipment needed for KA Oil manufacture from phenol is less complex and the process is safer than that based on cyclohexane oxidation, resulting in reduced investment costs. Moreover, current hydrogenation technology allows to obtain directly a mixture of cyclohexanol and cyclohexanone with the desired ratio. By increasing the quantity of ketone it is possible to save hydrogen in this step and nitric acid during oxidation. The hydrogenation process is very selective and the final product is extremely pure, if compared with KA Oil stemming from cyclohexane oxidation. This could render AA purification simpler.

Finally, another method to obtain cyclohexanol is the one developed by Asahi, where hydrogenation of benzene to cyclohexene is performed, followed by the hydration of cycloolefin.

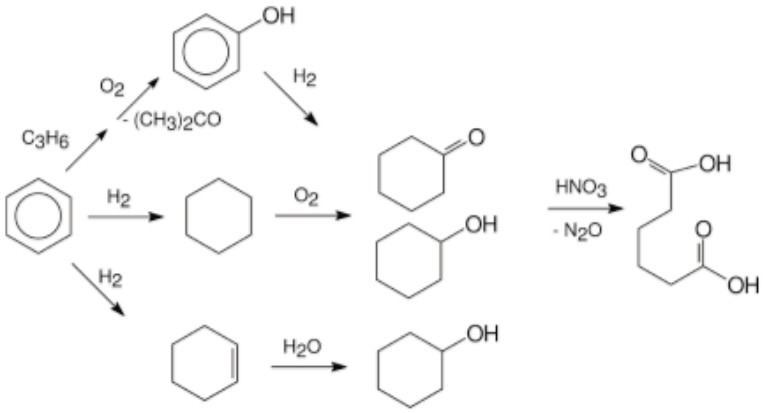

Figure 15: adipic acid synthesis

Currently the production of adipic acid can also be performed from renewable sources, for instance starting by muconic acid, obtained from glucose. Johnson Matthey signed a cooperation agreement with Rennovia for its production, by a catalytic process, aerobic oxidation of glucose. This process could be less expensive than the current one, based on petrochemicals.

Prices of the monomers described, on the industrial level, are here given and compared with the prices of similar molecules:

Product	**Price($/Kg)**
L-tartaric acid	1-2
α,α'-trehalose	5-10
D-glucose	0.3- 0.4
Saccharose	1
Cellobiose	1-100
Ethylenediamine	8.60 ($/L)
L-lysine	1-2

Prices have been obtained under the hypothesis of using an annual maximum quantity of 1000 kg. The prices of raw materials used in this work can be considered competitive to those prices of "standard" raw materials; consequently it is possible to envisage a industrial scale-up of the synthesis.

3 POLYAMIDES FROM DERIVATIVES OF L-TARTARIC ACID AND ADIPIC ACID

3.1 Copolymers

The synthesis of copolymers improves, or in general modulates, some properties of the polymeric materials. The "copolymer" class identifies all macromolecules whose polymeric chain contains repeating units deriving from two or more different species. In polycondensation polymers, two different monomer units participate to form the repeating unit (eg. diamine and diacid); the definition of "comonomers" and consequently the one of "copolymer" must then be referred to the presence of different monomer units that perform the same role in the repetitive unit (eg. two diacids and/or two diamine).

The copolymer structure may be formed by regular or random (statistical) alternation of the monomers, or by blocks of monomers of different type (block copolymers), or also by side chains (graft), where some monomers belong to the main chain and others to side chains. Similarly, in polycondensation copolymers different situations can be present, due to the concatenation of different repeating units.

There are many commercial copolymers:

- High Impact Polystyrene (HIPS), where polybutadiene molecules are grafted in the main chain of polystyrene to reduce brittleness and increase resilience (graft structure)[41]
- SBS resin, where the skeleton is composed by alternating chains of polystyrene and polybutadiene (block structure).
- ABS, a copolymer derived from styrene which is polymerized with acrylonitrile in presence of polybutadiene, and therefore can be defined as a terpolymer. The proportions may vary from 15% to 35% of acrylonitrile, from 5% to 30% of butadiene and from 40% to 60% of styrene (block copolymer structure).
- Among polycondensation copolymers, PETG is a PET containing a small amount (typically between 1 and 5%) of cyclohexanedimethanol, which disturbs the crystallinity and makes the polymer more amorphous and therefore transparent (statistical structure).

Physical and mechanical properties of the copolymer will depend on the constituent units and on their arrangement into the polymer chain.

An important factor to consider in this type of reactions is that, when the various monomers react with each other, a copolymer with composition different from that of the mixture of monomers present in the feed is obtained, because of the different reactivity ratios between them; typically, composition varies with the polymerization time. In conclusion, it is possible to say that the copolymer composition depends on the degree of conversion of the reaction and will be the same of the feed mixture composition only in case of total conversion of the reactants or similar reactivity of the monomers[42].

3.2 Research metodology

As above mentioned, recently, in collaboration with a company leader in the synthesis of polyamides, a study to evaluate a possible industrial scale-up of the oligo-L-tartaramide synthesis developed in our laboratory has been deepened. However, several problems in the scale-up from laboratory-scale to pilot-plant have been highlighted and have delayed a possible industrial development of the products.

The main problems arisen were attributed to the "drastic" conditions used for industrial scale-up (eg. high temperatures); in fact, in the scale-up reaction, the high amount of hydroxyl groups present in the polymer chain caused partial crosslinking favoring other structural changes, resulting in intense color variations.

To solve these problems it was decided to reduce the hydroxyl groups quantity in the chain by copolymerization between the unit derived by L-tartaric acid and another monomer derived from a diacid without hydroxyl groups in the structure. Therefore, some preliminary laboratory tests were carried out using dimethyl adipate obtained from adipic acid (Figure 16).

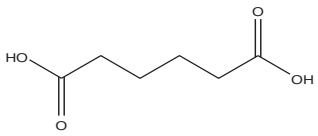

Figure 16: adipic acid structure

The reactivity of dimethyl adipate under the same reaction conditions used with the hydroxylated diesters has been evaluated. In fact, past researches demonstrated that hydroxyl or ether groups in α- or β- position with respect to the ester group strongly increase the reactivity of diesters in polycondensation reactions conducted in polar solvents[43].

In the last years, in our laboratories, tests on polycondensation between dimethyl adipate and ethylenediamine were performed under reaction conditions similar to those used for dimethyl L-tartrate and other diesters having heteroatoms, such as oxygen, in α position to the carbonyl groups, which allowed to have an easy polycondensation reaction with diamines in alcoholic solution. Syntheses were performed in different solvents (DMSO, THF or methanol), using different temperature (from room temperature up to 80°C) and reaction time (up to 17 days) to evaluate the best conditions for the activation of the new diester. The products obtained starting from dimethyl adipate had shown a low reactivity of the diester, obtaining the monocondensation product with a "mixed" termination (an ester and an amine) as show in Figure 17.

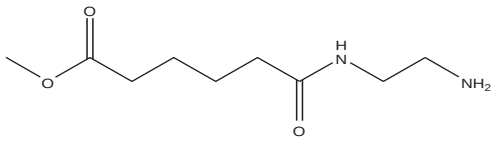

Figure 17: monocondensation product between dimethyladipate and ethylenediamine

In this study, the reaction conditions necessary to obtain polycondensation between dimethyl adipate and ethylenediamine, forming an homopolymer, were evaluated; subsequently, the conditions necessary for the optimization of the reactions, promoting the formation of the copolymer, were studied.

For the synthesis of the homopolymer, conditions completely different from those used for the other diesters have been used, in order to try to increase the reactivity of dimethyl adipate; these reactions were conducted using bulk polymerization.

The subsequent copolymerizations were carried out using two methods; one in bulk and the other in solution (with small amounts of solvent) to obtain products with higher molecular weight. Post-polymerization reactions with small amounts of solvent were also carried out.

Finally, to simplify the characterization of the products, extractions with solvent were performed, in order to separate the products in relation to the molecular weight or to their composition.

3.3 Results and discussion

3.3.1 Synthesis of the precursor: dimethyl L-tartrate

To promote the polycondensation reaction between diacids and diamines, the dicarboxylic acid must be activated; in this work an activation through esterification reaction was used, because this reaction is very simple and do not require the use of expensive reagents.

The esterification reaction of L-tartaric acid (Figure 18) was studied by Houston et al.[44], and was modified by Salvini[33]. Among the different methods used to promote the esterification reaction, the formation of the dimethyl ester by the corresponding diacid had already been optimized in our laboratory[33], using, boric acid as catalyst and excess methanol as esterifying agent.

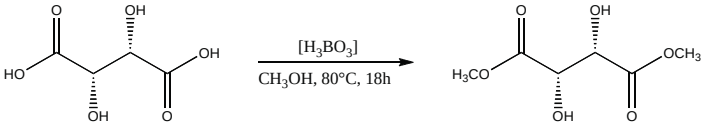

Figure 18: dimethyl L-tartrate synthesis

After 18 hours at 80 °C the reaction is almost complete (yield: 98%): ^{1}H-NMR analysis (Figure 19) confirms the presence of the ester thanks to the signal at δ 3.85 ppm, relative to 6 hydrogen atoms of the methylene ester groups.

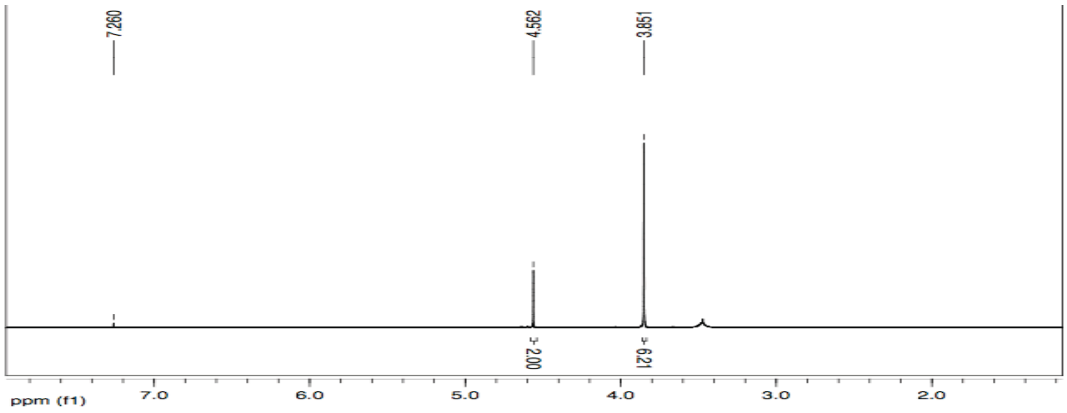

Figure 19: ^{1}H NMR spectrum in $CDCl_3$ of dimethyl L-tartrate

^{13}C NMR analysis (Figure 20) confirms the formation of an ester group due to the presence of a signals at δ 53.2 ppm related to the -O**C**H$_3$ groups and at δ 171.9 attributable to the ester carbonyl group. Moreover, also the signal at δ 72.0 ppm relative to -**C**HOH is present.

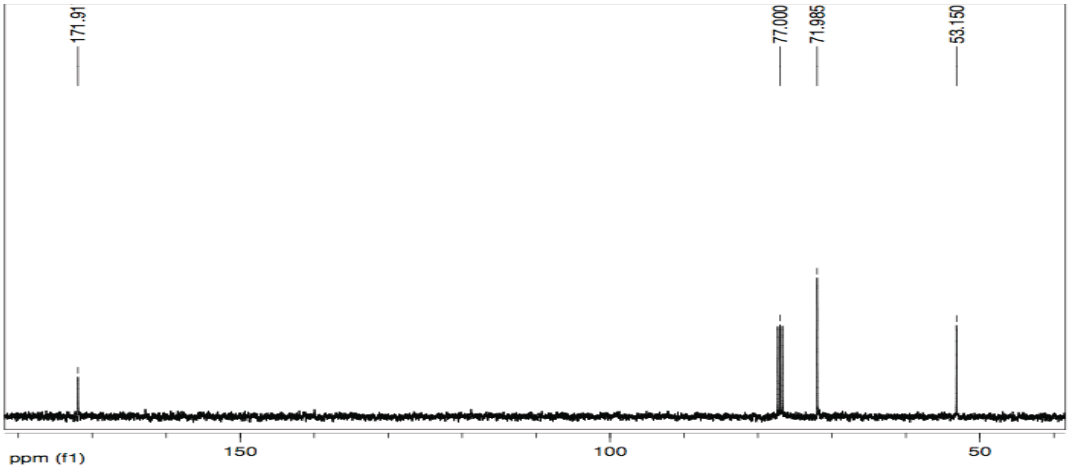

Figure 20: ^{13}C NMR spectrum in $CDCl_3$ of dimethyl L-tartrate

The boric acid used as catalyst at the end of the reaction turns into $B(OCH_3)_3$, having a boiling point of 68°C: this molecule can be removed easily during the work-up by distillation at reduced pressure.

The dimethyl L-tartrate obtained was then used together with commercial dimethyl adipate and ethylenediamine for the synthesis of the copolymers.

3.3.2 Syntheses of the homopolymers and copolymers

To promote the reactivity of dimethyl adipate, bulk polymerization of the homopolymer was carried out, while for the syntheses of the copolymers two approaches have been used: one in bulk and the other one in presence of small amounts of solvent, as previously stated.

All bulk polycondensation reactions were carried out without catalyst, at 80°C, with reaction times up to 2 days.

The reactions with small amounts of solvent were performed maintaining constant reaction temperature (80°C), carrying out the polymerization either with or without catalyst, increasing the reaction times up to 5 days.

Both reactions were performed in nitrogen atmosphere to avoid possible oxidation and carbonation of the diamine which consequently would become non-reactive.

The products obtained were subjected to selective extraction with solvents having different polarity (methanol, dimethyl sulfoxide, ethanol, acetone, chloroform) to try to separate fractions with different characteristics, based on the molecular weight or on the composition of the copolymer. The solvent giving the best results was methanol, which allowed the separation of two

fractions with different molecular weight. Precipitation tests were also carried out, by dissolving the product in water and re-precipitating in acetone, obtaining also in this case a separation of the product depending on the molecular weight.

Polyamides characterization was carried out by NMR and FT-IR spectroscopies. The molecular weight of the oligomers was calculated by integration of the signals of the ^{1}H NMR spectrum, leading to the determination of the numeral average molecular weight of the products similarly to the procedure described in literature for other oligoamides[33,34].

During the step-growth polymerization, as well as in the chain-growth polymerization, molecules of different lengths are formed and the final product will be composed by macromolecules with a different degree of polymerization. Necessarily, the molecular weight of the polymers must therefore be indicated using average values in order to take into account these differences. In the step-growth polymerization the molecular complexity increases with reaction time.

Table 1 and Table 2 describe the polycondensation reactions performed.

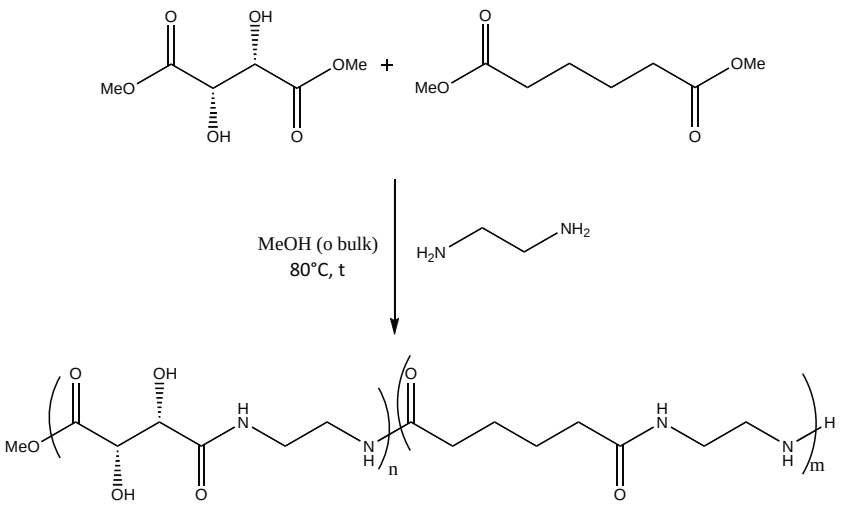

Figure 21: reaction scheme for the synthesis of the copolymers

Table 1: polycondensation reactions of homopolymers

Product	T (°C)	t	Solvent	Catalyst	Yield (%)	T_g (°C)	D.P.	MW (g/mol)
Oligoethyleneadipamide	80	8 hours	---	---	44.6	61.4	2.5*	457*
Oligoethylene-L-tartaramide	80	2.5 days	MeOH	NEt_3	63.6	104	5	930

*water soluble fraction

Table 2: polycondensation reactions of copolymers

Product	T (°C)	t (days)	Solvent	Catalyst	Yield (%)	T_g (°C)	D.P. A*	D.P. B**	MW (g/mol) A	MW (g/mol) B	A(%)	B (%)
1	80	1	---	---	61.6	---	n= 3 + m= 0.5	n= 0.5 + m= 0.5	667	202	64	36
2	80	2	---	---	63.6	N.D.	n= 4 + m= 1	n= 0.5 + m= 0.5	926	202	76.2	23.8
3	80	3	MeOH	---	65.5	108	n= 4 + m= 2.5	n= 0.5 + m= 2.5	1181	558	75	25
4	80	5	MeOH	---	67	109	n= 6 + m= 2	n= 0.5 + m= 2	1444	458	68.6	31.4
5	80	3	MeOH	NEt_3	70	120	n= 7 + m= 3	n= 0.5 + m= 2.5	1788	544	67.2	32.8
6	100	1	MeOH	---	80	---	n= 5 + m= 2	n= 0.5 + m= 3	1256	629	81.8	18.2

*A: methanol insoluble fraction; **B: Methanol soluble fraction; n: tartaric units; m: adipic units

3.3.2.1 Oligoethyleneadipamide

The synthesis between dimethyl adipate and ethylenediamine, two transparent liquids, was performed without solvent and catalyst at 80°C for 8 hours: the reaction was stopped because a white solid was formed, making magnetic stirring impossible. The work-up was carried on washing the solid with ethyl ether and filtering on büchner funnel: given the "pasty" nature of the product, this procedure caused a partial loss of the product itself, that had the tendency to remain on the filter. The residual solid was dried under reduced pressure at room temperature and was isolated giving a 44.6% yield. The white solid obtained is partially soluble in water but insoluble in DMSO, methanol, ethanol and acetone. Both fractions (water soluble and insoluble) were analysed via FT-IR; the soluble fraction was also analysed via NMR.

In FT-IR spectra (Figure 22) the formation of the amide bond is confirmed by the presence of signals at 1640 and 1556 cm^{-1} (amide I and II respectively), having higher intensity in the insoluble fraction. In the spectrum there are also the signals related to N-H stretching at 3298 cm^{-1} and to C-H stretching at 3084, 2941 e 2860 cm^{-1}; in both fractions the ester stretching signal attributable to the ester stretching is present at 1720 cm^{-1}, having higher intensity in the soluble fraction.

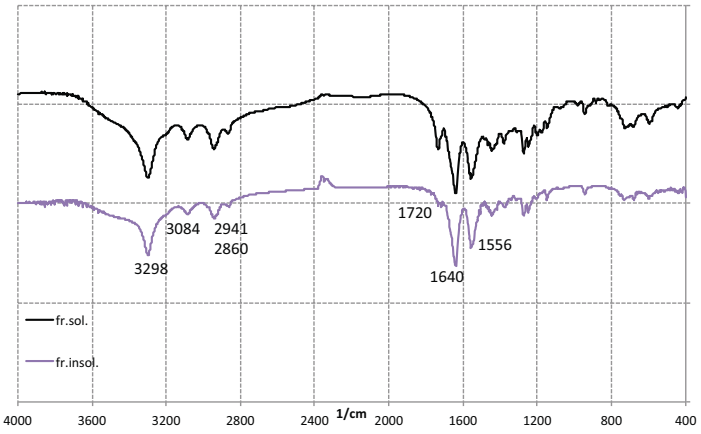

Figure 22: comparison between FT IR spectra of the soluble and insoluble fractions of the oligoethyleneadipamide

Soluble fraction was also characterized via NMR; in ^{1}H-NMR spectrum (Figure 23) the presence of a signal between 3.20 and 3.45 ppm attributable to the CH_2 group in α position to the amide group (C**H**$_2$NHCO) confirms the formation of an amide bond. A further confirmation of the oligoamide synthesis is given by the absence of the signal related to unreacted ethylenediamine at 2.60 ppm and by the presence of a signal that can be attributed to the CH_2 in α position to the terminal amino group at 2.94 ppm (C**H**$_2$NH$_2$). The spectrum shows signals indicating that the end

groups are both amino and ester groups, given the presence of the signal at 3.70 ppm (-OC**H**$_3$) besides the one at 2.94 ppm already discussed: the two signals have a 1:1 ratio.

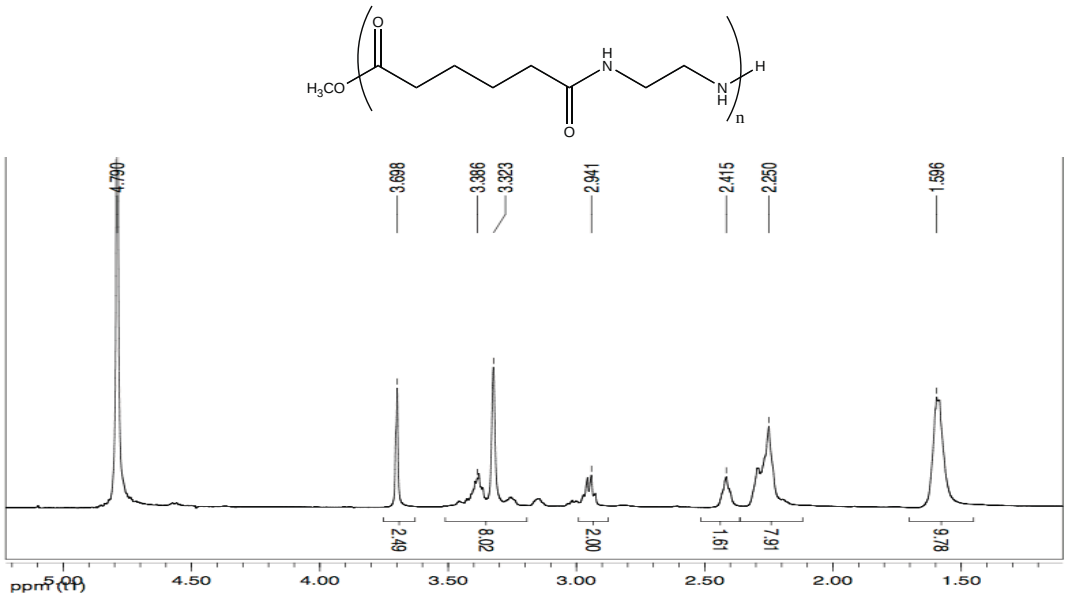

Figure 23: ^{1}H NMR spectrum in D_2O of the water soluble fraction of the oligoethyleneadipamide (400 MHz)

Through gCOSY spectrum (Figure 24), studying the correlations between the hydrogens of the molecule, it is possible to relate, in ^{1}H NMR spectrum, the signal at 3.39 ppm to the CH_2 in β position to the amino terminal group and the signals between 3.20 a 3.35 ppmto the other CH_2NHCO groups. It is also possible to relate the signal at 2.42 ppm to the CH_2 in α position to the terminal ester group (C**H**$_2$COOCH$_3$) and a new signal at 2.25 ppm to C**H**$_2$CONH groups, because of the presence of the coupling with the signal at 1.60 ppm (C**H**$_2$CH$_2$CONH).

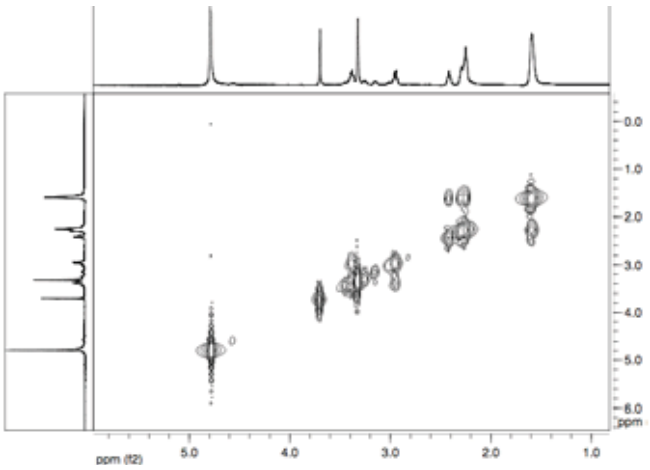

Figure 24: gCOSY spectrum in D_2O of the water soluble fraction of the oligoethyleneadipamide

In ^{13}C-NMR spectrum (Figure 25), formation of the product is confirmed by the presence of signals at 176.7 ppm (**C**ONH) and 38.5 ppm (**C**H_2NHCO). The presence of two different chain ends is in agreement with the two signals at 177.1 and 52.1 ppm related to -**C**OO**C**H_3 group and at 39.4 ppm related to CH_2 group in α position to the terminal amino group.

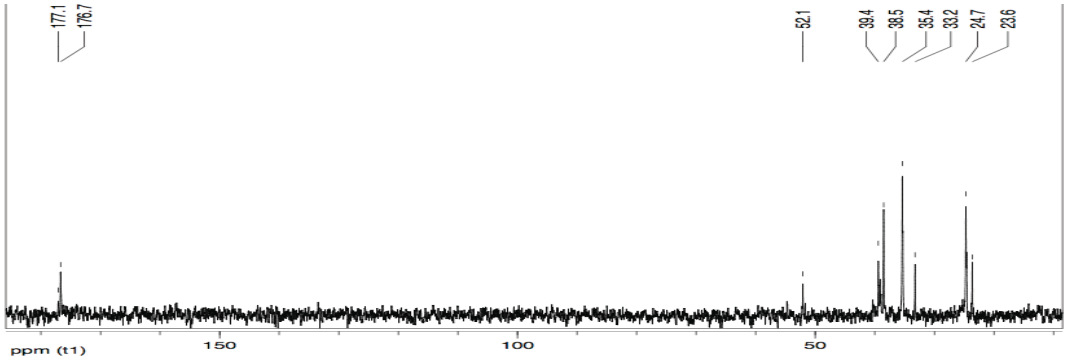

Figure 25: ^{13}C NMR spectrum in D_2O of the water soluble fraction of the oligoethyleneadipamide (100 MHz)

From gHSQC spectrum (Figure 26), studying the correlations between hydrogen and carbon atoms of the molecule, it is possible to relate the signal at 33.2 ppm in ^{13}C NMR spectrum to the CH_2 group in α position to the ester group (**C**H_2COOCH_3) and the one at 35.4 ppm to the **C**H_2CONH group. The correlations between the hydrogens of C**H**$_2$CH_2CONH and C**H**$_2$CH_2COOCH_3 groups with the corresponding carbon atoms at 24.7 ppm and 23.6 ppm respectively are visible.

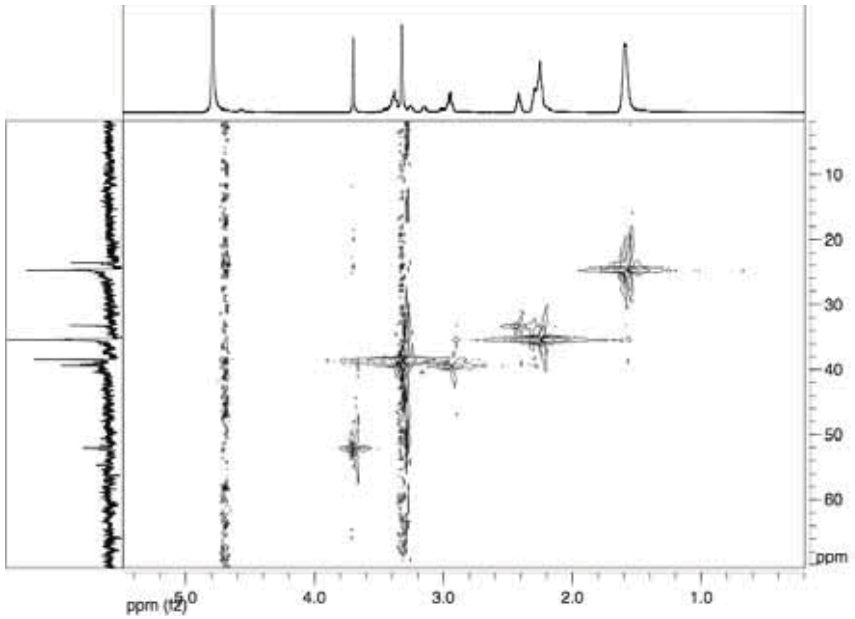

Figure 26: gHSQC spectrum in D_2O of the water soluble fraction of the oligoethyleneadipamide

As previously stated, the determination of the average molecular weight was first performed measuring the integrals present in ^{1}H-NMR. Indeed, identifying the signals related to the terminal groups (-$COOCH_3$, -CH_2NH_2), it is possible to use them as reference values to calculate the molecular weight of the product, comparing them with the integrals of the signals related to the protons present along the polymeric chain.

In the NMR analysis of the product synthesised, both terminal groups are present; following this consideration, it is possible to calculate the number (n) of the repeating units of the oligoethyleneadipamide according to the following data:

*integral of -OC**H**$_3$ signal = 3*

integral of -CH_2NH_2 signal = 2

*integral of -C**H**$_2$NHCO signal = 4n-2*

*integral of -CH_2C**H**$_2$$COOCH_3$ signal = 2*

*integral of -CH_2C**H**$_2$CONH- signal = 4n-2*

*integral of -C**H**$_2$$CH_2$CONH- signal = 4n*

The product is composed by an average of 2.5 repeating units, with an ester and an amino terminal group: consequently the average molecular weight is 457 g/mol (Figure 27).

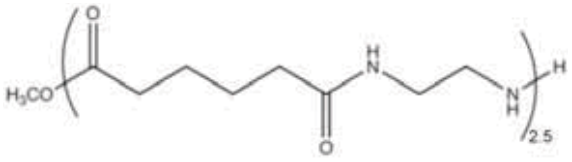

Figure 27: oligoethyleneadipamide

Glass transition temperature (T_g) of the product (Figure 28 left) is at 61.4°C, typical value of oligoadipamide with short chain.

Two peaks at about 128 and 225°C could be related two different melting points of the product (Figure 28 right), related to different DP; in fact, these values do not correspond to the boiling points of the two monomers (109°C for dimethyl adipate and 116°C for ethylenediamine).

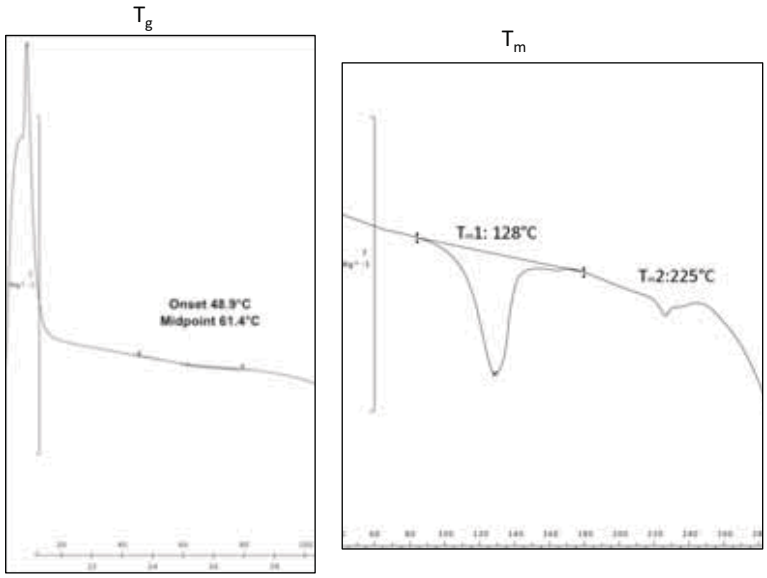

Figure 28: Glass transition temperature (T_g) and melting temperature (T_m) of oligoethylenadipamide

3.3.2.2 Oligoethylene-L-tartaramide

Synthesis of oligoethylene-L-tartaramide was carried out using the method of Cipriani et al.[33] reducing reaction time.

The synthesis between dimethyl L-tartrate and ethylenediamine was performed using methanol as solvent and triethylamine as catalyst, at 80°C for 2.5 days. The work-up was carried on washing the solid with methanol and filtering on büchner funnel; the residual solid was dried under reduced pressure at room temperature and was isolated giving a 63.6% yield. The product has light yellow colour and water soluble: it was analysed through FT-IR and NMR spectroscopies.

In FT-IR spectrum (Figure 29) the formation of the amide bond is confirmed by the signals at 1659 and 1539 cm^{-1} (amide I and II respectively); the presence of tartaric units in the chain is visible thanks to the peaks at 1120 and 1068 cm^{-1} characteristic of L-tartaric moiety. Moreover in N-H stretching range a broader band, in comparison to oligoethyleneadipamide, is present, thanks to the simultaneous presence of O-H stretching.

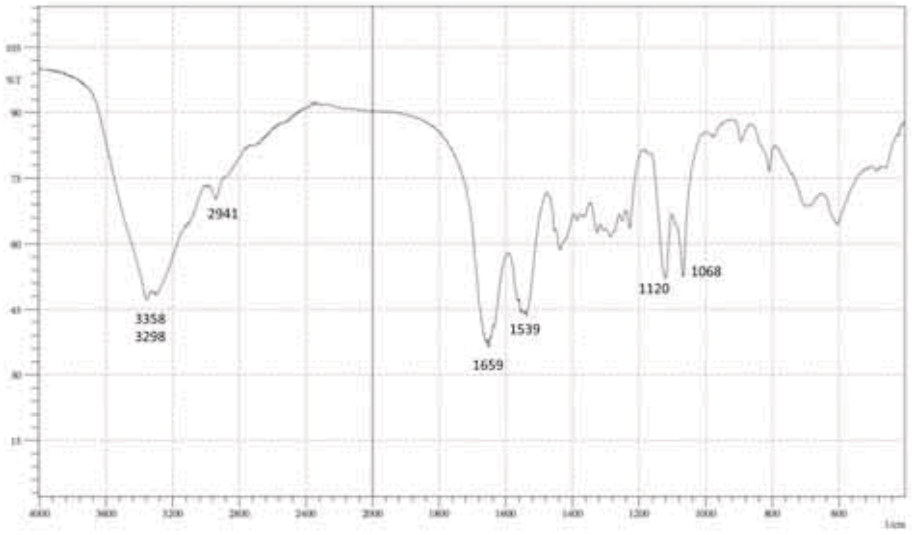

Figure 29: FT IR spectrum of the oligoethylene-L-tartaramide

^{1}H-NMR spectrum (Figure 30) confirms the formation of an amide bond, thanks to the presence of a signal at 3.48 ppm caused by the CH_2 group in α position to the amide group (C**H**$_2$NHCO). A further confirmation of the reaction is given by the absence of signals related to unreacted ethylenediamine at 2.60 ppm and by the presence of a signal that can be attributed to the CH_2 in α position to the terminal amino group at 3.09 ppm (C**H**$_2$NH$_2$); ester termination is not present, therefore the signal corresponding to the amino terminal groups is set equal to 4 idrogens. Moreover the signal related to the C**H**-OH at 4.58 ppm is present.

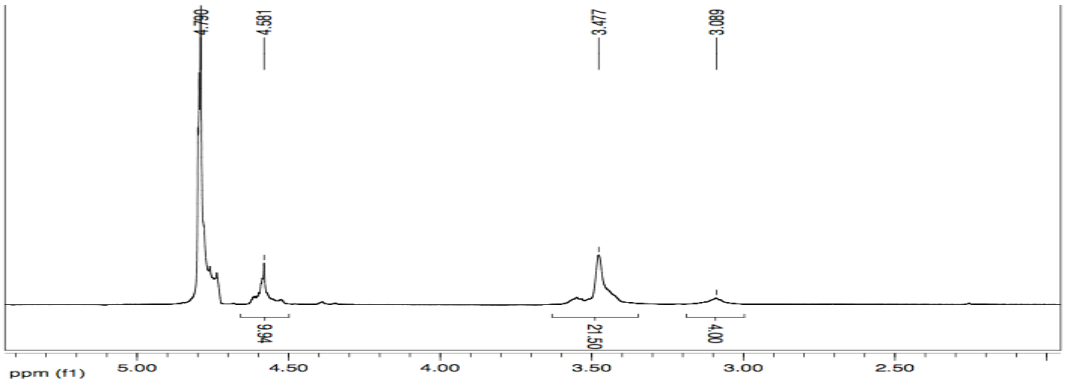

Figure 30: ^{1}H NMR spectrum in D_2O of the oligoethylene-L-tartaramide

In ^{13}C-NMR spectrum (Figure 31) the presence of two amino chain ends is confirmed by the signal at 39.4 ppm and by the absence of the signals related to the ester group. Besides, the formation

of the product is confirmed by the signal at 174 ppm (**C**ONH) and 38.5 ppm (**C**H_2NHCO); lastly, a signal at 72.3 ppm is present related to the **C**H-OH.

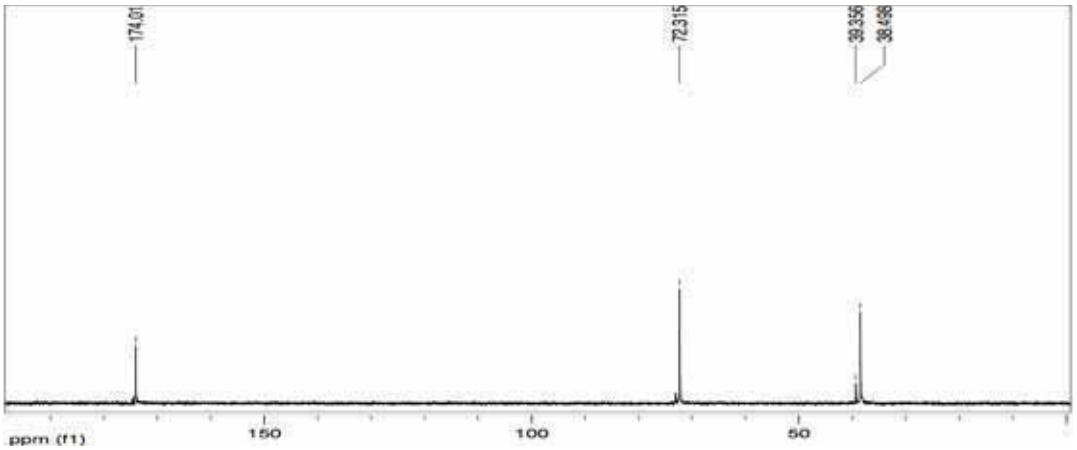

Figure 31: ^{13}C NMR spectrum in D_2O of the oligoethylene-L-tartaramide

As above reported, in the NMR spectra of the product synthesised, only amino termination signals are present,; following this consideration, it is possible to calculate the number (n) of the repeating units of the oligoethyleneadipamide according to the following data:

*integral of -C**H**$_2$NH$_2$ signal = 4*

*integral of -C**H**$_2$NHCO signal = 4n*

*integral of -C**H**OH- signal = 2n*

The product is composed by an average of 5 repeating units, with double amino termination: consequently the average molecular weight is 930 g/mol (Figure 32).

Finally, through glass transition temperature (T_g) was evaluated by DSC, obtaining a value of 104°C.

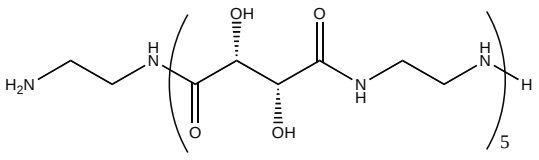

Figure 32: oligoethylene-L-tartaramide

3.3.2.3 Copolymers: bulk polycondensation (Synthesis 1 and Synthesis 2)

The reaction between dimethyl adipate, dimethyl L-tartrate and ethylenediamine, three transparent liquids, was performed without solvent and catalyst, with two reaction times: 24 hours (synthesis 1) and 48 hours (synthesis 2).

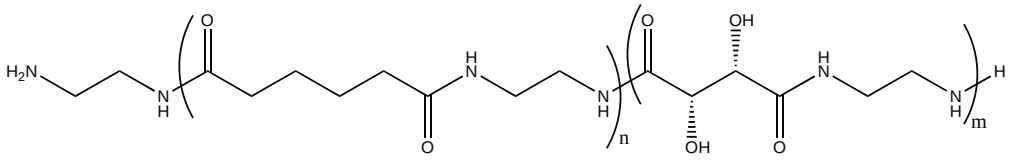

Figure 33: repeating units of the copolymer having two amino terminations

Synthesis 1. After 24 hours of reaction into the Sovirel® tube the disappearance of the liquid phase and the formation of a yellow solid was observed. In the work-up, the product was washed with ethyl ether, filtered on a büchner funnel, and then dried at reduced pressure giving a 61.6% yield. The product is a light yellow crystalline solid, water soluble.

Synthesis 2. The reaction was carried out for 2 days and then the product was subjected to the same work-up of the previous reaction, obtaining an intense yellow crystalline solid, with a slight increase of the reaction yield (63.6%). The product is water soluble.

Confirm of the formation of the copolymers in both syntheses, with respect to the possible presence of two homopolymers, is given by the good water solubility of both products, while the oligoethyleneadipamide homopolymers obtained after 8 hours of reaction, contain both a water soluble and a water-insoluble fraction.

Subsequently, in order to assess more accurately the oligomers synthesized and to simplify their characterization se, the products of both reactions were subjected to selective extraction in solvents. In fact, the possibility to separate different fractions according to molecular weight or according to the amount of hydroxylated or non-hydroxylated diester allows to study the different components that are part of the product. The extractions were carried out with solvents having different polarity (acetone, chloroform, methanol, ethanol, dimethyl sulfoxide); methanol resulted to be the best solvent and allowed the separation of two fractions.

Precipitation tests were carried out, by dissolving the product in water and precipitating in acetone, obtaining also in this case the separation of two fractions.

The characterization of the products was carried out by NMR and FT-IR spectroscopies.

In ^{1}H NMR spectrum (Figure 34) of **methanol insoluble fraction** (in synthesis 1: 64% yield; in synthesis 2: 76.2% yield), the oligomer formation is confirmed by the presence of a signal

between 3.30 and 3.55 ppm attributable to the CH_2 group in α position to the amide groups (C**H**$_2$NHCO from the tartaric and adipic units), by the presence of the signals related to C**H**$_2$CONH group at 2.30 ppm and by C**H**$_2$CH$_2$CONH group at 1.62 ppm, that confirm the presence of adipic unit; the presence of L-tartrate unit, is confirmed by the presence of the signal at 4.61 ppm.

A further proof of the reaction is given by the presence of the signal at 3.03 ppm due to the CH_2 group in α position to the terminal amino group (-C**H**$_2$NH$_2$) set equal to 4 hydrogens (double amino termination) due to the absence of signals at about 3.70 ppm that indicates that no ester termination is present.

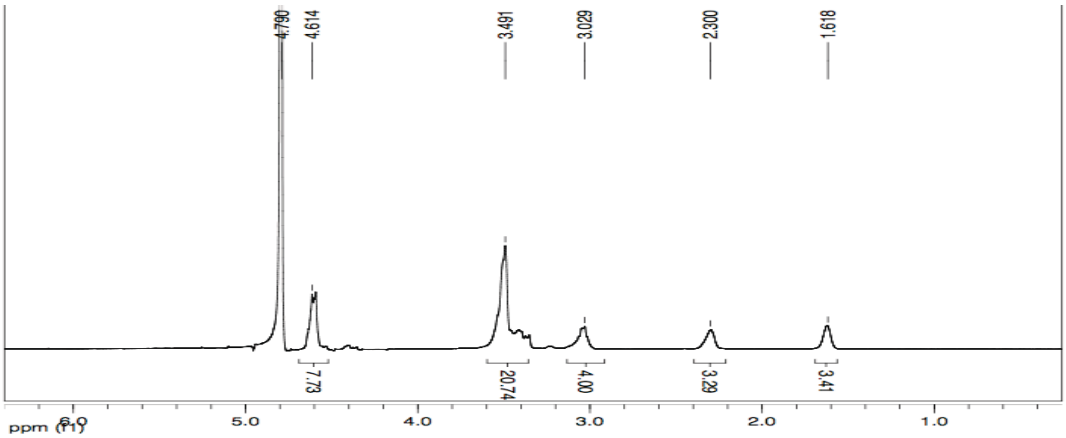

Figure 34: ^{1}H NMR spectrum in D$_2$O of the copolymer 2 (methanol insoluble fraction)

gCOSY spectrum (Figure 35) confirms this assignment, thanks to the couplings between the CH_2 in α and β positions to the CONH of the adipic chain at 2.30 and 1.62 ppm respectively and to the correlation between the CH_2 in α position to the terminal amino group at 3.03 ppm and the CH_2 in β position (CH_2NHCO) between 3.30 and 3.55 ppm.

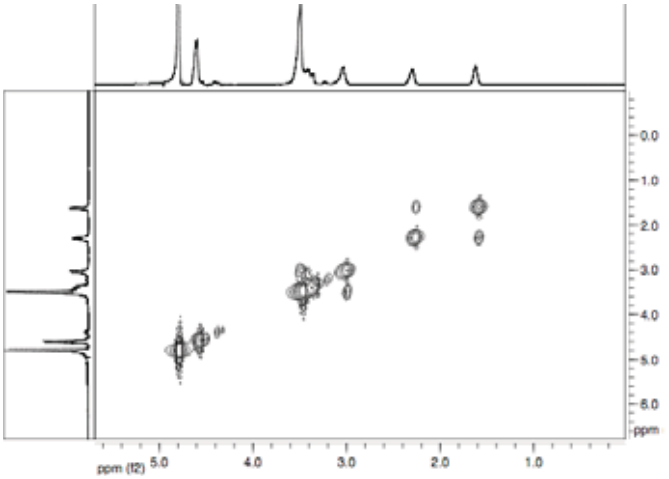

Figure 35: gCOSY spectrum in D$_2$O of the copolymer 2 (methanol insoluble fraction)

In ^{13}C-NMR spectrum (Figure 36) the presence of two amino termination is confirmed by the signal at 39.4 ppm and by the absence of the signals related to the terminal ester group. Besides, the formation of the product is confirmed by the signal at 174 ppm (**C**ONH) and 38.5 ppm (**C**H_2NHCO); a signal at 72.3 ppm is present related to the **C**H-OH and it is possible to observe a shift of the signals related to the CH_2 of the adipic chain at 23.5 (**C**$H_2CH_2COOCH_3$) and 33.2 ppm (**C**$H_2NHCOOCH_3$) to 24.7 ppm (**C**H_2CH_2CONH) and 35.4 ppm (**C**H_2NHCO) respectively.

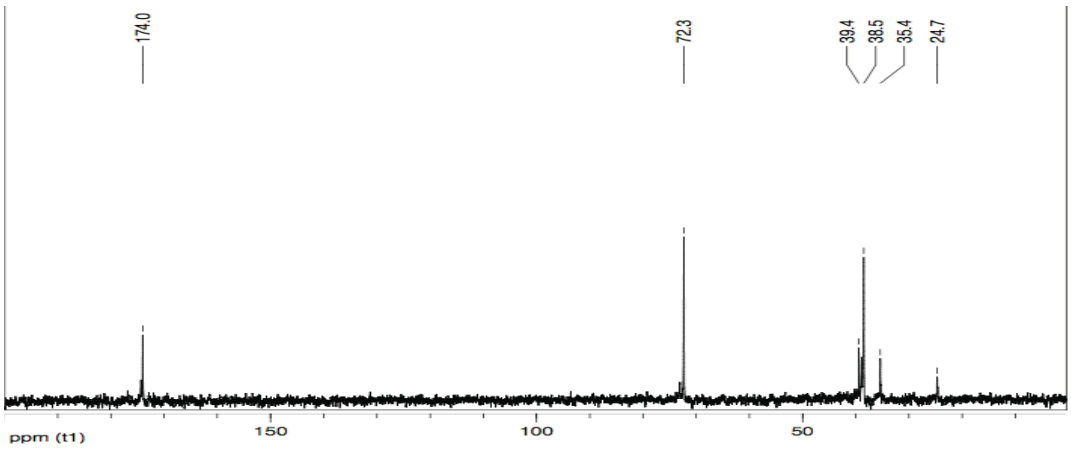

Figure 36: ^{13}C NMR spectrum in D_2O of the copolymer 2 (methanol insoluble fraction)

From gHSQC spectrum (Figure 37) the assignations made in ^{13}C NMR spectrum are confirmed, thanks to the couplings between the hydrogens previously attributed and corresponding carbons.

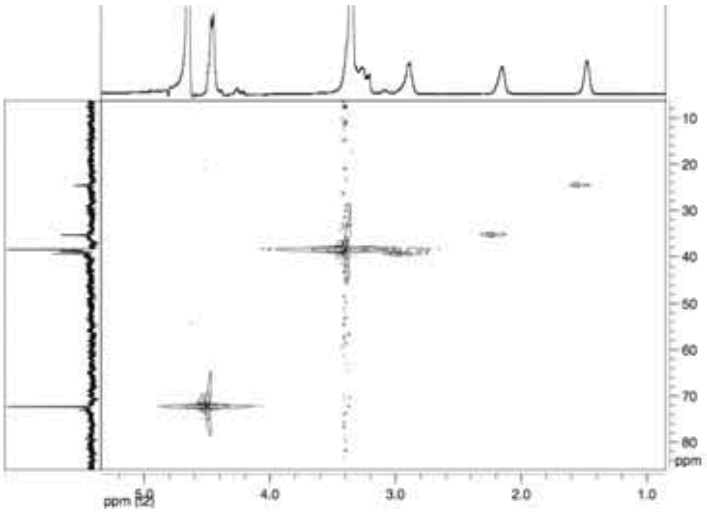

Figure 37: gHSQC spectrum in D_2O of the copolymer 2 (methanol insoluble fraction)

In FT IR spectrum (Figure 38) the formation of the amide bond is confirmed by the peaks at 1651 (I) and 1549 (II) cm^{-1}; moreover, two peaks are present related to C-O stretching at 1121 e 1069

cm^{-1}, absent in the oligoadipamide. Also in this case, the ester termination at about 1730 cm^{-1} is not present.

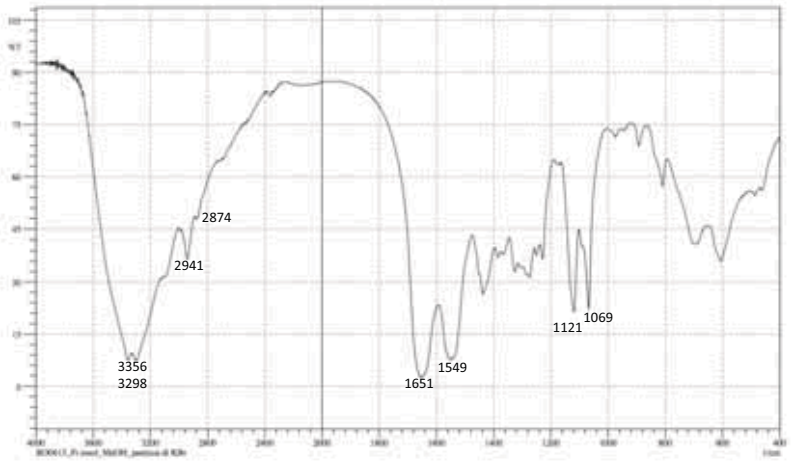

Figure 38: FT IR spectrum of the copolymer 2 (methanol insoluble fraction)

Determination of the average molecular weight was performed measuring the integrals present in ^1H NMR. In this case the calculation previously described for the homopolymer must be integrated with the addition of the integrals relating to the portion relative to dimethyl L-tartrate. It is possible to calculate the number "n" of the repeating units of the oligoamide according to the following data:

*integral of –C**H**OH signal = 2n*

*integral of -C**H**$_2$NHCO signal = 4n*

integral of -CH$_2$NH$_2$ signal = 4

*integral of -CH$_2$C**H**$_2$CONH- signal = 4n*

*integral of -C**H**$_2$CH$_2$CONH- signal = 4n*

In the synthesis with reaction time of 24 hours, the elaboration of the integrals obtained in ^1H NMR spectrum, permits to evaluate that the product is composed by repeating units having an average of 3 dimethyl L-tartrate and 0.5 of dimethyl adipate, with two amino terminations: consequently the average molecular weight is 667 g/mol.

In the reaction carried out for 2 days, the methanol insoluble fraction is composed by an average of 4 dimethyl L-tartrate repeating units and 1 of dimethyl adipate, with two amino termination, and consequently average molecular weight equal to 926 g/mol.

The ^1H NMR spectrum (Figure 39) of **methanol soluble fraction** (in synthesis 1: 36% yield; in synthesis 2: 23.8% yield) confirms the formation of the copolymer thanks to the presence of the

same signals present in the insoluble fraction. Both are composed by an average of 1 repeating unit (0.5 of dimethyl L-tartrate and 0.5 of dimethyl adipate), with two amino termination and consequently average molecular weight equal to 202 g/mol.

In this spectrum it is possible to observe the presence of a very weak signal at 3.72 ppm (OC**H**$_3$ termination), that has not been considered as chain termination for the evaluation of the average molecular weight, because of the low intensity compared to amino termination.

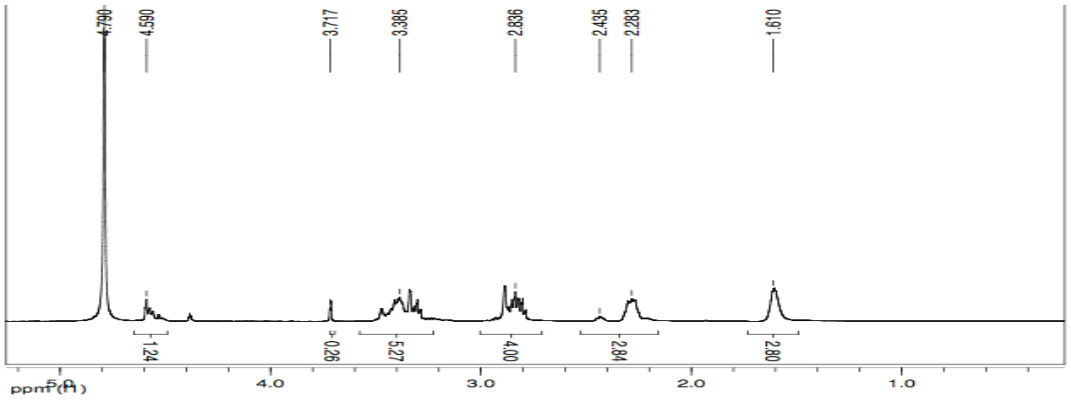

Figure 39: ^{1}H NMR spectrum in D_2O of the copolymer 2 (methanol soluble fraction)

In ^{13}C NMR spectrum (Figure 40) the presence of the amino termination is given by the signal at 39.7 ppm; the presence of the ester termination group, present in small quantities in the product, is not detectable through ^{13}C NMR spectrum, for the absence of the signals related to **C**OO**C**H$_3$ group. The formation of the product is confirmed by the signals at 174.1 and 176.9 ppm (C**O**NH), at 38.5 ppm (**C**H$_2$NHCO) and at 72.4, 73.1 ppm (**C**HOH). Finally there is a shift of the signals related to the CH_2 groups of the adipic backbone, from 23.5 and 33.2 ppm to 24.7 ppm (**C**H$_2$CH$_2$CONH) and 35.4 ppm (**C**H$_2$CONH) respectively, as in the insoluble fraction in methanol.

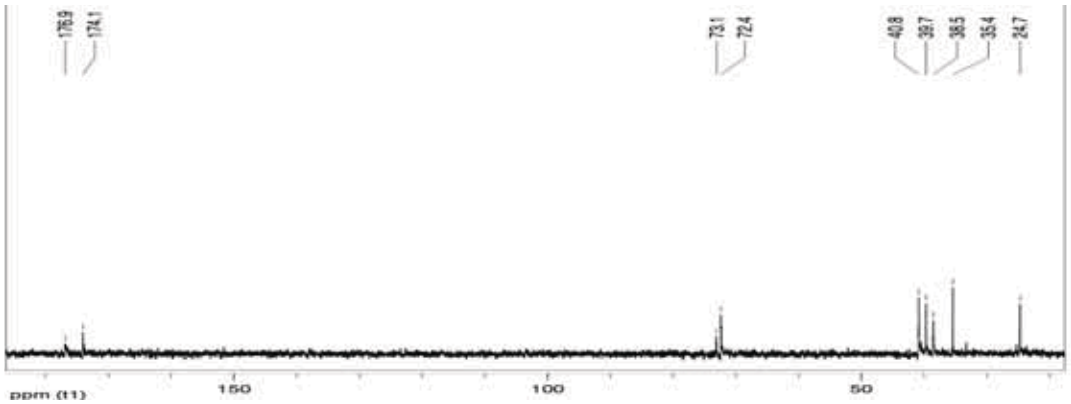

Figure 40: ^{13}C NMR spectrum in D_2O of the copolymer 2 (methanol soluble fraction). The signal at 40.8 ppm is owed to an impurity.

FT IR spectrum (Figure 41) is in agreement with NMR analysis, thanks to the presence of the peaks at 1641 and 1555 cm^{-1} (amide I and II respectively) and to the presence of a very weak peak at 1731 cm^{-1} related to ester termination. The presence of the tartaric units is confirmed by the weak peaks at 1130 and 1070 cm^{-1}, that are not present in the FT IR spectrum of the oligoethylenadipamide.

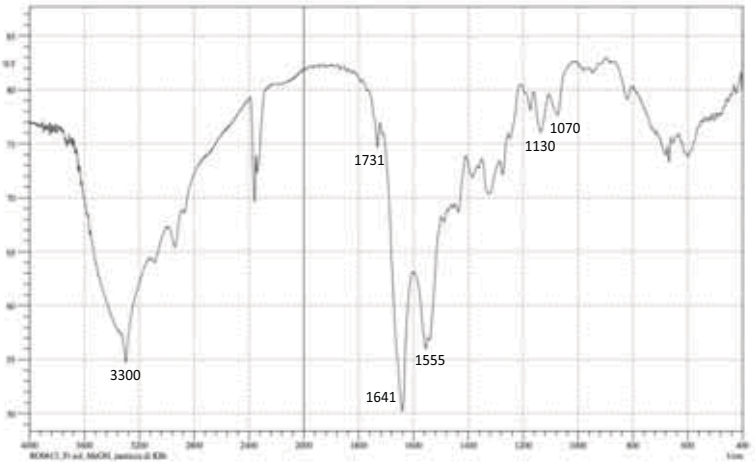

Figure 41: FT IR spectrum of the copolymer 2 (methanol soluble fraction)

Glass transition temperature (T_g) of **product 2**, i.e. the prduct obtained from synthesis 2 (Figure 42) is not visible; melting was observed but the transition is affected by the degradation of the oligomer, that starts immediately after the beginning of melting (Figure 43)

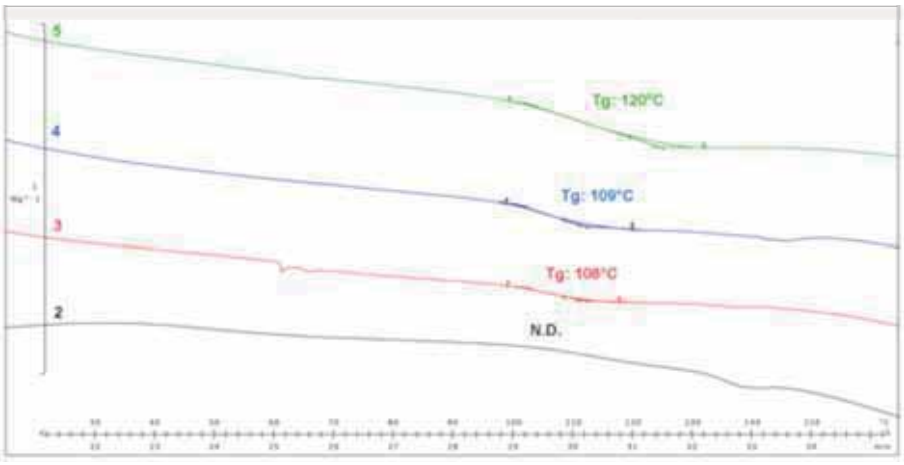

Figure 42: Glass transition temperature (T_g) of products 2, 3, 4 and 5

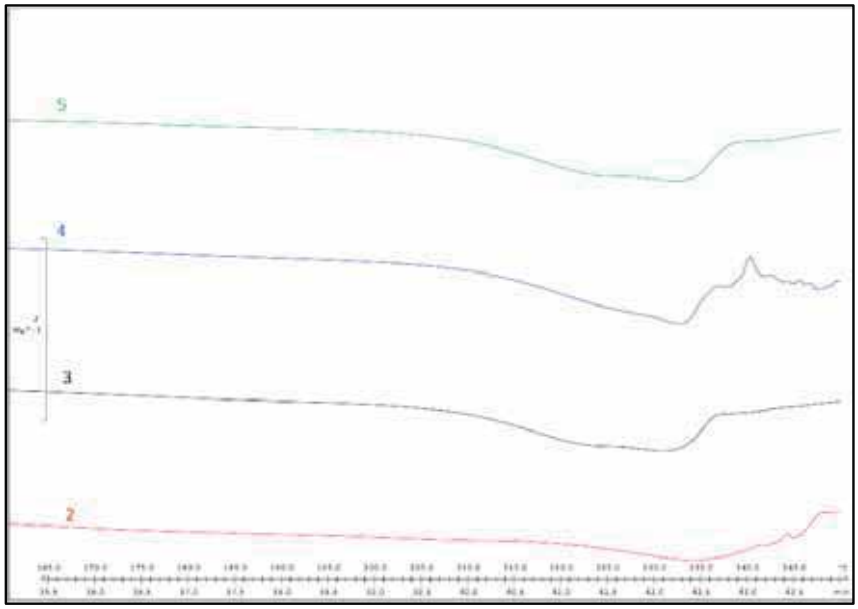

Figure 43: Temperature range between 165 and 250°C (product 2, 3, 4, 5)

In agreement with the results obtained, it can be concluded that higher reaction time allows a moderate increase of the average molecular weight of the product, probably limited by the absence of solvent, because the reactivity in the solid state is much lower and generally an increase of the temperature is necessary to promote the rate of the process.

Given these results, in order to obtain products with higher molecular weight, syntheses with a small amount of solvent have been performed (**synthesis 3 and 4**), with the aim to partially solubilize the solid formed during the reaction. To promote the kinetic of the reaction, a catalyst was also used (**synthesis 5**).

3.3.2.4 Copolymers: syntheses with solvent (Synthesis 3 and Synthesis 4)

The reaction was carried out in a Sovirel® tube, with methanol, at 80°C for 3 days (synthesis 3) or 5 days (synthesis 4). The work up was the same of the previous reactions: two yellow crystalline solids were obtained, both water soluble, isolated giving 65.5 e 67% yield (), in agreement with an increase in conversion thanks to higher reaction time.

Synthesis 3: the product was obtained with a yield similar to the one obtained with bulk polymerization, but with an increase of the average molecular weight.

This result is in good agreement with the consideration that, in a polycondensation reaction between diacids and diamines, the conversion is complete since the beginning of the reaction: increasing reaction time, molecular weight grows. Similarly, the presence of a solvent positively

affects the rate of the process, favouring the increase of molecular weight in comparison to bulk reactions.

The solid was extracted in methanol, obtaining two fractions, one insoluble and the other soluble. In ^{1}H NMR spectrum (Figure 44) of the **methanol insoluble fraction** (75% yield), an oligomer with two amino termination (and a small amount of ester termination) is present, composed by an average of 6.5 repeating units (4 of tartaric and 2.5 of adipic units) and consequently average molecular weight of 1181 g/mol.

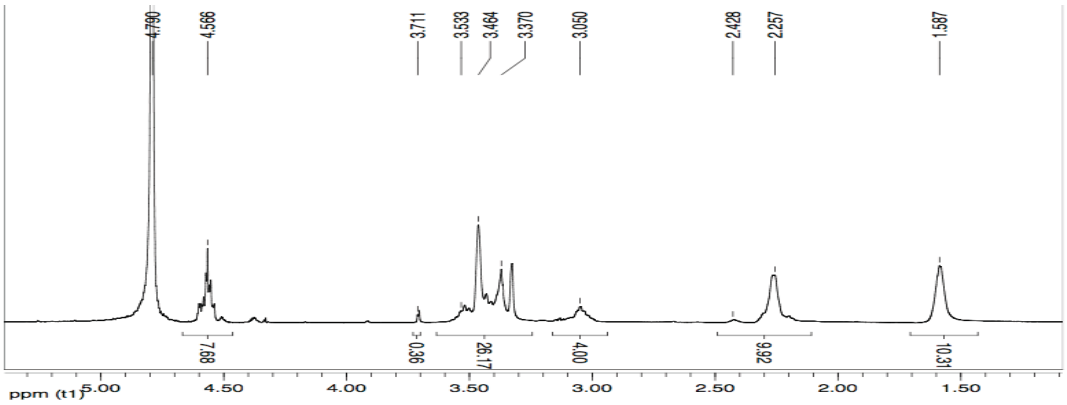

Figure 44: ^{1}H NMR spectrum in D_2O of the copolymer 3 (methanol insoluble fraction)

In ^{13}C NMR (Figure 45) the signals related to the ester terminal group (O**C**H_3) and the CH_2 in α or β position (**C**$H_2CH_2COOCH_3$ e CH_2**C**H_2COOCH_3) are not present because the signals, at about 52.0, 23.5 e 33.2 ppm respectively, are absent.

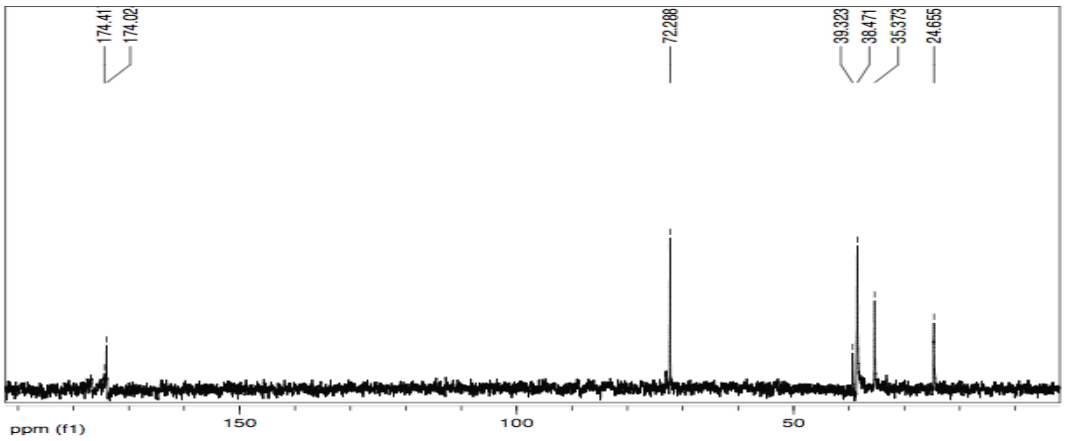

Figure 45: ^{13}C NMR spectrum in D_2O of the copolymer 3 (methanol insoluble fraction)

The **methanol soluble fraction** (25% yield) was also characterized via NMR; ^{1}H NMR (Figure 46) confirms the formation of a product in equimolar amount between "mixed termination" and

double amino termination by the presence of the signal at 2.96 ppm ($C\mathbf{H}_2NH_2$), at 3.71 and at 3.91 ppm ($OC\mathbf{H}_3$). The product is composed by an average of 6 repeating units (1 tartaric and 5 adipic units): consequently the average DP is equal to 3.

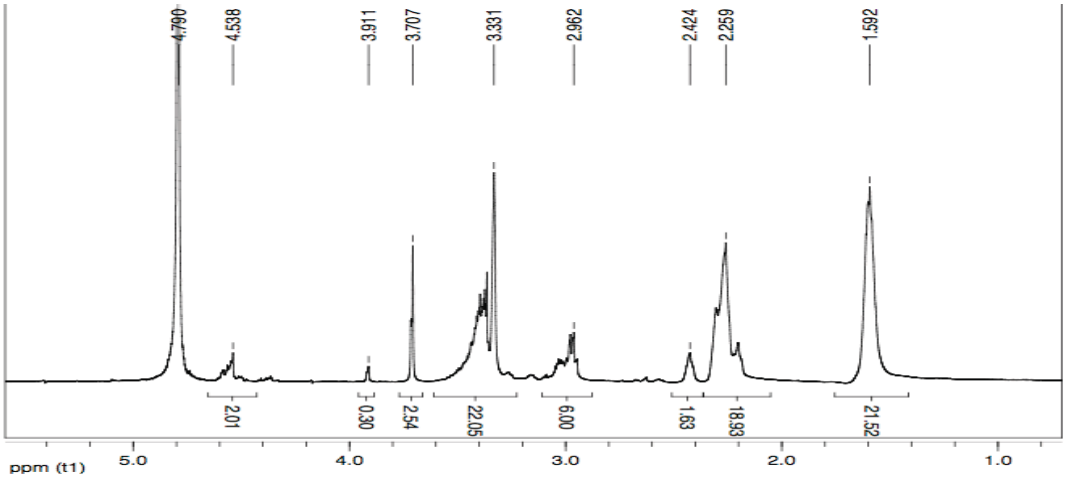

Figure 46: ^{1}H NMR spectrum in D_2O of the copolymer 3 (methanol soluble fraction)

In this case ^{13}C NMR spectrum (Figure 47), besides showing the same signals of the previous oligomers (see for example Figure 40), shows the presence of the ester termination at 52.1 ppm and the signals relating to $\mathbf{C}H_2CH_2COOCH_3$ and $CH_2\mathbf{C}H_2COOCH_3$ respectively at 23.6 and 33.2 ppm.

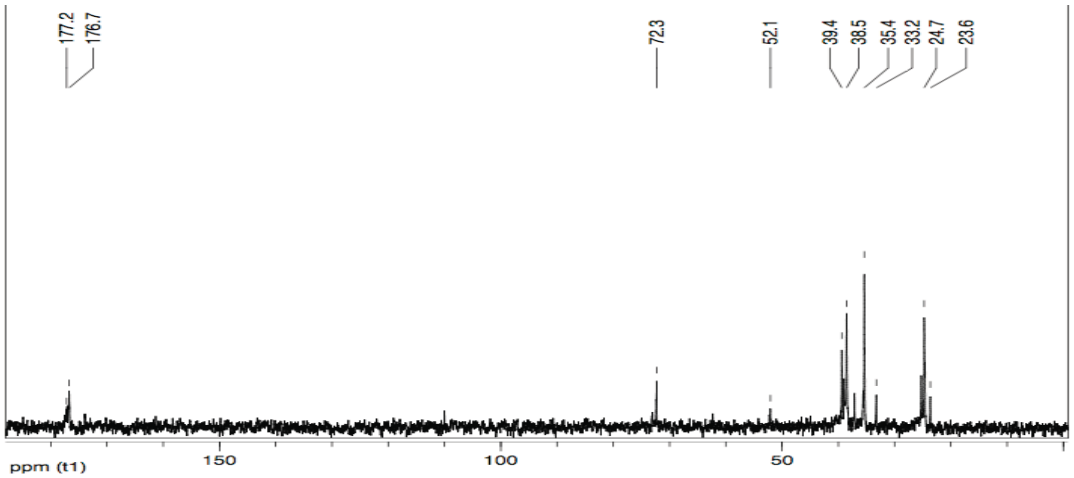

Figure 47: ^{13}C NMR spectrum in D_2O of the copolymer 3 (methanol soluble fraction)

Synthesis 4: the product was obtained using methanol as solvent, with reaction time equal to 5 days; however, the formation of a solid product in the Sovirel® tube was observed since the 3rd day: the mixture was left reacting in the same reaction conditions to promote a further growth of

the average molecular weight. The solid after the work up was dried under reduced pressure at room temperature and was isolated giving a 67% yield; this solid was extracted in methanol, obtaining two fractions, one insoluble and the other soluble.

In the **insoluble one** (68.6% yield), an oligomer with double amino termination (and only trace of ester termination) is present, with an average DP equal to 8 (6 tartaric and 2 adipic units).

In the **soluble fraction** (31.4% yield) a product with mixed termination in a ratio 1:1 (adipic ester and amino termination) is present, composed by 2.5 repeating units (2 adipic and 0.5 tartaric units).

Glass transition temperature (T_g) for products 3 and 4 (Figure 42) is visible at 108°C and 109°C respectively; melting, as the previous case, is affected by the degradation of the oligomer, that starts immediately after the beginning of melting (Figure 43).

3.3.2.5 Copolymer: syntheses with solvent and catalyst (Synthesis 5)

The reaction was carried out in a Sovirel® tube, with methanol as solvent, at 80°C for 3 days, in presence of a catalyst (NEt_3). After the same work up of the previous reactions, a yellow crystalline solid was obtained, water soluble, isolated giving a 70% yield (Table 2).

Through a methanol extraction, two fractions were obtained; the elaboration of the integrals present in ^1H NMR spectrum allows to understand that the **insoluble** fraction (67.2% yield) is composed by an average of 10 repeating units (7 tartaric and 3 adipic units) with double amino termination (average molecular weight : 1788 g/mol); however a small amount of ester termination is present, indicated in ^1H NMR spectrum (Table 4). In FT IR spectrum the peak attributable to ester groups present with low intensity is not visible, because it lies under the peak of amide; in ^{13}C NMR spectrum the signals related to the **C**OO**C**H_3 are non evaluable since ^{13}C NMR is less sensitive then ^1H NMR.

The **soluble fraction** (32.8% yield) is composed by an average of 3 repeating units (0.5 tartaric and 2.5 adipic units) with mixed termination in ratio 1:1 (average molecular weight: 544 g/mol).

In Table 3, Table 4 and Table 5 the signals related to this product are given.

Glass transition temperature (T_g) for product 5 (Figure 42) is visible at 120°C; melting, as the previous case, is affected by the degradation of the oligomer (Figure 43).

3.3.2.6 Copolymer: post-polymerization (Synthesis 6)

The post-polymerization reaction has been used to promote a further growth of the average molecular weight on the product with mixed termination. Based on of previous experience in the our research group, it was decided not to perform the post-polymerization in bulk, to avoid the formation of products with intense colors and low reproducibility.

Using small quantities of solvent it was possible to obtain products having mild coloration and a good reproducibility because solvent allows a better temperature control and because reaction temperatures are lower than the ones used for bulk synthesis.

Also in this case, the reaction was carried out in inert atmosphere to avoid possible oxidation and amine carbonation, that would make amine non reactive.

The post-polymerization reaction on the copolymer obtained in "synthesis 3" was carried out at 80°C for 24 hours with a small amount of methanol. The product, having intense yellow colour, was washed with ethyl ether, filtered on büchner funnel and dried under reduced pressure and room temperature, giving a 80% yield (Table 2).

The solid was extracted in methanol, obtaining two fraction, an insoluble (81.8% yield) and a soluble one (18.2% yield).

The insoluble fraction (81.8% yield) is composed by equimolecular amounts of mixed termination and double amino termination, with an average of 14 repeating units (10 tartaric and 4 adipic units): consequently the average DP is equal to 7 (average molecular weight: 1256 g/mol).

The soluble fraction (18.2% yield), with mixed termination, is composed by 3.5 repeating units (0.5 tartaric and 3 adipic units).

In Table 3, Table 4 and Table 5 the signals related to this product are present.

3.4 Conclusions

In this work new oligoamides with modified structure compared to oligotartaramides produced in the past in our laboratory have been synthesized, using two different diester, one aliphatic (dimethyladipate) and the other having hydroxyl groups in the chain (dimethyl L-tartrate), giving the presence in the final products of two different repeating units with characteristics of diacid.
This result is very important because new oligomers with a reduced density of hydroxyl groups along the chain have been obtained: this will allow to perform new tests for an industrial scale-up in collaboration with a leader company in the synthesis of polyamides,.
The presence of adipic units in the products synthesized should allow to solve the problems related to undesired cross-linking of the hydroxyl groups, previously observed under the reaction conditions of the scale-up synthesis. The preliminary study carried out in this research gives the possibility of an interesting development of the synthetic procedure, although to achieve the scale-up it will be necessary to conduct further tests using reaction conditions the most similar possible to the ones of the industrial process.

The laboratory syntheses have been carried out in different reaction conditions, in bulk and with small amounts of solvent, with and without catalyst, with times of up to 5 days and at 80°C.
The products obtained in the bulk polymerization have shown problems related to the low control on the molecular weight, with strong color variations, due to the difficulties of dissipation of heat the reaction. Furthermore, the chain growth was probably blocked due to the low rate of reaction within the solid mass that formed after a few hours of reaction.
Good results have been obtained when small amounts of solvent were used, thanks to a better temperature control.
This synthetic procedure allows to obtain products with milder colors, thanks to the improved control of temperature, with a good reproducibility.
Further increase of the molecular weight has been achieved with the addition of an activator (NEt_3).
Finally, post-polymerization reaction with small amounts of solvent (to promote uniform heating) was performed to increase the molecular weight of some products limiting colour changes. A slightly higher molecular weight was obtained, with no significant variations in color of the product.

All products were subjected to extraction in different solvents in order to obtain two product fractions. Methanol is the solvent that gave the best results, allowing to separate products according to their DP.

This step was very important for the characterization, because the determination of the average molecular weight of the product has been simplified and more accurate values were obtained.

In these syntheses, up to three different terminal moieties can be present (adipic ester, tartartic ester and two kind ester amino group): this feature makes the calculation of the average MW more complicated than in homopolymer syntheses (where only two terminal groups were present), because of the high number of possible combinations of these three terminal groups.

Through methanol extraction, two fractions for each product were obtained, one insoluble (higher average molecular weight) and one soluble (lower average molecular weight).

Moreover, in methanol insoluble fractions there is the presence of higher quantities of the tartaric repeating units compared to the adipic; in methanol soluble fraction there are low molecular weight products, with a higher amount of adipic acid. Modulating the molar ratio of the two diesters (in this study equimolar amounts of the two diesters have been used), it will be possible to tailor the properties of the final product.

It can be concluded that the reactions with the solvent allow to obtain products, with good yields and higher molecular weight; this is possible thanks to the chains mobility and reactivity in the presence of solvent compared to the reactions in bulk polymerization. The addition of the catalyst allows a further increase in the yield and in DP.

Post-polymerization reaction with small amount of solvent was carried out at 100°C, obtaining a moderate DP increase.

The properties of the oligomers synthesized have been evaluated via DSC, measuring T_g and melting points, to compare the differences with the oligethylene-L-tartaramide studied in the past. T_g becomes visible when higher MW are obtained (products 3, 4, 5), since when the oligomer chain is very short no glass transition is possible: the higher the MW, the higher T_g. Melting was observed starting over 200°C but the transitions are affected by the degradation of the oligomers, that starts immediately after the beginning of melting.

Table 3: FT-IR signals

Product	N-H stretching	O-H stretching	C-H stretching	C=O stretching (ester group)	C=O stretching (Amide I)	N-H bending (Amide II)	C-O stretching
Oligoethylenadipamide	3298 (s)	---	3084 (m) 2941 (m) 2860 (m)	1720 (m)	1640 (vs)	1556 (vs)	---
Oligoethylene-L-tartaramiwe	3358 (s) 3298 (s)	3358 (s) 3298 (s)	2941 (w)	---	1659 (vs)	1539 (vs)	1120 (s) 1068 (s)
1 e 2 **insoluble fraction in MeOH**	3356 (s) 3298 (s)	3356 (s) 3298 (s)	2941 (w) 2874 (w)	---	1651 (vs)	1549 (vs)	1121 (s) 1069 (s)
1 e 2 **soluble fraction in MeOH**	3300 (s)	3300 (s)	2941 (w) 2873 (w)	1731 (w)	1641 (vs)	1555 (vs)	1130 (w) 1070 (w)
3 e 4 **insoluble fraction in MeOH**	3354 (vs) 3300 (vs)	3354 (vs) 3300 (vs)	3085 (w) 2945 (w) 2870 (w)	---	1645 (vs)	1553 (s)	1121 (s) 1069 (s)
3 e 4 **soluble fraction in MeOH**	3299 (vs)	3299 (vs)	3086 (w) 2945 (w) 2870 (w)	1732 (vw)	1643 (vs)	1556 (vs)	1130 (w) 1070 (w)
5 **insoluble fraction in MeOH**	3358 (vs) 3302 (vs)	3358 (vs) 3302 (vs)	3086 (w) 2943 (w) 2870 (w)	---	1651 (vs)	1553 (vs)	1121 (s) 1069 (s)
5 **soluble fraction in MeOH**	3298 (vs)	3298 (vs)	3086 (w) 2945 (w) 2870 (w)	1731 (w)	1641 (vs)	1556 (vs)	1130 (w) 1070 (w)
6 **insoluble fraction in MeOH**	3298 (vs)	3298 (vs)	3086 (w) 2945 (w) 2870 (w)	1731 (w)	1641 (vs)	1556 (vs)	1121 (s) 1069 (s)
6 **soluble fraction in MeOH**	3297 (vs)	3297 (vs)	3086 (w) 2945 (w) 2870 (w)	1733 (w)	1646 (vs)	1556 (vs)	1130 (w) 1070 (w)

Table 4: ^{1}H NMR peaks attribution (400 MHz, δ, ppm, D_2O)

Product	CH_2CH_2CONH	CH_2CH_2CONH	CH_2COOCH_3	CH_2NH_2	CH_2NHCO	$-OCH_3$	CH-OH
Oligoethyleneadipamide	1.60	2.25	2.42	2.94	3.20- 3.45	3.70	---
Oligoethylene-L-tartaramide	---	---	---	3.09	3.48	---	4.58
1 e 2 insoluble fraction in MeOH	1.62	2.30	---	3.03	3.30- 3.55	---	4.61
1 e 2 soluble fraction in MeOH	1.61	2.28	2.44	2.84	3.20- 3.50	3.72	4.59
3 e 4 insoluble fraction in MeOH	1.59	2.26	2.43	3.05	3.30- 3.55	3.71	4.57
3 e 4 soluble fraction in MeOH	1.59	2.26	2.42	2.96	3.20- 3.50	3.71 3.91	4.54
5 insoluble fraction in MeOH	1.60	2.28	2.43	2.97	3.30- 3.50	3.72	4.59
5 soluble fraction in MeOH	1.62	2.28	2.44	2.95	3.25- 3.50	3.72	4.56
6 insoluble fraction in MeOH	1.60	2.28	2.43	2.97	3.20- 3.55	3.72 3.92	4.59
6 soluble fraction in MeOH	1.62	2.28	2.44	2.95	3.20- 3.45	3.72 3.92	4.56

Table 5: ^{13}C NMR peaks attribution (100 MHz, δ, ppm, D_2O)

Product	$CH_2CH_2COOCH_3$	CH_2CH_2CONH	CH_2COOCH_3	CH_2CONH	CH_2NHCO	CH_2NH_2	$-OCH_3$	CH-OH	C=O
Oligoethyleneadipamide	23.6	24.7	33.2	35.4	38.5	39.4	52.1	---	176.7 177.1
Oligoethylene-L-tartaramide					38.5	39.4		72.3	174.0
1 e 2 **insoluble fraction in MeOH**	---	24.7	---	35.4	38.5	39.4	---	72.3	174.0
1 e 2 **soluble fraction in MeOH**	---	24.7	---	35.4	38.5	39.7	---	72.4 73.1	174.1 176.9
3 e 4 **insoluble fraction in MeOH**	---	24.7	---	35.4	38.5	39.3	---	72.3	174.0
3 e 4 **soluble fraction in MeOH**	23.6	24.7	33.2	35.4	38.5	39.4	52.1	72.3	176.7 177.2
5 **insoluble fraction in MeOH**	---	24.7	---	35.3	38.4	39.4	---	72.2	174.2 176.7
5 **soluble fraction in MeOH**	23.6	24.6	33.2	35.3	38.4	39.4	52.1	72.3	174.2 176.7 177.0
6 **insoluble fraction in MeOH**	23.6	24.7	33.2	35.4	38.5	39.7	52.0	72.3 73.1	174.1 177.0
6 **soluble fraction in MeOH**	23.6	24.6	33.2	35.3	38.4	39.4	52.1	72.3	174.0 176.7 177.1

3.5 Experimental

3.5.1 Materials

3.5.1.1 Solvents

- Methanol, product Normapur, 99.9% pure
- Ethyl ether

3.5.1.2 Reagents and products

- Boric acid, product Aldrich, 99,5% pure
- Dimethyl adipate, by Radici Chimica S.p.A.
- 1,2- ethylenediamine, product Aldrich, 99% pure
- L-tartaric acid, product Aldrich, 99% pure
- Triethylamine, product Carlo Erba, 97% pure

3.5.2 Instruments

3.5.2.1 NMR spectroscopy

^{1}H NMR, ^{13}C NMR, gCOSY and gHSQC spectra were recorded with a Varian Mercury Plus 400 spectrometer and a Varian VXR 200 spectrometer, working at 399.921 MHz and 199.985 MHz, respectively. All spectra are reported in ppm and referred to TMS as internal standard. Spectra elaboration was performed with the software Mestre-C 4.3.2.0. Solvents used (D_2O, $CDCl_3$) are produced by Aldrich Co.

3.5.2.2 FT IR spectroscopy

FT IR spectra were recorded with a Shimadzu FT-IR-8400S model, and elaborated with the Spectrum v.3.0202. Solutions were analyzed using KBr or CaF_2 round cell windows, after deposition and evaporation of solvent. Spectra of solid samples were recorded as KBr pellets.

3.5.2.3 Differenzial scanning calorimetry (DSC)

DSC analyses were conducted using a Mettler Toledo DSC 820, on samples weighting from 7 to 10 mg each.

Dynamic DSC analyses samples were first heated from 25°C to 100°C at 10°C/min and maintained at 100°C for 2 min to eliminate residue water, then cooled down to 25°C at 20°C/min, maintained at 25°C for 2 min; for T_m and T_g determination a second thermal cycle from 25°C to 250°C was then used to evaluate the behavior of the material.

3.5.3 Syntheses of the homopolimers

3.5.3.1 Synthesis of oligoethyleneadipamide

In a Sovirel® tube, dimethyl adipate (1.742 g, 10 mmol) is added, under nitrogen atmosphere and under continuous stirring, to a ethylenediamine (601 mg, 10 mmol). The reaction mixture is allowed to react at 80°C for 8 hours. After cooling to room temperature, a white solid is recovered by filtration, washed with ethyl ether, and dried at room temperature (1. 044 g, 44.6% yield). 50 mg of the solid are extracted in water, obtaining a soluble fraction (33 mg, 66% yield) and an insoluble one (17 mg, 34% yield).

Soluble fraction:

^{1}H-NMR (D_2O, 400 MHz, Table 4): signals at δ 1.60 (m, 4H, C**H**$_2$CH$_2$CONH), 2.25 (m, 4H, CH$_2$C**H**$_2$CONH), 2.42 (m, 2H, C**H**$_2$COOCH$_3$), 2. 94 (m, 2H, C**H**$_2$NH$_2$), 3.20- 3.45 (m, 4H, C**H**$_2$NHCO), 3.70 ppm (s, 3H, OC**H**$_3$).

^{13}C-NMR (D_2O, 100 MHz, Table 5): signals at δ 23.6 (CH$_2$CH$_2$COOCH$_3$), 24.7 (CH$_2$CH$_2$CONH), 33.2 (CH$_2$COOCH$_3$), 35.4 (CH$_2$CONH), 38.5 (CH$_2$NHCO), 39.4 (CH$_2$NH$_2$), 52.1 (OCH$_3$), 176.7 (CONH), 177.1 ppm (COOCH$_3$).

Soluble and insoluble fractions:

FT-IR (KBr pellet, Table 3): peaks at 3298 cm^{-1} (s, stretching N-H), 3084, 2941, 2860 (m, C-H stretching), 1720 (m, C=O ester stretching), 1640 (vs, C=O amide stretching), 1556 (vs, N-H amide bending).

T_g: 61.4°C

3.5.3.2 Synthesis of oligoethylene-L-tartaramide

Into a Sovirel® tube, triethylamine (54.6 mg, 0.54 mmol) is added under continuous stirring to 9 mL of a methanol solution of dimethyl L-tartrate (360 mg, 2.02 mmol). Ethylenediamine (121.4 mg, 2.02 mmol) is added and the mixture is heated at 80°C for 2.5 days. After cooling to room temperature, the mixture is filtered on a Büchner funnel and washed with methanol; then the solid obtained is dried under vacuum at room temperature (305.4 mg, 63.6% yield).

^{1}H-NMR (D_2O, 400 MHz, Table 4): signals at δ 3.09 (m, 4H, C**H**$_2$NH$_2$), 3.48 ppm (m, 4H, C**H**$_2$NHCO), 4.58 ppm (m, 2H, CHOH).

^{13}C-NMR (D_2O, 100 MHz, Table 5): signals at δ 38.5 ppm (CH$_2$NHCO), 39.4 (CH$_2$NH$_2$), 72.3 ppm (CHOH), 174.0 ppm (CONH).

FTIR (KBr pellet, Table 3): peaks at 3358, 3298 (s, broad, N-H and O-H stretching), 2941 (w, C-H stretching), 1659 (s, C-O amide stretching), 1539 (s, N-H amide bending), 1120, 1068 (w, C-O stretching) cm^{-1}.

T_g: 104°C.

3.5.4 Syntheses of the copolymers

3.5.4.1 Synthesis 1 and Synthesis 2

In a Sovirel® tube, dimethyl adipate (522.6 mg, 3 mmol) and dimethil L-tartrate (534.42 mg, 3 mmol) are added, under nitrogen atmosphere and under continuous stirring, to ethylenediamine (360.6 mg, 6 mmol). The reaction mixture is allowed to react at 80°C for 24 hours (**synthesis 1**). After cooling to room temperature, a yellow solid is recovered by filtration, washed with ethyl ether, and dried at room temperature (873.7 mg, 61.6% yield). 50 mg of the solid are extracted in methanol, obtaining an insoluble fraction (32 mg, 64% yield) and an soluble one (18 mg, 36% yield).

The reaction was repeated increasing the reaction time to 2 days (synthesis 2), at 80°C.

A yellow solid obtained was recovered by filtration, washed with ethyl ether, and dried at room temperature (902 mg, yield 63.6%).

50 mg of solid were extracted in methanol, obtaining an insoluble fraction (38.1 mg, 76.2% yield) and a soluble one (11.9 mg, 23.8% yield).

Insoluble fraction:

^{1}H-NMR (D_2O, 400 MHz, Table 4): signals at δ 1.62 (m, 4H, C**H**$_2$CH$_2$CONH), 2.30 (m, 4H, CH$_2$C**H**$_2$CONH), 3.03 (m, 4H, C**H**$_2$NH$_2$), 3.30- 3.55 (m, 4H, C**H**$_2$NHCO), 4.61 ppm (m, 2H, C**H**OH).

^{13}C-NMR (D_2O, 100 MHz, Table 5): signals at δ 24.7 (CH$_2$CH$_2$CONH), 35.4 (CH$_2$CH$_2$CONH), 38.5 (CH$_2$NHCO), 39.4 (CH$_2$NH$_2$), 72.3 (CHOH), 174.0 (CONH).

FT-IR (KBr pellet, Table 3): peaks at 3356, 3298 (s, N-H and O-H stretching), 2941, 2874 (w, C-H stretching), 1651 (vs, C=O amide stretching), 1549 (vs, N-H amide bending), 1121, 1069 (s, C-O stretching) cm^{-1}.

Soluble fraction:

^{1}H-NMR (D_2O, 400 MHz, Table 4): signals at δ 1.61 (m, 4H, -C**H**$_2$CH$_2$CONH-), 2.28 (m, 4H, CH$_2$C**H**$_2$CONH), 2.44 (m, 0.17, C**H**$_2$COOCH$_3$), 2.84 (m, 4H, C**H**$_2$NH$_2$), 3.20- 3.50 (m, 4H, C**H**$_2$NHCO), 3.72 (s, 0.2H, OCH$_3$), 4.59 ppm (m, 2H, C**H**OH).

^{13}C-NMR (D_2O, 100 MHz, Table 5): signals at δ 24.7 (CH$_2$CH$_2$CONH), 35.4 (CH$_2$CH$_2$CONH), 38.5 (CH$_2$NHCO), 39.7 (CH$_2$NH$_2$), 72.4, 73.1 (CHOH), 174.1, 176.9 (CONH).

FT-IR (KBr pellet, Table 3): peaks at 3300 (s, N-H and O-H stretching), 2941, 2873 (w, C-H stretching), 1731 (s, C=O ester stretching), 1641 (vs, C=O amide stretching), 1555 (vs, N-H amide bending), 1130, 1070 (w, C-O stretching) cm^{-1}.

3.5.4.2 Synthesis 3 and Synthesis 4

In a Sovirel® tube, dimethyl adipate (522.6 mg, 3 mmol) and dimethil L-tartrate (534.42 mg, 3 mmol) are added, under nitrogen atmosphere and under continuous stirring, to a methanol solution (1 mL) of ethylenediamine (360.6 mg, 6 mmol). The reaction mixture is allowed to react at 80°C for 3 days (**synthesis 3**). After cooling to room temperature, a yellow solid is recovered by filtration, washed with ethyl ether, and dried at room temperature (928 mg, 65.5% yield). 50 mg of the solid are extracted in methanol, obtaining an insoluble fraction (37.5 mg, 75% yield) and an soluble one (12.5 mg, 25% yield). T_g: 108°C

The reaction was repeated increasing the reaction time to 5 days (**synthesis 4**) at 80°C.

A yellow solid obtained was recovered by filtration, washed with ethyl ether, and dried at room temperature (949 mg, 67% yield). T_g: 109°C

50 mg of solid were extracted in methanol, obtaining an insoluble fraction (34.4 mg, 68.6% yield) and a soluble one (15.7 mg, 31.4% yield).

Insoluble fraction:

^{1}H-NMR (D_2O, 400 MHz, Table 4): signals at δ 1.59 (m, 4H, C**H**$_2$CH$_2$CONH), 2.26 (m, 4H, CH$_2$C**H**$_2$CONH), 2.43 (m, 0.16H, C**H**$_2$COOCH$_3$), 3.05 (m, 4H, C**H**$_2$NH$_2$), 3.30-3.55 (m, 4H, C**H**$_2$NHCO), 3.71 (m, 0.24H, OC**H**$_3$), 4.57 ppm (m, 2H, C**H**OH).

^{13}C-NMR (D_2O, 100 MHz, Table 5): signals at δ 24.7 (CH$_2$CH$_2$CONH), 35.4 (CH$_2$CH$_2$CONH), 38.4 (CH$_2$NHCO), 39.4 (CH$_2$NH$_2$), 72.2 (CHOH), 174.2, 176.7 (CONH) ppm.

FT-IR (KBr pellet, Table 3): peaks at 3354, 3300 (ff, N-H and O-H stretching), 3085, 2945, 2870 (d, C-H stretching), 1645 (ff, C=O amide stretching), 1553 (ff, N-H amide bending), 1121, 1069 (m, C-O stretching) cm^{-1}.

Soluble fraction:

^{1}H-NMR (D_2O, 400 MHz, Table 4): signals at δ 1.59 (m, 4H, C**H**$_2$CH$_2$CONH), 2.26 (m, 4H, CH$_2$C**H**$_2$CONH), 2.42 (m, 1.70H, C**H**$_2$COOCH$_3$), 2.96 (m, 2H, C**H**$_2$NH$_2$), 3.20-3.50 (m, 4H, C**H**$_2$NHCO), 3.71, (s, 2H, OC**H**$_3$), 3.91 (s, 1H, OC**H**$_3$), 4.54 ppm (m, 2H, C**H**OH).

^{13}C-NMR (D_2O, 100 MHz, Table 5): signals at δ 23.6 (CH$_2$CH$_2$COOCH$_3$), 24.7 (CH$_2$CH$_2$CONH), 33.2 (CH$_2$CH$_2$COOCH$_3$), 35.4 (CH$_2$CH$_2$CONH), 38.5 (CH$_2$NHCO), 39.4 (CH$_2$NH$_2$), 52.1 (OCH$_3$), 72.3 (CHOH), 176.7 (CONH), 177.2 (COOCH$_3$).

FT-IR (KBr pellet, Table 3): peaks at 3299 (vs, N-H and O-H stretching), 3086, 2945, 2870 (w, C-H stretching), 1732 (vw, C=O ester stretching), 1643 (vs, C=O amide stretching), 1556 (vs, N-H amide bending), 1130 (w, C-O stretching), 1070 (w, C-O stretching) cm^{-1}.

3.5.4.3 Synthesis 5

In a Sovirel® tube, dimethyl adipate (348.4 mg, 2 mmol) and dimethyl L-tartrate (356.3 mg, 2 mmol) are added, under nitrogen atmosphere and under continuous stirring, to a methanol solution (1 mL) of ethylenediamine (240.4 mg, 4 mmol). Finally triethylamine (109.3 mg, 1.08 mmol) is added and the reaction mixture is allowed to react at 80°C for 3 days. After cooling to room temperature, a yellow solid is recovered by filtration, washed with ethyl ether, and dried at room temperature (660.8 mg, 70% yield). 50 mg of solid were extracted in methanol, obtaining an insoluble fraction insoluble (33.6 mg, 67.2% yield) and a soluble one (32.8 mg, 32.8% yield). T_g: 120°C

Insoluble fraction:

^{1}H-NMR (D_2O, 400 MHz, Table 4): signals at δ 1.60 (m, 4H, C**H**$_2$CH$_2$CONH), 2.28 (m, 4H, CH$_2$C**H**$_2$CONH), 2.43 (m, 0.05H, C**H**$_2$CH$_2$COOCH$_3$), 2.97 (m, 4H, C**H**$_2$NH$_2$), 3.30-3.50 (m, 4H, C**H**$_2$NHCO), 3.72 (s, 0. 2H, OC**H**$_3$), 4.59 ppm (m, 2H, C**H**OH).

^{13}C-NMR (D_2O, 100 MHz, Table 5): signals at δ 24.7 (CH$_2$CH$_2$CONH), 35.3 (CH$_2$CH$_2$CONH), 38.4 (CH$_2$NHCO), 39.4 (CH$_2$NH$_2$), 72.2 (CHOH), 174.2, 176.7 (CONH).

FT-IR (KBr pellet, Table 3): peaks at 3358, 3302 (vs, N-H e O-H stretching), 3086, 2943, 2870 (w, C-H stretching), 1651 (vs, C=O amide stretching), 1553 (vs, N-H amide bending), 1121, 1069 (s, C-O stretching) cm^{-1}.

Soluble fraction:

^{1}H-NMR (D_2O, 400 MHz, Table 4): signals at δ 1.62 (m, 4H, C**H**$_2$CH$_2$CONH), 2.28 (m, 4H, CH$_2$C**H**$_2$CONH), 2.44 (m, 0.17H, C**H**$_2$CH$_2$COOCH$_3$), 2.95 (m, 4H, C**H**$_2$NH$_2$), 3.25-3.50 (m, 4H, C**H**$_2$NHCO), 3.72 (s, 0. 2H, OC**H**$_3$), 4.56 ppm (m, 2H, C**H**OH).

^{13}C-NMR (D_2O, 100 MHz, Table 5): signals at δ 23.6 (CH$_2$CH$_2$COOCH$_3$), 24.6 (CH$_2$CH$_2$CONH), 33.2 (CH$_2$CH$_2$COOCH$_3$), 35.3 (CH$_2$CH$_2$CONH), 38.4 (CH$_2$NHCO), 39.4 (CH$_2$NH$_2$), 52.1 (COOCH$_3$) 72.3 (CHOH), 174.2, 176.7 (CONH), 177.1 (COOCH$_3$) ppm.

FT-IR (KBr pellet, Table 3): peaks at 3298 (vs, N-H and O-H stretching), 3086, 2945, 2870 (w, C-H stretching), 1731 (w, C=O ester stretching), 1641 (vs, C=O amide stretching), 1556 (vs, N-H amide bending), 1130, 1072 (m, C-O stretching) cm^{-1}.

3.5.4.4 Synthesis 6: post-polymerization reaction

In a Sovirel® tube, copolymer 3 (150 mg) is added, under nitrogen atmosphere and under continuous stirring, to a 1mL of methanol. The reaction mixture is allowed to react at 100°C for 1 day. After cooling to room temperature, a yellow solid is recovered by filtration, washed with ethyl ether, and dried at room temperature (120 mg, 80% yield).

50 mg of the solid was extracted in methanol, obtaining an insoluble fraction (40.9 mg, 81.8% yield) and an soluble one (9.1 mg, 18.2% yield).

Insoluble fraction:

^{1}H-NMR (D_2O, 400 MHz, Table 4): signals at δ 1.60 (m, 4H, C**H**$_2$CH$_2$CONH), 2.28 (m, 4H, CH$_2$C**H**$_2$CONH), 2.43 (m, 0.5H, C**H**$_2$COOCH$_3$), 2.97 (m, 2H, C**H**$_2$NH$_2$), 3.20-3.55 (m, 4H, C**H**$_2$NHCO), 3.72 (s, 2H, OC**H**$_3$), 3.92 (s, 1H, OC**H**$_3$), 4.59 ppm (m, 2H, C**H**OH).

^{13}C-NMR (D_2O, 100 MHz, Table 5): signals at δ 23.6 (CH$_2$CH$_2$COOCH$_3$), 24.7 (CH$_2$CH$_2$CONH), 33.2 (CH$_2$CH$_2$COOCH$_3$), 35.4 (CH$_2$CH$_2$CONH), 38.5 (CH$_2$NHCO), 39.7 (CH$_2$NH$_2$), 52.0 (OCH$_3$), 72.3, 73.1 (CHOH), 174.1 (CONH), 177.0 (COOCH$_3$).

FT-IR (KBr pellet, Table 3): peaks at 3298 (vs, N-H and O-H stretching), 3086, 2945, 2870 (w, C-H stretching), 1731 (w, C=O ester stretching) 1641 (vs, C=O amide stretching), 1556 (vs, N-H amide bending), 1121, 1069 (m, C-O stretching) cm^{-1}.

Soluble fraction:

^{1}H-NMR (D_2O, 400 MHz, Table 4): signals at δ 1.62 (m, 4H, C**H**$_2$CH$_2$CONH), 2.28 (m, 4H, CH$_2$C**H**$_2$CONH), 2.44 (m, 1.2H, C**H**$_2$COOCH$_3$), 2.95 (m, 2H, C**H**$_2$NH$_2$), 3.20-3.45 (m, 4H, C**H**$_2$NHCO), 3.72 (s, 2H, OCH$_3$), 3.92 (s, 1H, OCH$_3$), 4.56 ppm (m, 2H, C**H**OH).

^{13}C-NMR (D_2O, 100 MHz, **Table 5**): signals at δ 23.6 (**C**H$_2$CH$_2$COOCH$_3$), 24.6 (**C**H$_2$CH$_2$CONH), 33.2 (CH$_2$**C**H$_2$COOCH$_3$), 35.3 (CH$_2$**C**H$_2$CONH), 38.4 (**C**H$_2$NHCO), 39.4 (**C**H$_2$NH$_2$), 52.1 (O**C**H$_3$), 72.3 (**C**HOH), 174.0, 176.7 (**C**ONH), 177.1 (**C**OOCH$_3$).

FT-IR (KBr pellet, Table 3): peaks at 3297 (vs, N-H e O-H stretching), 3086, 2945, 2870 (w, C-H stretching), 1733 (w, C=O ester stretching), 1646 (vs, C=O amide stretching), 1556 (vs, N-H amide bending), 1130, 1070 (vw, C-O stretching) cm^{-1}.

4 Polyamides based on polyamines

4.1 Kinetic hydrate inhibitors (KHIs)

Gas hydrates (clathrate) are very complex structures where a molecule (host) contains another type of molecule (guest). In natural gas hydrates, gases (host) occupy cages within a lattice of water molecules (host). They are white ice-like solids formed from water and small hydrocarbons under pressure, usually at temperatures below about 25°C.

Hydrogen bonds and Van der Waals interactions are the chemical bonds that allow the formation of these structures; the first type of bond is involved in the reticular structure formed by water molecules, while Van der Waals interactions arise between host and guest molecules; this type of bond stabilizes water crystalline phase through an increase of melting temperature[45].

In the petroleum industry, natural gas and petroleum fluids contain a variety of small molecules which can form gas hydrates. They include hydrocarbons such as methane, ethane, propane, isobutane as well as nitrogen, carbon dioxide and hydrogen sulphide. Also larger hydrocarbons such as cyclopentane, cyclohexane and benzene can be present. When these hydrate-forming components are present with water at elevated pressures and reduced temperatures, the mixture tends to form gas hydrate crystals. For example, in patent WO2013/053770 it is reported that ethane at a pressure of 1 MPa forms hydrates only below 4 °C, whereas at 3 MPa gas hydrates can be formed below 14 °C[46]. These temperatures and pressures, suited to hydrate formation, are typical operating environments where petroleum fluids are produced and transported.

The formation of hydrates should be avoided, since they could cause problems for the regular functioning of the system, with the possibility to clog of the pipes, resulting in blocking of the production line.

Hydrocarbons can form three types of gas hydrates, named “structure I”, “structure II” and “structure H”. The molecules that typically form hydrates of type I are carbon dioxide and methane. Hydrates of type II are the most common type of structure since they are thermodynamically stable when formed from a mixture of gases such as methane, ethane, propane and butane but can also be formed by gases such as oxygen and nitrogen. It is possible to have coexistence cases of hydrates of type I and II[47].

The formation of H-type structure requires the cooperation of two gases guests (large and small) to be stable. In fact, the characteristic that distinguishes hydrates H from those of type I and II is that hydrates H always exist as mixed hydrates, and therefore require the presence of at least two

different types of guest molecules, as molecules able to stabilize larger cavities cannot enter into smaller cavities.

In a production line, to reduce the possibility of hydrate formation, it is necessary to eliminate water from gas to liquid state and that the gas is at higher temperature than the one of hydrate formation. If at least one of these conditions cannot be satisfied, it is necessary to use other means to prevent the formation of hydrates, such as the use of inhibitors, or substances able to lower the temperature of hydrate formation.

There are a variety of ways to prevent gas hydrate from forming including the use of chemicals acting as thermodynamic hydrate inhibitors (THIs), Anti-Agglomerants (AAs) and Kinetic Hydrate Inhibitors (KHIs). These last two are low dosage hydrate inhibitors (LDHIs) because they require lower concentrations in comparison to conventional thermodynamic inhibitors. Generally AAs and KHIs are used in concentrations from 0.01 to 3%, unlike THIs that reach high concentrations, typically 10-60% w/w of the water present. THIs work shifting the equilibrium conditions for hydrate formation to lower temperatures or high pressures; methanol, ethanol and ethylene glycol are the most used THIs. They generally are anti-freezing, acting on lowering the melting point; the problem of these products is that they must be added in large quantities and often require their recovery from the pipes; for these reasons their use is a very long and expensive procedure.

AAs are classes of surfactants, as quaternary ammonium salts or phosphonium salts, that work on the surface of hydrate crystals to keep them from agglomerating and to transform them into a transportable slurry in a liquid hydrocarbon phase. They do not interrupt the crystals nucleation, but the agglomeration of gas hydrates. These systems allow to maintain a low viscosity of the system, to permit transport along the pipeline. Unfortunately, these salts have often high toxicity and low biodegradability, factors that limit their use[46,48].

KHIs are composed by water-soluble polymers which slow the kinetics of nucleation.

Many types of polymers can be used as KHIs[47], but those giving better results contain polar groups near to hydrophobic groups. In the past, poly-N-vinyllactam (poly-N-vinylpyrrolidone (PVP), poly-N-vinyl-N-caprolactam (PVCap) and N-vinylpyrrolidone:N-vinylcaprolactam copolymer (VP:VCap)) have been used; also chitosan partially or completely acetylated, modified polyacrylamide, polyvinilamides, polyallylamides and hyper-branched polyesteramides were investigated[47,49,50].

In general, products with amide groups close to hydrophobic groups have the ability to act as KHIs according to the hydrophobic group present[47].

In recent years, in the Department of Chemistry "Ugo Schiff" of Università degli Studi di Firenze many types of functionalized oligoamides were synthesized, based on L-tartaric acid, D-glucaric acid and α,α'-trehaluronic acid with different diamines (ethylenediamine and hexamethylenediamine), to be used as consolidant for archaeological wood[33].

During the preliminary study of these polyamides for their use as consolidant, the attention towards other possible application fields has raised, because they are similar to other polar matrices besides being often water-soluble.

To expand the field of interest of these materials, synthesis of new oligoamides were carried out increasing the diamines choice, in order to obtain final products with characteristics very different from one another. In particular, diamines with higher number of carbon atoms (1,12-dodecamethylenediamine), having higher polarity (2,2 '(ethylenedioxy) bis-ethylenediamine), or being aromatic (p-xylylenediamine) or polyamines were used.

Thanks to the different characteristics of the products synthesized, their different molecular weights and solubility, it was possible to find different applications for this class of polymeric compounds, as for example the use as additives in polymeric formulations, in the treatment of cotton fabrics or polyamide fibers. Polyamides deriving from polyamines, could be used as catchers of formaldehyde; this application was subject of a preliminary study, showing good results in laboratory.

Polyamides based on polyamines are water-soluble, and present characteristics similar to those of the KHIs products: the introduction of appropriate structural modifications should improve performances for this type of application.

4.2 Research methodology

The polyamides based on polyamines (Figure 48), recently synthesized in our laboratory, can be studied as KHIs modifying their structure, adding hydrophobic pendants bonded to nitrogen secondary atoms of the oligoamide or through oxidation of amino groups to obtain the corresponding N-oxides.

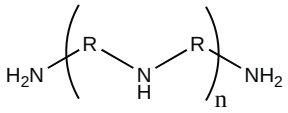

Figure 48: polyamines structure

In order to synthesise oligoamides that could be used as KHIs, the synthesis and characterization of oligomers based on polyamines and α,α'-trehaluronic acid was deepened: the preliminary synthesis of these products had already been studied but it had not been optimized. Besides, in this work the synthesis of a new product based on polyamine and L- tartaric acid was performed.
To obtain a progressive and regular chain growth, it is necessary to use stoichiometric amounts of the two monomers: generally in industrial processes this is accomplished working in bulk starting from the salt between the diamine and diacid. However, the sensitivity of the monomers towards high temperatures makes difficult to use this method of activation of the diacid. Therefore in our syntheses the dimethyl esters of trehaluronic and tartaric acids were used, in order to work with low temperature (80°C) to avoid alteration of the carbohydrate units.

The product based on polyamines and L-tartaric acid was subjected to further alkylation and oxidation reactions. In particular, the alkylation on the secondary amino groups was carried out on oligodiethyleneamino-L-tartaramide (Figure 49) through substitution reaction using two different procedures, with acyl chloride (valeroyl chloride) and alkyl bromide (bromobutane) respectively. The reaction with acyl chloride did not give good results and therefore only the second methodology will be described.

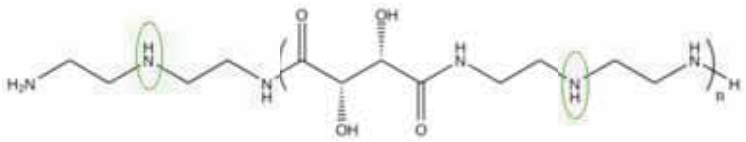

Figure 49: Oligodiethylenamino -L-tartaramide

Bromobutane was chosen for the alkylation reaction because it is less toxic than the lower homologue, bromopropane, but can anyway maintain good water solubility of the final product, which would decrease in presence of substitution with its higher homologues.

The reaction scheme is here presented, showing that the reaction is not selective between primary and secondary amino groups (Figure 50).

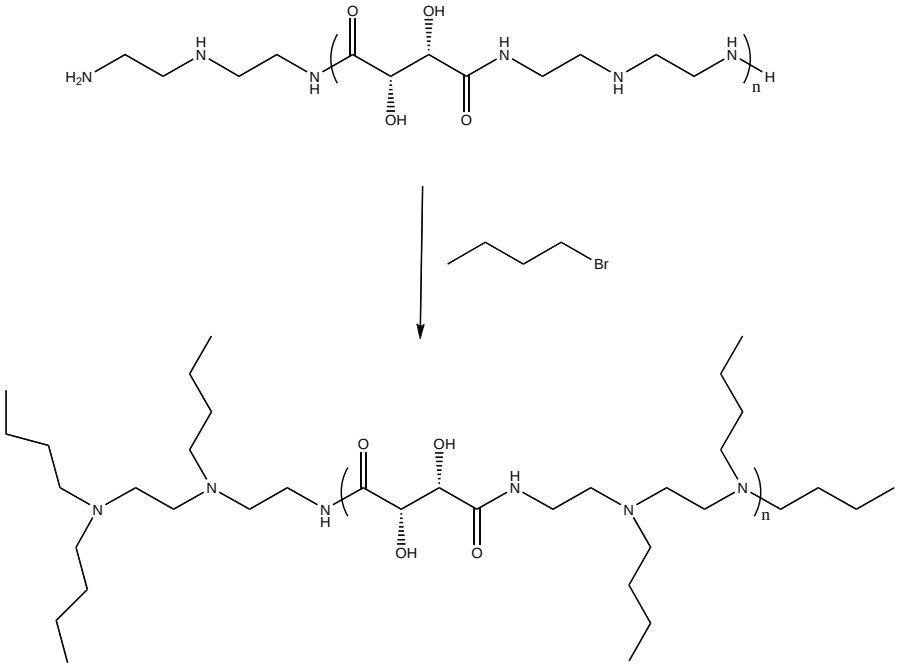

Figure 50: scheme of alkylation reaction with bromobutane

Using a modified version of the synthetic procedure reported by Blicke et al.[51] various syntheses were performed by changing reaction conditions to try to obtain a product with the highest degree of alkylation possible:

- Molar ratio oligoamide: bromobutane equal to 1:2 or 1:3;
- Reaction time between 8 and 48 hours;
- With and without addition of $CaCO_3$
- In presence of methanol or ethanol as solvent
- The reaction was performed in a flask with condenser or in a Sovirel tube, to reach temperature higher than the ones used with reflux solvent (80°C using Sovirel® tube).

After the substitution reaction, the product of N-alkylation was subjected to an oxidation reaction with H_2O_2 (Figure 51). The purpose of this reaction was to oxidize the tertiary amino groups of the

oligomer to make the product more suitable as KHIs. In this study, two methods of oxidation were studied, one with H_2O_2 aqueous solution (Method 1)[52]and the other with H_2O_2 aqueous solution and NH_4HCO_3 (Method 2)[53].

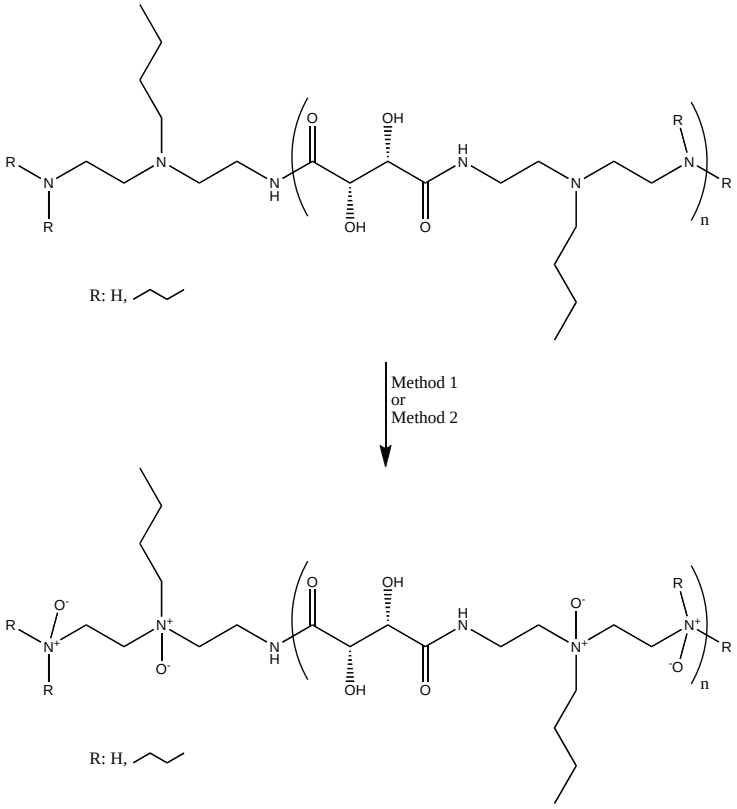

Figure 51: scheme of oxidation reaction to the alkylated oligoamide

4.3 Results and discussion

Several syntheses of oligoamides with polyamines were performed using five aliphatic polyamines (diethylenetriamine; triethylenetetramine; tetraethylenepentamine; bis-(3-aminopropyl)amine; 1,2-bis-(3-aminopropyl)aminoethane). Polymers characterization was carried out by NMR and FT IR spectroscopies. The average molecular weight of the products was determined by ^{1}H NMR spectroscopy, since the results obtained with this method for other polyamides have proved to be equivalent with those obtained by ESI-MS analysis[34].

The value obtained is the numeral average molecular weight since in step-growth polymerization, even if the monomer is consumed in the first step of the reaction and the molecular weight increases over time, macromolecular chains having different length can statistically be formed.

The syntheses were performed using the diacids activated as diester, using stoichiometric amounts of diester and diamine in the feed: the difficulty in having a very good molar balance between the two monomers represents a limit of this approach, since it can influence the molecular weight of the product.

In Table 6 the reaction conditions of all syntheses are reported while the details of the synthesis are described in the paragraphs below:

Table 6: reaction conditions of the syntheses

Product	Diamine	T (°C)	t (days)	Yield (%)	D.P.*	M.W. (g/mol)	Water solubility
A	diethylenetriamine	80	7	93.2	19	8406	Yes
B	triethylenetetramine	80	7	87.0	3	1586	Yes
C	tetraethylenepentamine	80	7	92.0	4	2281	Yes
D	bis-(3-aminopropyl)amine	80	7	90.0	N.D.**	N.D.	Yes
E	1,2-bis-(3-aminopropyl)aminoethane	80	7	87.0	N.D.	N.D.	Yes
F	diethylenetriamine	80	2	70.1	20	4443	Yes

**DP = degree of* polymerization; **N.D.: not determined.

Reaction time was set equal to 7 days for products from A to E (based on dimethyl α,α'-trehaluronate). For oligodiethylenamino-L-tartaramide (F), preliminary tests have shown satisfactory results, regarding yield and MW even after only 2 days.

Product F (Figure 49), which contains secondary amino groups in the chain available for reaction with hydrophobic groups and a simpler structure compared to the one of other products based on acid-α,α'-trehaluronic (A-E), was used to test different methods of alkylation of secondary amino groups and subsequent oxidation of the tertiary amino groups, to make it suitable to the function as KHI.

4.3.1 Syntheses of the products[34]

4.3.1.1 Oligodiethylenamino- α,α'- trehaluronamide (A)

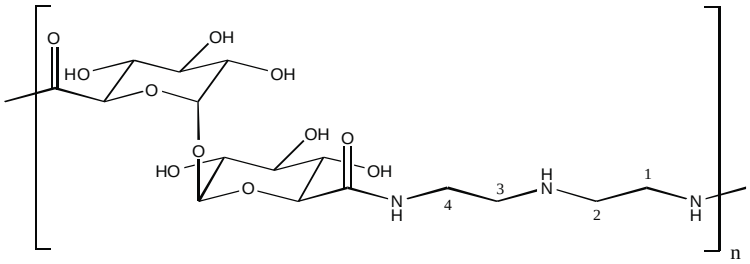

The synthesis between dimethyl α-α'-trehaluronate and diethylenetriamine was performed under stirring with methanol as solvent, in a Sovirel® tube, at 80°C for 7 days. After 24 hours a brown precipitate and a clear yellow solution were obtained.

The final product, washed with methanol and dried at reduced pressure and room temperature (93.2% yield), was analyzed by NMR and FT IR spectroscopies.

In FT IR spectrum (Figure 52) the formation of the amide bond is confirmed by the peaks at 1651 and 1550 cm^{-1} (amide I and II respectively). In the spectrum there are also the peaks related to C-O stretching at 1111, 1065, 1029 cm^{-1}, typical of α-α'- trehaluronic unit.

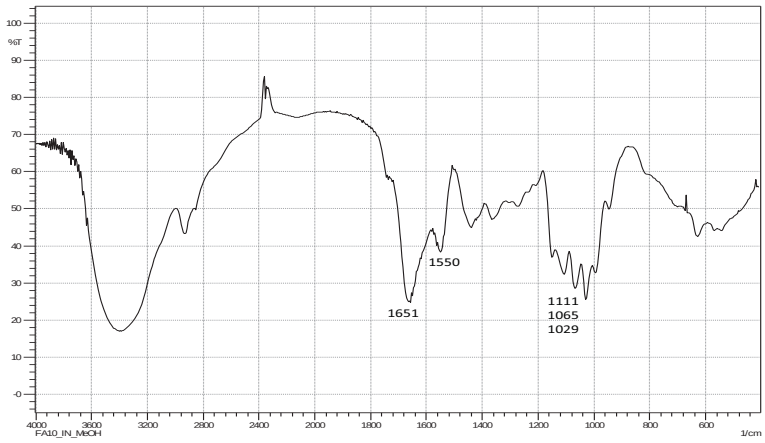

Figure 52: FT IR spectrum of the oligodiethylenamino-α,α'- trehaluronamide A

In ^{1}H NMR spectrum (Figure 53), the formation of an amide bond is confirmed thanks to the presence of a signal at 3.42 ppm owed to the methylene group in α position to the amide group (C**H**$_2$NHCO). Moreover there are changes in the shape of the signals in the trehaluronic portion between 3.50 and 3.95 ppm, between 4.00 and 4.28 ppm and at 5.22 ppm. The signal at 3.06 ppm

is attributed to the methylene group in α position to the amino end group (C**H**$_2$NH$_2$), whereas the signal related to the terminal ester group is not visible in the spectrum. At last the signal attributable to the methylene groups in the internal chain of the amine is present at 2.85 ppm.

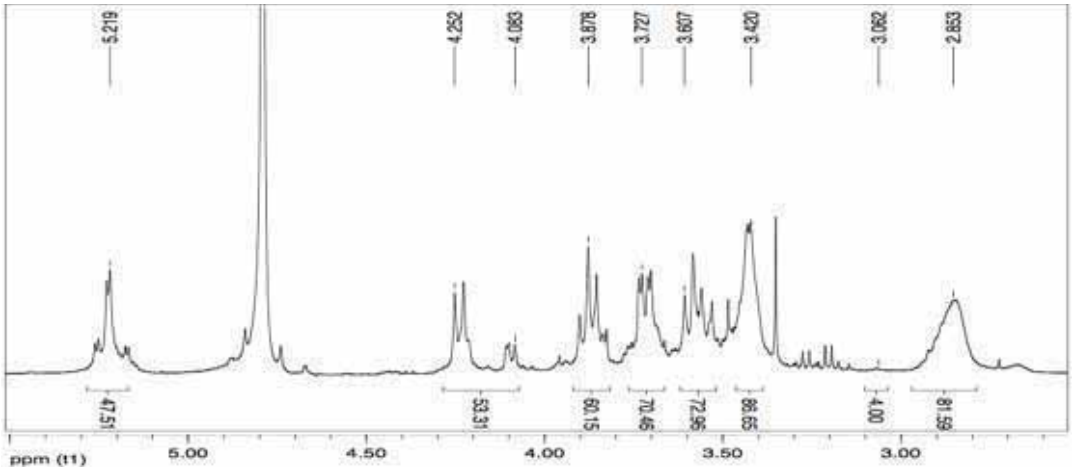

Figure 53: ^{1}H-NMR spectrum in D$_2$O of the oligodiethylenamino-α,α'-trehaluronamide A

Through the gCOSY spectrum (Figure 54), it is possible to relate the signal at 3.06 ppm to the methylene group in α position to the amino terminal group (C**H**$_2$NH$_2$) because of the presence of the coupling with the signal at 2.92 related to methylene group in β position at the same terminal group. Moreover the signal at 2.85 ppm is attributable to the methylene group near the C**H**$_2$NHCO because of the presence of the coupling with its signal at 3.42 ppm. Finally it is possible to assign the signals of the sugar backbone thanks to the couplings between the different vicinal hydrogens, at 3.61 ppm (H_4-H_4'), at 3.73 ppm (H_2-H_2'), at 3.88 ppm (H_3-H_3'), to 4.00- 4.28 ppm (H_5-H_5'), and to 5.22 (H_1-H_1') respectively.

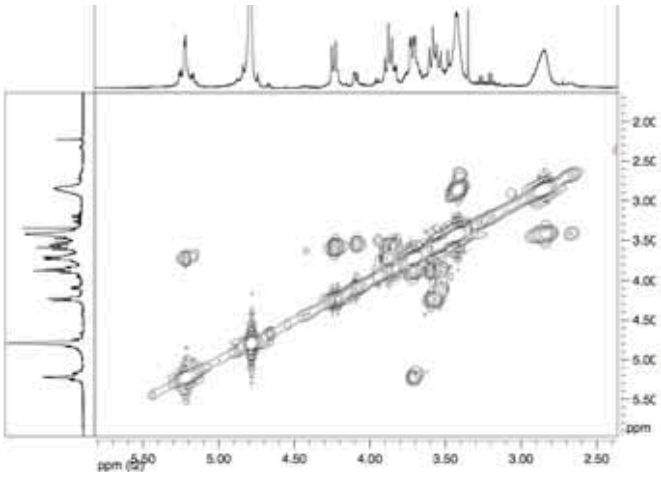

Figure 54: gCOSY spectrum in D$_2$O of the oligodiethylenamino-α,α'-trehaluronamide A

In ^{13}C NMR spectrum (Figure 55), the formation of the product is confirmed by the presence of signals at 37.8 ppm (**C**H_2NHCO) and at 171.3 ppm (**C**ONH).

Signals between 70.5 and 72.1 (**C**HOH: C_2-C_2' at 70.5 ppm, C_4-C_4' at 71.6 ppm, C_3-C_3' and C_5-C_5' at 72.1 ppm) and at 94.6 ppm (**C**HOH: C_1-C_1') are present, due to the presence of trehaluronic backbone whereas the signal related to the methylene groups in α position to the amino internal groups (**C**H_2NH) is visible at 47.0 ppm. Also in this spectrum signals related to the ester termination are not detectable.

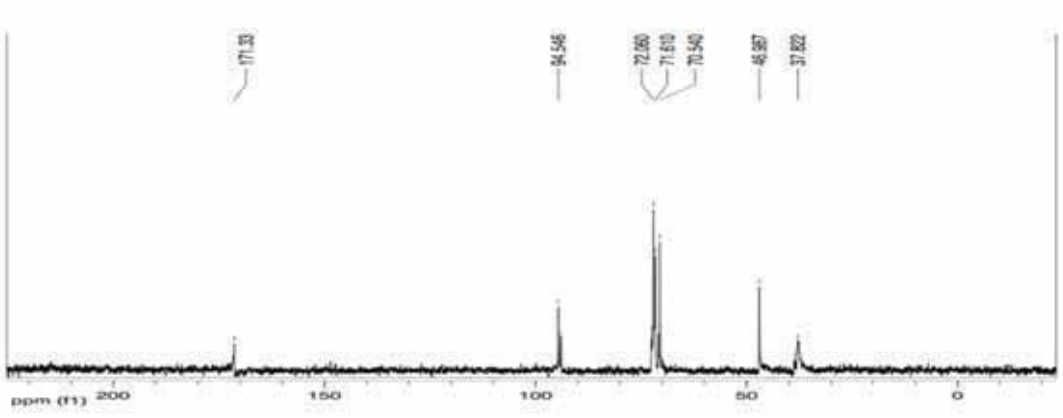

Figure 55: ^{13}C-NMR spectrum in D_2O of the oligodiethylenamino-α,α'-trehaluronamide A

The determination of the average molecular weight was performed measuring the integrals present in ^{1}H-NMR, assuming the double amino termination. The integrals of all the other signals were calculated in relation to the reference CH_2NH_2 set equal to 4H.

In Table 7, data used for the determination of the degree of polymerization (DP) of all products synthesized are shown; the oligoethyleneamino-α,α'-trehaluronate (A) is composed of 19 repeating units, with average molecular weight of 8406 g/mol.

Table 7: equations used to determine the average DP of the products, through ^{1}H NMR

		Equation	
Product	Type of terminal group	CH_2NH	CH_2NHCO
A	2 CH_2NH_2 groups	k= 4(DP + 1)	x= 4DP
B	2 CH_2NH_2 groups	k= 8(DP+1)	x= 4DP
C	2 CH_2NH_2 groups	k= 12(DP+1)	x= 4DP
D	N.D.	---	---
E	N.D.	---	---

4.3.1.2 Oligotriethylenediamino-α,α'- trehaluronamide (B)

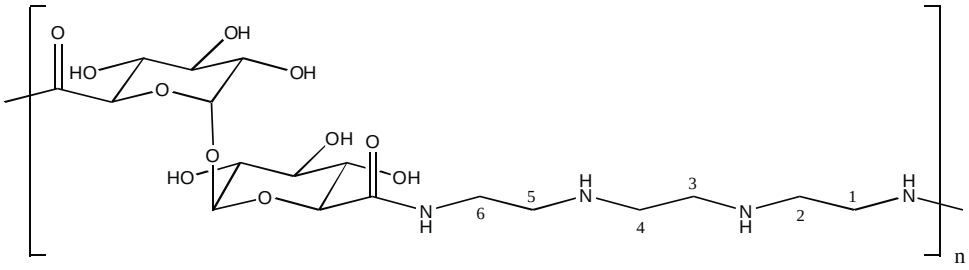

The reaction between dimethyl α-α'-trehaluronate and diethylenetriamine was performed under stirring with methanol as solvent, in a Sovirel® tube, at 80°C for 7 days. After 24 hours a brown precipitate and a clear yellow solution were obtained.

At the end of the reaction, the product was subjected to the same work up of the previous reaction, and then the solid residue was dried at reduced pressure and room temperature (87% yield) and analyzed by NMR and FT IR spectroscopies.

Similarly to the previous reaction, FT IR spectrum (Figure 56) confirms the formation of the amide compound by the peaks at 1651 and 1550 cm^{-1} (amide I and II) and at 1112, 1065 and 1025 cm^{-1}, relative to the C-O stretching.

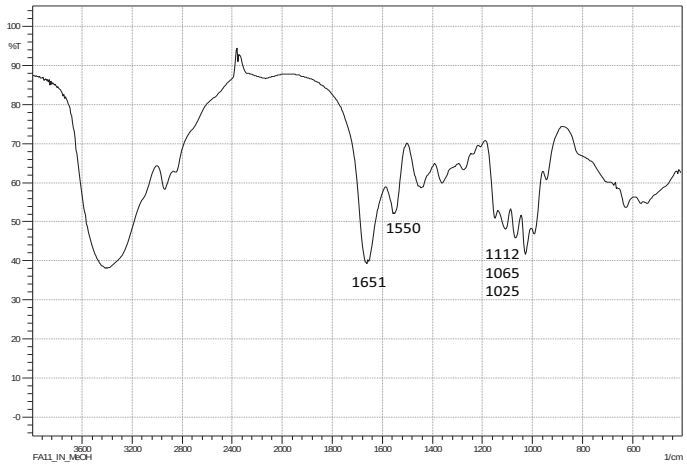

Figure 56: FT IR spectrum of the oligotriethylendiamino-α,α'- trehaluronamide B

In ^{1}H NMR spectrum (Figure 57), it is possible to evaluate the presence of methylene group in α position to the amide group at 3.41 ppm (C**H**$_2$NHCO); the change of shape of the signals relative to the sugar backbone between 3.50 and 3.95 ppm relative to the hydrogens H_2- H_2', H_3- H_3', H_4- H_4', between 4.00 and 4.29 to H_5- H_5' and at 5.22 ppm to H_1- H_1', is observed. Moreover a signal at

3.00 ppm is present relative to the methylene group in α position to the amino terminal group (C**H**$_2$NH$_2$) and there are no signals relative to ester terminal group; this indicates that also in this case two amino terminal groups are present, with the integral set equal to 4H to calculate the molecular weight.

Through gCOSY analysis is possible to assign the signals of the sugar backbone thanks to the couplings between the different vicinal hydrogens, at 3.58 ppm (H_4-H_4'), at 3.72 ppm (H_2-H_2'), at 3.87 ppm (H_3-H_3'), to 4.00- 4.29 ppm (H_5-H_5'), and to 5.22 (H_1-H_1') respectively. Moreover the signals present between 2.50 and 2.91 ppm can be attributable to the methylene groups of the internal amine

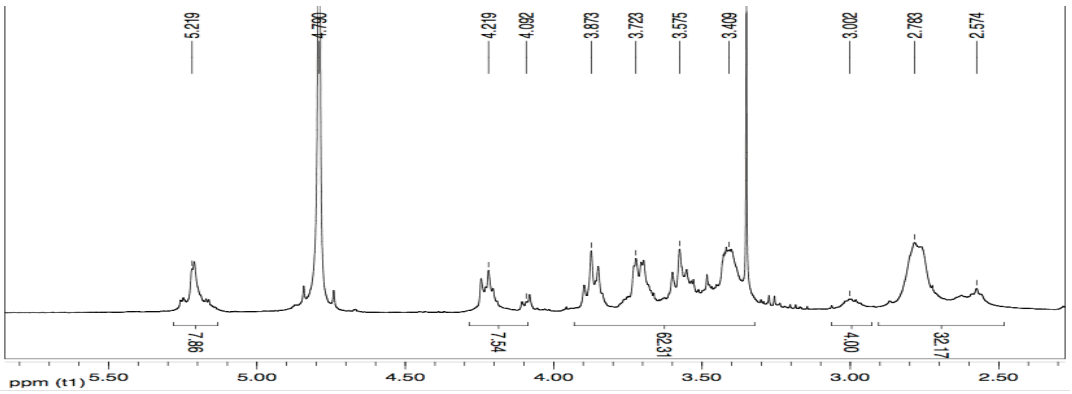

Figure 57: ^{1}H NMR spectrum in D_2O of the oligotriethylendiamino-α,α'- trehaluronamide B

In ^{13}C-NMR spectrum (Figure 58), in agreement with the formation of an amide compound, a signal at 37.4 ppm attributable to the methylene group in α position to the amide group (**C**H$_2$NHCO) and the signal at 170.3 ppm relative to the carbonyl of the amide group (**C**ONH) are present. The signals between 46.0 and 46.3 ppm are owed to the carbons of aliphatic amine (**C**H$_2$NH).

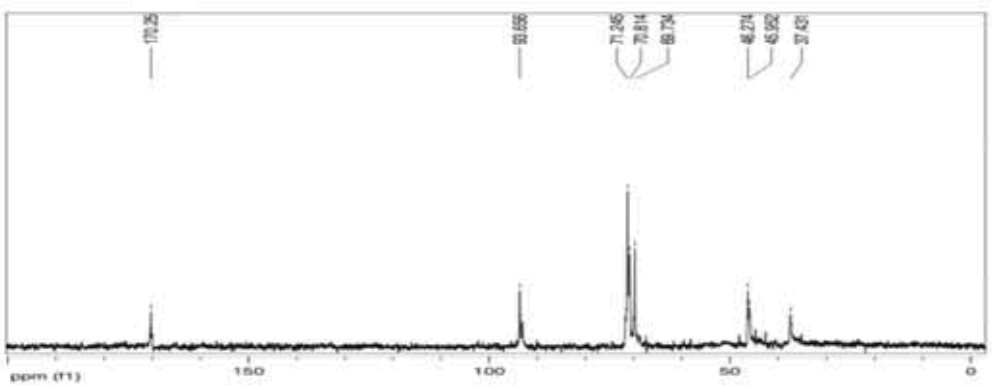

Figure 58: ^{13}C NMR spectrum in D_2O of the oligotriethylendiamino-α,α'- trehaluronamide B

According to the integrals (Table 7), the product is composed by 3 repeating units, resulting in an average molecular weight of 1586 g/mol.

4.3.1.3 Oligotetraethylenetriamino-α,α'- trealuronamide (C)

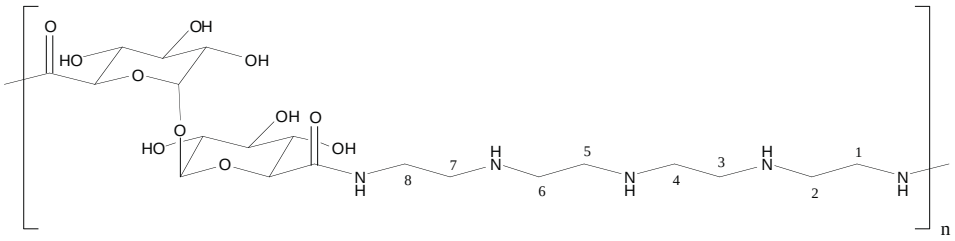

The reaction between dimethyl α-α'-trehaluronate and tetraethylenepentamine, was performed under stirring with methanol as solvent, in a Sovirel® tube, at 80°C for 7 days.

Also in this case, as in the previous reactions, after 24 hours it was possible to observe the precipitation of a brown solid in the Sovirel® tube and the formation of a clear yellow solution.

The product, washed with methanol and dried at reduced pressure and room temperature (92.0% yield), was analyzed by NMR and FT IR spectroscopies.

FT IR spectrum (Figure 59) confirms the presence of the product thanks to the peaks at 1662 and 1550 cm^{-1} (amide bond) and the peaks related to trehaluronic backbone at 1108, 1065 and 1029 cm^{-1}.

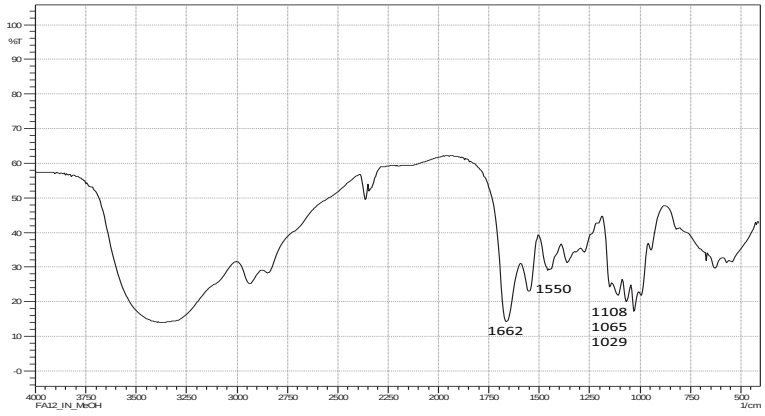

Figure 59: FT IR spectrum of the oligotetraethylentriamino-α,α'- trehaluronamide C

In ^{1}H NMR spectrum (Figure 60) the formation of an amide bond is confirmed by the presence of a signal at 3.43 ppm attributable to the methylene group in α position to the amide group (C**H**$_2$NHCO). The signals relating to the trehaluronic backbone are at 3.52- 3.95 ppm for H_2- H_2', H_3-

H_3', H_4- H_4', at 4.05 - 4.28 ppm for H_5- H_5' and at 5.23 ppm for H_1- H_1' The signal at 3.05 ppm is attributed to the methylene group in α position to the amino end group (C**H**$_2$NH$_2$).

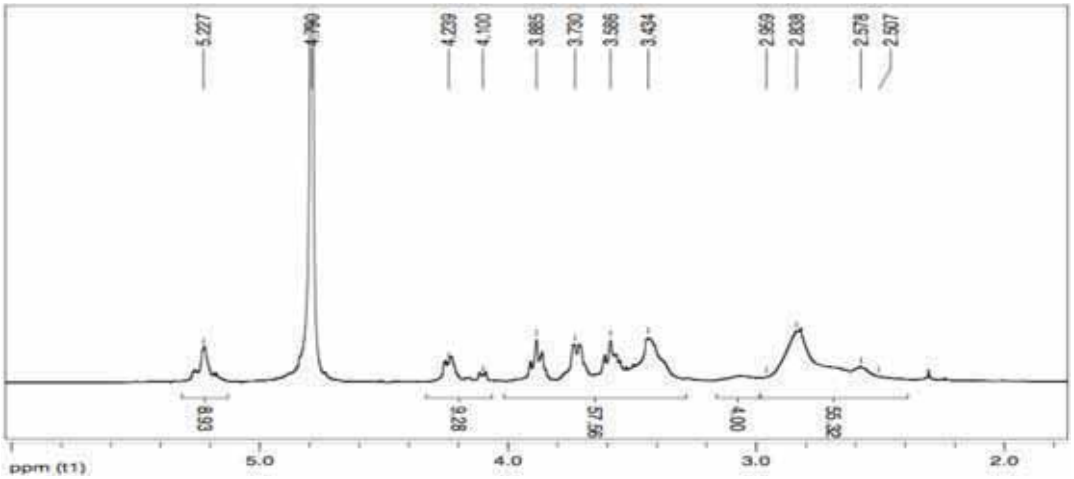

Figure 60: ^{1}H NMR spectrum in D_2O of the oligotetraethylentriamino-α,α'- trehaluronamide C

The gCOSY analysis distinguishes between various hydrogens of trehaluronic backbone [H_2- H_2', H_3- H_3', H_4- H_4' at 3.59 ppm (H_4- H_4'), 3.73 ppm (H_2- H_2') and 3.89 ppm (H_3- H_3') and between methylene groups of the internal amine chain (between 2.50 and 2.96 ppm).

^{13}C NMR spectrum (Figure 61) confirms the formation of an amide compound by the signals at δ 38.3 ppm (**C**H$_2$NHCO) and at 170.9 ppm (**C**ONH). The signal at 46.9 ppm is related to the methylene groups in α position to the internal amine groups (**C**H$_2$NH).

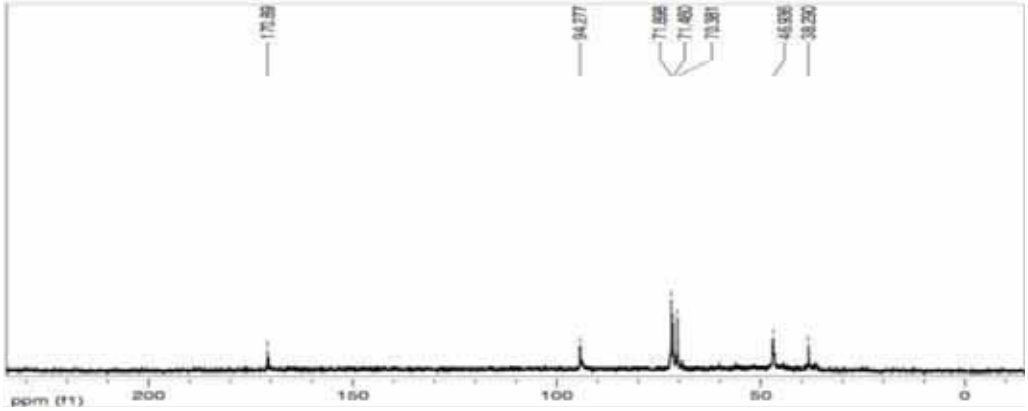

Figure 61: ^{13}C NMR spectrum in D_2O of the oligotetraethylentriamino-α,α'- trehaluronamide C

According to the integrals (Table 7), the product is composed by 4 repeating units, with average molecular weight equal to 2281 g/mol.

4.3.1.4 Oligo-diproylenamino-α,α'- trehaluronamide (D)

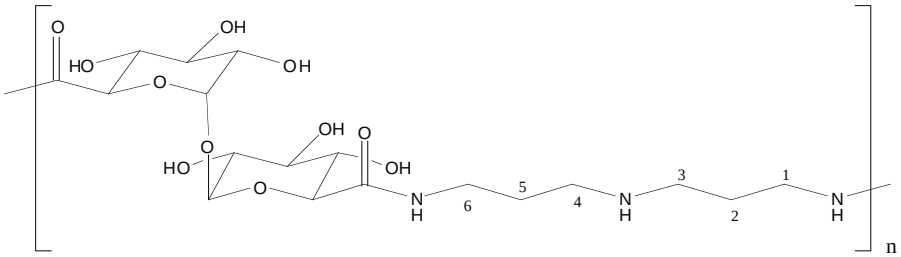

The reaction between bis(3-aminopropyl)amine and dimethyl- α,α'- trehaluronate was performed under stirring in methanol as solvent, in a Sovirel® tube, at 80°C for 7 days. After 24 hours a brown solid precipitates and a clear yellow solution forms.

The product, washed with methanol and dried at reduced pressure and room temperature (90.0% yield), was analyzed by NMR and FT IR spectroscopies.

In FT IR spectrum (Figure 62) amide characteristic peaks at 1654 and 1550 cm^{-1} are present. Moreover the typical peaks of the trehaluronic C-O stretching at 1108 1068 and 1025 cm^{-1} are visible.

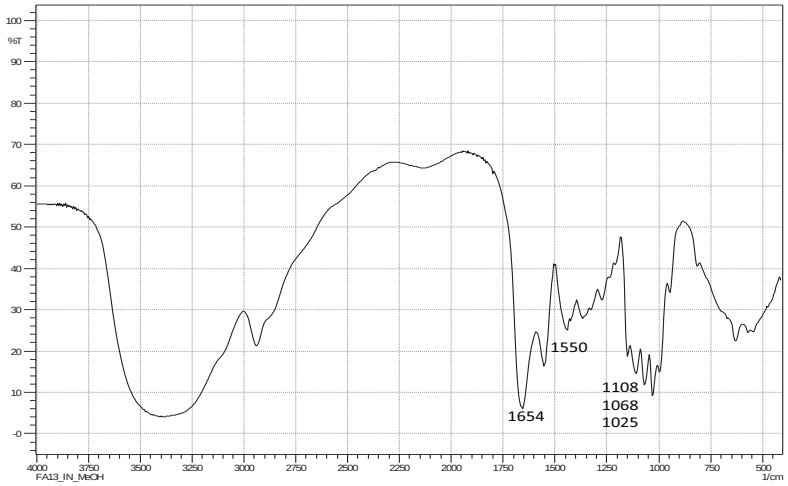

Figure 62: FT IR spectrum of the o*ligo-diproylenamino*-α,α'- trehaluronamide D

^{1}H-NMR spectrum (Figure 63) is in agreement with the formation of the oligoamide, thanks to the signals at δ 3.29 and 1.74 ppm relative to the presence of the methylene groups in α and β positions to amide group (-CHC**H**$_2$NHCO and -C**H**$_2$CH$_2$NHCO) and at 2.65 ppm the signal related to the methylene group near the internal amino group (**C**H$_2$NH). The signals of the trehaluronic backbone are located between 3.51- 3.92 ppm (C**H**-OH: H_2- H_2', H_3- H_3', H_4- H_4'), 4.00- 4.29 ppm (C**H**-OH: H_5- H_5') and at 5.20 ppm (C**H**-OH: H_1- H_1'). The ester termination is not present and

methylene terminal amino groups are not detectable; for these reasons it was not possible to calculate the DP of the oligomer and consequently its average molecular weight by ^{1}H NMR spectroscopy.

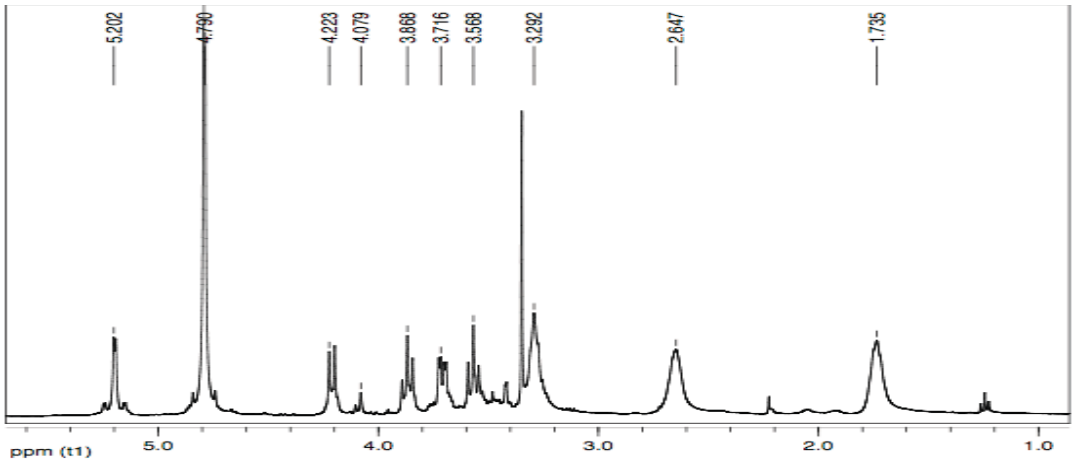

Figure 63: ^{1}H NMR spectrum in D_2O of the oligo-diproylenamino-α,α'- trehaluronamide D

In ^{13}C NMR spectrum (Figure 64) the formation of the amide compound is confirmed by the presence of the signals at 36.2 ppm (**C**H_2NHCO) and at 169.9 ppm (**C**ONH). The signal at 44.9 ppm confirms the presence of the methylene groups in α position to the internal amino group (**C**H_2NH). The signal at 26.7 ppm is relative to the internal methylene groups on the propylene groups (CH_2**C**H_2CH_2).

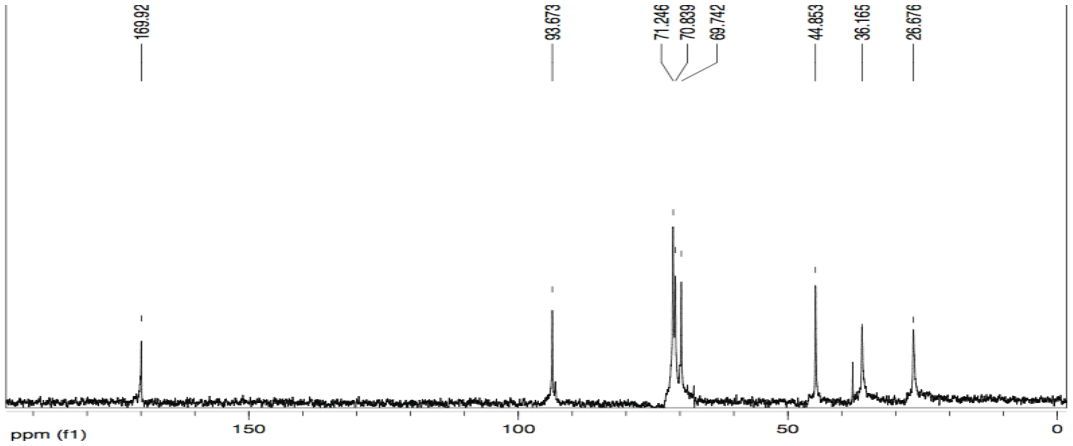

Figure 64: ^{13}C NMR spectrum in D_2O of the oligo-diproylenamino-α,α'- trehaluronamide D

4.3.1.5 Oligo-bis(propylenamino)ethane-α,α'- trehaluronamide (E)

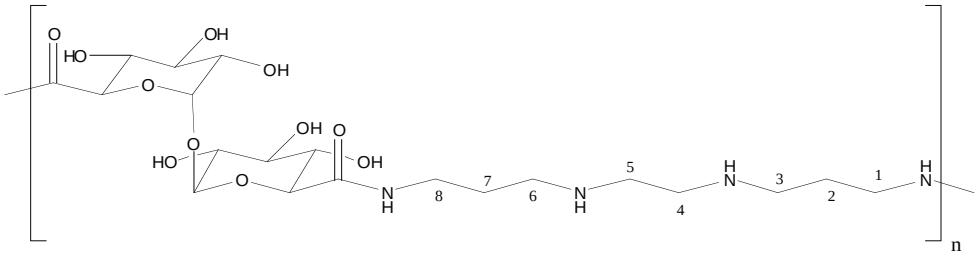

This synthesis with dimethyl- α,α'-trehaluronate and 1,2-bis(3-aminopropylamino)ethane, was carried out under stirring using methanol as solvent, in a Sovirel® tube, for 7 days at 80°C, like the previous reactions. The product was subjected to the same work up of the previous reactions, and then dried at reduced pressure and room temperature (87.0% yield), before the analyses with NMR and FT IR spectroscopies.

FT IR spectrum (Figure 65) confirms the formation of the amide compound thanks to the peaks at 1658 and 1550 cm^{-1} (amide I and II) and at 1108, 1065 and 1025 cm^{-1} related to the C-O stretching.

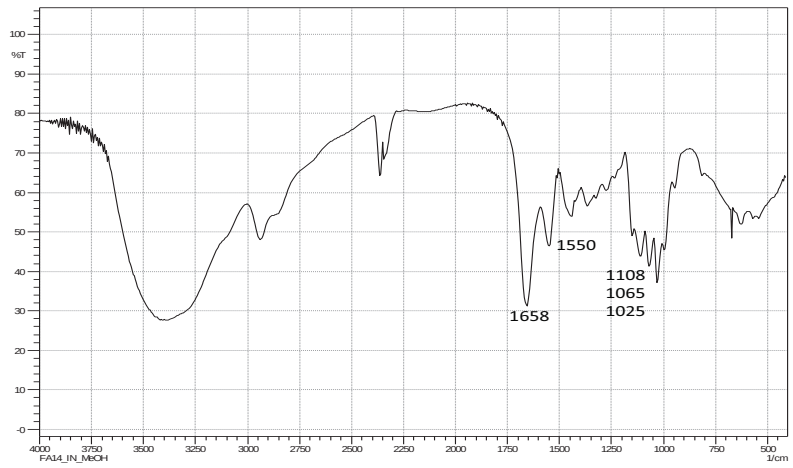

Figure 65: FT IR spectrum of the oligo-bis(propylenamino)ethane-α,α'- trehaluronamide E

^{1}H NMR spectrum (Figure 66) shows the presence of methylene group in α position to the amide group at 3.29 ppm (C**H**$_2$NHCO), the signals related to the trehaluronic backbone (H_2-H_2', H_3-H_3', H_4-H_4' between 3.51 and 3.95 ppm, H_5- H_5' at 4.00- 4.29 ppm and H_1- H_1' at 5.20 ppm), the signal attributable to the internal methylene group of the amino chain at 2.61 ppm and at 1.72 ppm the signal attributable to the methylene group in β position to the amide bond.

The methylene group in α position to the terminal amino group (C**H**$_2$NH$_2$) is not distinguishable, and terminal ester groups are not present:, therefore it was not possible to calculate the DP of the oligomer and the corresponding average molecular weight by ^{1}H NMR spectroscopy.

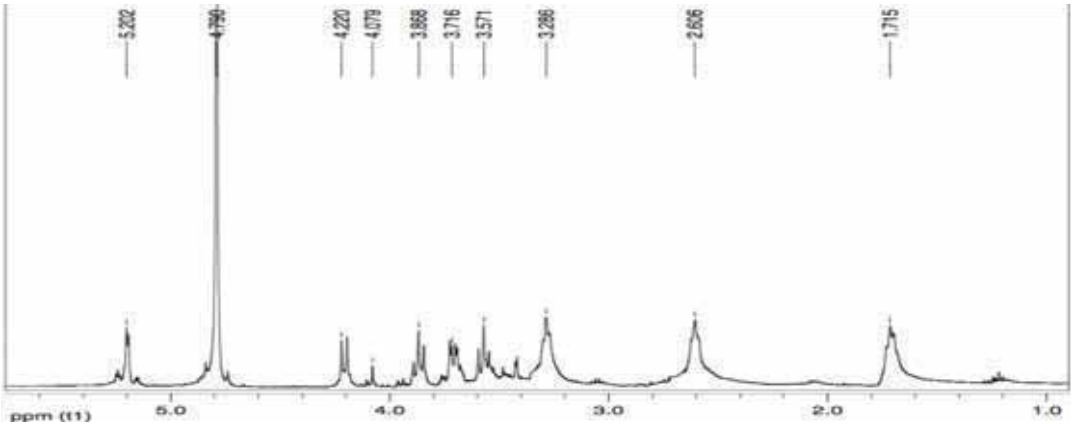

Figure 66: ^{1}H NMR spectrum in D$_2$O of the oligo-bis(propylenamino)ethane-α,α'- trehaluronamide E

The formation of the amide compound is confirmed by ^{13}C-NMR spectrum (Figure 67) for the presence of the signal at 36.4 ppm relative to the carbon of the methylene group near the amide groups (**C**H$_2$NHCO) and the signal at 169.9 ppm relative to the carbonyl amide group (**C**ONH). The methylene groups of the amine portion are represented by three signals: the -**C**H$_2$- group at the centre of the two propylene groups at 27.0 ppm, and the two signals of the methylene groups near nitrogen at 45.0 and 46.3 ppm (**C**H$_2$NH).

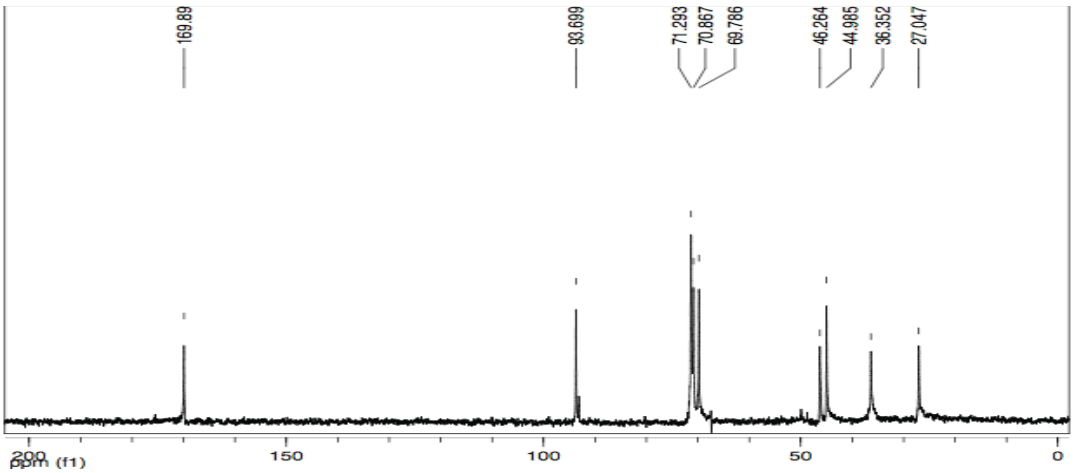

Figure 67: ^{13}C NMR spectrum in D$_2$O of the oligo-bis(propylenamino)ethane-α,α'- trehaluronamide E

4.3.1.6 Oligodiethylenamino -L-tartaramide

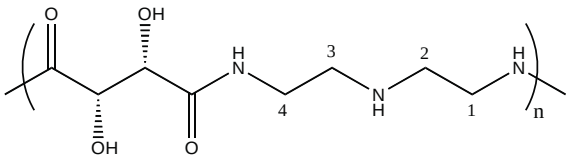

The synthesis between dimethyl L-tartrate and diethylenetriamine was performed under stirring with methanol as solvent, in a Sovirel® tube, at 80°C for 2 days. During the reaction a brown precipitate and a clear yellow solution were obtained.

The final product, washed with methanol and dried at reduced pressure and room temperature (70.1% yield), was analyzed by NMR and FT IR spectroscopies.

In FT IR spectrum (Figure 68) the characteristic peaks of the oligoamide at 1650 and 1540 cm^{-1} are present as well as the peaks related to C-O stretching at 1135 and 1072 cm^{-1}, typical of L-tartaric units.

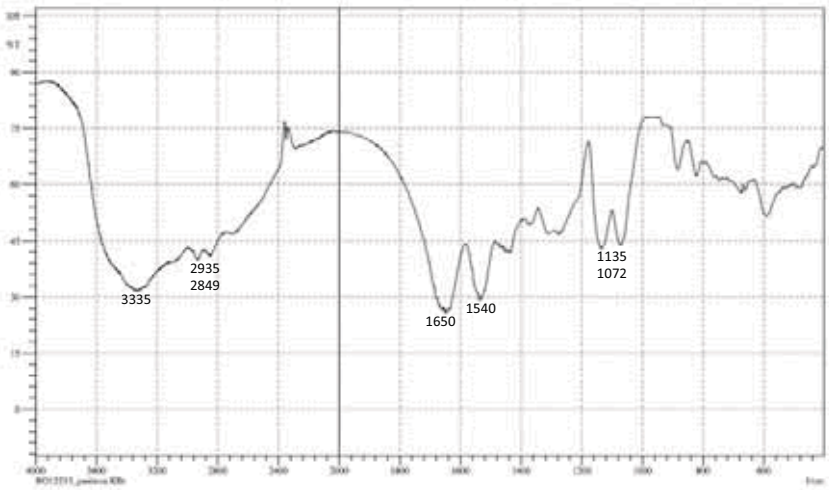

Figure 68: FT IR spectrum of the oligodiethylenamino -L-tartaramide (F)

^{1}H-NMR spectrum (Figure 69) confirms the formation of the oligoamide, thanks to the presence of a signal at 3.41 ppm owed to the methylene group in α position to the amide group (**C**H_2NHCO) and to a signal at 2.99 ppm attributable to the methylene group near to the terminal amine group (**C**H_2NH_2). Moreover the methylene groups present near to the internal amino groups (**C**H_2NH) and the signal relative to **C**H-OH group at 2.79 and 4.57 ppm respectively, are present. These signals were used for the evaluation of DP. In fact, the signal at 3.41 ppm cannot be used because overlapped to a signal relating to methanol. In this kind of product, the formation of very strong interactions between the solvent and the polar groups of the oligoamide is possible, and do not

allow the complete removal of the solvent. In this spectrum the signal relating to an ester termination is not visible, in accordance with the hypothesis that the molecule has two amino terminal groups.

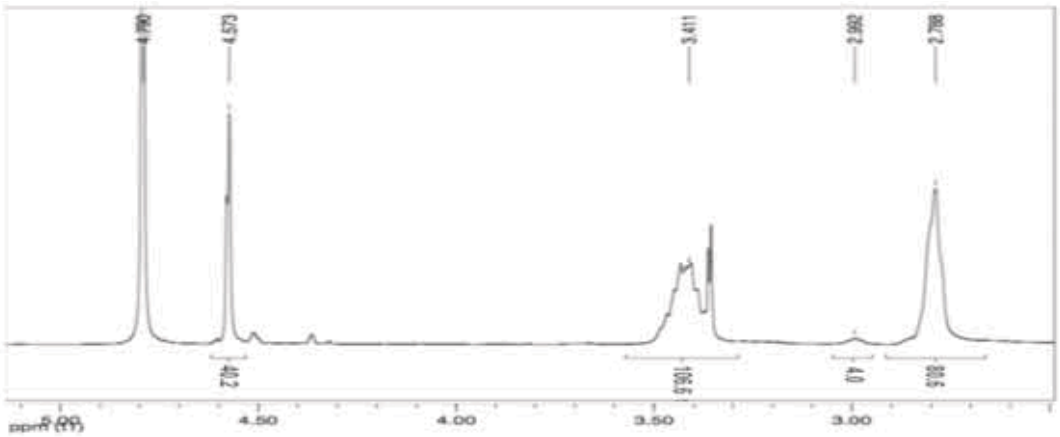

Figure 69: ^{1}H NMR spectrum in D_2O of the oligodiethylenamino -L-tartaramide (F)

In ^{13}C NMR spectrum (Figure 70) ester terminal groups are not present since no signals at about 53 ppm (O**C**H_3) and at 170- 171 ppm (**C**OOCH_3) are present. The formation of the product is confirmed by the presence of the signal at 38.3 ppm related to the methylene group in α position to the amide group (**C**H_2NHCO). The signal of the **C**H-OH group at 72.4 ppm and the methylene groups in α position to the internal amino groups (C**H**$_2$NH) at 46.9 ppm are present. Also in this case there is a signal having low intensity at 48.8 ppm relative to the solvent. A 173.9 ppm it is possible to find the signal relative to the amide C=O.

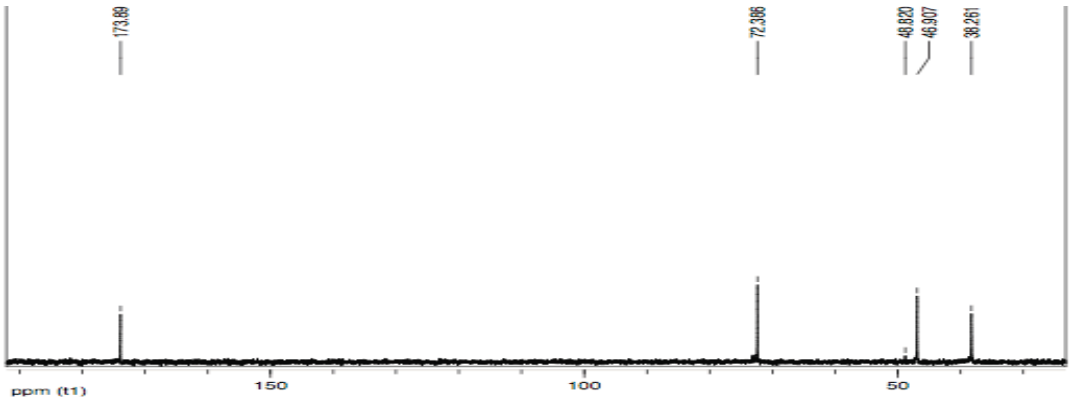

Figure 70: ^{13}C NMR spectrum in D_2O of the oligodiethylenamino -L-tartaramide (F)

Determination of the average molecular weight was performed measuring the integrals present in ^{1}H NMR spectrum, using the double amino termination as reference value; then, the integral of

the C**H**$_2$NH$_2$ group is set equal to 4H. In this product there are three signals useful to determine the DP: the C**H**-OH one, the one related to methylene groups in α position to the amide group (C**H**$_2$NHCO) and the one of the methylene groups near to the amino group (C**H**$_2$NH). However, for these compounds the integral of the signal in α position to the amide group, as mentioned previously, is higher because of the presence of methanol.
Below, the three calculations used to determine the number of repeating units (n) are reported:

Integral of CH-OH signal = 2n
*Integral of C**H**$_2$NH signal = 4 (n+1)*
Integral of CH$_2$NHCO signal = 4n

The degree of polymerization is equal to 20 indicating an average molecular weight of 4443 g/mol.

4.3.1.7 Oligoamide alkyl substituted (Method 1)

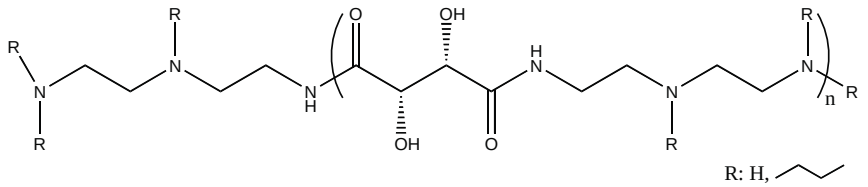

The reaction between oligodiethyleneamino-L-tartaramide and bromobutane was performed in a Sovirel® tube, with methanol as solvent, at 80°C, in different molar ratio oligoamide: bromobutane (1: 2 and 1: 3) for 24 and 48 hours.

At the end of the reactions solvent and volatile reagents (unreacted bromobutane) were removed from the mixture by distillation at reduced pressure at 50°C. The solid obtained was dried at reduced pressure and room temperature.

Degree of substitution was evaluated taking the C**H**OH integral value as reference; the product with the highest degree of substitution is obtained from the reaction left to react for 48 hours. Higher bromobutane quantities do not increase the degree of substitution, therefore the ratio 1: 2 was used, obtaining a product with DS of secondary and primary amino groups of about 28-30% (DS= 7- 8).

The low value of alkylation degree can be attributed to the negative effect of the hydrobromic acid, formed as a result of the reaction between the alkyl halide and the amino groups of the oligoamide. Indeed, the presence of HBr can form quaternary ammonium salts hindering further substitution reactions on primary or secondary amine groups.

The solid obtained was characterized by NMR analysis.

Alkylated product formation is confirmed by ^{1}H NMR spectrum (Figure 71) thanks to the presence of a signals at 0.98 ($C\mathbf{H}_3CH_2CH_2CH_2N$), at 1.43 ppm ($CH_3C\mathbf{H}_2CH_2CH_2N$) and at 1.74 ppm ($CH_3CH_2C\mathbf{H}_2CH_2N$). Besides, a shift of the signals relative to the previous product is visible and new signals are also present.

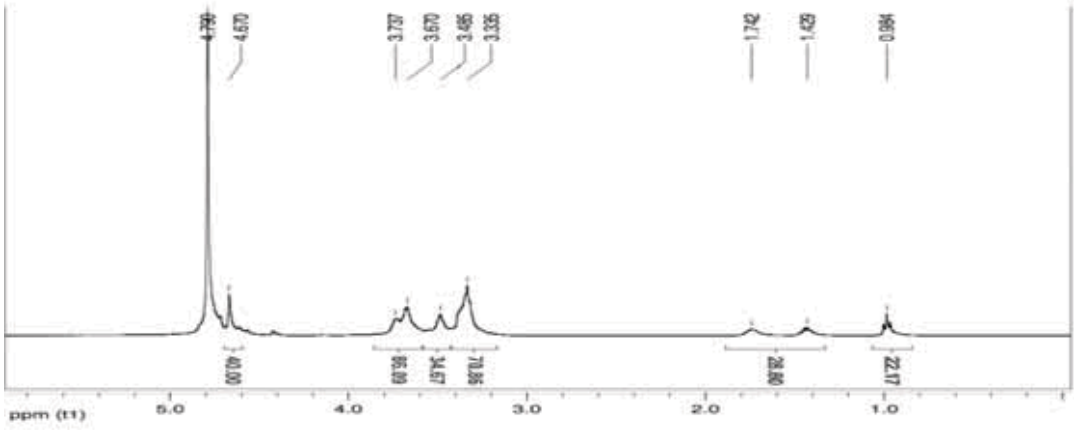

Figure 71: ^{1}H NMR spectrum in D_2O of the alkylated- oligodiethylenamino-L-tartartaramide (Method 1)

Through gCOSY spectrum (Figure 72) it is possible to identify different methylene groups between 3.30 and 3.80 ppm, such as the one at 3.34 ppm ($CH_3CH_2CH_2C\mathbf{H}_2N$) thanks to the coupling to the $CH_3CH_2C\mathbf{H}_2CH_2N$ at 1.74 ppm. Moreover the signal at 3.34 ppm coupled with that at 3.67 and another one at 3.49 ppm coupled with the one at 3.74 ppm; these signals are attributed to the methylene groups in α position to the amino group and to the amide group respectively, adjacent to the secondary and tertiary amino groups.

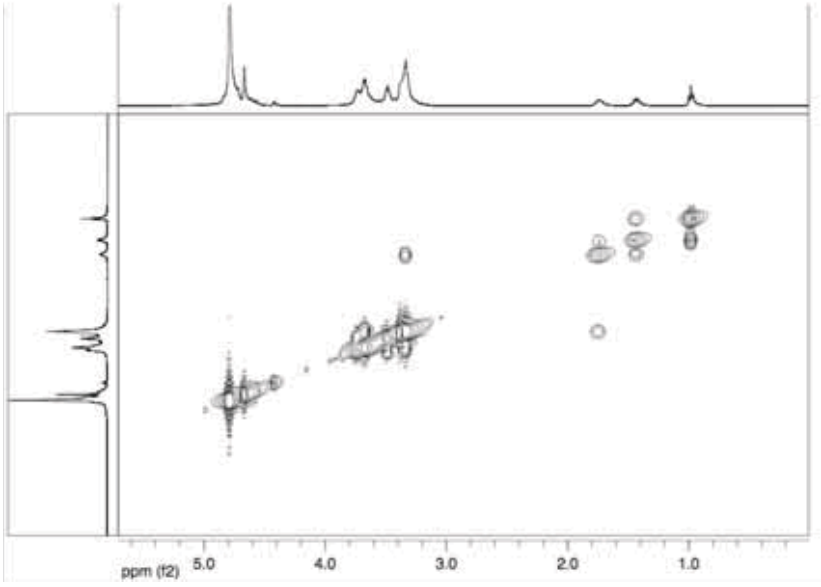

Figure 72: gCOSY spectrum in D_2O of the alkylated- oligodiethylenamino-L-tartartaramide (Method 1)

In ^{13}C NMR spectrum (Figure 73) the presence of the new alkyl group on the nitrogen atom is confirmed by the signals at 52.6 and 53.6 ppm, relative to CH_2N groups of the substituent and of the oligoamide chain. Moreover, the other signals related to the alkyl chain at 12.8 ($\mathbf{C}H_3CH_2CH_2CH_2N$), 19.2 ($CH_3\mathbf{C}H_2CH_2CH_2N$) e 25.0 ($CH_3CH_2\mathbf{C}H_2CH_2N$) are present.

Signals at 174.7 (**C**ONH), at 72.3-73.2 (**C**H-OH), and at 47.2 ppm (**C**HNH) have not changed compared to the starting compound. Finally there are two signals, at 34.2 and 35.7 related to the methylene groups in α position to the amide groups.

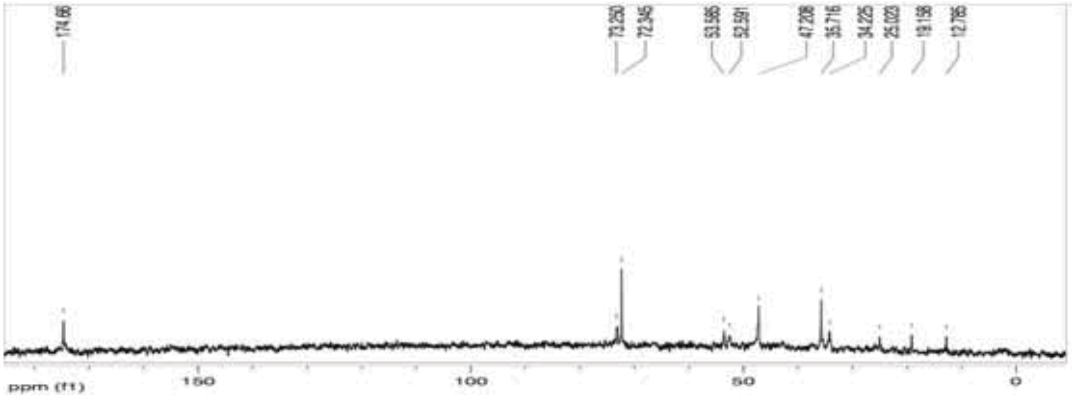

Figure 73: ^{13}C NMR spectrum in D_2O of the alkylated- oligodiethylenamino-L-tartartaramide (Method 1)

gHSQC spectrum (Figure 74) confirm this assignment thanks to the coupling between the hydrogen atoms (already attributed by ^{1}H NMR analysis and gCOSY) with those of ^{13}C NMR spectrum. In this spectrum it is possible to confirm that the signal at 3.34 ppm is relative to two methylene groups: CH_2NH oligoamide chain (un-substituted amino group) and CH_2N of the alkyl substituent, thanks to the correlation with the signals at 47.2 and 53.6 ppm respectively; the one at 3.49 ppm to the CH_2N of the oligoamide is correlated with the signal at 52.6 ppm. Thus the signal at 35.7 ppm is attributable to CH_2NHCO in α position to the CH_2NH, while the one at 34.2 ppm is related to the carbon in α to CH_2N.

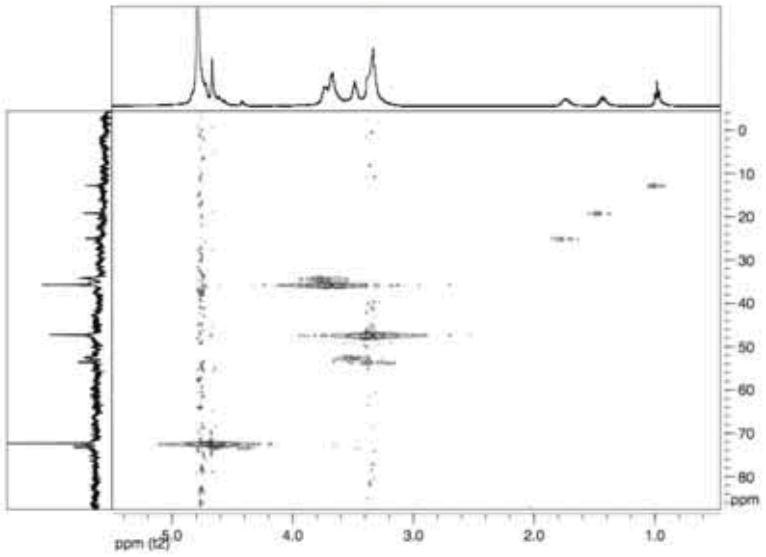

Figure 74: gHSQC spectrum in D_2O of the alkylated- oligodiethylenamino-L-tartartaramide (Method 1)

4.3.1.8 Oligoamide alkyl substituted (Method 2)

Method 1 was modified, in order to improve the degree of substitution: oligodiethyleneamino-L-tartaramide and bromobutane were put in a flask with condenser, using ethanol as solvent, in different molar ratios oligoamide: bromobutane (1: 2 and 1: 3), in presence of $CaCO_3$ (stoichiometric amount to bromobutane), for 24 and 48 hours, and the reaction was performed at the reflux temperature of ethanol.

Ethanol was chosen as solvent thanks to the optimal boiling point and minimal toxicity problems. The addition of $CaCO_3$ was performed to remove hydrobromic acid formed during the reaction and to prevent the formation of ammonium salts which would have hindered the progress of the substitution reaction on the amino groups, that probably occurred in reaction 1.

At the end of the reaction, solvent and volatile reagents (unreacted bromobutane) were removed from the mixture by distillation at reduced pressure at 50°C. The solid obtained was washed with water to separate the alkyl-oligoamide from the salts ($CaCO_3$ and $CaBr_2$); then the solution containing the product was distilled at reduced pressure (T = 40°C) and the resulting solid dried under reduced pressure and room temperature.

The characterization of the product was carried out by NMR analysis confirming the same characteristics of the previous reactions. The DS of secondary and primary amino groups in this case is about 20-25% (DS= 5-6), therefore lower than the one obtained using the Sovirel® reaction.

4.3.1.9 Oligoamide alkyl substituted (Method 3)

The reaction between oligodiethyleneamino-L-tartaramide and bromobutane was performed in a Sovirel® tube, with methanol as solvent, in molar ratio oligoamide: bromobutane equal to 1: 2, and $CaCO_3$ in a stoichiometric amount to bromobutane, for 24 and 48 hours, at 80°C. At the end of the reactions, the work-up was performed as in Method 2.

The reaction with the highest degree of substitution was the one left to react for 48 hours; the 1: 2 molar ratio between oligoamide and bromobutane was used because it gave the best results in the previous reactions. The degree of substitution evaluated via NMR, using the integral of the CH-OH group as reference signal, results in an alkylation of secondary and primary amino groups of 70- 80% (DS= 17-19).

The conditions used in these syntheses have proved to be better than those used in previous methods. In fact, compared to Method 1, the addition of $CaCO_3$ avoids the formation of ammonium salts that prevented the complete substitution reaction on the remaining primary and

secondary amino groups; furthermore, compared to Method 2, using a closed reactor allows to carry out the reaction at slightly higher temperature and with a slight overpressure determined both by the vapors of the solvent and by carbon dioxide developed as a result of the reaction of $CaCO_3$ with HBr. Below, the ^1H NMR spectrum of one of these products, with DS of about 17.5 is discussed.

As in the previous reaction, ^1H NMR spectrum (Figure 75) confirms the presence of the signals related to the butyl group at δ 0.97 ppm ($C\mathbf{H}_3CH_2CH_2CH_2N$), at 1.41 ppm ($CH_3C\mathbf{H}_2CH_2CH_2N$), at 1.71 ppm ($CH_3CH_2C\mathbf{H}_2CH_2N$) and at 3.31 ppm ($CH_3CH_2CH_2C\mathbf{H}_2N$); moreover at 4.66 ppm the signal related to the CH-OH group is present and used as reference for the determination of the alkylation degree.

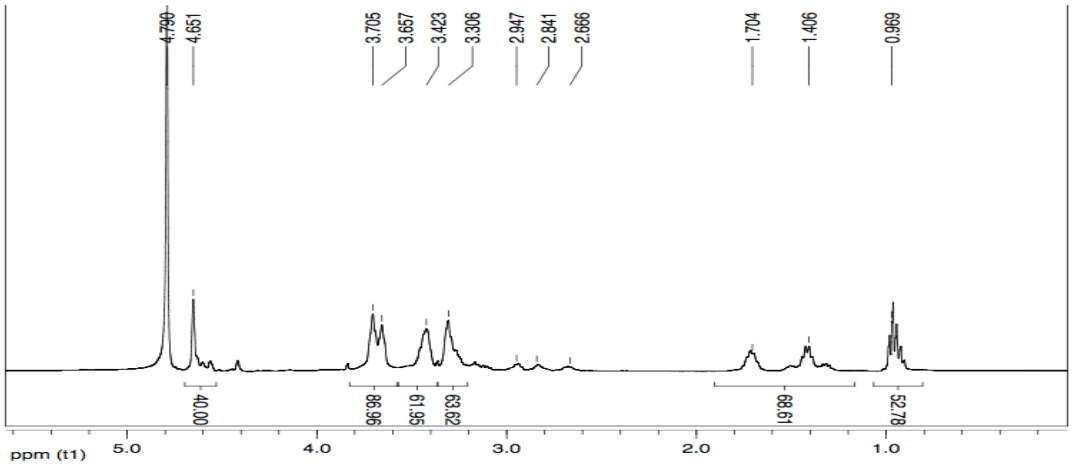

Figure 75: ^1H-NMR spectrum in D_2O of the alkylated- oligodiethylenamino-L-tartartaramide (Method 3)

gCOSY spectrum (Figure 76) allows to assign the pattern of signals between 3.30 and 3.80 ppm: at 3.31 ppm there are the $CH_3CH_2CH_2C\mathbf{H}_2N$ group and the CH_2NH group of the oligoamide chain (without alkylation); the signal at 3.66 ppm is related to the CH_2NHCO group. Moreover the coupling between the signal at 3.42 ppm and that at 3.71 ppm is present, attributable to the methylene groups in α position to the internal amino group and in α position to the amide group, adjacent to the tertiary amine groups ($-CH_2N$) respectively.

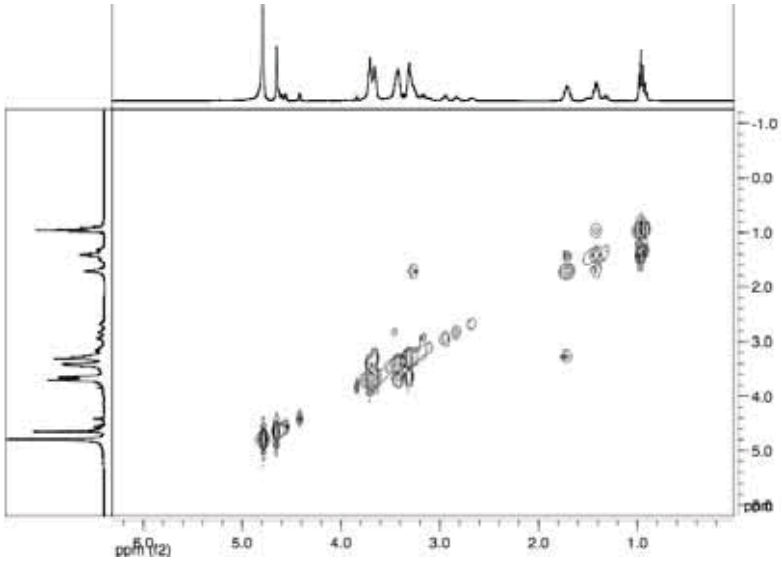

Figure 76: gCOSY spectrum in D_2O of the alkylated- oligodiethylenamino-L-tartartaramide (Method 3)

These assignments are confirmed by ^{13}C NMR spectra and gHSQC (Figure 77); it is possible to assign the signals at δ 12.9 ppm to **C**$H_3CH_2CH_2CH_2N$, at 19.3 ppm to CH_3**C**$H_2CH_2CH_2N$, at 25.3 ppm to CH_3CH_2**C**H_2CH_2N and 53.6 ppm to the $CH_3CH_2CH_2$**C**H_2N. The presence of the signals at 52.7 ppm (**C**H_2N of the alkylated oligoamide chain), at 47.3 ppm (**C**H_2NH of the not-alkylated oligoamide chain), at 34.5 ppm (NCH_2**C**H_2NHCO of the alkylated oligoamide chain) and at 35.9 ppm (-$NHCH_2$**C**H_2NHCO of the oligoamide chain not alkylated) are in agreement with a partial oligoamide alkylation as shown and quantified also by ^1H NMR spectroscopy.

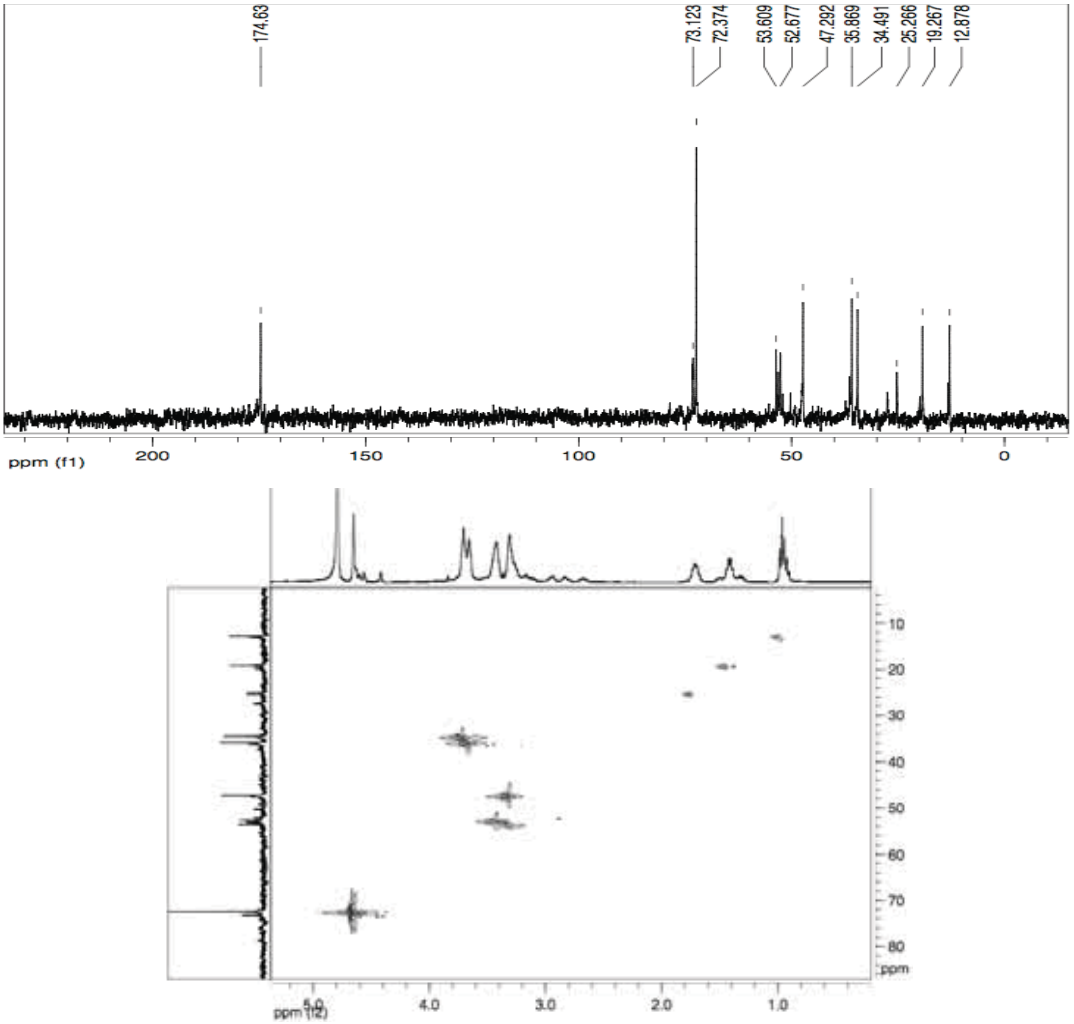

Figure 77: ^{13}C NMR e gHSQC spectra in D_2O of the alkylated- oligodiethylenamino-L-tartartaramide (Method 3)

4.3.1.10 Oxidation reaction (Method 1)

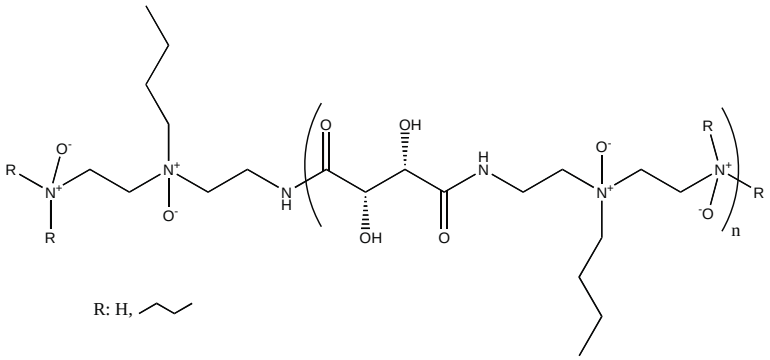

The oxidation reaction of the alkylated oligoamide (3) has been carried out in a single neck flask, by addition of H_2O_2 (30%) to the oligoamide either as such or in aqueous solution[52]. Molar ratios between oligoamide and H_2O_2 equal to 1:1, 1:2, 1:4 and 1:6 were used, for 24 hours at room temperature .

At the end of the reaction the mixture was heated at 70°C for 1 hour with a condenser, to remove the excess H_2O_2; then the solution was distilled under reduced pressure at 50°C, obtaining a solid that was dried at reduced pressure and room temperature. The products obtained in all the reactions were analyzed by NMR and FT IR spectroscopies.

The reaction in ratio equal to 1: 4 with an aqueous solution of oligoamide proved to be the one giving the best results.

In the ^{1}H NMR analysis (Figure 78) the signal at 4.64 attributable to C**H**-OH is taken as a reference in the count of the integrals by placing it equal to 40 hydrogens as in the polydiethyleneamino-L-tartaramide not alkylated.

The signals related to methylene groups in the oligoamide chain at 0.98 (**C**$H_3CH_2CH_2CH_2N$), 1.42 (CH_3**C**$H_2CH_2CH_2N$) and 1.70-1.80 (CH_3CH_2**C**H_2CH_2N) ppm, are also present.

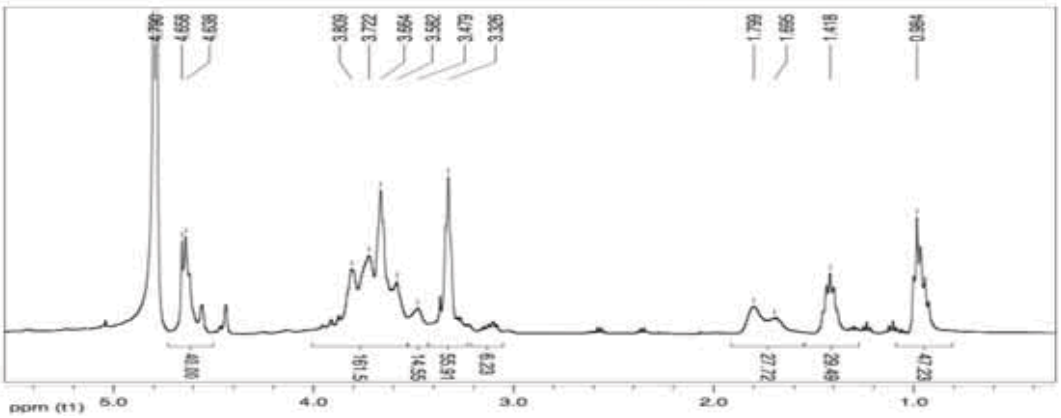

Figure 78: ^{1}H NMR spectrum in D_2O of the alkylated oligoamide after oxidation (Method 1)

gCOSY spectrum (Figure 79) confirms the attributions made for the signals in ^{1}H NMR spectrum, relative to C**H**$_3$CH$_2$CH$_2$CH$_2$N, CH$_3$C**H**$_2$CH$_2$CH$_2$N e CH$_3$CH$_2$C**H**$_2$CH$_2$N groups.

The CH$_3$CH$_2$CH$_2$C**H**$_2$N group, that can be identified thanks to coupling with near hydrogens, is in a wide range, between 3.12 and 3.80 ppm, according to the position of the alkyl group either on a non-oxidized or on an oxidized nitrogen.

Finally the coupling between the signal at 3.33 and at 3.66 ppm is present, related to the C**H**$_2$NH of the oligoamide chain in α position to C**H**$_2$NHCO.

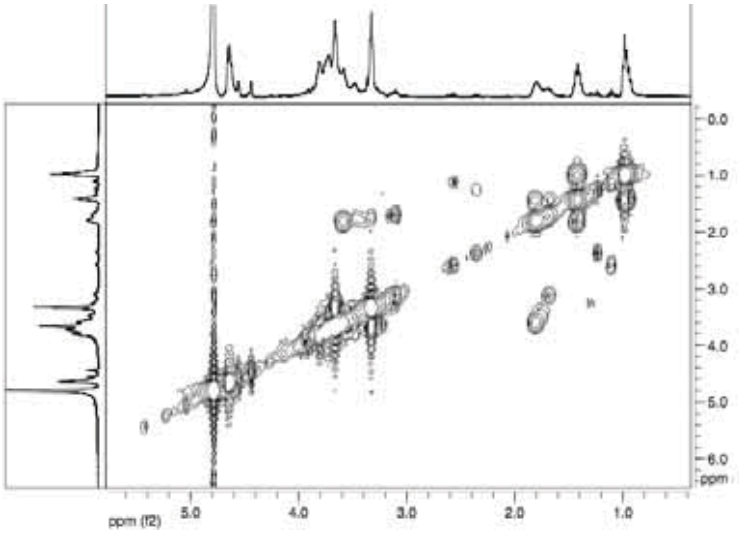

Figure 79: gCOSY spectrum in D$_2$O of the alkylated oligoamide after oxidation (Method 1)

In ^{13}C NMR (Figure 80) it is possible assign the signals of the substituent related to the **C**H$_3$CH$_2$CH$_2$CH$_2$N and the CH$_3$**C**H$_2$CH$_2$CH$_2$N at 12.9 and 19.1 ppm respectively. Moreover the signals at 174.7 and 72.4- 73.0 ppm are relative to the amide **C**=O and **C**H-OH groups respectively.

The signals at 35.8 and 47.3 ppm, unchanged compared to the starting compound, are those relating to the CH$_2$ in α position to the amide group and secondary amino group, respectively.

A decrease of the signals at 52.7 and 53.7 ppm is observed, related to the CH$_2$ in α position to the not-oxidized tertiary amino group in the substituent and in the oligoamide, whereas is present a new set a signals at 61- 62 ppm related to the CH$_2$ in α position to the oxidized nitrogen atoms.

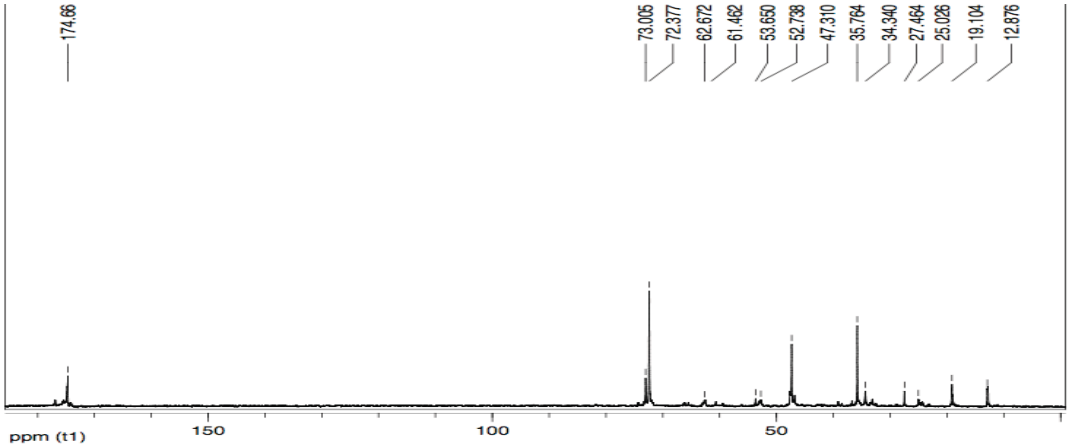

Figure 80: ^{13}C NMR spectrum in D_2O of the alkylated oligoamide after oxidation (Method 1)

gHSQC spectrum (Figure 81) is not useful to determine the structure of the molecule, because the spectrum is very complex.

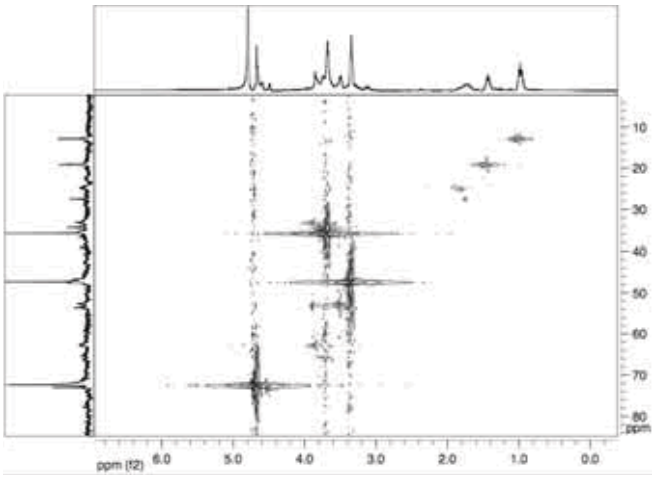

Figure 81: gHSQC spectrum in D_2O of the alkylated oligoamide after oxidation (Method 1)

Given the complexity of the system and the spectral resolution of the instrument, it is not possible to understand all the signals of the NMR spectrum, but the oxidation can be confirmed comparing the spectra collected before and after the reaction. Since ^{1}H NMR signals could not be used to evaluate the conversion of the oxidated product, this parameter was calculated considering ^{13}C NMR spectrum: an approximation was used, considering the same responsivity between the signals of the corresponding groups in the product before and after oxidation. With this approximation, the conversion results to be about 50%.

To try to push the reaction towards a higher degree of oxidation, a different oxidation method was tested, by combining the action of hydrogen peroxide with the presence of NH_4HCO_3 as described in literature[53].

4.3.1.11 Oxidation reaction (Method 2)

The oxidation reaction of the alkylated oligoamide (3) was carried out in the presence of an aqueous solution of H_2O_2 (30%) and NH_4HCO_3 (as oxidizing agents).

The oxidizing solution was prepared in a flask with one neck and left under stirring for 15 minutes, then the alkylate oligoamide was added (3). The reaction was carried out using a ratio oligoamide: H_2O_2 equal to 1: 5 for 24 hours.

At the end of the reaction, volatile products were removed from the mixture by distillation at reduced pressure at 50°C, obtaining a solid which was dried under reduced pressure at room temperature.

The products obtained in all the reactions were analyzed by NMR spectroscopy.

^{1}H NMR spectrum (Figure 82) confirms the presence of the signals at 0.98 ($CH_3CH_2CH_2CH_2N$), at 1.41 ($CH_3CH_2CH_2CH_2N$), and at 1.76 ($CH_3CH_2CH_2CH_2N$) with unchanged values respect to the alkylate product. The signal related to the $CH_3CH_2CH_2CH_2N$ is shifted respect to the same signal in the alkylated product, from 3.31 ppm to 3.37 ppm, thanks to the N-oxide formation.

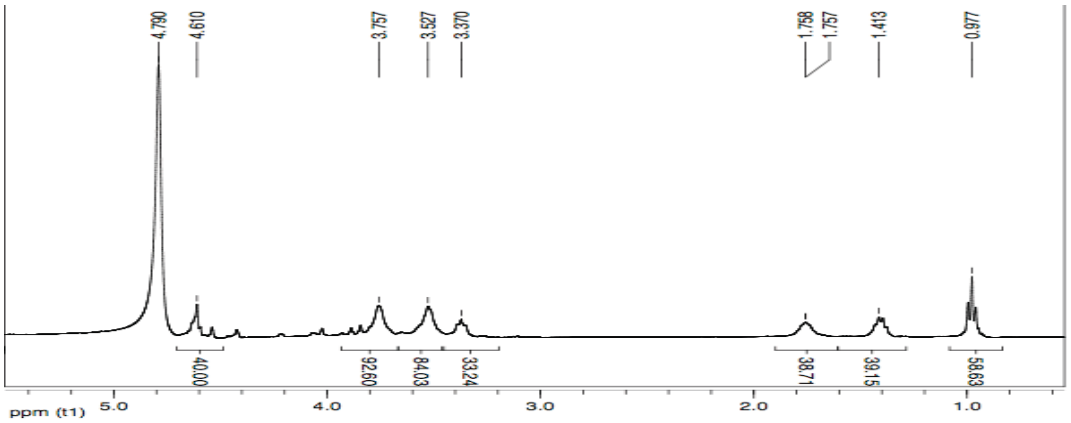

Figure 82: ^{1}H NMR spectrum in D_2O of the alkylated oligoamide after oxidation (Method 2)

In gCOSY spectrum (Figure 83) it is possible evaluate the couplings between the signal at 3.53 ppm to that at 3.76 ppm, related to the methylene group in α and β position to oxidized nitrogen atom (secondary or tertiary).

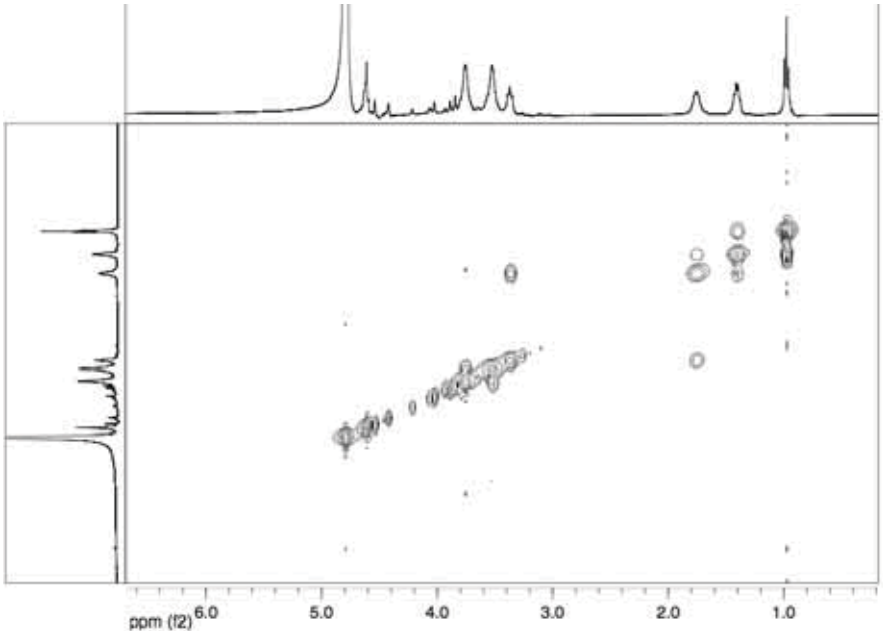

Figure 83: gCOSY spectrum in D_2O of the alkylated oligoamide after oxidation (Method 2)

^{13}C NMR spectrum (Figure 84) confirms the absence of the signals at about 47.0 and 34.0 - 36.0 ppm, that show the complete oxidation of secondary and tertiary amino groups. Other signals at 63.2 and 66.0 ppm and at 24.6 and 33.5 ppm (methylene groups in α and β position to N-oxide of the substituent and of the oligoamide) appear.

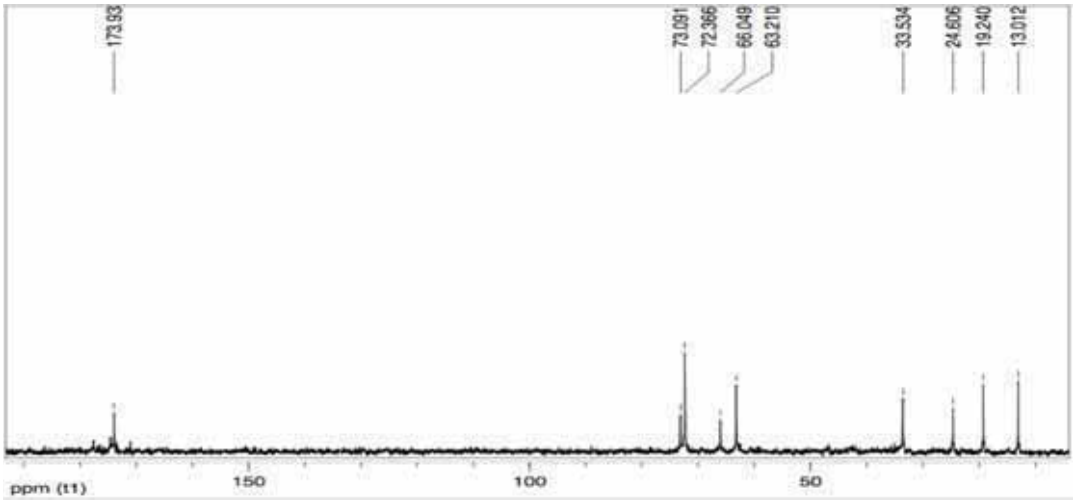

Figure 84: ^{13}C NMR spectrum in D_2O of the alkylated oligoamide after oxidation (Method 2)

On the base of gHSQC spectrum (Figure 85), according to correlations between hydrogens and carbons directly linked, it is possible to assign the signal at 66.0 ppm and that at 63.2 ppm to the carbon atoms linked to the tertiary nitrogen atoms and to the C**H**$_2$NO of the alkyl groups of the substituent and of oligoamide respectively.

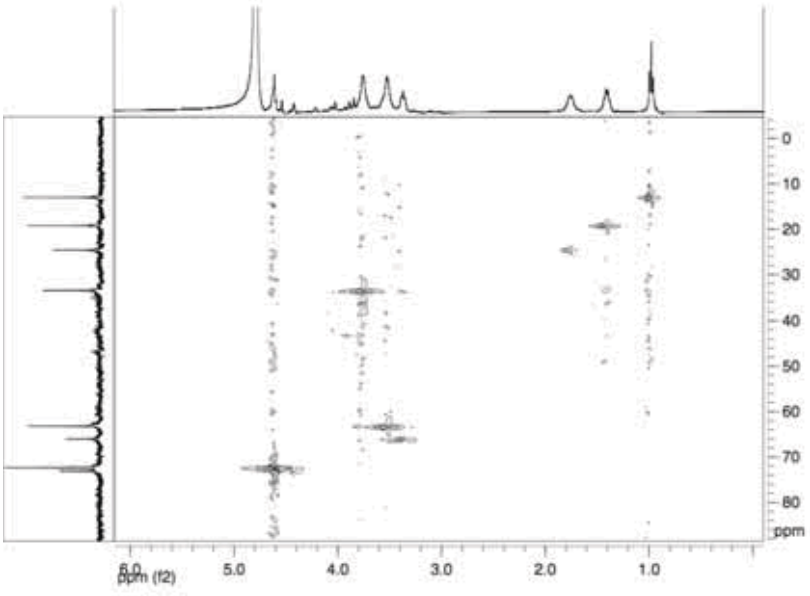

Figure 85: gHSQC spectrum in D_2O of the alkylated oligoamide after oxidation (Method 2)

Table 8: significant signals of ^{1}H NMR spectra of the products synthesized (400 MHz, δ, ppm, *D_2O*)

	Dicarboxylic moiety							Diamine moiety				
Product	C**H**-OH	H-4	H-2	H-3	H-5	H-5 end chain	H-1	C**H**$_2$NHCO	C**H**$_2$CH$_2$NHCO	N-R-N[a]	C**H**$_2$CH$_2$NH$_2$	C**H**$_2$NH$_2$
A	---	3.61	3.73	3.88	4.00-4.28	---	5.22	3.42	2.85	–	2.92	3.06
B	---	3.58	3.72	3.87	4.00-4.29	---	5.22	3.41	2.50-2.91	2.50-2.91	2.57	3.00
C	---	3.59	3.73	3.89	4.05-4.28	---	5.23	3.43	2.50-2.96	2.50- 2.96	2.51	3.05
D	---	3.57	3.72	3.87	4.00-4.29	---	5.20	3.29	1.74	2.65	N.D.	N.D.
E	---	3.57	3.72	3.87	4.00-4.29	---	5.20	3.29	1.72	2.61	N.D.	N.D.
F	4.57	---	---	---	---	---	---	3.41	2.79	---	---	2.99

B-F: -NH-(CH$_2$)$_2$-NH-(C**H**$_2$)$_2$-NH-(CH$_2$)$_2$-NH; C: -NH-(CH$_2$)$_2$-NH-(C**H**$_2$)$_2$-NH-(C**H**$_2$)$_2$-NH-(CH$_2$)$_2$-NH; D: -NHCH$_2$CH$_2$C**H**$_2$NHC**H**$_2$CH$_2$CH$_2$NH; E: -NHCH$_2$CH$_2$C**H**$_2$NH-(C**H**$_2$)$_2$NHC**H**$_2$CH$_2$CH$_2$NH.

Table 9: significant signals of ^{1}H NMR spectra of the products synthesized (400 MHz, δ, ppm, *D_2O*)

Prodotto	C**H**$_3$CH$_2$CH$_2$CH$_2$N	CH$_3$C**H**$_2$CH$_2$CH$_2$N	CH$_3$CH$_2$C**H**$_2$CH$_2$N	CH$_3$CH$_2$CH$_2$C**H**$_2$N	C**H**$_2$NH	CH$_3$CH$_2$CH$_2$C**H**$_2$NO	C**H**$_2$NO	C**H**$_2$N	C**H**$_2$NHCO near NH	C**H**$_2$NHCO near N	C**H**$_2$NHCO near NO	C**H**-OH
Alkylated oligoamide (1) e (2)	0.98	1.43	1.74	3.34	3.34	---	---	3.49	3.67	3.74	---	4.67
Alkylated oligoamide (3)	0.97	1.41	1.71	3.31	3.31	---	---	3.42	3.66	3.71	---	4.66
Oxidated oligomide (1)	0.98	1.42	1.70- 1.80	3.33	3.33	N.D.	N.D.	N.D.	3.66	N.D.	N.D.	4.64
Oxidated oligomide (2)	0.98	1.41	1.76	---	---	3.37	3.53	---	---	---	3.76	4.61

N.D.: not determined

Table 10: significant signals of ^{13}C NMR spectra of the products synthesized (50 MHz, δ, ppm, D_2O)

	Dicarboxylic moiety							Diamine moiety			
Product	**C**H-OH	C-4	C-2	C-3	C-5	C-1	C=O	**C**H_2NHCO	**C**H_2CH_2NHCO	N-R-N[a]	**C**H_2NH_2
A	---	71.6	70.5	72.1	72.1	94.6	171.3	37.8	47.0	---	N.D.
B	---	70.8	69.7	71.2	71.2	93.7	170.3	37.4	46.0 46.3	46.0 46.3	N.D.
C	---	71.5	70.4	71.9	71.9	94.3	170.9	38.3	46.9	46.9	N.D.
D	---	70.8	69.7	71.2	71.2	93.7	169.9	36.2	26.7	44.9	N.D.
E	---	70.9	69.8	71.3	71.3	93.7	169.9	36.4	27.0	45.0 46.3	N.D.
F	72.4	---	---	---	---	---	173.9	38.3	46.9	---	N.D.

B: -NH-$(CH_2)_2$-NH-(**C**$H_2)_2$-NH-$(CH_2)_2$-NH; C: -NH-$(CH_2)_2$-NH-(**C**$H_2)_2$-NH-(**C**$H_2)_2$-NH-$(CH_2)_2$-NH; D: -NHCH_2CH_2**C**H_2NH**C**$H_2CH_2CH_2$NH; E: -NHCH_2CH_2**C**H_2NH-(**C**$H_2)_2$-NH**C**$H_2CH_2CH_2$NH.

Table 11: significant signals of ^{13}C NMR spectra of the products synthesized (100 MHz, δ, ppm, D_2O)

Product	**C**$H_3CH_2CH_2CH_2$N	CH_3**C**$H_2CH_2CH_2$N	CH_3CH_2**C**H_2CH_2N	$CH_3CH_2CH_2$**C**H_2N	**C**H_2NH	$CH_3CH_2CH_2$**C**H_2NO	C**H**$_2$NO	**C**H_2N	C**H**$_2$NHCO near NH	C**H**$_2$NHCO near N	CONHC**H**$_2CH_2$NO	**C**H-OH	**C**=O
Alkylated oligoamide (1) e (2)	12.8	19.2	25.0	53.6	47.2	---	---	52.6	35.7	34.2	---	72.3 73.2	174.7
Alkylated oligoamide (3)	12.9	19.3	25.3	53.6	47.3	---	---	52.7	35.9	34.5	---	72.4, 73.1	174.6
Oxidated oligomide (1)	12.9	19.1	25.0	53.7	47.3	61.5- 62.7		52.7	35.8	34.3	---	72.4, 73.0	174.7
Oxidated oligomide (2)	13.0	19.2	24.6	---	---	66.0	63.2	---	---	---	33.5	72.4- 73.1	173.9

4.4 Conclusions

In this work a study on functionalized water soluble polyamides of type (m, n), that has been carried on for the last years in a laboratory of the Chemistry Department of the University of Florence, was continued. One of the products synthesized was subjected to structural modifications (alkylation and oxidation reactions) to use it as KHI in oil and gas pipelines.

The interest about functionalized oligoamides, that had been studied for testing their use as consolidant of waterlogged wood, has been then extended to other possible applications in the field of industrial formulations. The class of polyamides is in fact characterized by a great versatility and high chemical resistance, and this allows to use these materials in various industrial sectors. Besides these aspects, the use of monomers directly derived from renewable natural resources and low cost is an added value.

The results obtained in this research have allowed to expand the library of functionalized polyamide compounds deriving from L-tartaric acid and α,α'- trehaluronic acid, synthesizing oligoamides with different molecular structure.

The polyamides, all water soluble, were synthesized through polycondensation in solution at 80°C, using five aliphatic polyamines (diethylenetriamine; triethylenetetramine; tetraethylenepentamine; bis-(3-aminopropyl)amine; 1,2-bis-(3-aminopropyl)aminoethane) with -NH- bridges along the chain.

Polydiethyleneamino-L-tartaramide (F) underwent alkylation with bromobutane of secondary amine groups and subsequent oxidation of the tertiary amine groups (and of the remaining secondary amino groups).

Various methods and reaction conditions have been studied to perform the alkylation reaction: the one that led to the higher degree of substitution was the one performed in a Sovirel® tube, using methanol as solvent, with a molar ratio between oligoamide and bromobutane equal to 1: 2, in the presence of $CaCO_3$, at 80°C for a time of 48 hours. In these conditions, a 70-80% degree of substitution of the amino groups was obtained.

The subsequent oxidation reaction was conducted using two different methods; the first leads to a partial oxidation of the secondary and tertiary amino groups with a conversion of about 50% in the presence of an aqueous solution of H_2O_2.

The second method, using an aqueous solution of H_2O_2 with the addition of NH_4HCO_3, allowed the complete oxidation of the secondary and tertiary amine groups without having to destroy the excess hydrogen peroxide.

The chemistry of this method, described by Balagam and Richardson[53], is associated with the labile hydration/dehydration equilibrium of carbon dioxide in water. Authors hypothesized that peroxymonocarbonate is be formed via a labile pre-equilibrium reaction between bicarbonate ion and hydrogen peroxide and subsequently it oxidizes the amine (secondary and tertiary) to amine oxide.

$$H_2O_2 + HCO_3^- \rightleftharpoons HCO_4^-$$

$$HCO_4^- + R_3N \rightleftharpoons R_3NO + HCO_3^-$$

Moreover the use of NH_4HCO_3 as the source of HCO^{3-} allows higher catalyst concentration than the use of alkali metal salts, before solubility saturation effects become apparent. In addition, NH_4HCO_3 conveniently decomposes to NH_3, CO_2, and H_2O, allowing the catalyst to be removed by evaporation so that it is not necessary to heat the mixture at 70°C to decompose the oxidizing agent in excess, as done when only hydrogen peroxide is used. In this way a product with a higher degree of oxidation is obtained, using a step less than when using only H_2O_2.

These products (70-80% alkylated oligoamide, 50% oxidized oligoamide and totally oxidized oligoamide), will be used in the next months in the Norwegian University of Stavanger, within a scientific collaboration with Prof. Kelland, to test the properties as KHIs.

4.5 Experimental

4.5.1 Materials

4.5.1.1 Solvents

- milliQ water
- 1,4-dioxane, product Aldrich, 99% pure
- Isopropanol, product Aldrich, 99,5% pure
- Methanol, product Normapur, 99.9% pure
- Ethanol, So. Co. Fi., 96% pure

4.5.1.2 Reagents

- L-tartaric acid, product Aldrich, 99% pure
- Boric acid, product Aldrich, 99,5% pure
- Amberlite IR-120H, product Aldrich
- α,α'-trehalose dihydrate, product Aldrich, 99% pure
- 2,2,6,6-Tetramethylpiperidine-1-oxyl(TEMPO), product Aldrich, 98% pure
- Triethylamine, product Carlo Erba, 97% pure
- Acid solution of vanillin for TLC:

  3 g of vanillin are dissolved in a solution of 4 ml of H_2SO_4 (conc) and 250 ml of ethanol.
- Boric acid, product Aldrich, 99,5% pure
- Bis(3-aminopropyl)amine, product Aldrich, 98% pure
- 1,2-bis-(3-aminopropyl)aminoethane, product Aldrich, 94% pure
- Diethylenetriamine, product Aldrich, 99% pure
- Tetraethylenepentamine, product Aldrich, tecnical grade
- Triethylenetetramine, product Aldrich, 60% pure
- $CaCO_3$: product Carlo Erba, 99.5% pure
- H_2O_2 (30%): product Aldrich
- Bromobutane: product Aldrich, 99% pure
- NH_4HCO_3, product Aldrich, 99% pure

4.5.2 Instruments

4.5.2.1 NMR spectroscopy

^{1}H NMR, ^{13}C NMR, gCOSY and gHSQC spectra were recorded with a Varian Mercury Plus 400 spectrometer and a Varian VXR 200 spectrometer, working at 399.921 MHz and 199.985 MHz, respectively. All spectra are reported in ppm and referred to TMS as internal standard. Spectra elaboration was performed with the software Mestre-C 4.3.2.0. Solvents used (D_2O, $CDCl_3$) are produced by Aldrich Co.

4.5.2.2 FT IR spectroscopy

FT IR spectra were recorded with a Shimadzu FT-IR-8400S model, and elaborated with the Spectrum v.3.0202. Solutions were analyzed using KBr or CaF_2 round cell windows, after deposition and evaporation of solvent. Spectra of solid samples were recorded as KBr pellets.

4.5.3 Syntheses of the products

4.5.3.1 Oligodietyleneamino-α,α'- trehaluronamide (A)

Into a Sovirel tube, triethylamine (16.4 mg, 0.162 mmol) is added, under nitrogen atmosphere and under continuous stirring to a methanol solution (2.5 mL) of dimethyl-α,α'- trehaluronate (238.8 mg, 0.6 mmol). Diethylenetriamine (61.9 mg, 0.6 mmol) is added and the mixture is allowed to react at 80°C for 7 days. After cooling to room temperature, the mixture is filtered on a büchner funnel and the brown solid obtained is washed with methanol and dried at room temperature (280.3 mg, 93.2% yield).

^{1}H-NMR (D_2O, 400 MHz, Table 8): signals at δ 2.85 ppm (m, 4H, C**H**$_2$NH), 2.92 ppm (m, 4H, C**H**$_2$CH$_2$NH$_2$), 3.06 ppm (m, 4H, C**H**$_2$NH$_2$), 3.42 ppm (m, 4H, C**H**$_2$NHCO), 3.61 ppm (m, 2H, H_4, H_4'), 3.73 ppm (m, 2H, H_2, H_2'), 3.88 ppm (m, 2H, H_3, H_3'), 4.00-4.28 ppm (m, 2H, H_5, H_5'), 5.22 ppm (m, 2H, H_1, H_1').

^{13}C-NMR (D_2O, 50 MHz, Table 10): signals at δ 37.8 ppm (**C**H$_2$NHCO), 47.0 ppm (**C**H$_2$NH), 70.5 ppm (C_2, C_2'), 71.6 ppm (C_4, C_4') e 72.1 ppm (C_3, C_3',C_5, C_5'), 94.6 ppm (C_1, C_1'), 171.3 ppm (**C**ONH).

FT-IR (KBr pellet): peaks at 1651 cm^{-1} (vs, C=O amide stretching), 1550 cm^{-1} (s, N-H bending), 1111, 1065, 1029 cm^{-1} (s, C-O stretching).

4.5.3.2 Oligotriethylendiamino-α,α'- trealuronamide (B)

Into a Sovirel tube, triethylamine (16.4 mg, 0.162 mmol) is added, under nitrogen atmosphere and continuous stirring, to a methanol solution (2.5 mL) of dimethyl-α,α'- trehaluronate (238.8 mg, 0.6 mmol). Triethylenetetramine (87.74 mg, 0.6 mmol) is added and the mixture is allowed to react at 80°C for 7 days. After cooling to room temperature, the mixture is filtered on a büchner funnel and the brown solid obtained is washed with methanol and dried at room temperature (284 mg, 87% yield).

^{1}H-NMR (D_2O, 400 MHz, Table 8): signals at δ 2.57 ppm (m, 2H, C**H**$_2$CH$_2$NH$_2$), 2.50- 2.91 ppm (m, 8H, internal C**H**$_2$NH), 3.00 ppm (m, 4H, C**H**$_2$NH$_2$), 3.41 ppm (m, 4H, C**H**$_2$NHCO), 3.58 ppm (m, 2H, H_4, H_4'), 3.72 ppm (m, 2H, H_2, H_2'), 3.87 ppm (m, 2H, H_3, H_3'), 4.00- 4.29 ppm (m, 2H, H_5, H_5'), 5.22 ppm (m, 2H, H_1, H_1').

^{13}C-NMR (D_2O, 50 MHz, Table 10): signals at δ 37.4 ppm (**C**H$_2$NHCO), 46.0- 46.3 ppm (**C**H$_2$NH), 69.7 (C_2, C_2'), 70.8 ppm (C_4, C_4'), 71.2 ppm (C_3, C_3', C_5, C_5'), 93.7 ppm (C_1, C_1'), 170.3 ppm (**C**ONH).

FT-IR (KBr pellet): peaks at 1651 cm^{-1} (vs, C=O amide stretching), 1550 cm^{-1} (s, N-H bending), 1112, 1065, 1025 cm^{-1} (s, C-O stretching).

4.5.3.3 Oligotetraethylenpentamino-α,α'- trehaluronamide (C)

Into a Sovirel tube, triethylamine (16.4 mg, 162 mmol) is added, under nitrogen atmosphere and under continuous stirring to a methanol solution (2.5 mL) of dimethyl-α,α'- trehaluronate (238.8 mg, 0.6 mmol). Tetraethylenepentamine (113.6 mg, 0.6 mmol) is added and the mixture is allowed to react at 80°C for 7 days. After cooling to room temperature, the mixture is filtered on a büchner funnel and the brown solid obtained is washed with methanol and dried at room temperature (324.2 mg, 92% yield).

^{1}H-NMR (D_2O, 400 MHz, Table 8): δ 2.50-2.96 (m, 12H, internal C**H**$_2$NH), 2.51 (m, 4H, C**H**$_2$CH$_2$NH) 3.05 (m, 4H, C**H**$_2$NH$_2$), 3.43 (m, 4H, C**H**$_2$NHCO), 3.59 (m, 2H, H_4,H_4'), 3.73 (m, 2H, H_2,H_2'), 3.89 (m, 2H, H_3, H_3'), 4.05- 4.28 ppm (2H, H_5, H_5'), 5.23 ppm (2H, H_1, H_1').

^{13}C-NMR (D_2O, 50 MHz, Table 10): δ 38.3 ppm (**C**H$_2$NHCO), 46.9 ppm (**C**H$_2$NH), 70.4 ppm (C_2, C_2'), 71.5 (C_4, C_4'), 71.9 ppm (C_3, C_3', C_5, C_5'), 94.3 ppm (C_1, C_1'), 170.9 ppm (**C**ONH).

FT-IR (KBr pellet): peaks at 1662 cm^{-1} (vs, C=O amide stretching), 1550 cm^{-1} (s, N-H bending), 1108, 1065, 1029 (s, C-O stretching) cm^{-1}.

4.5.3.4 Oligo-dipropylenamino-α,α'- trehaluronamide (D)

Into a Sovirel tube, triethylamine (16.4 mg, 162 mmol) is added, under nitrogen atmosphere and continuous stirring, to a methanol solution (2.5 mL) of dimethyl-α,α'- trehaluronate (238.8 mg, 0.6 mmol). Bis(3-aminopropyl)amine (78.7 mg, 0.6 mmol) is added and the mixture is allowed to react at 80°C for 7 days. After cooling to room temperature, the mixture is filtered on a on a büchner funnel and the brown solid obtained is washed with methanol and dried at room temperature (285.8 mg, 90% yield).

^{1}H-NMR (D_2O, 400 MHz, Table 8): signals at δ 1.74 ppm (m, 4H, C**H**$_2$CH$_2$NHCO), 2.65 ppm (m, 4H, **C**H$_2$NH), 3.29 ppm (m, 4H, C**H**$_2$NHCO), 3.57 ppm (m, 2H, H_4, H_4'), 3.72 ppm (m, 2H, H_2, H_2'), 3.87 ppm (m, 2H, H_3, H_3'), 4.00- 4.29 ppm (m, 2H, H_5, H_5'), 5.20 ppm (m, 2H, H_1, H_1').

^{13}C-NMR (D_2O, 50 MHz, Table 10): signals at δ 26.7 ppm (**C**H$_2$CH$_2$NHCO), 36.2 ppm (**C**H$_2$NHCO), 44.9 ppm (**C**H$_2$NH), 69.7 ppm (C_2, C_2'), 70.8 ppm (C_4, C_4'), 71.2 ppm (C_3, C_3', C_5, C_5'), 93.7 ppm (C_1, C_1'), 169.9 ppm (**C**ONH).

FT-IR (KBr pellet): peaks at 1654 cm^{-1} (vs, C=O amide stretching), 1550 cm^{-1} (s, N-H bending), 1108, 1068, 1025 cm^{-1} (s, C-O stretching).

4.5.3.5 Oligo-bis(propylenamino)ethane-α,α'- trehaluronamide (E)

Into a Sovirel tube, triethylamine (16.4 mg, 0.162 mmol) is added, under nitrogen atmosphere and under continuous stirring to a methanol solution (2.5 mL) of dimethyl-α,α'- trehaluronate (238.8 mg, 0.6 mmol). 1,2-bis-(3-aminopropyl)aminoethane (104.6 mg, 0.6 mmol) is added and the mixture is allowed to react at 80°C for 7 days. After cooling to room temperature, the mixture is filtered on a on a büchner funnel and the brown solid obtained is washed with methanol and dried at room temperature (400.5 mg, 92.2 % yield).

^{1}H-NMR (D_2O, 400 MHz, Table 8): signals at δ 1.72 (m, 4H, C**H**$_2$CH$_2$NHCO), 2.61 (m, 8H, internal -C**H**$_2$-), 3.29 (m, 4H, C**H**$_2$NHCO), 3.57 (m, 2H, H_4, H_4'), 3.72 (m, 2H, H_2, H_2'), 3.87 (m, 2H, H_3, H_3'), 4.00-4.29 (m, 2H, H_5, H_5'), 5.20 ppm (m, 2H, H_1, H_1').

^{13}C-NMR (D_2O, 50 MHz, Table 10): signals at δ 27.0 (**C**H$_2$CH$_2$NHCO), 36.4 (**C**H$_2$NHCO), 45.0-46.3 ppm (**C**H$_2$NH), 69.8 (C_2, C_2'), 70.9 (C_4, C_4'), 71.3 (C_3, C_3', C_5, C_5'), 93.7 (C_1, C_1'), 169.9 ppm (**C**ONH).

FT-IR (KBr pellet): peaks at 1658 cm^{-1} (vs, C=O amide stretching), 1550 cm^{-1} (s, N-H bending), 1108, 1065, 1025 cm^{-1} (s, C-O stretching).

4.5.3.6 Oligodiethylenamino-L-tartartaramide (F)

Into a Sovirel tube, triethylamine (110.3 mg, 1.09 mmol) is added, under nitrogen atmosphere and under continuous stirring to a methanol solution (6.5 mL) of dimethyl-α,α'- tartrate (720 mg, 4.04 mmol). Diethylenetriamine (416.8 mg, 4.04 mmol) is added and the mixture is allowed to react at 80°C for 2 days. After cooling to room temperature, the mixture is filtered on a on a büchner funnel and the brown solid obtained is washed with methanol and dried at room temperature (796.9 mg, 70.1% yield).

^{1}H-NMR (D_2O, 400 MHz, Table 8): signals at δ 2.79 (m, 4H, CH$_2$NH), 2.99 (m, 4H, CH$_2$NH$_2$), 3.41 (m, 4H, CH$_2$NHCO), 4.57 ppm (m, 2H, CHOH).

^{13}C-NMR (D_2O, 100 MHz, Table 10): signals at δ 38.3 (**C**H$_2$NHCO), 46.9 (**C**H$_2$NH), 72.4 (**C**H-OH), 173.9 ppm (**C**ONH).

FT IR (KBr pellet): peaks at 1650 (vs, CO amide stretching), 1540 (vs, NH amide bending), 1135, 1072 (s, C-O stretching).

All alkylation reactions and oxidation reactions were referred to an oligoamide with DP equal to 20, to uniform the syntheses. In real cases, the functionalized oligoamides DP can be vary in a little range.

4.5.3.7 Alkylation reaction with bromobutane (Method 1)

Into a Sovirel® tube, a solution of bromobutane (308.3 mg, 2.25 mmol) in methanol (0.7 mL) is added, under nitrogen atmosphere and under continuous stirring to olidiethyleneamino-L-tartaramide (200 mg, 0.045 mmol), using a ratio oligoamide: bromobutane equal to 1:2. The mixture is allowed to react at 80°C for 24 and 48 hours. After cooling to room temperature, the mixture is distilled at reduced pressure and the solid obtained is dried at reduced pressure and room temperature (DS: 28-30%).

The reaction was repeated with ratio oligoammide: bromobutane equal to 1: 3 (bromobutane: 3.38 mmol), for times of 24 and 48 hours (DS: 28-30%).

^{1}H-NMR (D_2O, 400 MHz, Table 9): signals at δ 0.98 (m, 3H, C**H**$_3$CH$_2$CH$_2$CH$_2$N), 1.43 (m, 2H, CH$_3$C**H**$_2$CH$_2$CH$_2$N), 1.74 (m, 2H, CH$_3$CH$_2$C**H**$_2$CH$_2$N), 3.34 (m, 2H, CH$_3$CH$_2$CH$_2$C**H**$_2$N, 4H, C**H**$_2$NH), 3.49 (m, 4H, C**H**$_2$N), 3.67, 3.74 (m, 4H, C**H**$_2$NHCO), 4.67 ppm (m, 2H, -C**H**OH).

^{13}C-NMR (D_2O, 100 MHz, Table 11): signals at δ 12.8 (**C**H$_3$CH$_2$CH$_2$CH$_2$N), 19.2 (CH$_3$**C**H$_2$CH$_2$CH$_2$N), 25.0 (CH$_3$CH$_2$**C**H$_2$CH$_2$N), 34.2, 35.7 (C**H**$_2$NHCO), 47.2 (C**H**$_2$NH), 52.6 (C**H**$_2$N), 53.6 (CH$_3$CH$_2$CH$_2$**C**H$_2$N) 72.3, 73.2 (**C**HOH), 174.7 ppm (**C**ONH).

4.5.3.8 Alkylation reaction with bromobutane (Method 2)

Into a two-neck flask with condenser, a solution of bromobutane (308.3 mg, 2.25 mmol) in ethanol (0.7 mL) is added, under nitrogen atmosphere and continuous stirring, to 200 mg olidiethyleneamino-L- tartaramide (0.045 mmol). After the addition of $CaCO_3$ (112.6 mg, 1.125 mmol), the mixture is reacted at 80 ° C for 24 and 48 hours under magnetic stirring. At the end, the reaction is cooled and distilled at reduced pressure. The solid residue is dissolved in water, and the solution is distilled at reduced pressure, washed with methanol and dried (DS: 20-25%).

The reaction was repeated with ratio oligoammide: bromobutane equal to 1: 3 (bromobutane: 3.38 mmol), for times of 24 and 48 hours (DS: 20-25%).

^{1}H-NMR (D_2O, 200 MHz, Table 9): signals at δ 0.87 (m, 3H, C**H**$_3$CH$_2$CH$_2$CH$_2$N), 1.28 (m, 2H, CH$_3$C**H**$_2$CH$_2$CH$_2$N), 1.46 (m, 2H, CH$_3$CH$_2$C**H**$_2$CH$_2$N), 2.70- 3.05 (m, 2H, CH$_3$CH$_2$CH$_2$C**H**$_2$N, 4H, C**H**$_2$NH, 4H, C**H**$_2$N), 3.35- 3.60 (m, 4H, C**H**$_2$NHCO), 4.56 ppm (m, 2H, -CH-OH).

^{13}C-NMR (D_2O, 50 MHz, Table 11): signals at δ 12.8 (**C**$H_3CH_2CH_2CH_2N$), 19.2 (CH_3**C**$H_2CH_2CH_2N$) e 25.0 (CH_3CH_2**C**H_2CH_2N), 34.2, 35.7 (C**H**$_2$NHCO), 47.2 (C**H**$_2$NH), 52.6, 53.6 (C**H**$_2$N), 72.3, 73.2 (-**C**HOH), 174.7 ppm (**C**ONH).

4.5.3.9 Alkylation reaction with bromobutane (Method 3)

Into a Sovirel® tube, a solution of bromobutane (308.3 mg, 2.25 mmol) in methanol (0.7 mL) is added, under nitrogen atmosphere and under continuous stirring to olidiethyleneamino-L-tartaramide (200 mg, 0.045 mmol). After the addition of $CaCO_3$ (112.6 mg, 1.125 mmol), the mixture is reacted at 80°C for 48 hours under magnetic stirring. At the end, the reaction is cooled and distilled at reduced pressure. The solid residue is dissolved in water, and the solution is distilled at reduced pressure, washed with methanol and dried (DS: 70- 80%).

^{1}H-NMR (D_2O, 400 MHz, Table 9): signals at δ 0.97 (m, 3H, C**H**$_3CH_2CH_2CH_2N$), 1.41 (m, 2H, CH_3C**H**$_2CH_2CH_2N$), 1.71 (m, 2H, CH_3CH_2C**H**$_2CH_2N$), 3.31 (m, 2H, $CH_3CH_2CH_2$C**H**$_2$N, 4H, -C**H**$_2$NH-), 3.42 (m, 4H, C**H**$_2$N), 3.66, 3.71 (m, 4H, C**H**$_2$NHCO), 4.65 ppm (m, 2H, C**H**OH).

^{13}C-NMR (D_2O, 100 MHz, Table 11): signals at δ 12.9 (**C**$H_3CH_2CH_2CH_2N$), 19.3 (CH_3**C**$H_2CH_2CH_2N$), 25.3 (CH_3CH_2**C**H_2CH_2N), 34.5, 35.9 (C**H**$_2$NHCO), 47.3 (C**H**$_2$NH), 52.7 (C**H**$_2$N), 53.6 ($CH_3CH_2CH_2$**C**H_2N), 72.4, 73.1 (**C**HOH), 174.7 ppm (**C**ONH).

4.5.3.10 Oxidation reaction (Method 1)

A solution of alkylated oligoamide (3) (500 mg, 0.092 mmol) in milliQ water (1.1 mL) is put in a one neck flask. After adding H_2O_2 (30%) (169.1 mL, 1.656 mmol), the mixture is reacted at room temperature (25°C) for 24 hours.

At the end of the reaction the mixture is heated at 70°C for 1 hour with a condenser, then distilled under reduced pressure (T: 50°C); the solid obtained is dried and characterized by NMR analysis.

The reaction was repeated with ratio oligoamide: H_2O_2 equal to 1: 2 (H_2O_2: 3.31 mmol), 1: 4 (H_2O_2: 3.31 mmol) and 1: 6 (H_2O_2: 9.94 mmol); in all case, oxidation of about 50%.

^{1}H-NMR (D_2O, 400 MHz, Table 9): signals at δ 0.98 (m, 3H, C**H**$_3CH_2CH_2CH_2N$), 1.42 (m, 2H, CH_3C**H**$_2CH_2CH_2N$), 1.70-1.80 (m, 2H, CH_3CH_2C**H**$_2CH_2N$), 3.33 (m, 2H, $CH_3CH_2CH_2$C**H**$_2$N, 4H, CH_2NH), 3.66 (m, 4H, C**H**$_2$NHCO), 4.64 ppm (m, 2H, C**H**OH).

^{13}C-NMR (D_2O, 100 MHz, Table 11): signals at δ 12.9 (**C**$H_3CH_2CH_2CH_2N$), 19.1 (CH_3**C**$H_2CH_2CH_2N$), 25.0 (CH_3CH_2**C**H_2CH_2N), 34.3, 35.8 (C**H**$_2$NHCO), 47.3 (**C**H_2NH), 52.7 (**C**H_2N), 53.4 ($CH_3CH_2CH_2$**C**H_2N) 61.5, 62.7 (**C**H_2NO, $CH_3CH_2CH_2$**C**H_2NO), 72.4- 73.0 (-**C**HOH), 174.7 ppm (**C**ONH).

4.5.3.11 Oxidation reaction (Method 2)

A solution of H_2O_2 (30%) (0.846 mL, 8.28 mmol) in milliQ water (9.1 mL) is added to NH_4HCO_3 (327.06 mg, 4.14 mmol) in a one neck flask. After the addition of the alkylated oligoamide (3) (500 mg, 0.092 mmol), the mixture is reacted at room temperature (25°C) for 24 hours.

At the end of the reaction the product is distilled under reduced pressure (T: 50°C), obtaining a white solid, dried and characterized by NMR analysis (oxidation: 100%).

^{1}H-NMR (D_2O, 400 MHz, Table 9): signals at δ 0.98 (m, 3H, C**H**$_3$CH$_2$CH$_2$CH$_2$NO), 1.41 (m, 2H, CH$_3$C**H**$_2$CH$_2$CH$_2$NO), 1.76 (m, 2H, CH$_3$CH$_2$C**H**$_2$CH$_2$NO), 3.37 (m, 2H, CH$_3$CH$_2$CH$_2$C**H**$_2$NO), 3.53 (m, 4H, -C**H**$_2$NO), 3.76 (m, 4H, C**H**$_2$NHCO), 4.61 ppm (m, 2H, C**H**OH).

^{13}C-NMR (D_2O, 100 MHz, Table 11): signals at δ 13.0 (**C**H$_3$CH$_2$CH$_2$CH$_2$NO), 19.2 (CH$_3$**C**H$_2$CH$_2$CH$_2$NO), 24.6 (CH$_3$CH$_2$**C**H$_2$CH$_2$NO), 33.5 (C**H**$_2$NHCO), 63.2 (CH$_2$NO), 66.0 (CH$_3$CH$_2$CH$_2$**C**H$_2$NO), 72.4- 73.1 (**C**HOH), 173.9 ppm (**C**ONH).

5 Biobased oligoamides based on tartaric L-acid and L-lysine.

5.1 Choice of natural diamines for the synthesis of new oligoamides

Many polyamides and oligoamides present in literature[31,24,25,22,23,28,54,29,30]as well as those prepared in our laboratories, are synthesized using acids having natural origin and synthetic diamines.

To synthetize new oligoamides, completely derived from renewable sources, the possibility of replacing diamines with other products that are derived from natural sources was evaluated.

A suitable class of compounds is the one of basic amino acids, thanks to the presence of two amino groups in the chain; 3 out of the 20 natural amino acids are included in this category: lysine, histidine and arginine (Figure 86).

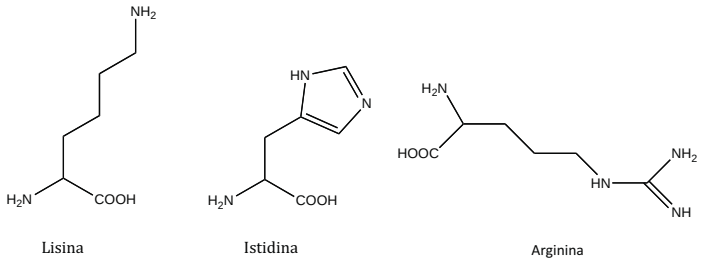

Figure 86: basic amino acids

Among these amino acids, the one with the best characteristics, in relation to the arrangement of the amino groups in the structure and complexity of the final molecule, is L-lysine (Figure 87), an amino acid which is industrially produced by fermentation.

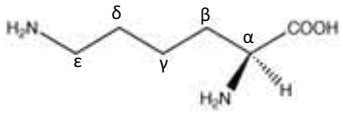

Figure 87: L-lysine structure

Lysine is an essential amino acid, polar, with chiral structure, having a R group constituted by an aliphatic chain that terminates with an amino group.

In literature, lysine is reported in several works as a reagent for new materials, discussed below, mainly in the formation of **2,5-diketopiperazinic structures** but also in the **polymers synthesis**.

5.1.1 2,5-diketopiperazines

Several amino acids can be used in the formation of 2,5-diketopiperazine structures (Figure 88), which are highly polar compounds, with symmetrical rings having side chains functionalized based on the starting amino acid. According to the nature of R group, diketopiperazines may contain aliphatic, aromatic, sulfur or amino groups. Out of simplicity, in this chapter they will be simply referred to as "diketopiperazine".

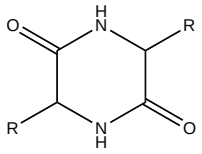

Figure 88: 2,5-diketopiperazine structure

The first work about the synthesis of diketopiperazines based on L-lysine date back to the beginning of 20th century, described by Fischer and Suzuki (1905) who obtained them heating DL-lysine methyl ester at 100°C and assumed to have obtained the diketopiperazine structure; Adamson[55], many years later (1943), showed that the substance obtained by Fischer contained at least 40% of the volatile intramolecular anhydride of lysine (Figure 89). Katchalski[56] in 1946, in order to prevent intramolecular anhydridization, protected ε-amino group of lysine by Bergmann's method, introducing a carbobenzoxy group. ε-carbobenzoxy-L-lysine methyl ester was liberated from the corresponding hydrochloride and was converted to ε,ε'-dicarbobenzoxylysine anhydride by eating at 100°C. The two carbobenzoxy groups were removed by reduction through the procedure used by Harington and Mead.

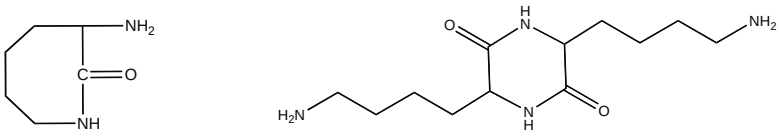

Figure 89: intramolecular anhydride (left) and diketopiperazine (right) of L-lysine

An interesting study on this type of structures was carried out by Ishibashi et al.[57] where, to estimate the steric distance between sites determinant for the bitter taste in peptides, some cyclic dipeptides, amino acid anilides, amino acid cyclohexylamides and benzoyl amino acids, were synthesized and their tastes were evaluated.

The diketopiperazine ring of cyclic dipeptides acted as a bitter taste determinant site due to its hydrophobicity.

23 cyclic dipeptides and corresponding linear dipeptides were synthetized and their tastes were compared. Both cyclic and linear products containing neutral amino acids (glycine and alanine) were tasteless; cyclic dipeptides composed by valine and glycine were bitter, while the corresponding linear peptides had no bitterness or were only slightly bitter. All cyclic and linear dipeptides containing leucine, isoleucine and phenylalanine, typical hydrophobic amino acids, were considerably bitter, but the bitter taste of cyclic dipeptides was more intense than the one of linear dipeptides. This behaviour can be explained considering that hydrophobic groups of the peptide bond on mouth's bitter taste receptor. According to the results obtained, authors demonstrate that the intensity of bitterness is dependent on the features of the monomer constituting the peptide and on the distance between different units.

Borthwick[58] in 2012 publshed a review on 2,5-diketopiperazines synthesis, their reactions and function.

5.1.2 Polymers based on amino acids.

In literature, there are several papers dealing with polymers based on amino acids[59–61], used in a wide application range[62–64], from that of standard plastic materials to the biomedical field. A polymer class largely used for the latter is that of the poly(ester-amides)[65–68] and polyamides because they can maintain the typical properties of nylons, becoming also biocompatible and biodegradable, according to constituting monomers.

Gachard et al.[64] in 1997 described the synthesis of polyamides based on two natural monomers, L-lysine and L-aspartic acid; both the monomers were protected to avoid secondary reactions. The products obtained were subjected to enzymatic or hydrolytic degradation, converting the polymers into metabolizable compounds. Consequently, these products could be used in biomedical field as new materials for sutures and drug-delivery systems.

Akerlund[69] synthesised high-melting point polymers with heterocyclic backbone units from common amino acids, with properties and cost similar to the common industrial nylons. Acids were first converted to methyl ester salts, that were dimerized to form diketopiperazines, which were polymerized in solution. Aspartic acid, serine, lysine, glycine, and tyrosine were used as starting materials for the diketopiperazines. Aromatic and aliphatic comonomers were used. Thus, authors demonstrated the technical feasibility of producing strong, durable resins from abundant domestic resources. These resins showed great potential for high-performance polymers to be used in films, fibers, and composites.

In a paper by Terada[70], aspartic and glutamic acid-based diketopiperazines, *cyclo*(l-asparaginyl-l-asparaginyl) (DKPD) and *cyclo*(l-glutaminyl-l-glutaminyl) (DKPE) were synthesized. Polycondensation of DKPD and DKPE with α,α′-dibromoxylenes was carried out using K_2CO_3 as a base in DMF to obtain polymers with weight-average molecular weights (M_w) of 1100–3500 Da. Furthermore, polycondensation of DKPE with various diamines was carried out using 4-[4,6-dimethoxy-1,3,5-triazin-2-yl]-4-methylmorpholinium chloride as a condensation agent in DMF to obtain polymers with M_w of 1200–4100 Da. The polymers were insoluble in common organic solvents except DMF.

Alborzi et al.[71] synthesised L-lysine hydrochloride-derived poly (amide-imide)s, through microwave-assisted polycondensation. These polymers have inherent viscosities in the range of 0.23–0.66 dl g^{-1}, display optical activity from +8.02 to +15.11 (as there is no regioselectivity between alpha and epsilon amino groups of the chiral diacid during the polymerization step, therefore random orientation of diacid moieties along the polymer backbone can be predicted and the concept of ‘‘tacticity’’ cannot be addressed in this research), and are readily soluble in polar aprotic solvents. They start to decompose ($T_{10\%}$) above 362°C and display glass-transition temperatures at 119–153°C.

In a paper by Kunisaki et al.[72], the dichlorodihydropyrazines derived from 2,5-diketopiperazine were treated with diols in a basic condition to obtain polyethers containing cyclodipeptide moiety in the main chain, which were found to be degraded into amino acid components in an acidic condition.

Rafiemanzelat[73] in 2012 has carried out the synthesis and characterization of poly(ether-urethane)s derived from 3,6-diisobutyl-2,5-diketopiperazine, obtained from L-Leucine. These copolymers are biodegradable and thermally stable. Some structural characterization and physical properties of these polymers before and after degradation in soil, river water and sludge are reported. The environmental degradation of the polymer films was investigated by SEM, FT-IR, TGA, DSC, GPC and XRD techniques. A significant rate of degradation occurred in PEU samples under river water and sludge condition. The polymeric films were not toxic to Escherichia coli (Gram negative), Staphylococcus aureus and Micrococcus (Gram positive) bacteria and showed good biofilm formation on polymer surface. Results show that hard segment degraded selectively as much as soft segment and these polymers are susceptible to degradation in soil and water.

In literature many polyamides based on diketopiperazine synthesis are also found.

Crescenzi was among the precursors of the study of this type of products: in 1968[74] he carried out a polyamides synthesis from diketopiperazine based on L-lysine with adipoil chloride; in 1973[75] he

published a patent on the synthesis of polymers via polyaddition or polycondensation, based on diketopiperazine obtained from modified amino acids.

In 2000, Parrish et al.[76] carried out a polymer synthesis by reaction between diketopiperazine (obtained by L-glutamic acid dimerization) and various diamines. The polymers synthesized showed good thermal stability and high glass transition temperatures, compared to those of common aliphatic nylon.

In literature there are also papers on the synthesis of polyamides based on monomers having completely natural origin. In these studies, the amino, carboxyl or hydroxyl groups of the functionalized diacid or of the amino acid are often protected to avoid side reactions.

Bou et al. synthesized various cyclic and linear polyamides starting from lysine and tartaric acid.

In a 1995[77] paper the synthesis of a polyamide entirely based on naturally occurring compounds has been carried out by polycondensation of N,N-bis(trimethylsilyl)L-lysine ethyl ester and bis(pentachlorophenyl) di-O-methyl-L- tartrate in a chloroform solution (Figure 90).

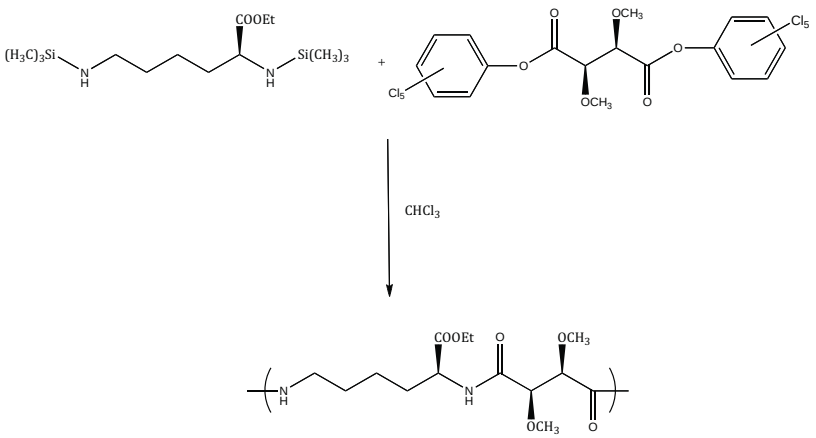

Figure 90: reaction scheme for the polyamides synthesis based on L-lysine and tartaric acid derivatives

The polytartaramide obtained has a molecular weight of about 6000 Da, displays high optical activity and is soluble in water. The regioregularity of the polymer has been examined by ^{13}C NMR, with the support of model compounds, which revealed that the chain is predominantly syndioregic in nature

The same polyamides (PLyTA) were synthesized[78] from natural compounds L-lysine and D- or L-tartaric acid via the active ester polycondensation method. The carboxyl and hydroxyl side groups were orthogonally protected as methyl ester and methyl ether, respectively. Direct reaction of methyl L-lysinate dihydrochloride with bis(pentachlorophenyl) di-O-methyl tartaric acid led to the aregic ar-PLyTA polyamide, whereas isoregic (ir-PLyTA) and syndioregic (sr-PLyTA) polyamides

were obtained by polycondensation of particular precursors to obtain the polymer with specific provision.

These polyamides have intrinsic viscosities in the 0.50– 0.76 dl g^{-1} range, display optical activity, and are readily soluble in chloroform. They start to decompose well above 200°C and display glass-transition temperatures at 100–105°C. DSC and X-ray diffraction results indicated that these polyamides are not crystalline but they seem to adopt a partially ordered phase. No differences in properties other than optical rotation were observed between PLyTA made of D- and L-tartaric acid respectively.

In 2006[63] the same authors synthesized cyclic oligomers based on L-lysine 2,5-diketopiperazine and tartaric acid. L-lysine was selectively N-protected (-NH_2 in ε position) and esterified with methanol via copper complex, then it was self-condensed heating at 100°C for 24h. Diketopiperazine was obtained treating with HBr in acetic acid, whit a 55% yield. On the other hand, active esters of di-O-methyl tartaric acid (D or L) to be used as diacidic monomers were obtained from methyl tartrate (D or L). Polycondensation of L-lysine 2,5-diketopiperazines with the pentachlorophenyl ester of di-O-methyl tartaric acid, at room temperature in dry DMF was carried out, with triethylamine to neutralize HBr that is released in the process..

5.2 Research methodology

In the present work, oligoamides based on dimethyl L-tartrate and L-lysine were synthesized decreasing the reaction steps and simplifying the purification steps of the product in comparison to the procedures already known in the scientific literature. The purpose of this study is to use 100% biobased products as consolidating for archaeological wood and make the product potentially interesting from an industrial point of view, performing the synthesis with a "one pot" process. Using this type of products, the classical properties of nylons and the ones of biocompatible and biodegradable polymers could be present at the same time[64,76].

The reactions were carried out with two different synthetics methods, obtaining the same type of polycondensation product.

The **first method** proceeds through a reaction in solution in Sovirel® tube, under nitrogen atmosphere, at with a slight overpressure. This method, used for the synthesis of all oligoamides we studied in the past, requires the presence of triethylamine as catalyst and methanol as solvent. The advantage of this method relies on the presence of the solvent which guarantees a good temperature control, preventing the formation of products with colors intense and leads to a good reproducibility of the results.

In the **second method** a process without catalyst and solvent has been used, similarly to industrial polycondensation process. To let the polycondensation proceed, the reaction was performed using the vacuum evaporation technique, to remove the by-product formed (methanol).

The advantages of this method rely on the elimination of the solvent and catalyst and on lower reaction times; moreover reaction temperatures are milder (60°C).

The same reactions were also carried out using L-lysine alone to evaluate its reactivity without the diester.

5.3 Results and discussion

The two monomers used for the synthesis of these biobased oligoamides are tartaric acid and L-lysine.

Tartaric acid was activated by esterification, as discussed in the previous chapter. L-lysine (Figure 2) contains two amino groups with different reactivity, having different basicity and hindrance; this feature can lead to the formation of different types of products.

Two types of synthesis were carried out, the first in a Sovirel® tube in the presence of solvent, and the second at reduced pressure, through the use of a rotary evaporator.

All syntheses were performed at different reaction times (1, 3, 7 days), with a ratio of diester: amino acid equal to 1: 1 and 1: 2 at 80°C (temperature giving the best results of chain growth in the synthesis of polytartaramides and polytrehaluronamides[33,34]). The work-up of the reaction is very simple, performed washing the solid precipitated during the reaction with methanol and via filtration on a büchner funnel.

The second method, does not exhibit the typical problems of bulk polymerization, even if the reaction occurs in the absence of solvent, because temperatures are lower and reaction time is reduced. The work-up was performed as in Method 1, but the product washing step is faster because the catalyst is not present and therefore must not be removed. The products obtained have the same characteristics as those obtained with the first method.

The same reactions were also carried out using L-lysine alone to evaluate its reactivity without dimethyl L-tartrate.

The products were characterized by NMR (^{1}H NMR, ^{13}C NMR, gCOSY, gHSQC) and FT IR spectroscopy, MALDI, DSC, GPC and potentiometric titration.

Below (Table 12 and the following paragraphs) the syntheses are described in detail.

Table 12: reaction conditions of the polycondensation between L-lysine and dimethyl L-tartrate

Product	T (°C)	t (days)	Method	Ratio diester: lysine	Solvent	Catalyst	Yield (%)	DP	MW (g/mol)	Diketopiperazine oligoamide (%)	Tg (°C)	Tf (°C)
1	80	1	**1** (Sovirel®)	1:1	MeOH	NEt_3	40.5	3	1366	85.65	---	---
2	80	1	**1** (Sovirel®)	1:2	MeOH	NEt_3	53.6	3	1366	79.17	121.7	N.D.
3	80	3	**1** (Sovirel®)	1:1	MeOH	NEt_3	46.5	3	1366	84.37	---	---
4	80	3	**1** (Sovirel®)	1:2	MeOH	NEt_3	66.3	3	1366	79.31	120.8	N.D.
5	80	7	**1** (Sovirel®)	1:1	MeOH	NEt_3	53.8	5	2105	80.85	---	---
6	80	7	**1** (Sovirel®)	1:2	MeOH	NEt_3	71.8	4	1736	82.37	120.2	N.D.
7	60	9 hours	**2** (Rotary evaporator)	1:2	---	---	36.0	2	996	90.58	N.D.*	N.D.
8	80	7	**1** (Sovirel®)	Lysine	MeOH	NEt_3	---	---	---	---	---	---
9	60	9 hours	**2** (Rotary evaporator)	Lysine	---	---	---	---	---	---	---	---
10	60	12 hours	**2** (Rotary evaporator)	Lysine	---	---	---	---	---	---	---	---

*N.D.: not determined

5.3.1 Syntheses of the oligoamides

5.3.1.1 Method 1: in a "Sovirel® tube"

Polycondensation reactions between dimethyl L-tartrate and L-lysine were carried out in a Sovirel® tube at 80°C for 1, 3 and 7 days, using methanol as solvent and triethylamine as catalyst. The polymer formed during the reaction was separated as a solid into the Sovirel® tube and at the end of the reaction was separated from the liquid phase by filtration on a büchner funnel and washed with methanol.

The syntheses were carried out with dimethyl L-tartrate: L-lysine = 1: 1 and 1: 2 ratio, obtaining in both cases the formation of the same oligoamide. All products showed good water solubility and good yields (Table 13). As Table 13 shows, yield increases for the products having longer reaction times; within the same reaction length, yield is always higher when 1: 2 ratio between the monomers was used.

Table 13: syntheses reaction conditions

Product	t (days)	Method	Ratio diester:lysine	Yield (%)
1	1	Sovirel®	1:1	40.5
2	1	Sovirel®	1:2	53.6
3	3	Sovirel®	1:1	46.5
4	3	Sovirel®	1:2	66.3
5	7	Sovirel®	1:1	53.8
6	7	Sovirel®	1:2	71.8
7	9 hours	Sovirel®	1:2	36.0

After **1 day** of reaction (**product 1 and 2**) confirmation of product formation is given by the precipitation of a solid in the Sovirel® tube and by NMR and FT IR analyses.

FT IR analysis (Figure 91) confirmed the oligoamide formation for the presence of a band at 1654 cm^{-1} relative to the C=O amide and those at 1130 and 1074 cm^{-1} relative to C-O stretching. There are also other bands related to $-NH_3^+$ stretching around 2130 and 2632 cm^{-1} typical of amino acids and two peaks at 1581 and 1520 cm^{-1} are present.

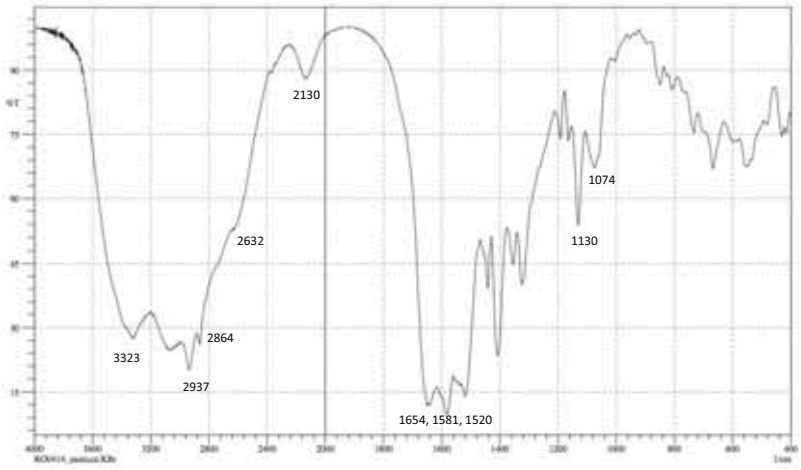

Figure 91: FT IR spectrum of the Product 1

In ^{1}H-NMR spectrum (Figure 92) the ratio L-lysine: dimethyl L-tartrate appears equal to 2:1, then it was hypothesized that part of the product is represented by the oligoamide based on dimethyl ester/L-lysine diketopiperazine (this data will be confirmed by other analyses). The presence of an amide compound is confirmed by the signals between 3.20 and 3.40 ppm (C**H**$_2$NHCO, ε in the figure), and at 3.68 ppm (C**H**NHCO, α in the figure); furthermore there is a separation of the signal related to H_δ and H_β between 1.56 and 1.83 ppm (in L-lysine they give a single signal at 1.61 ppm) and C**H**OH from 4.70 ppm to 4.50 ppm. Signals related to an ester termination of the dimethyl L-tartrate at about 3.75 ppm and the C**H**NH$_2$ amino (α terminal) at 3.30 ppm are not present; the lack of this last signal is also confirmed by gCOSY analysis; termination to be taken as a reference is relative to C**H**$_2$NH$_2$ of the L-lysine side chain to 2.98 (H_ε terminal).

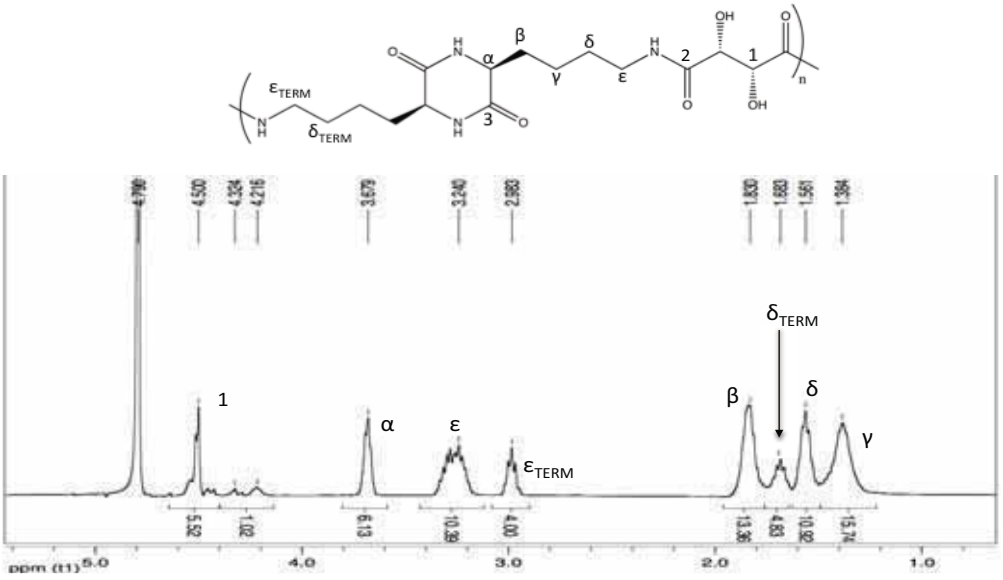

Figure 92: ^{1}H NMR spectrum in D_2O of the Product 1 (400 MHz)

From gCOSY spectrum (Figure 93), analyzing the correlations between the hydrogens of the molecule, it is possible to confirm the attribution made by ^{1}H NMR for the presence of coupling between the C**H**$_2$NH$_2$ group (ε terminal) at 2.98 ppm with H_δ terminal at 1.68 ppm and between C**H**$_2$NHCO group (ε internal) to 3.20- 3.40 ppm with internal H_δ at 1.56 ppm.
Furthermore, the correlation between the H_β at 1.83 ppm with the C**H**NHCO group (α internal) to 3.68 ppm, and with another signal at 4.22 ppm is shown; this weak coupling will be discussed later.

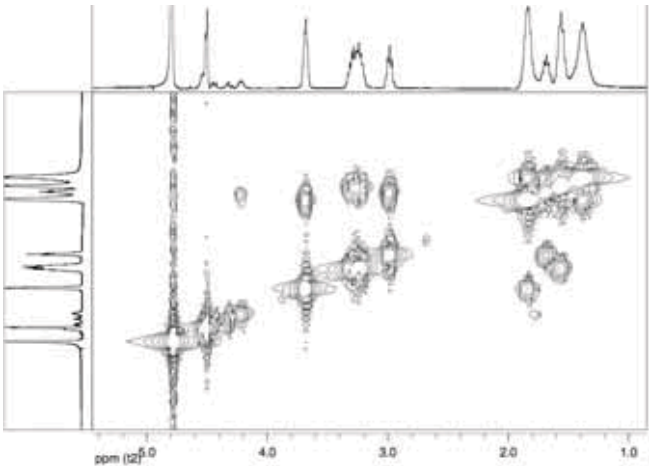

Figure 93: gCOSY spectrum in D_2O of the Product 1

^{13}C NMR (Figure 94) and gHSQC (Figure 95) spectra, confirm the product formation, thanks to the presence of the signals at 38.6 and 54.7 ppm, related to the signals of **C**H$_2$NHCO (ε in the figure) and **C**HNHCO (α in the figure), respectively. It is also possible to assign the signal to 21.6 ppm to C_γ, at 26.4 ppm to terminal C_δ, at 28.0 ppm to internal C_δ and at 30.2 to C_β. In the carbonyl amide range there are two signals, one at 173.6, the other one at 175.2 ppm, with the same intensity. Moreover in gHSQC spectrum a correlation between the signal to 4.22 ppm with another at 54.7 ppm is present. Moreover ^{13}C NMR spectrum confirms the absence of the ester termination due to the absence of signals at about 171.5 ppm and the amino termination (CH(COOH)NH$_2$) given the absence of a signal at about 55.5 ppm. Signals relating to the lysine carboxyl group at about 181 ppm (COOH) are not detectable.

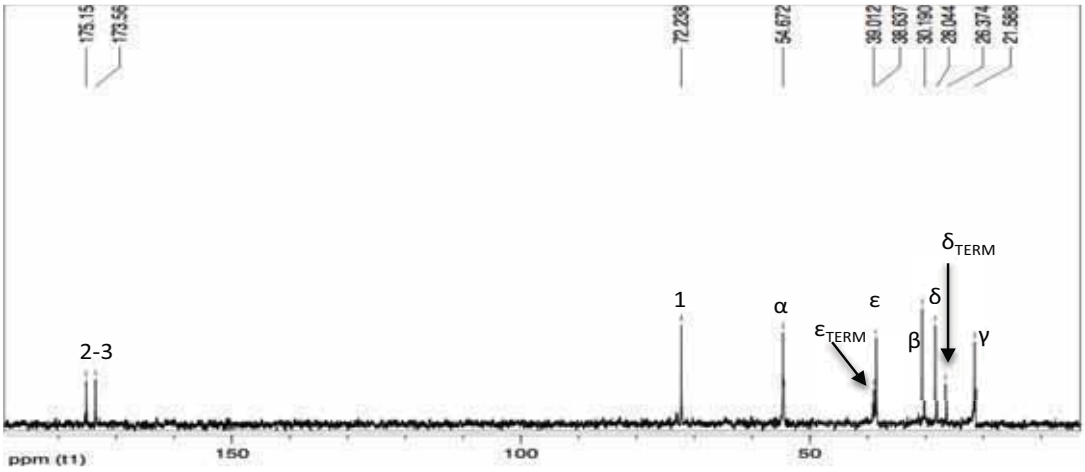

Figure 94: ^{13}C NMR spectrum in D_2O of the Product 1

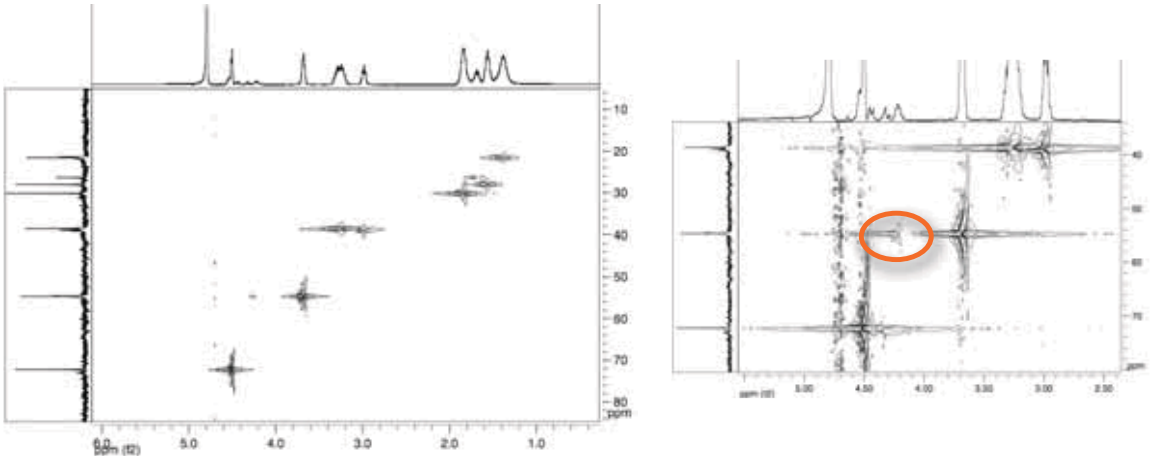

Figure 95: gHSQC spectrum in D_2O of the Product 1 (left) and magnification (right)

It is evident that the signal at 4.22 ppm is related to an H_α because it has a coupling in gCOSY and gHSQC spectra, with the same signals of the H_α at 3.68 ppm. This point show the presence of two polyamide species, one in higher concentration than the other, which will be discussed later. Out of simplicity, the signal at 3.73 ppm will be defined"α_D" and that at 4.22 will be "α_L".

The determination of the size (i.e. molecular weight) of the molecules synthesized was performed, at first, via calculation of the integrals of the signals in ^{1}H-NMR spectrum. In fact, identifying the signals for the different end groups (-CO_2CH_3, -CH_2NH_2, -$CHNH_2$), they can be used as reference values to determinate the average molecular weight, comparing them with the integrals of the signals related to protons inside the polymer chain.

In the NMR analysis of the product synthetized, only the signal related to the terminal amino group (**CH_2NH_2**) is present. Based on this consideration, it is possible to calculate the number (n) of repeating units, according to the following calculations:

integral of H_γ signal = 4(n+1)

integral of H_β signal = 4(n+1)

integral of H_δ internal signal= 4n

integral of H_δ terminal signal= 4

*integral of C**H**$_2NH_2$ in ε to L-lysine signal= 4*

*integral of C**H**$_2$NHCO in ε to L-lysine signal= 4n*

*integral of C**H**NHCO in α to L-lysine signal ($\alpha_D + \alpha_L$)= 2(n+ 1)*

*integral of C**H**OH signal = 2n*

From the integrals elaboration by ^{1}H NMR, it was concluded that the product obtained consists of 3 repeating units with double amino termination, with resulting molecular weight of 1366 g/mol (Figure 96).

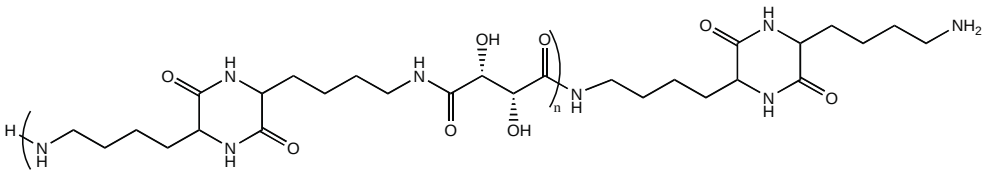

Figure 96: polyamides structure based on diketopiperazine structure

After **3 days** of reaction (**product 3 and 4**) the precipitation of a solid was observed and the formation of the polycondensation product was confirmed by ^{1}H NMR, ^{13}C NMR and FT IR spectra, as in the previous case.

From the integrals of the signals in ^{1}H NMR spectrum, the product results composed by 3 repeating units with double amino termination (1366 g/mol), as in the previous case, but with increased yield (Table 13).

After **7 days** of reaction (**product 5 and 6**) two products were obtained, with 53.8% and 71.8% yield respectively (Table 13); both are water soluble and composed by 5 and 4 repetitive units with double amino termination, respectively.

The evaluation of the DP of the products was made considering all the signals present in the spectrum (**Table 14**). Regarding the amide signals H_α, the evaluation was performed considering the sum of two signals at 3.68 ppm (α_D) and 4.22 ppm (α_L); in fact NMR analysis shows that they have the same couplings, both in gCOSY and gHSQC spectra.

Table 14: degree of polymerization of the products, calculated with all the signals of the ^{1}H NMR spectrum

Product	*t (days)*	*Ratio diester: lysine*	*CH_2NH_2 $\varepsilon_{terminal}$*	*DP CH-OH*	*DP CH_2NHCO (ε)*	*DP CHNHCO (α_D+ α_L)*	*DP β,γ,δ*
1	1	1:1	4	3.15	3.09	3.04	3.21
2	1	1:2	4	2.76	2.60	2.58	2.77
3	3	1:1	4	3.1	3.25	3.31	3.2
4	3	1:2	4	3.09	2.90	2.73	3.07
5	7	1:1	4	4.44	4.69	4.44	4.80
6	7	1:2	4	3.89	3.80	3.50	4.02
7	9 hours	1:2	4	2.21	2.16	2.10	2.28

On the contrary, if the DP evaluation was performed considering only the signal α_D, a DP value about 10-20% lower than that of the total CH_2NHCO (Table 15) was obtained.

Table 15: integral calculation *CH_2NHCO and CHNHCO*

Product	*DP CH_2NHCO (ε)*	*DP CHNHCO (α_D)*	*Δ**
1	3.09	2.47	20.06
2	2.60	2.06	20.77
3	3.25	2.68	17.54
4	2.90	2.26	22.07
5	4.69	3.83	18.34
6	3.80	3.13	17.63
7	2.16	1.98	8.33

*[(C**H**$_2$NHCO- C**H**NHCO)/ C**H**$_2$NHCO]*100

Therefore, the value at 3.68 ppm, for the component present in higher amounts, can be attributed to the $H\alpha_D$ (CHNHCO) of diketopiperazine structure, while that at 4.22 ppm to the $H\alpha_L$ (CH(COOH)NHCO), relative to a linear structure with dimethyl L-tartrate: L-lysine equal to 1:1 (not diketopiperazine).

Difference of chemical shift between the two hydrogen types Hα is explained by the formation of these two structures, with very different chemical environment: in the diketopiperazine structure, $H\alpha_D$ has a classic "amide-type" neighbourhood, in the linear oligomer diester/lysine as 1:1 (Figure 97) $H\alpha_L$ has a higher de-shielding effect due to the presence of a free carboxylic group.

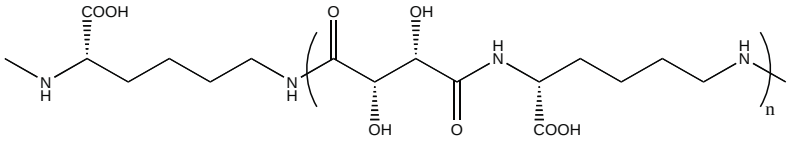

Figure 97: dimethyl L-tartrate/L-lysine equal to 1:1 oligoamide

The oligoamide with no diketopiperazine structure, theoretically present in small amounts, is not detectable accurately by NMR analysis; therefore, to try to better understand the composition of the product, other analyses, such as potentiometric titration, GPC analysis and MALDI were carried out.

MALDI analysis (Figure 98) has allowed to identify the presence of oligomers up to 8 repeating units with a ratio diester: L-lysine equal to 1: 1.

The data obtained with this technique allow to quantify the molecular weight of the not-diketopiperazine oligomer, that was not evidenced in the NMR spectra, probably because present in minimal quantities. On the contrary, the oligomers based on tartaric-lysine diketopiperazine were not easily detectable by MALDI because of their high polarity, owed to the cyclic structure.

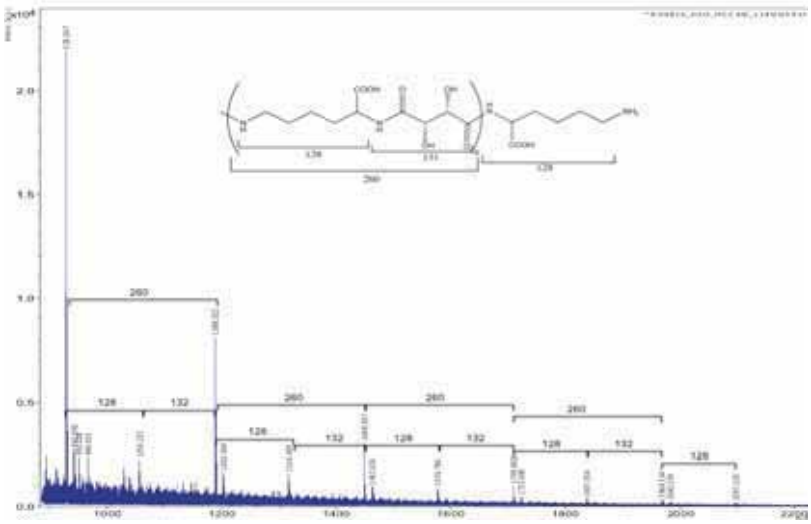

Figure 98: MALDI spectrum of the sample 5

Potentiometric titration (Table 16), confirms the presence of two types of amino groups and a carboxyl group in all products; however, the presence of the acid group and of one of the two amine is confirmed only performing the analysis with relatively high amounts of sample (over 115 mg). Performing the analysis with lower quantities, only the presence of a type of terminal amine group can be detected; also this result can be correlated with the presence of very low amounts

of oligoamide with no diketopiperazine structure, detectable only at relatively high concentrations.

Table 16: values of the potentiometric titration of samples

Product	*NH_2 (I)**	*NH_2 (II)**	*COOH**	*M_n (g/mol)*
1	123.76	56.38	40.59	11102.48
2	294.62	89.69	72.14	5204.13
3	53.03	73.72	42.38	15779.10
4	182.09	82.28	50.62	7565.15
5	60.46	104.70	99.73	12109.47
6	72.48	89.56	108.72	12342.63
7	264.58	216.15	175.91	4160.34

*meq/Kg

As example, the titration of product 6 (Figure 99) is shown: the first image shows amino groups titration with HCl (0.01 M), the second the acid groups back-titration with NaOH (M 0.01).

In Table 16 all the values obtained are shown with Mn calculated based on the total value of the NH_2 groups.

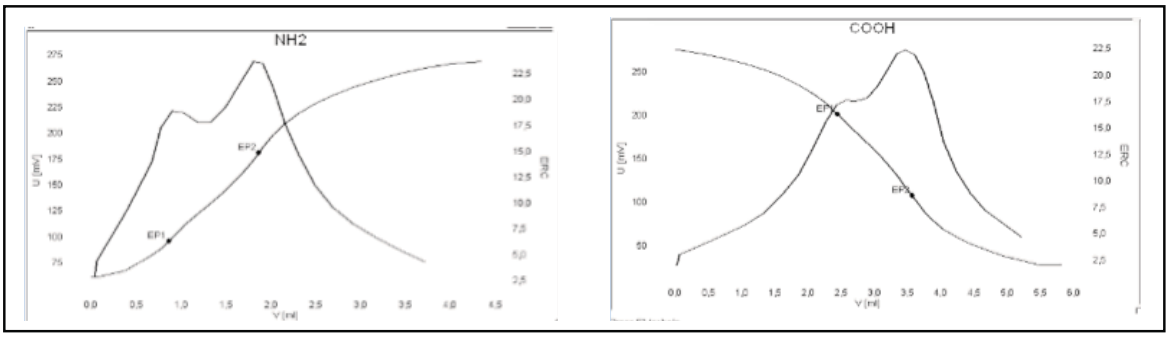

Figure 99: potentiometric titration of NH_2 groups (left) and -COOH groups (right)

The molecular weights calculated by NMR analysis and potentiometric titration are not in agreement: the first gives values of about 1500- 2000 g/mol, the second give MWs that are 5 times higher.

To understand which of the two analyses is more reliable for the molecular weight determination, GPC analysis were performed on two samples for which the NMR showed a higher molecular weight (samples 5 and 6), (Figure 100) .

The shape and hydrodynamic volume of the peaks obtained don't indicate the formation of products with high molecular weight, and therefore it is possible to conclude that the molecular weight obtained via NMR are more reliable. The evaluation of the absolute molecular weight by

GPC cannot be performed due to the lack of appropriate calibration curves and the impossibility to locate a reference standard used for this type of compounds.

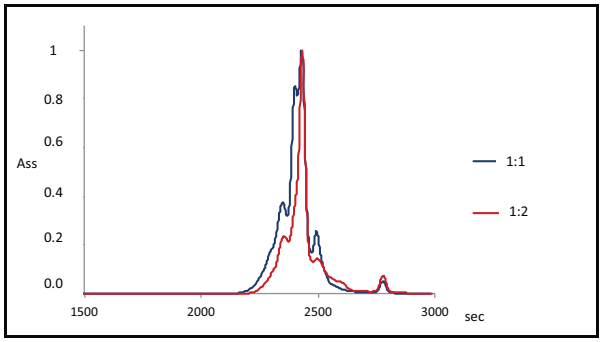

Figure 100: chromatogram of the samples 5 and 6

The products were characterized also by polarimetric analysis, to evaluate their optical activity and all showed values ranging between +54° and +56°.

The properties of the oligomers synthesized have been evaluated via DSC, measuring glass transition (T_g) and melting temperature (T_m), to compare the products synthetized. T_g becomes visible when higher MWs are obtained (products 2, 3 and 5), since when the oligomer chain is very short no glass transition exist (product 7). T_m is not visible before 290°C; over this temperature, melting and degradation occur at the same time. Thermal degradation was studied by TGA (Figure 102), that shows two decomposition stages, the first between 175-280°C and the second between 300-450 °C.

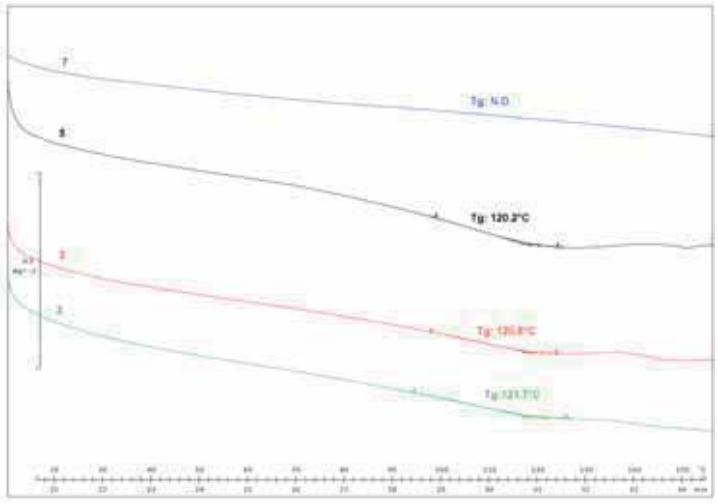

Figure 101: Glass transition temperature (Tg) of products 2,3,5,7

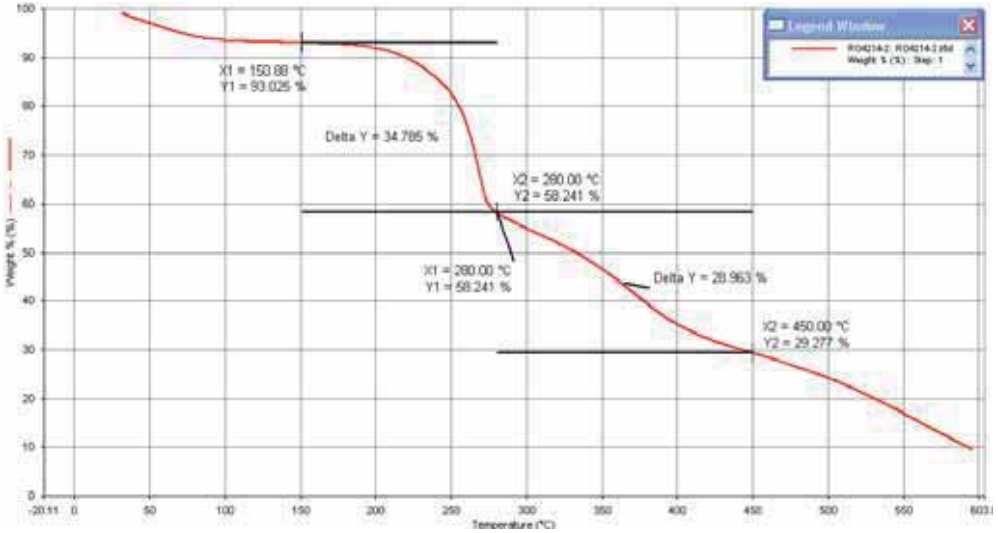

Figure 102: Thermal degradation studied by TGA

For this series of syntheses, comparing the results obtained with the different analytical techniques, it is possible to conclude that about 80-90% of the product has a ratio diester: amino acid equal to 1: 2 and the remaining has a ratio 1 : 1.

The presence of a product with 1:1 ratio in small quantity, may be deduced from the analyses carried out on the basis of the following considerations:

- ^{1}H NMR analysis: for the integral related to Hα at 3.68 ppm (CHNHCO) with a value about 15-20% lower than the other signals in the spectrum, and the presence of a signal at about 4.22 ppm having weak intensity, related to the group [CH(COOH)NHCO], which is more de-shielded of the previous one.
- No NMR spectra show the presence of COOH and $CHNH_2$ groups.
- Potentiometric titration: titration shows the presence of two amino groups and an acid group, when using quantities of sample higher than 115 mg; the analyses with low amounts of samples show the presence of only one amino group.
- The final confirmation of the formation of the linear product (not-diketopiperazine), is obtained through MALDI analysis, which reveals the presence of a product with a ratio of diester: amino acid equal to 1: 1 consisting of oligomers having up to 8 repeating units. The oligomers based on tartaric-lysine diketopiperazine were not detectable because of their high polarity.

5.3.1.2 Method 2: in a "Rotary evaporator"

The polycondensation reaction between dimethyl L-tartrate and L-lysine is conducted in a flask, placed in a rotary evaporator at 60°C for 9 hours, without solvent and catalyst. The polymer formation (**product 7**) is highlighted by color and consistency changes of the reaction mixture; in fact, dimethyl L-tartrate is a transparent oil and L-lysine is a white solid, while the end product is a yellow solid. After washing the solid with methanol, a product was obtained with a 36% yield, water soluble. This product was analysed by NMR and potentiometric titration.

From NMR analysis *(^{1}H NMR, ^{13}C NMR, gCOSY e gHSQC)*, the product exhibits the same signals of the product synthesized by Method 1, but with lower molecular weight, (about 2 repeating units less than the product of Method 1) with double amino termination and an average molecular weight of 996 g/mol.

In potentiometric titration also in this case two amino terminations and an acid termination were detected when using quantities of sample higher than 115 mg. Mn evaluation indicates a value higher than the one calculated by ^{1}H NMR, as for the synthesis of Method 1.

T_g (Figure 101), in this case is not detectable, according to the lower average molecular weight of the product, compared to those obtained in Method 1.

5.3.2 Diketopiperazine

5.3.2.1 Method 1: in a "Sovirel® tube"

The same syntheses were carried out with L-lysine alone, maintaining other reaction conditions constant (temperature, catalyst, solvent), varying reaction times from 1 to 7 days (**product 8**). ^{1}H NMR analysis shows that the diketopiperazine structure was not formed in any reaction; in fact, in all NMR spectra, signals of unreacted L-lysine are present.

In ^{1}H NMR spectrum (Figure 103) signals at 1.39 ppm, 1.65 ppm, 2.95 ppm and 3.35 ppm respectively are present, attributable to hydrogens γ, β e δ, ε and α in the L-lysine.

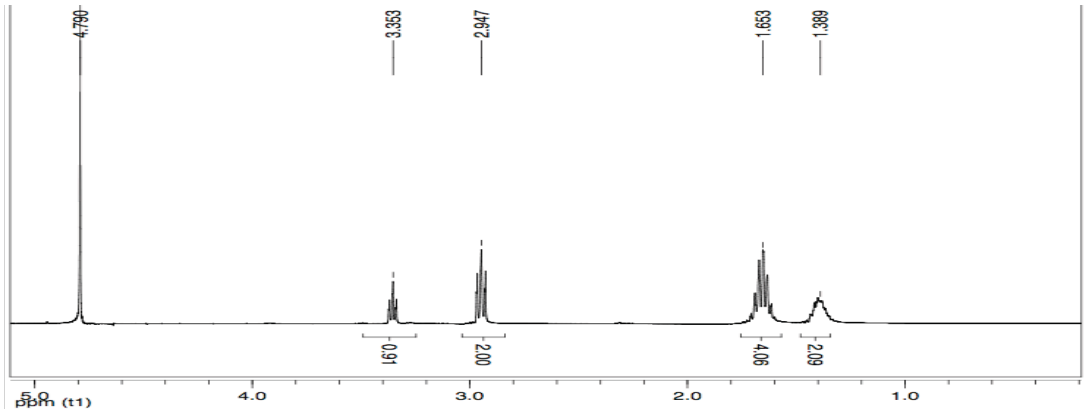

Figure 103: ^{1}H NMR spectrum in D_2O of the product 8 (400 MHz)

In ^{13}C NMR spectrum (Figure 104), 6 signals at 21.8 ppm (C_γ), 27.1 ppm (C_δ), 32.9 ppm (C_β), 39.2 ppm (C_ε), 55.3 ppm (C_α) and 181.1 ppm (C=O) are present, that also in this case correspond to those present in the L-lysine.

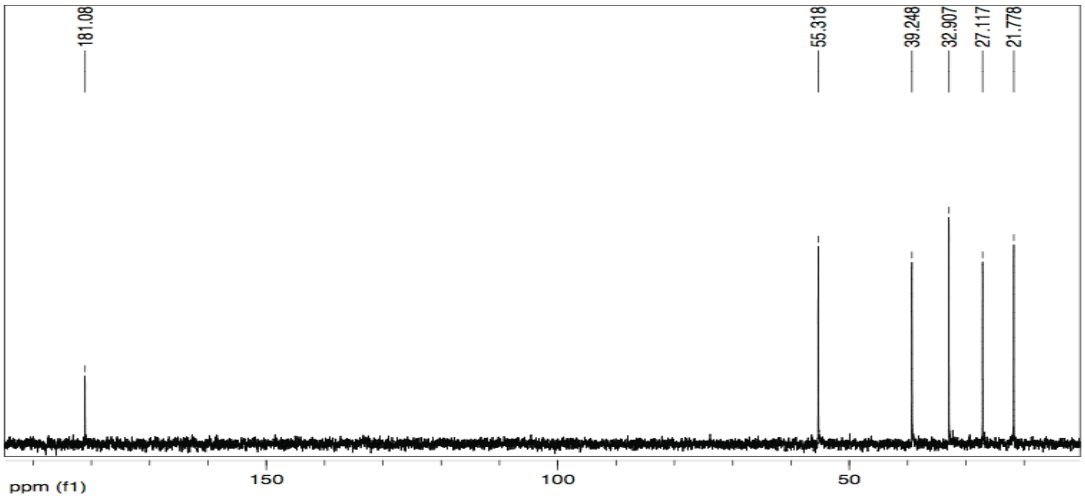

Figure 104: ^{13}C NMR spectrum in D_2O of the product 8

In FT IR spectrum (Figure 105) the bands present in the product are perfectly overlapped to those of the starting monomer, confirming that the reaction has not occurred.

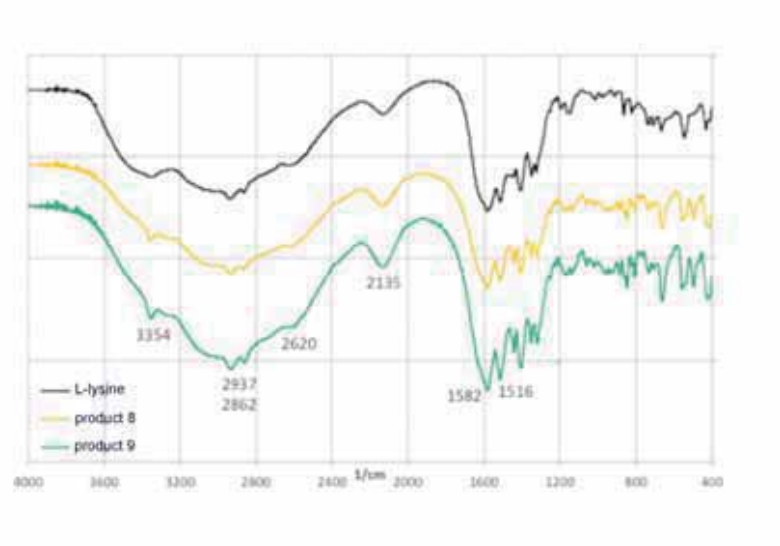

Figure 105: FT IR spectra comparison of samples 8 and 9 with L-lysine

In the reactions carried out for 7 days at 80°C, a partial degradation of the product was evidenced; in fact, in ^{1}H NMR spectrum (Figure 106), in addition to the signals characteristic of L-lysine, signals having low intensity at 1.90, 3.16, 3.69 and 3.86 ppm are present, not attributable to any hydrogen of the monomer or polymer, as confirmed by gCOSY analysis.

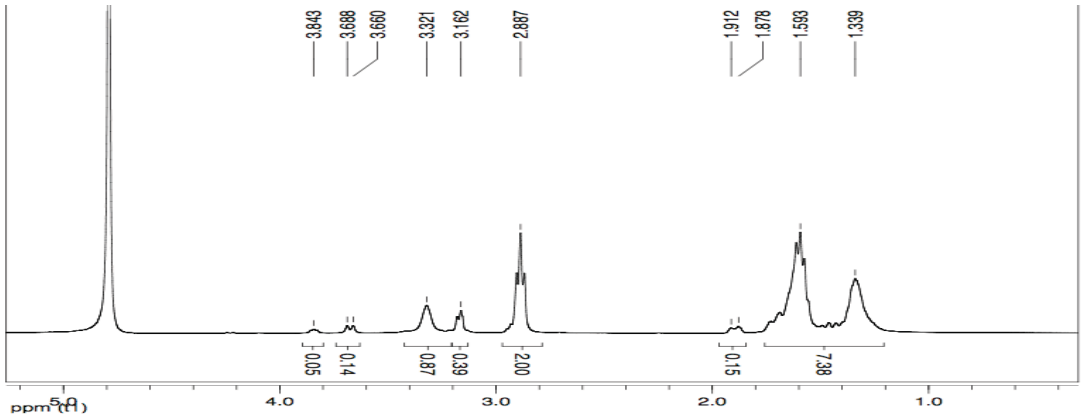

Figure 106: ^{1}H NMR spectrum in D_2O of the degradation product, Method 1 (400 MHz)

^{13}C NMR spectrum (Figure 107) confirms the absence of the diketopiperazine structure thanks to the lack of signal at 173-174 ppm related to the C=O amide; furthermore there are many signals that can be attributed to alteration products of lysine.

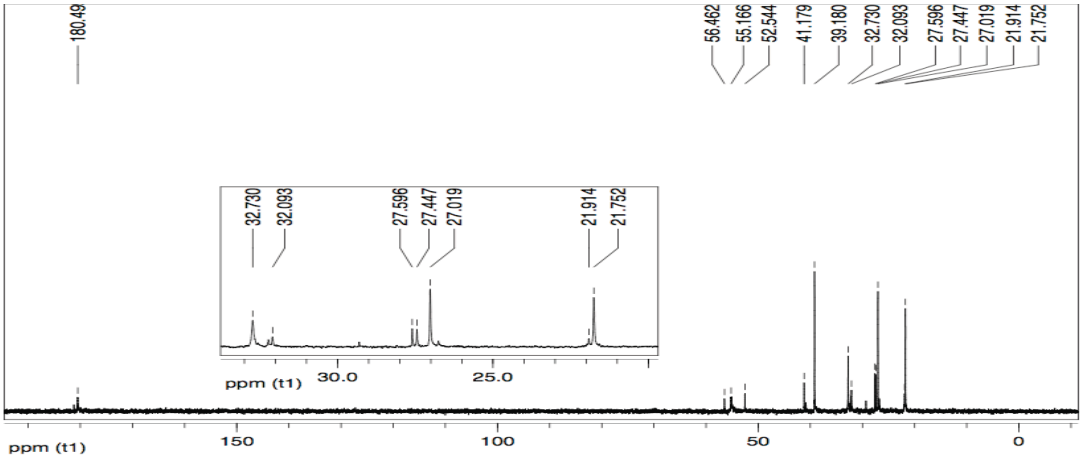

Figure 107: ^{13}C NMR spectrum in D_2O of the degradation product, Method 1

This result confirms that the diketopiperazine structure is formed only when the amino group in ε position is *"activated"*, in this case by formation of an amide bond with dimethyl L-tartrate; in this case the molecule can form the cyclic structure.

5.3.2.2 Method 2: in a "Rotary evaporator"

Syntheses of L-lysine alone were carried out also using Method 2, maintaining constant the other conditions and varying the reaction time from 9 hours (**product 9**) to 12 hours (**product 10**).

All products were characterized by NMR and FT IR spectroscopy, obtaining spectra corresponding to the previous reaction (Method 1 with only L-lysine); in fact, also in this case, formation of diketopiperazine structure is not observed, confirming the presence of unreacted L-lysine. Using lower reaction temperature compared to Method 1, no signals related to products degradation are visible.

5.4 Conclusions

This work was performed to expand the library of hydrophilic polyamide compounds that has been ongoing for several years in the laboratory of the Department of Chemistry of Università degli Studi di Firenze.

Only reagents recovered from natural sources were used, to obtain completely bio-based products, replacing synthetic diamines used up to now with others that are derived from natural products.

L-lysine was used as "diamine" because it has natural origin and in its structure two amino groups and an acid group are present.

In the literature polymers based on dimethyl L-tartrate and L-lysine are known, obtained using several reaction steps. Now, respecting the principles of green chemistry, we have synthesized this type of oligoamides decreasing the number of the reaction step and simplifying the product purification compared to the procedures already known in literature, with the purpose to obtain a product potentially interesting from an industrial point of view.

Two synthetic methods were used, achieving the same type of polycondensation product. The reactions performed with “Method 1” were carried out in ratio diester: amino acid equal to 1: 1 and 1: 2, leading to the same product.

In Method 1 the reaction was carried out in a Sovirel® tube, in solution, using nitrogen atmosphere and atmospheric pressure (or slightly higher). This method, used for all oligoamide syntheses studied, requires the presence of triethylamine as catalyst and methanol as solvent. In this way a good temperature control is guaranteed, preventing the formation of intense colors of the products and maintaining a good reproducibility of the results.

In Method 2 a process without catalyst and solvent was used, as commonly used in industrial polycondensation. To let the polycondensation proceed, the reaction was performed with a rotary evaporator, to remove the methanol formed in the polycondensation from the reaction. Temperatures lower than the ones of Method 1 and reduced reaction times were used,.

The advantages of this method rely on the elimination of the solvent and catalyst, the reduction of reaction times and the use of milder temperatures. The work-up was performed as in Method 1, but the product washing step was faster because it was not necessary to remove the catalyst.

In both reactions, products having the same characteristics were obtained, composed by oligoamides based on dimethyl L-tartrate and L-lysine diketopiperazine (about 80-90%) and on dimethyl L-tartrate and L-lysine in ratio 1:1 (the remaining 10-20%). The products, with average molecular weights of about 1000- 2100 g/mol, show a good water solubility.

The structure of the products was determined using different techniques: NMR and FT IR spectroscopies, potentiometric titrations, GPC and MALDI analyses.

The product obtained by Method 2 will need optimizations to obtain higher molecular weights and higher yields. The possibility to synthesize the oligoamides even with this alternative method is a noteworth result, since it doesn't require solvents and catalysts, as happens in bulk reactions, but at the same time uses lower reaction temperatures, that allow to perform reproducible syntheses and do not lead to intense color variations of the product. It is therefore possible to synthesize in a one-pot process the products that in the literature are obtained with more reaction steps; typically, amino ε group undergoes protection or activation step to be able to condense forming diketopiperazine; it was possible to get the same product without protecting the amino ε group, because dimethyl L-tartrate has this function, while promoting the formation of the cyclic structure and, consequently, the formation of the polymer.

Table 17: FT IR spectra signals

Product	NH stretching	O-H stretching	C-H stretching	$-NH_3^+$ amino acids stretching	$-COO^-$ stretching	C=O stretching (Amide I)	N-H bending (amide II)	C-O stretching
L-lysine	3350 (m)	---	2939 (vs) 2862 (vs)	2632 (w) 2135 (w)	1582 (vs)	---	1518 (vs)	---
1 and 2	3323 (vs)	3323 (vs)	2937 (w) 2864 (w)	2632 (w) 2130 (w)	(1581)	1654 (vs)	1581, 1520 (vs)	1130 (m) 1074 (m)
3 and 4	3323 (vs)	3323 (vs)	2939 (w) 2865 (w)	2630 (w) 2135 (w)	(1583)	1650 (vs)	1583, 1520 (vs)	1132 (m) 1074 (m)
5 and 6	3323 (vs)	3323 (vs)	2939 (w) 2864 (w)	2630 (w) 2131 (w)	(1582)	1645 (vs)	1582, 1516 (vs)	1131 (m) 1075 (m)
7	3321 (vs)	3321 (vs)	2939 (w) 2864 (w)	2624 (w) 2132 (w)	(1583)	1650 (vs)	1583, 1520 (vs)	1130 (m) 1068 (m)
8, 9, 10	3354 (m)	---	2937 (w) 2862 (w)	2620 (w) 2135 (w)	1582 (vs)	---	1516 (vs)	---

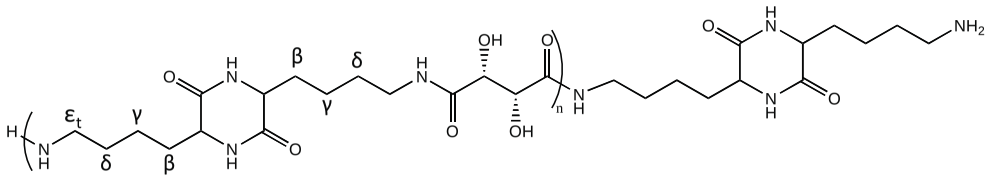

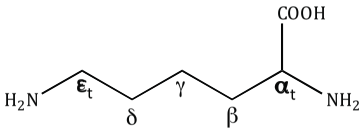

Table 18: ^{1}H NMR spectra signals (400 MHz, δ, ppm, *D_2O*)

Product	γ	δ	$\delta_{terminal}$ ($CH_2CH_2NH_2$)	β	ε terminal (CH_2NH_2)	ε (CH_2NHCO)	α ($CHNHCO$)	α [CH(COOH)NHCO]	α terminal ($CHNH_2$)	CH-OH	-OCH_3
L-lysine	1.36	---	1.61		2.90	---	---	---	3.30	---	---
1 and 2	1.38	1.56	1.68	1.83	2.98	3.20- 3.40	3.68	4.22	---	4.50	---
3 and 4	1.41	1.59	1.71	1.88	3.01	3.18- 3.38	3.72	4.21	---	4.52	---
5 and 6	1.41	1.59	1.72	1.88	3.02	3.20-3.40	3.73	4.22	---	4.52	---
7	1.41	1.59	1.71	1.87	3.01	3.18- 3.38	3.71	4.23	---	4.52	3.80
8, 9, 10	1.39	---	1.65		2.95	---	---	---	3.35	---	---

Table 19: ^{13}C NMR spectra signals (100 MHz, δ, ppm, *D_2O*)

Product	γ	δ terminal ($CH_2CH_2NH_2$)	δ	β	ε (CH_2NHCO)	ε terminal (CH_2NH_2)	α ($CHNHCO$)	α terminal ($CHNH_2$)	CH-OH	C=O	-OCH_3
L-lysine	21.8	27.4	---	33.2	---	39.3	---	55.5	---	181.8	
1 and 2	21.6	26.4	28.0	30.2	38.6	39.0	54.7	---	72.2	173.6 175.2	---
3 and 4[a]	20.8	25.6	27.3	29.3	37.8	38.2	53.8	---	71.4	172.7 174.1	---
5 and 6[a]	20.8	25.6	27.3	29.3	37.9	N.D.	53.8	---	71.4	172.7 173.9	---
7	21.4	26.3	28.0	30.0	38.6	39.0	54.4	---	72.4	173.5 175.6	---
8, 9, 10	21.8	27.1	---	32.9	---	39.2	---	55.3	---	181.1	---

[a]spectra recorded at 50 MHz

5.5 Experimental

5.5.1 Materials

5.5.1.1 Solvents

- MilliQ water
- Methanol, Normapur product, 99.9% pure

5.5.1.2 Reagents and products

- Boric acid, produced Aldrich, purity> 99.5%
- L-tartaric acid, Aldrich product purity to 99%
- L-lysine, product Aldrich, purity> 98%
- Triethylamine, product Carlo Erba, purity> 97%

5.5.2 Instruments

5.5.2.1 NMR spectroscopy

^{1}H NMR, ^{13}C NMR, gCOSY and gHSQC spectra were recorded with a Varian Mercury Plus 400 spectrometer and a Varian VXR 200 spectrometer, working at 399.921 MHz and 199.985 MHz, respectively. All spectra are reported in ppm and referred to TMS as internal standard. Spectra elaboration was performed with the software Mestre-C 4.3.2.0. Solvents used (D_2O, $CDCl_3$) are produced by Aldrich Co.

5.5.2.2 FT IR spectroscopy

FT IR spectra were recorded with a Shimadzu FT-IR-8400S model, and elaborated with the Spectrum v.3.0202. Solutions were analyzed using KBr or CaF_2 round cell windows, after deposition and evaporation of solvent. Spectra of solid samples were recorded as KBr pellets.

5.5.2.3 Differenzial scanning calorimetry (DSC)

DSC analyses were conducted using a Mettler Toledo DSC 820, on samples weighting from 7 to 10 mg each.

Dynamic DSC analyses samples were first heated from 25°C to 100°C at 10°C/min and maintained at 100°C for 2 min to eliminate residue water, then cooled down to 25°C at 20°C/min, maintained at 25°C for 2 min; for T_m and T_g determination a second thermal cycle from 25°C to 250°C was then used to evaluate the behavior of the material.

5.5.2.4 Thermogravimetric analysis (TGA)

TGA analyses were conducted on a Perkin Elmer TGA4000 under nitrogen atmosphere on samples weighting 6 mg, heating from 25°C to 600°C (20° C/min).

5.5.2.5 Gel permeation chromatography (GPC)

GPC analysis system having Waters 1515 Isocratic HPLC pump and a six styragel columns set (HR2-HR3-HR5) with a Waters 2487 Dual λ Absorbance Detector using a flow rate of 1 mL/min and 20 µL as injection volume; samples were prepared dissolving 30 mg of product in 1 mL of anhydrous CH_2Cl_2; before the analysis, the solution was filtered with 0.45 µm filters

5.5.2.6 Potentiometric titration:

Potentiometric titration were performed with Metrohm Titrino 751. Amino groups were titrated with HCl (0.01 M); the acid groups were back-titrated with NaOH (M 0.01).

5.5.2.7 Matrix-assisted laser desorption/ionization (MALDI)

MALDI analysis were performed with Bruker Daltonic Ultraflex MALDI TOF/TOF spectrometer

5.5.2.8 Optical rotation:

Polarimetric measurements were performed on a JASCO DIP-370". Samples were prepared dissolving 7 mg of product in 1 mL of water

5.5.3 Synthesis of the oligoamides

5.5.3.1 Method 1: in a "Sovirel® tube" (1:1)

Into a Sovirel tube, triethylamine (58.7 mg, 0.58 mmol) is added, under nitrogen atmosphere and under continuous stirring to 4 mL of a methanol solution of L-lysine (314.3 mg, 2.148 mmol). A methanolsolution (4 mL) of dimethyl L-tartrate (382.7 mg, 2.148 mmol) is added and the mixture is allowed to react at 80°C for 24 hours (**product 1**). After cooling to room temperature, the mixture is filtered on a on a büchner funnel and the solid obtained is washed with methanol and dried at room temperature (282.3 mg, 40.5% yield).

The reaction was repeated increasing the reaction time to 3 days (**product 3**) and 7 days (**product 5**) under a nitrogen atmosphere, respectively, with 46.5% yield (324.2 mg) and 53.8% yield (375 mg).

Product 1

^{1}H-NMR (D_2O, 400 MHz, Table 18): signals at δ 1.38 ppm (m, 4H, H_γ), 1.56 ppm (m, 4H, H_δ), 1.68 ppm (m, 4H, $H_{\delta terminal}$), 1.83 ppm (m, 4H, H_β), 2.98 ppm (m, 4H, $H_{\varepsilon terminal}$, CH_2NH_2), 3.20- 3.40 ppm (m, 4H, H_ε, CH_2NHCO), 3.68, 4.22 ppm (2H, H_α, CHNHCO, 1H, CH(COOH)NHCO), 4.50 ppm (m, 2H, CHOH).

^{13}C-NMR (D_2O, 100 MHz, Table 19): signals at δ 21.6 ppm (C_γ), 26.4 ppm ($C_{\delta terminal}$), 28.0 ppm (C_δ), 30.2 (C_β), 38.6 ppm (C_ε), 39.0 ($C_{\varepsilon\ terminal}$), 54.7 ppm ($C_\alpha$), 72.2 (**C**HOH), 173.6, 175.2 ppm (**C**ONH).

FT-IR (KBr pellet, Table 17): peaks at 3323 (vs, N-H and O-H stretching), 2937, 2864 (w, C-H stretching), 2632, 2130 (w, NH_3^+ stretching), 1654 (vs, C=O amide stretching), 1581, 1520 (vs, N-H amide bending), 1130, 1074 (m, C-O stretching) cm^{-1}.

Potentiometric titration: NH_2 (I flex) at 123.76meq/Kg; NH_2 (II flex) at 56.38 meq/Kg; COOH at 40.59 meq/Kg.

Optical rotation: $[\alpha]_D$= 56.40 (23°C)

Product 3:

^{1}H-NMR (D_2O, 400 MHz, Table 18): signals at δ 1.41 ppm (m, 4H, H_γ), 1.59 ppm (m, 4H, H_δ), 1.71 ppm (m, 4H, $H_{\delta\ terminal}$), 1.88 ppm (m, 4H, H_β), 3.01 ppm (m, 4H, $H_{\varepsilon terminal}$, CH_2NH_2), 3.18- 3.38 ppm (m, 4H, H_ε, CH_2NHCO), 3.72, 4.21 ppm (2H, H_α, CHNHCO, 1H, CH(COOH)NHCO), 4.52 ppm (m, 2H, CHOH).

^{13}C-NMR (D_2O, 50 MHz, Table 19): signals at δ 20.8 ppm (C_γ), 25.6 ppm ($C_{\delta terminal}$), 27.3 ppm (C_δ), 29.3 ppm (C_β), 37.8 ppm (C_ε), 38.2 ($C_{\varepsilon\ terminal}$), 53.8 ppm ($C_\alpha$), 71.4 (**C**H-OH), 172.7, 174.1 ppm (**C**ONH).

FT-IR (KBr pellet, Table 17): 3323 (vs, N-H and O-H stretching), 2939, 2865 (w, C-H stretching), 2630, 2135 (w, NH_3^+ stretching), 1650 (vs, C=O amide stretching), 1583, 1520 (vs, N-H amide bending), 1132, 1074 (m, C-O stretching) cm^{-1}.

Potentiometric titration: NH_2 (I flex) at 53.03 meq/Kg; NH_2 (II flex) at 73.72 meq/Kg; COOH at 42.38 meq/Kg.

Optical rotation: $[\alpha]_D$= 55.40 (23°C)

Product 5:

^{1}H-NMR (D_2O, 400 MHz, Table 18): signals at δ 1.41 ppm (m, 4H, H_γ), 1.59 ppm (m, 4H, H_δ), 1.72 ppm (m, 4H, $H_{\delta\ terminal}$), 1.88 ppm (m, 4H, H_β), 3.02 ppm (m, 4H, $H_{\varepsilon\ terminal}$, C**H**$_2$$NH_2$), 3.20- 3.40 ppm (m, 4H, H_ε, C**H**$_2$NHCO), 3.73, 4.22 ppm (2H, H_α, C**H**NHCO, 1H, C**H**(COOH)NHCO), 4.52 ppm (m, 2H, C**H**OH).

^{13}C-NMR (D_2O, 50 MHz, Table 19): signals at δ 20.8 ppm (C_γ), 25.6 ppm ($C_{\delta terminal}$), 27.3 ppm (C_δ), 29.3 ppm (C_β), 37.9 ppm (C_ε), 53.8 ppm (C_α), 71.4 (**C**HOH), 172.7, 173.9 ppm (**C**ONH).

FT-IR (KBr pellet, Table 17): 3323 (vs, N-H and O-H stretching), 2939, 2864 (w, C-H stretching), 2630, 2131 (w, NH_3^+ stretching), 1645 (vs, C=O amide stretching), 1582, 1516 (vs, N-H amide bending), 1131, 1075 (m, C-O stretching) cm^{-1}.

Potentiometric titration: NH_2 (I flex) at 60.46 meq/Kg; NH_2 (II flex) at 104.70 meq/Kg; COOH at 99.73 meq/Kg.

Optical rotation: $[\alpha]_D$= 54.40 (23°C)

MALDI: fragments at 928, 1188, 1448, 1709, 1969, 2097 g/mol.

5.5.3.2 Method 1: in a "Sovirel® tube" (1:2)

Into a Sovirel tube, triethylamine (58.7 mg, 0.58 mmol) is added, under nitrogen atmosphere and under continuous stirring to 4 mL of a methanol solution of L-lysine (314.3 mg (2.148 mmol). A methanol solution (2 mL) of dimethyl L-tartrate (191.3 mg, 1.074 mmol) is added and the mixture is allowed to react at 80°C for 24 hours (**product 2**). After cooling to room temperature, the mixture is filtered on a büchner funnel and the solid obtained is washed with methanol and dried at room temperature (271.0 mg, 53.6% yield).

The reaction was repeated by increasing the reaction time to 3 days (**product 4**) and 7 days (**product 6**) under a nitrogen atmosphere, respectively, with 66.3% (335.2 mg) and 71.8% (368 mg) yields.

Product 2

^{1}H-NMR (D_2O, 400 MHz, Table 18): signals at δ 1.38 ppm (m, 4H, H_γ), 1.56 ppm (m, 4H, H_δ), 1.68 ppm (m, 4H, $H_{\delta terminal}$), 1.83 ppm (m, 4H, H_β), 2.98 ppm (m, 4H, $H_{\varepsilon terminal}$, CH_2NH_2), 3.20- 3.40 ppm (m, 4H, H_ε, CH_2NHCO), 3.68, 4.22 ppm (2H, H_α, CHNHCO, 1H, CH(COOH)NHCO), 4.50 ppm (m, 2H, CHOH).

^{13}C-NMR (D_2O, 100 MHz, Table 19): signals at δ 21.6 ppm (C_γ), 26.4 ppm ($C_{\delta terminal}$), 28.0 ppm (C_δ), 30.2 (C_β), 38.6 ppm (C_ε), 39.0 ($C_{\varepsilon\ terminal}$), 54.7 ppm ($C_\alpha$), 72.2 (**C**HOH), 173.6, 175.2 ppm (**C**ONH).

FT-IR (KBr pellet, Table 17): peaks at 3323 (vs, N-H and O-H stretching), 2937, 2864 (w, C-H stretching), 2632, 2130 (w, NH_3^+ stretching), 1654 (vs, C=O amide stretching), 1581, 1520 (vs, N-H amide bending), 1130, 1074 (m, C-O stretching) cm^{-1}.

Potentiometric titration: NH_2 (I flex) at 294.62meq/Kg; NH_2 (II flex) at 89.69 meq/Kg; COOH at 72.14 meq/Kg.

Optical rotation: $[\alpha]_D$= 55.80 (23°C)

Product 4:

^{1}H-NMR (D_2O, 400 MHz, Table 18): signals at δ 1.41 ppm (m, 4H, H_γ), 1.59 ppm (m, 4H, H_δ), 1.71 ppm (m, 4H, $H_{\delta\ terminal}$), 1.88 ppm (m, 4H, H_β), 3.01 ppm (m, 4H, $H_{\varepsilon terminal}$, CH_2NH_2), 3.18- 3.38 ppm (m, 4H, H_ε, CH_2NHCO), 3.72, 4.21 ppm (2H, H_α, CHNHCO, 1H, CH(COOH)NHCO), 4.52 ppm (m, 2H, CHOH).

^{13}C-NMR (D_2O, 50 MHz, Table 19): signals at δ 20.8 ppm (C_γ), 25.6 ppm ($C_{\delta terminal}$), 27.3 ppm (C_δ), 29.3 ppm (C_β), 37.8 ppm (C_ε), 38.2 ($C_{\varepsilon\ terminal}$), 53.8 ppm ($C_\alpha$), 71.4 (**C**H-OH), 172.7, 174.1 ppm (**C**ONH).

FT-IR (KBr pellet, Table 17): 3323 (vs, N-H and O-H stretching), 2939, 2865 (w, C-H stretching), 2630, 2135 (w, NH_3^+ stretching), 1650 (vs, C=O amide stretching), 1583, 1520 (vs, N-H amide bending), 1132, 1074 (m, C-O stretching) cm^{-1}.

Potentiometric titration: NH_2 (I flex) at 182.09 meq/Kg; NH_2 (II flex) at 82.28 meq/Kg; COOH at 50.62 meq/Kg;

Optical rotation: $[\alpha]_D$= 55.80 (23°C)

Product 6:

^{1}H-NMR (D_2O, 400 MHz, Table 18): signals at δ 1.41 ppm (m, 4H, H_γ), 1.59 ppm (m, 4H, H_δ), 1.72 ppm (m, 4H, $H_{\delta\ terminal}$), 1.88 ppm (m, 4H, H_β), 3.02 ppm (m, 4H, $H_{\varepsilon\ terminal}$, C**H**$_2$$NH_2$), 3.20- 3.40 ppm (m, 4H, H_ε, C**H**$_2$NHCO), 3.73, 4.22 ppm (2H, H_α, C**H**NHCO, 1H, C**H**(COOH)NHCO), 4.52 ppm (m, 2H, C**H**OH).

^{13}C-NMR (D_2O, 50 MHz, Table 19): signals at δ 20.8 ppm (C_γ), 25.6 ppm ($C_{\delta terminal}$), 27.3 ppm (C_δ), 29.3 ppm (C_β), 37.9 ppm (C_ε), 53.8 ppm (C_α), 71.4 (**C**HOH), 172.7, 173.9 ppm (**C**ONH).

FT-IR (KBr pellet, Table 17): 3323 (vs, N-H and O-H stretching), 2939, 2864 (w, C-H stretching), 2630, 2131 (w, NH_3^+ stretching), 1645 (vs, C=O amide stretching), 1582, 1516 (vs, N-H amide bending), 1131, 1075 (m, C-O stretching) cm^{-1}.

Potentiometric titration: NH_2 (I flex) at 72.48 meq/Kg; NH_2 (II flex) at 89.56 meq/Kg; COOH at 108.72 meq/Kg.

Optical rotation: $[\alpha]_D$= 54.61 (23°C)

5.5.3.3 Method 2: in a "Rotary evaporator" (1:2)

Into a 10 mL a neck flask, L-lysine (146.20 mg, 1 mmol) is added to dimethyl L-tartrate (89.07 mg, 0,5 mmol). The mixture is allowed to react at 60°C for 9 hours in the rotary evaporator (**product 7**).

At the end of the reaction, the formation of a yellow solid is observed: the solid is washed with methanol, filtered on a büchner funnel and dried under vacuum at room temperature (85.2 mg, 36.2% yield).

^{1}H-NMR (D_2O, 400 MHz, Table 18): signals at δ 1.41 ppm (m, 4H, H_γ), 1.59 ppm (m, 4H, H_δ), 1.71 ppm (m, 4H, $H_{\delta\ terminal}$), 1.87 ppm (m, 4H, H_β), 3.01 ppm (m, 4H, $H_{\varepsilon\ terminal}$, C**H**$_2NH_2$), 3.18- 3.38 ppm (m, 4H, H_ε, C**H**$_2$NHCO), 3.71, 4.23 ppm (2H, H_α, C**H**NHCO, 1H, C**H**(COOH)NHCO), 3.80 (s, 0.2H, OCH_3), 4.52 ppm (m, 2H, C**H**OH).

^{13}C-NMR (D_2O, 50 MHz, Table 19): signals at δ 21.4 ppm (C_γ), 26.3 ppm ($C_{\delta\ terminal}$), 28.0 ppm (C_δ), 30.0 ppm (C_β), 38.6 ppm (C_ε), 39.0 ppm ($C_{\varepsilon\ terminal}$), 54.4 ppm ($C_\alpha$), 72.4 (**C**H-OH), 173.5, 175.6 ppm (**C**ONH).

FT-IR (KBr pellet, Table 17): peaks at 3321 (vs, N-H and O-H stretching), 2939, 2864 (w, C-H stretching), 2624, 2132 (w, NH_3^+ stretching), 1650 (vs, C=O amide stretching), 1583, 1520 (vs, N-H amide bending), 1130, 1068 (m, C-O stretching) cm^{-1}.

Potentiometric titration: NH_2 (I flex) at 264.58 meq/Kg; NH_2 (II flex) at 216.15 meq/Kg; COOH at 175.91 meq/Kg;

5.5.4 L-lysine reactivity

5.5.4.1 Method 1: in a "Sovirel® tube"

Into a Sovirel® tube, triethylamine (58.7 mg, 0.58 mmol) is added, under nitrogen atmosphere and under continuous stirring to 4 mL of a methanol solution of L-lysine (314.3 mg (2.148 mmol). The mixture is allowed to react at 80°C for 24 hours (**product 8**). After cooling to room temperature, the solid is filtered on a büchner funnel, washed with methanol and dried at room temperature.

^{1}H-NMR (D_2O, 400 MHz, Table 18): signals at δ 1.39 ppm (m, 2H, H_γ), 1.65 ppm (m, 4H, H_δ, H_β), 2.95 ppm (m, 2H, H_ε, CH_2NH_2), 3.35 ppm (m, 1H, H_α, CHNHCO).

^{13}C-NMR (D_2O, 100 MHz, Table 19): signals at δ 21.8 ppm (C_γ), 27.1 ppm (C_δ), 32.9 ppm (C_β), 39.2 ppm (C_ε), 55.3 ppm (C_α), 181.1 ppm (**C**=O).

FT-IR (KBr pellet, Table 17): peaks at 3354 (m, N-H stretching), 2937, 2862 (vs, C-H stretching), 2620, 2135 (w, NH_3^+ stretching), 1582 (vs, COO^- stretching), 1516 (vs, N-H amino bending) cm^{-1}.

5.5.4.2 Method 2: in a "Rotary evaporator"

Into a 10 mL a neck flask, L-lysine (146.20 mg, 1 mmol) is introduced. The solid is allowed to react at 60°C for 8 hours in the rotary evaporator (**product 9**). At the end of the reaction the solid is dried under vacuum at room temperature.

The reaction was repeated by increasing the reaction times to 12 hours (**product 10**).

^{1}H-NMR (D_2O, 400 MHz, Table 18): signals at δ 1.39 ppm (m, 2H, H_γ), 1.65 ppm (m, 4H, H_δ, H_β), 2.95 ppm (m, 2H, H_ε, CH_2NH_2), 3.35 ppm (m, 1H, H_α, CHNHCO).

^{13}C-NMR (D_2O, 100 MHz, Table 19): signals at δ 21.8 ppm (C_γ), 27.1 ppm (C_δ), 32.9 ppm (C_β), 39.2 ppm (C_ε), 55.3 ppm (C_α), 181.1 ppm (**C**=O).

FT-IR (KBr pellet, Table 17): peaks at 3350 (m, N-H stretching), 2940, 2868 (vs, C-H stretching), 2620, 2135 (w, NH_3^+ stretching), 1584 (vs, COO^- stretching), 1520 (vs, N-H amino bending) cm^{-1}.

6 TiO_2- oligoamide nanocomposites

6.1 Nanocomposites

Nanocomposites materials (also simply called "nanocomposites") are materials composed by a polymeric, ceramic or metallic matrix in which another material, mainly inorganic, is dispersed, the latter having nanometric (0.1-100 nm) dimensions. Consequently, a polymeric nanocomposite is composed by a polymeric matrix (being thermoplastic or thermosetting) and by nanoparticles, used to give peculiar properties to the material, regarding for example mechanical, thermal, optical, electrical, rheological or catalytic features.

Generally, in nanocomposites, the properties of the final material are better than the simple sum of the properties of the single phases[79,80].

Given these features, nanocomposites have been intensively studied for the last years, since they can have interesting applications both on an academic and on an industrial level in many different fields, such as the E&E, diagnostic, biomedical or environmental ones[81,82].

In most cases, the nanocomposite material is composed by a core-shell system, which can be broadly defined as comprising a core (inner material) and a shell (outer layer material). In order to get this kind of system, different nanoparticles can be used, having different nature and composition according to the features that the final material should have. Nanoparticles most commonly used in this field are metal oxides (i.e. ZnO, SiO_2, TiO_2), metals (Ag nanopowders), carbon-based materials (nanotubes and nanofibers) and clays.

In nanocomposites, nanoparticles are generally present in low quantities within the polymeric matrix (5-10% maximum) but, thanks to their very small dimensions, they can remarkably influence the properties of the final material; the kind of influence they have depends according to the chemical nature of the nanoparticle and the matrix, on their shape and dimensions, on their concentration and on the interactions that arise between the organic and inorganic phases. Usually it is very important to get the desired properties without significantly change the weight and the ductility of the polymeric matrix, and without altering the production process of the material, in order to limit production costs increase.

The efforts of the researches have therefore been dedicated to the study of procedures useful to obtain optimal dispersion of the nanoparticles within the polymeric matrices, in order to understand the "limit" properties that can be achieved with traditional polymeric matrices. Zhang

et al.[83] for example, studied 1 vol.% TiO_2-PA6,6 nanocomposites, demonstrating an increase of creep resistance and a better dimensional stability in comparison to Nylon 6,6 alone (DuPont Zytel® 101).

Jia et al.[84] in 2007 evaluated the properties of nanosilica/polyvinylalcohol (PVA-SNs) nanocomposites obtained by in situ radical polymerization, deriving from the functionalization of silica nanoparticles with VTEOS (vinyltriethoxysilane) and their reaction with VAM (Vinyl acetate monomer). The product they obtained was saponified via hydrolysis with a NaOH solution and the nanocomposite showed an increase of mechanical and thermal properties in comparison to pure PVOH, thanks to the presence of chemical bonds between the nanoparticles and the polymeric matrix. It indicated that the interfacial actions between polymer and inorganic components were very important for their enhancement of hybrid properties.

Inclusions of nanoparticles can modify thermal properties of the material because they act as thermal insulator and as mass transport barrier for volatile products that are generated during thermal decomposition.

Tang et al.[85] for instance, evaluated via TGA the improvement in thermal stability owed to the nano-ZnO/P(MMA–MAA)composite particles, prepared by dispersion of ZnO nanoparticles in a P(MMA-MAA) matrix, comparing the results with pure polymer. (MMA: methyl methacrylate; MAA: methacrylic acid).

Patra et al.[86] conducted a study using thermal analyses on pure PMMA and on a nanocomposite PMMA containing TiO_2 nanorods, demonstrating that the higher weight loss of the material is obtained at higher temperatures when nanorods are used, confirming the higher thermal stability and that this behaviour becomes more marked as the quantity of nanorods increases. This feature can be attributed to the barrier effect of nanoparticles, that lower heat diffusion in the polymeric matrix, limiting thermal degradation.

Generally, several studies evidence the improvements obtained with nanocomposite materials in comparison to pure polymers, however, it is also possible to find studies where a loss of properties is obtained when nanoparticles are used. In a study by Motaung et al.[87] the T_g of a pure PMMA was compared to the one of a PMMA composite having 5% of TiO_2, evidencing a significant increase of glass transition when TiO_2 is present; conversely, in some nanocomposites a lower T_g was observed in comparison to the polymeric matrix alone[88]. This phenomenon can be explained considering the attractive or repulsive interactions between the nanoparticles causing, respectively, an increase or a lowering of T_g.

Also other factors can influence the features of the final product, as the quality of the dispersion, the adhesion on the interface between the phases and the dimension of the interphase itself, the preparation method of the nanocomposite and possible surface modifications of the nanoparticle[89–92].

The first researches on the synthesis of polymeric nanocomposites were conducted by simply dispersing raw nanoparticles in a polymer. This approach can lead to the formation of agglomerates, that can cause a decrease of mechanical properties and of the optical transparency (in case the matrix is transparent) of the nanocomposite[93,94] (Figure 108).

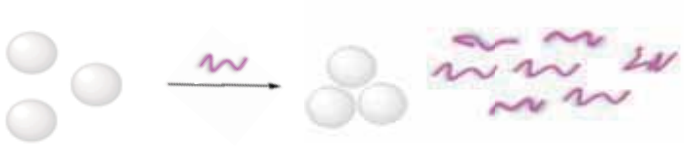

Figure 108: bad mixing between nanoparticles and polymeric matrix.

In order to get "high performance" polymeric nanocomposites it is fundamental not to have aggregates: this can be achieved when a good affinity between nanoparticles and the polymeric matrix is present.

In literature, examples of nanocomposites obtained from properly modified nanoparticles mixed with a polymeric matrix are present, giving improved homogeneity of the final material[95] (Figure 109). Nevertheless, also functionalization is not always the best way to achieve good dispersion, due to dimensional and structural changes of the nanoparticles, that can even lead to the formation of aggregates[94,96].

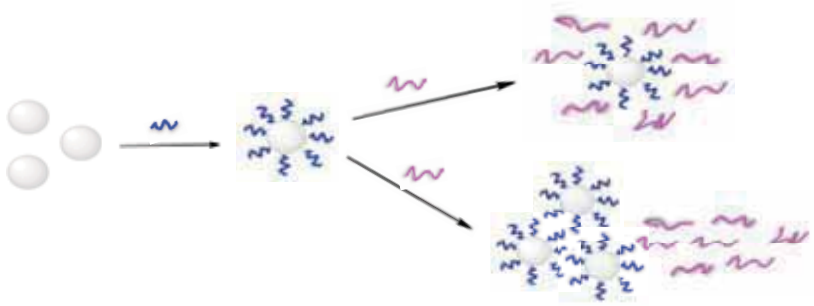

Figure 109: functionalisation of nanoparticles and subsequent mixing with the polymer: effective dispersion (top right) and ineffective dispersion (bottom right).

One of the best way to get nanocomposites having an high degree of dispersion relies on an initial functionalization of the nanoparticles with coupling agents having within their structure a functional group potentially reactive with the polymeric matrix: this allows obtaining a chemical

reaction between the polymer and the nanoparticles, favoring an homogeneous dispersion being stable over time (Figure 110).

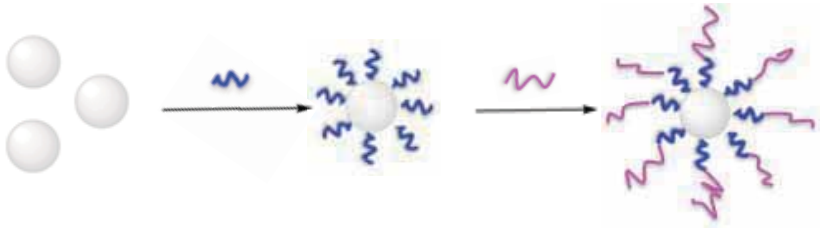

Figure 110: functionalization of nanoparticles and subsequent polymerization reaction.

This approach is very simple and effective and allows having a good covering of the inorganic nanoparticles' surface, that is stable over time, thanks to the formation of covalent bonds between coupling agent and nanoparticle.

With inorganic oxides nanoparticles, the most frequently used coupling agents belong to the silanes family, mainly chloro- and alkoxy-silanes, that tend to react with the hydroxyl groups present on the surface of the nanoparticles. One limit of silanes is that they also have the tendency to react with themselves more than with nanoparticles, forming a polysiloxane network, favoured in water, that leads to poor coverage of the surface of the nanoparticles. As a consequence, at the end of the reaction, an organic-inorganic phase separation can occur[97].

In literature there are, anyway, examples of effective functionalizations in water or water/organic solvent[98].

Liquid phase, i.e. an organic solvent, and inert atmosphere are required to have an effective reaction[99]: these conditions lead to cover the nanoparticles, with consequent formation of a functionalized product stable over time.

The reaction required for the formation of nanocomposites can be obtained by grafting polymers on the functionalized nanoparticles[93] or mixing the nanoparticles with monomers and having a bulk "in situ" polymerization[93,100–102], as for example Basilissi et al. did with nanocomposites between PLA and functionalized nanosilica[103].

Li et al.[104] performed studies on mesoporous titania grafted poly(styrene-divinylbenzene)/maleic anhydride [P(ST-DVB)/MA] nanocomposite microspheres, prepared by an open ring reaction method. Nanoparticles were modified through functionalization with silanes (having amino terminal groups) to avoid their aggregation; later, they were reacted with the mesoporous polymer, whose surface had previously been modified with MA to allow the reaction with amino terminal groups of the silane present on TiO_2 nanoparticles. The nanocomposite synthesized

showed a good homogeneity (uniform distribution of nanoparticles on the surface of the polymer), a very good UV protection effect and a slow release of agents inserted in the mesoporous polymer, such as cosmetic or photo-reactive agents.

Yuvaraj et al.[105] conducted syntheses of TiO_2-polypyrrole nanocomposites using supercritical CO_2. In this case, nanoparticles were surface modified with 3-(trimethoxy)propyl metacrylate, to try to homogeneously disperse CO_2 before polymerization between pyrrole and functionalized TiO_2 particles.

In a work by Rong et al.[106] the synthesis of TiO_2-polystyrene nanocomposites was performed through modification of the nanoparticles with 3-(trimethoxysilyl)propylmetacrylate followed by incorporation in the polymeric matrix, via polystyrene radical polymerization.

The effective interaction between the organic matrix and the inorganic part of nanoparticles is fundamental also to lower toxicity issues related to the presence of free nanoparticles[107,108]. When nanoparticles are chemically bonded with the polymer, their mobility is greatly reduced, with a higher safety for health.

The synthetic method used for the production of nanocomposite materials influences markedly the features of the material. The methods that are most commonly used are mainly four[81]:

1) **Solution synthesis**: the polymer is dissolved in a solvent and nanoparticles are dispersed in it. The nanocomposite can be obtained via precipitation in a non-solvent or through solvent evaporation. Problems related to this method are:
   a) the need to avoid nanoparticles aggregation.
   b) it is often necessary to use of organic solvents, that have often toxicity and flammability issues.
   c) dilute solutions are used, therefore a lot of solvents required to produce small quantities of nanocomposite.
2) **"In situ" synthesis** (of nanoparticles, polymer or both): polymerization is carried out in the presence of the nanoparticles, starting from their dispersion in the monomer(s) or in a monomer solution[102]. It is an easy procedure and no sophisticated equipment is required. In some cases the synthesis of nanocomposite in the presence of the polymer can be obtained[109].
3) **Melt mixing**: the polymer/nanoparticle mixture is heated at high temperature (generally over polymer melt temperature) and then the organic phase is mixed with the inorganic one.

This method has many advantages, since no organic solvents are used and since it is compatible with industrial production methods such as extrusion or injection molding[110]. Besides it is a good alternative when polymeric matrices that are not suitable to solution or "in situ" synthesis are used[110].

The problems related to "melt mixing" are owed to the necessity of having high temperatures, especially for polymers requiring processing at hight temperatures (i.e. polyamides, polycarbonates); in this case, organic compatibilizer present in the nanoparticles could undergo degradation, jeopardizing the quality of the nanocomposite[111,112].

6.2 Nanocomposites based on Titanium dioxide (TiO_2)

Titanium dioxide (TiO_2) for the last years has been widely studied due to its interesting physico-chemical properties, that include high stability and hydrophilicity, high refractive index and good photocatalytic activity, besides having low price and very good availability. It is commonly used in many fields, such as cosmetics, catalysis, pigments and solar cells devices[113,114].

It is present in 3 crystalline forms, one stable (rutile) and two metastable, anatase and brookite: between the two metastable ones, anatase has a higher stability[114].

Rutile, being the most abundant form, is used in many fields and mainly in the pigments sector to give dullness and white color in paints, plastics, inks and papers, thanks to its high refractive index[114,115].

In the last years, TiO_2 has found applications also in new sectors, such as the photocatalysis[113,114] since, through the direct absorption of photons, it can take part in photochemical processes on the surface.

When it is irradiated with a radiation having an energy higher or similar to its band gap, electron/hole pairs can be generated that can give redox reactions on the surface of the oxide (electrons go from valence to conduction band).

The steps involved in the process are the following ones[116] (Figure 111):

1) photoexcited TiO_2 catalyst produces electron-hole pairs that migrate to TiO_2 surface;
2) photogenerated holes (oxidant feature) in TiO_2 can react with adsorbed H_2O or OH^- at the catalyst/water interface to produce the highly reactive hydroxyl radicals; the electrons (reducing feature) can react with oxygen vacancies to form superoxide ions (O_2^{-}).

3) The species generated, highly reactive, can oxidate many organic compounds.

The increase of band gap reduces the ricombination rate of the electron/vacancy coupling, increasing therefore photocatalytic efficiency.

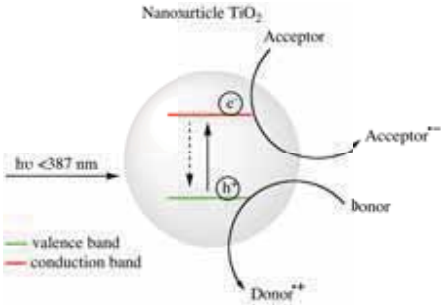

Figure 111: TiO_2 nanoparticle activation thanks to UV radiation

Anatase form shows higher photoactivity, in accordance with the band gap energy being 3,00 eV for rutile and 3,23 eV for anatase[117]. Therefore, radiations having wavelength <387 nm can selectively excite anatase TiO_2: this phenomenon is of great interest for many applications.

Titanium oxide nanoparticles (<100 nm) exhibit also peculiar properties since their band gap increases as their dimensions become lower[116].

Titanium dioxide photocatalitic activity can be used in many fields, such as:

- **Air purification processes**[118,119]: a remarkable reduction of organic and inorganic substrates - mainly VOC and nitrogen oxides (NO_x) – deriving from indoor and outdoor pollution can be achieved.

  This effect has also been studied mixing TiO_2 with concrete (5% w/w on concrete) and comparing the effects using the same material with no TiO_2[118]. The process is as follows: TiO_2 nanoparticles are activated through UV radiation absorption, gaining the ability to degrade NO and NO_2. NO is oxidated to NO_2 thanks to reaction with •OH radical and NO_2 is oxidized and adsorbed as nitrate.

  Another useful feature in this field is the ability to reduce bioaerosols, one of the main indoor pollution sources, that involves the presence of more than 60 patogens microorganisms (bacteria, viruses and fungi). Diseases transmitted via bioaerosols include tuberculosis, Legionaries, influenza, colds, mumps, measles, rubella, small pox, aspergillosis, pneumonia, meningitis, diphtheria, and scarlet fever[120].
- **Deodorizing action**[118,119]: through decomposition of organic substrates causing indoor pollution, such as ammonia (NH_3), trimethylamine ($(CH_3)_3N$), hydrogen sulphide (H_2S),

methylmercaptane (CH_3SH), dimethylsulfide ($(CH_3)_2S$, formaldehyde and molecules responsible for cigarette smell.

Titanium dioxide, applied on tiles, can decompose toxic gases that are the cause of domestic illness and bad smell.

- **Reduction of textile yellowing**[121–125]: generally, in textile fibers, there are chromophores (aminoacids residues as cysteine, phenylalanine, tryptophan) that can absorb UV radiation. This absorbance causes molecules to reach excited states that, later, release energy: as a consequence, radicals are produced, forming chromophores on the aminoacids that are responsible for the yellowing. When TiO_2 is present, UV radiation absorption by chromophores is blocked and all the process is therefore altered. Yellowing is then reduced.
- **Super-hydrophilic properties**[118,126]: it is a very important feature of TiO_2 that is evident when the surface of the material is exposed to UV light. Super-hydrophilicity during irradiation and super-hydrophobicity ("lotus effect") at the end of irradiation represent the two features required to obtain self-cleaning materials, as for example for cleaning external walls of buildings, that get dirty because of car exhaust gases. With a titanium dioxide cover, a thin water layer is formed on the surface of the material, that is taken away by rain, preserving the aesthetic features of the building. Super-hydrophilicity is based on the production of electrons and holes after irradiation with UV light, but the reactions occurring are different in comparison to the ones of photocatalysis. Electrons reduce Ti^{4+} to Ti^{3+}, and holes ("h" in Figure 112) oxidate O^{2-} thus eliminating a O atom from the surface and creating the so-called "oxygen vacancy":

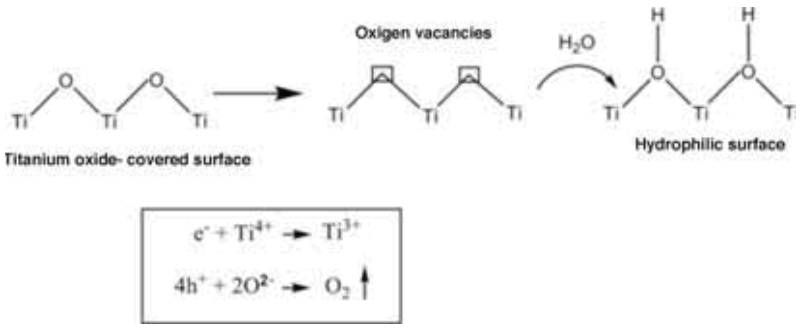

Figure 112: mechanism at the basis of hydrophylicity in TiO_2-covered surfaces

In this way, oxygen vacancies are accessible and are replaced by dissociated water molecules (OH^- groups), making the surface able to absorb water molecules. The higher the exposure to UV radiation, the lower the contact angle between surface and water. After about 30

minutes under a mild UV radiation, contact angle tends to 0° meaning that water tends to perfectly cover the surface itself. Stopping UV radiation, hydrophilic behavior remains for about 2 hours and then the surface becomes hydrophobic again.

- **Antimicrobial activity**[118,127,128]: titanium dioxide has a strong oxidant feature and can decompose bacteria and fungi that attack surfaces.
  It has been discovered that TiO_2 has antibacterial effect higher than any other antimicrobial agent since its catalytic activity continue also when cells are actively propagating. This effect is valid for fungi, bacteria and mold.
  Possible practical applications can be in hospitals (in surfaces and room disinfection), sanitary (prosthesis production), food and pharmaceutical field, in waste or clear water clearing, for the protection of trees from patogens[120] and in the cultural heritage field, to preserve degrading artifacts.
  This effect is attributed to the positive species formed by the photocatalytic activity of titanium dioxide, that react with the negative components present on the cell membrane of bacteria, causing its breakage. Bacterium metabolism ceases, causing its death.

The versatility of titanium dioxide has therefore allowed the development of many nanocomposite materials formed by a polymeric matrix and TiO_2 nanoparticles dispersion.
Kubacka et al.[129] conducted a study on the preparation of films based on iPP-TiO_2 nanocomposites with biocide features, adding 0.5-5% w/w of TiO_2. Nanocomposite characterization puts in evidence the formation of a nanometer-level dispersion of the titanium dioxide in the polymeric matrix, with aggregates having average dimension of 100 nm and with no significant changes on the structural features of the polymeric matrix.
The film showing higher biocide features is the one obtained using the nanocomposite having 2% w/w of TiO_2, regardless the microorganism used for the tests (Gram positive or negative bacteria). The nanocomposite enhances the antimicrobial activity of TiO_2 through an efficient movement of the charges through the organic-inorganic interface, making the whole system a biocide. These systems can find applications in a lot of fields, as food or biomedical packaging, for example as cover for surfaces or for general disinfection purposes.
Zhaobo Wang et al.[130] studied the synthesis of TiO_2-High impact polystyrene (HIPS) nanocomposites with antibacterial effect, to be used for packaging, toys, bottles, houseware and E&E applications. The introduction of TiO_2 only slightly influences the processability of HIPS, besides, with a low TiO_2 quantity, rheologic behaviour is enhanced. The surface of the

nanocomposite shows high UV light absorption in 250-400 nm range and it has been demonstrated that an increase on the quantity of inorganic fraction in the organic one increases the absorbance in that range. The germicide activity was evaluate checking the killing rate on *E. Coli* and *S. aureus*, counting vital cells. The antibacterial effect after 12 hours is relatively low, but significantly increases as the contact time increases up to 24 hours.

Among the many TiO_2-polyamide nanocomposites described in literature, examples on products obtained via melt mixing are present.

Ou Baoli et al.[131] studied the morphology of nanocomposites deriving from functionalized TiO_2 nanoparticles in a PP/PA6 (70/30) mixture, and the effects of the compatibility between the components. Usually, binary mixture of PP/PA6 polymers have low mechanical properties, due to the non-miscibility of the two polymers. It is therefore necessary to control and stabilize the desired morphology in the polymeric matrix to get materials with optimal properties. One of the methods used to reach this goal is the addition of TiO_2 nanoparticles to the polymeric matrix to modify interphase properties.

In a work of Yonglin Lei et al.[132] the photocatalytic activity under visible light of nanocomposites based on TiO_2 and dendrimeric aromatic polyamides having molecular switches based of spyrolactams (RG-TiO_2) was studied. Results show that the photo-catalys RG-TiO_2 improves the photocatalytic efficiency of the photodegradation of phenol in comparison to pure TiO_2 in the visible light spectrum. When RG-TiO_2 is acidified at pH 3, it turns from the spyrolactamic form (OFF) to the open-ring amidic form (ON). This new method for the production of photocatalytic TiO_2 gives an efficient way to develop photocatalysts with high efficiency that can be controlled via molecular switches.

6.3 Research methodology

In the Department of Chemistry of Università degli Studi di Firenze, after synthesizing and characterizing hydroxylated oligoamides and polyamides to be used as consolidant for waterlogged archaeological wood[33,34], the synthesis of nanocomposites deriving from oligoamides and titanium dioxide nanoparticles was performed, to complete the surface treatment of archaeological wood.

Nanocomposites having core-shell structure were synthesized, favouring the growth of oligoamides on TiO_2 nanoparticles functionalized with coupling agents, in order to get polymeric films having an homogeneous distribution of the nanoparticles.

Anatase titanium dioxide was used, since this crystalline form possesses a photoactivity higher than the one of rutile and brookite forms. Radiations with wavelength < 387 nm can therefore selectively excite this form, having antimicrobial features. Since another important factor in the choice of the nanoparticles is related to their dimension, (the band gap increases as the dimensions become lower, with a further enhancement of photo-activity), nanoparticles having diameter lower than 25 nm were chosen for the present study.

Antimicrobial activity has great importance in wood conservation, a field where hydroxylated oligoamides showed very good features but the use of organic consolidants can favour the attack of microorganisms and the development of fungi on the surface. Formulations containing TiO_2-polyamide nanocomposite could therefore be used on wood surfaces treated with the corresponding consolidants based on natural substrates.

The synthesis was performed in more steps, via activation of the nanoparticles, followed by functionalizing with coupling agents and then by “in situ” polymerization on the functionalized nanoparticles.

Different methods for the activation of nanoparticle powders were investigated, through acidification processes. Afterwards, activated nanoparticles underwent a functionalization step with two coupling agents, (3-aminopropyl)trimethoxysilane and [3-(2-aminoethylamino)propyl]trimethoxysilane, both containing a terminal amino group reactive in the subsequent polycondensation reaction.

Different nanocomposites were synthesized, changing the diacid and the reaction steps, obtaining core-shell systems where the polymer forms covalent bonds with the nanoparticles.

All the reactions were performed using diesters deriving from hydroxyl carboxylic acids (L-tartaric acid or α,α’-trehaluronic acid) and a diamine (1,2-ethylenediamine) to get the corresponding polyamides.

The products were characterized by NMR and FT IR spectroscopies, Dynamic Light Scattering (DLS) and by Transmission Electron Microscope (TEM)

The photocatalytic activity of the nanocomposites was studied via preliminary trials; at first, the degrading ability of the nanocomposite towards methylene blue under UV radiation[114,126,133] was tested and then the resistance to photo-degradation was evaluated, studying the possible structure variations by FT IR and NMR spectroscopies and evaluating color changes by colorimetric measurements.

After this phase, applicative studies were performed to evaluate the antimicrobial effectiveness of a nanocomposite on beech wood (Fagus sylvatica) using a fungus (*Trametes versicolor).*

6.4 Results and discussion

6.4.1 Synthesis and characterization of the products

6.4.1.1 Activation and characterization of titanium oxide nanoparticles

Various activation methods by acidification of the nanoparticles in powder form were investigated. The one that gave the best results was a modified version of K.K. Suma[134], in which TiO_2 powder and HNO_3 (2M) are placed in a flask, maintaining the dispersion at reflux (95°C) for 8 hours.

Subsequently the dispersion was centrifuged to remove the counter-ion of the acid and redispersed in MilliQ water, obtaining a dispersion at 4.5% w/w. The dispersion appears very stable: conversely, the dispersion obtained using the not-activated titanium dioxide is not stable, since TiO_2 tends to sink on the bottom.

After having distilled at reduced pressure the volatile components from a fraction of the dispersion, the characterization of the activated nanoparticles was performed by FT IR spectroscopy and TEM analysis. In FT IR spectrum (Figure 113) there are two bands of medium intensity at 3396 and 1635 cm^{-1} and a very intense broad band between 450 and 800 cm^{-1}. In agreement to what reported by Mesnage[113], the first two absorption bands are attributable to the stretching and bending of the hydroxyl groups surface, while the third band, more intense, is characteristic of the Ti-O stretching of titanium dioxide nanoparticles. Moreover there is a band at 1386 cm^{-1} attributable to the N-O stretching of the NO^{3-} residue, still present in the nanoparticles after activation.

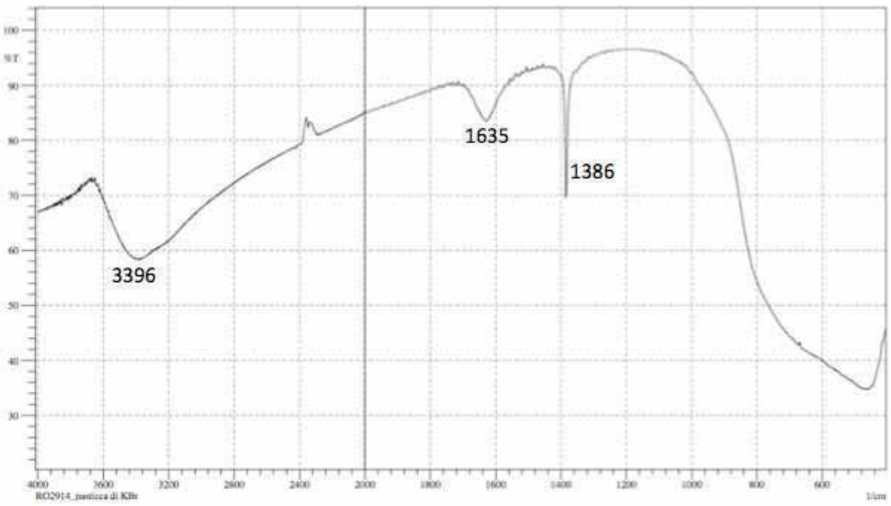

Figure 113: FT IR spectrum of TiO_2 nanoparticles activated with HNO_3

TEM image (Figure 114) confirm the presence of nanoparticles with a diameter of about 10-20 nm.

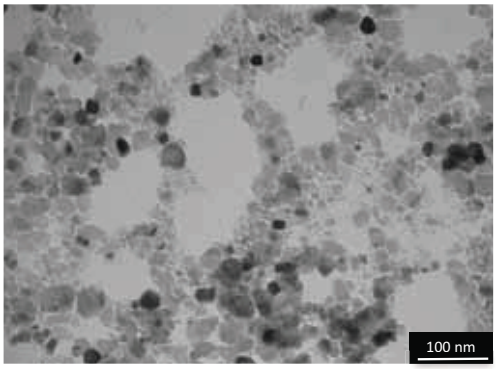

Figure 114: TEM image of TiO_2 nanoparticles on carbon grid

The reactions carried out on activated nanoparticles are summarized below, showing the codes of the synthesized products (Table 20) and the type of nanocomposites synthesized (Table 21).

Table 20: Codes of the synthesized products

Code product		Reagents
FNP	FNP.1	TiO_2- [3-(2-aminoethylamino)propyl]trimethoxysilane (AEAPTMS)
	FNP.2	TiO_2- (3-aminopropyl)trimethoxysilane (APTMS)
FNPE	FNPE.1	FNP.1 + dimethyl L-tartrate
	FNPE.2	FNP.1 + dimethyl α,α'-trehaluronate
	FNPE.3	FNP.2 + dimethyl L-tartrate
	FNPE.4	FNP.2 + dimethyl α,α'-trehaluronate
FNPO	FNPO.1	FNP.1 + dimethyl L-tartrate + 1,2-ethylendiamine
	FNPO.2	FNP.1 + dimethyl α,α'-trehaluronate + 1,2-ethylendiamine
	FNPO.3	FNP.2 + dimethyl L-tartrate + 1,2-ethylendiamine
	FNPO.4	FNP.2 + dimethyl α,α'-trehaluronate + 1,2-ethylendiamine
FNPEO	FNPEO.1	FNPE.1 + dimethyl L-tartrate + 1,2-ethylendiamine
	FNPEO.2	FNPE.2 + dimethyl α,α'-trehaluronate + 1,2-ethylendiamine
	FNPEO.3	FNPE.3 + dimethyl L-tartrate + 1,2-ethylendiamine
	FNPEO.4	FNPE.4 + dimethyl α,α'-trehaluronate + 1,2-ethylendiamine

Table 21: Syntheses of nanocomposites

Product	Molar ratio[a]	Yield A+ B (%)	DP[b] (A)
FNPO.1	1:3:2	67.3	2
	1:4:3	72.5	3
	1:10:9	75.0	6
FNPO.2	1:3:2	57.0	2
FNPO.3	1:3:2	63.0	3
FNPO.4	1:3:2	31.0	2
FNPEO.1	1:5:6	66.0	8
	1:9:10	74	12
FNPEO.2	1:5:6	77.8	9
FNPEO.3	1:5:6	74.6	17
FNPEO.4	1:2:3	70.4	14

[a]Molar ratio FNPE (or FNP): diester: diamine;

[b]DP= degree of polymerization of the soluble fraction (A).

6.4.1.2 Functionalized nanoparticle syntheses with the coupling agents (FNP)

The functionalized nanoparticles were synthesized using two different silylating agents, 3-(2-aminoethylamino)propyl]trimethoxysilane and (3-aminopropyl)trimethoxysilane, obtaining respectively FNP.1 and FNP.2 (Figure 115) as reported in Table 20, with the purpose of introducing an amino terminal group onto TiO_2 nanoparticles by reaction between hydroxyl groups and a silylating coupling agent

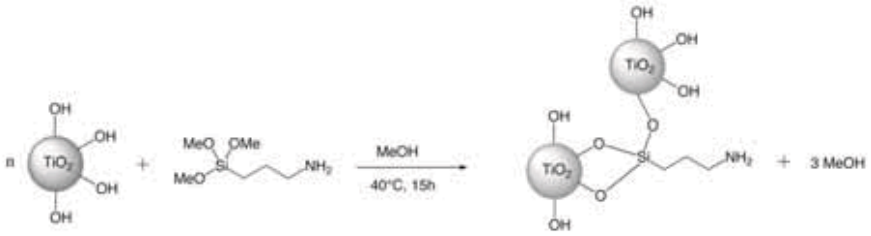

Figure 115: Functionalization reaction between TiO_2 nanoparticles with (3-aminopropyl)trimethoxysilane (FNP.2).

A water-dispersion of NPs (4.5% w/w) was added to the coupling agent diluted in methanol and the mixture was sonicated for 30' at room temperature, giving a stable, white dispersion.

Two syntheses were conducted, one by subjecting the mixture to heating at 40°C for 8 hours, the other for 15 hours.

In both cases, the reactions were monitored taking a portion of the dispersion that was distilled under reduced pressure to remove the solvent and volatile reagents. The solid obtained was washed in chloroform to separate the unreacted coupling agent or its soluble derivatives, from the functionalized nanoparticles.

The chloroform soluble fraction was distilled at reduced pressure, the insoluble one was dried at room temperature and reduced pressure. Both fractions were characterized by NMR and FT IR spectroscopies.

In the reaction carried out for 8 hours, in chloroform-soluble fraction, derivatives of the coupling agent are present, that are not found when the reaction is conducted for 15 hours. This means that increasing reaction time leads to a higher degree of functionalization of the nanoparticles.

In **FNP.1,** product formation is confirmed by ^{1}H-NMR analysis (Figure 116) thanks to the disappearance of a signal at 3.26 ppm relative to C**H**$_3$O- groups of the coupling agent; formation of covalent Si-O-Ti bond was confirmed by the change in chemical shifts of the other signals compared to those of the coupling agent as such; the shift of the signals from 0.53 ppm (SiC***H***$_2$), 1.58 ppm (SiCH$_2$C***H***$_2$) and 2.75 ppm (SiCH$_2$CH$_2$C***H***$_2$NHC***H***$_2$C***H***$_2$NH$_2$) to 0.63, 1.67 and 2.87 ppm is present respectively.

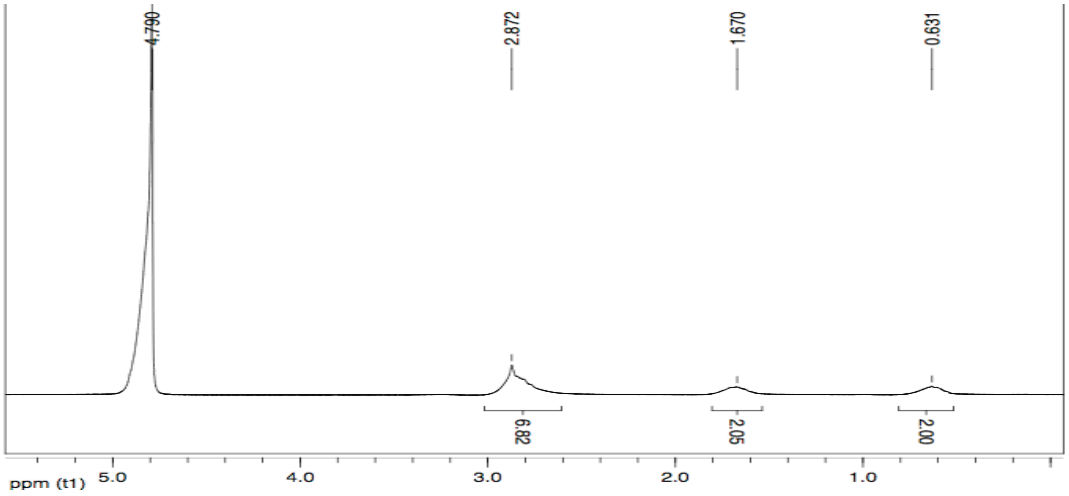

Figure 116: ^{1}H NMR spectrum in D2O of FNP.1

Analogously, **FNP.2** product formation (Figure 117) is confirmed by the disappearance of the signal at 3.26 ppm, and by the chemical shift of the other signals respect to the coupling agent unreacted from 0.54 ppm ($SiC\boldsymbol{H}_2$), 1.60 ppm ($SiCH_2C\boldsymbol{H}_2$) and 2.78 ppm ($SiCH_2CH_2C\boldsymbol{H}_2NH_2$) at 0.62, 1.70 and 2.90 ppm, respectively.

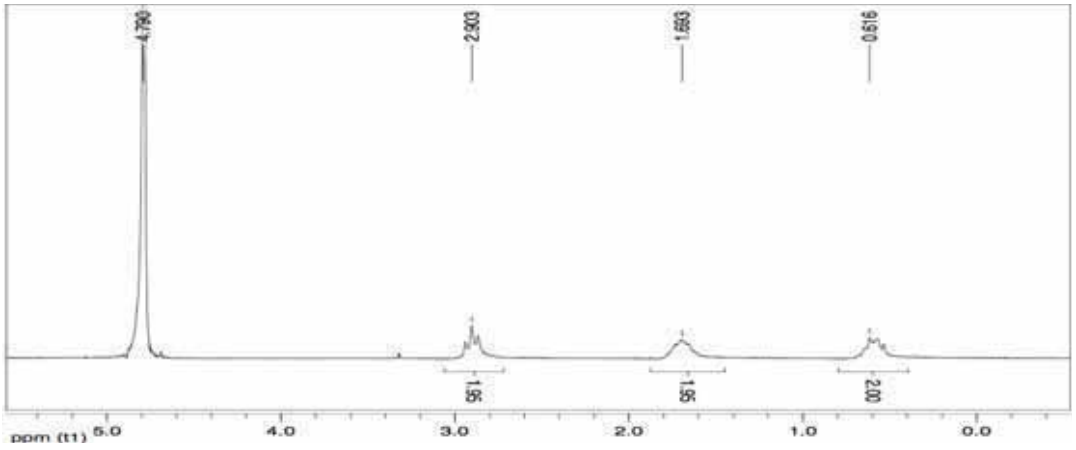

Figure 117: ^{1}H NMR spectrum in D_2O of FNP.2

Further, in FT IR spectrum (Figure 118) the product formation is confirmed by the peaks at 912 cm^{-1} due to Si-O-Ti stretching. The shape change and the shift of the product absorption bands relative to the Si-O stretching (1115 and 1032 cm^{-1}) is in agreement with the presence of functionalized nanoparticles, compared to the unreacted coupling agent: the shift is attributable to a change of the bond from $Si\text{-}OCH_3$ to Si-O-Ti. Also the bands related to the N-H stretching and

bending (3246, 1596 cm^{-1}), C-H stretching and bending (2924-2870, 1457 cm^{-1}) and C-N stretching (1353 cm^{-1}) are present.

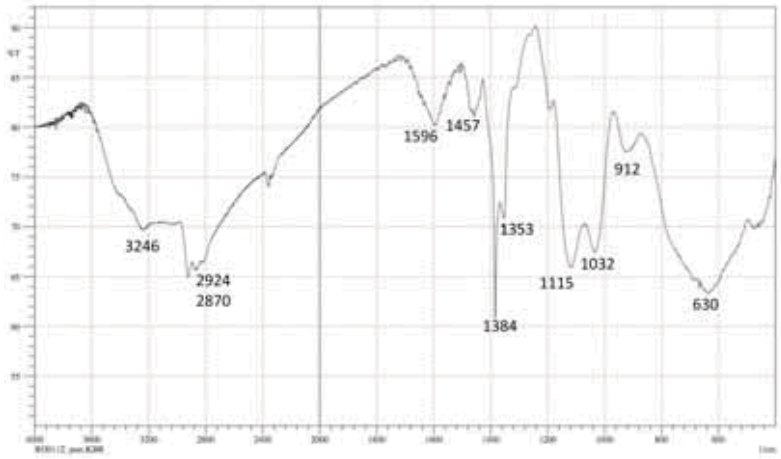

Figure 118: FT IR spectrum of the products FNP.1- FNP.2

6.4.1.3 Amide syntheses: reaction between FNP and dimethyl ester (FNPE)

To evaluate the reactivity of the terminal amino group on the functionalized nanoparticles (FNP) a reaction between the dispersion of the FNP products (FNP.1 or FNP.2) and a dimethyl ester (dimethyl L-tartrate or dimethyl α,α'-trehaluronate) was carried out, obtaining an amide compound with the terminal ester group (**Figure 119**).

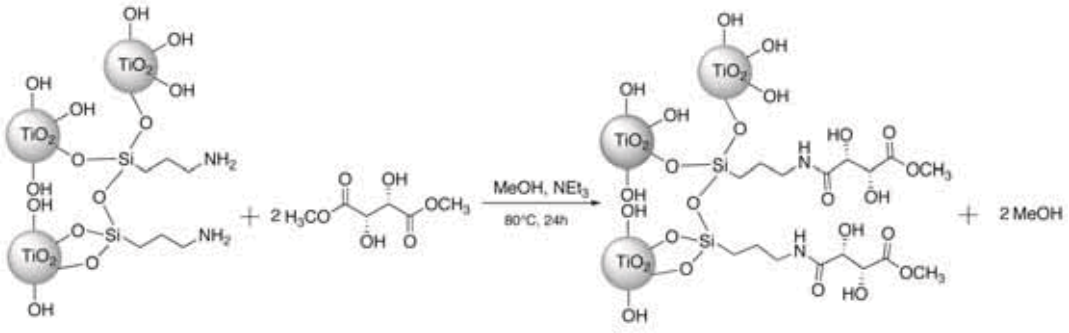

Figure 119: synthesis of FNPE

Syntheses were carried out with a molar ratio diester/ FNP equal to 1: 1 and 2: 1 obtaining in the first case "non-reactive" products (Figure 120), while in the second case the products exhibit reactive groups (Figure 119).

The structural characterization by ^{1}H NMR analysis was confirmed for all the synthesized products; in the spectrum of the FNPE.3 product obtained from the synthesis between FNP.2 and dimethyl L-tartrate in ratio 1: 1 (Figure 121) the signal relating to the OC**H**$_3$ terminal ester group at 3.80 ppm is not present. Moreover the integral ratio between diester and coupling agent signals is equal to 1: 2; therefore the product can be considered "non-reactive" because both ester units of dimethyl ester have reacted.

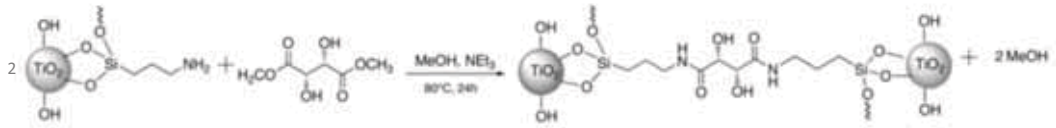

Figure 120: General synthesis scheme of a "non-reactive" product

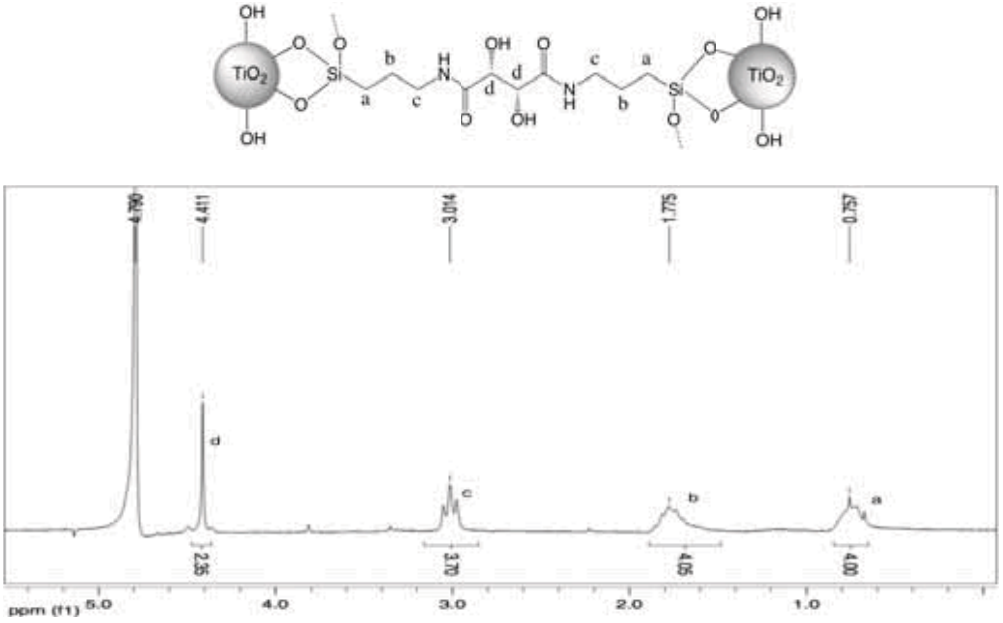

Figure 121: ^{1}H NMR spectrum in D_2O of the "non-reactive" FNPE.3 product obtained between FNP.2 and dimethyl L-tartrate in ratio equal to 1:1

All syntheses in ratio diester: coupling agent equal to 2: 1 (Figure 119) led to the formation of the expected product

FNPE.1- FNPE.3: based dimethyl L-tartrate compounds

FNP.1 and FNP.2 were subjected to condensation reactions with dimethyl L-tartrate. At the end of reaction each product was distilled at reduced pressure, washed with methanol and centrifuged, in order to remove the excess of dimethyl L-tartrate.

In ^{1}H NMR spectra of FNPE.1 and FNPE.3 (Figure 122) the product formation is confirmed by the presence of a signal related to the terminal ester group at 3.84 ppm, to the C**H**-OH group near amide at 4.42 ppm and to the C**H**-OH group near ester end group at 4.68 ppm.

The signals of coupling agent were subjected to a small shift in **FNPE.3** at 0.77 ppm ($SiC\mathbf{H}_2CH_2CH_2NH_2$), 1.81 ppm ($SiCH_2C\mathbf{H}_2CH_2NH_2$) and 3.05 ppm ($SiCH_2CH_2C\mathbf{H}_2NH_2$), as shown in Figure 122. **FNPE.1** presents the same signals of FNPE.3, but the coupling agent shifted at 0.73 ppm ($SiC\mathbf{H}_2CH_2CH_2NHCH_2CH_2$), 1.81 ppm ($SiCH_2C\mathbf{H}_2CH_2NHCH_2CH_2NH$), 3.00- 3.28 ppm ($SiCH_2CH_2C\mathbf{H}_2NHC\mathbf{H}_2CH_2NH$) and 3.60 ppm ($SiCH_2CH_2CH_2NHCH_2C\mathbf{H}_2NH$).

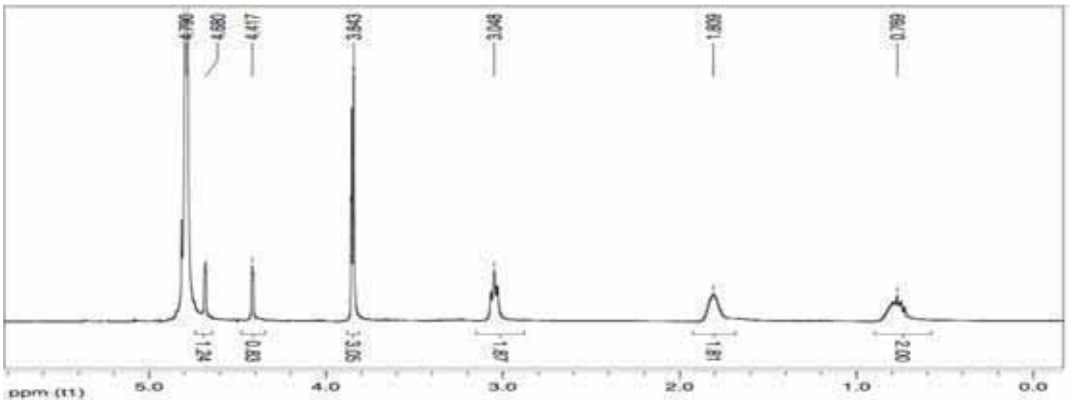

Figure 122: ^{1}H NMR spectrum of the product FNPE.3

In FT-IR spectrum (Figure 123) the band attributable to the ester group at 1738 cm^{-1} was present. The amide bands I and II were not observed separately because of the presence of other overlapped bands. In fact, H-OH bending, probably due to coordinated water, is present for all FNPE products; moreover a band attributable to N-H amine bending is present near 1600 cm^{-1} for FNPE.1. Several attempts for reduce water presence in these samples were unsuccessful.

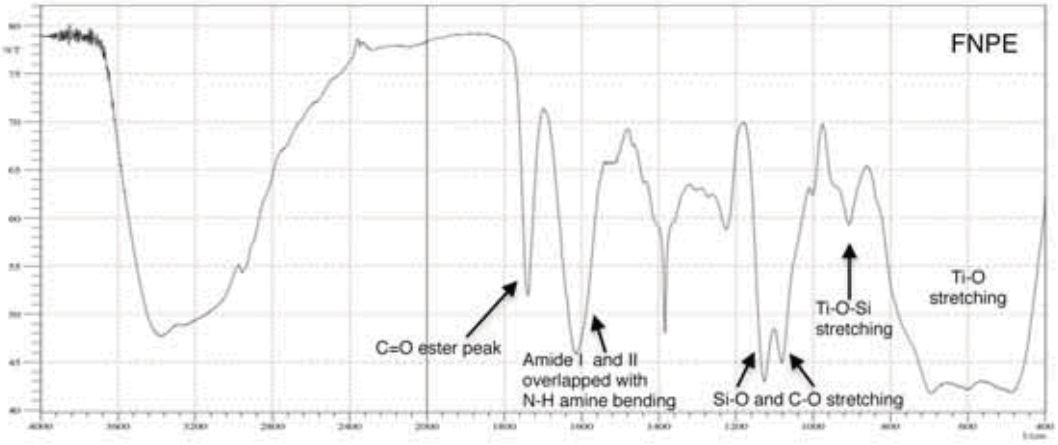

Figure 123: FT-IR spectrum of the products FNPE.1 and FNPE.3

FNPE.2- FNPE.4: : based dimethyl α,α'-trehaluronate

The products FNP.1 and FNP.2 were subjected to condensation reactions with dimethyl L-trehaluronate. Also in this case, at the end of reaction each product was distilled at reduced pressure, washed with methanol and centrifuged, in order to remove the excess of dimethyl α,α'-trehaluronate.

In ^{1}H NMR spectra of the products FNPE.2 and FNPE.4 (Figure 124) the amide formation is confirmed by the presence of a signal related to the H_1-H_1' at 5.19 ppm and those relating to terminal H_5 at 4.40 ppm which is separated from the one at 4.07 ppm (H_5 in α position to amide). Moreover in the range between 3.40 and 3.95 ppm signals related to H_2-H_2', H_3-H_3'- H_4-H_4' and -OC**H**$_3$ (singlet at 3.80 ppm) are present. As in the previous case the signals related to the coupling agent are visible, in **FNPE.2** these signals are present at 0.68 ppm (SiC**H**$_2$CH$_2$CH$_2$NHCH$_2$CH$_2$NH), 1.75 ppm (SiCH$_2$C**H**$_2$CH$_2$NHCH$_2$CH$_2$NH), 2.98 ppm (SiCH$_2$CH$_2$C**H**$_2$NHC**H**$_2$CH$_2$NH) and in the range 3.40- 3.95 ppm (SiCH$_2$CH$_2$CH$_2$NHCH$_2$C**H**$_2$NH) whereas in **FNPE.4** the coupling agent signals are present at 0.77 ppm (SiC**H**$_2$CH$_2$CH$_2$NH), 1.83 ppm (SiCH$_2$C**H**$_2$CH$_2$NH) and 3.10 ppm (SiCH$_2$CH$_2$C**H**$_2$NH).

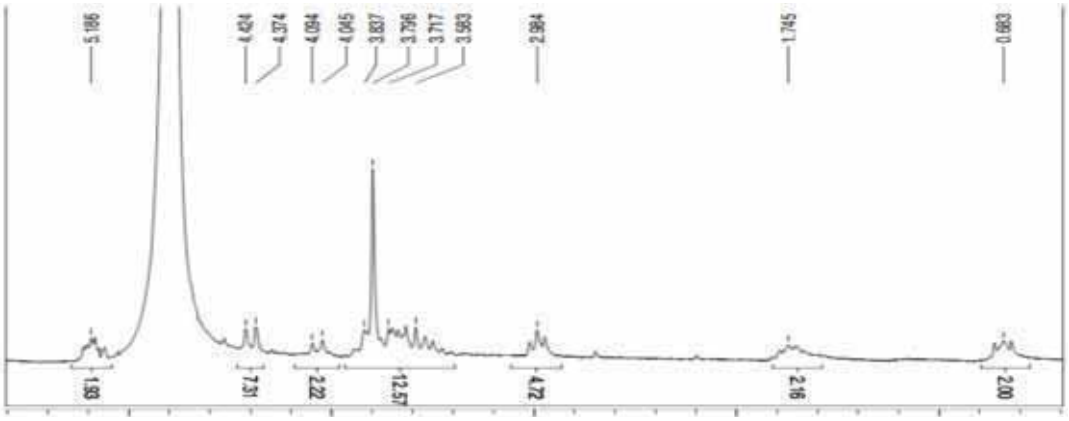

Figure 124: ^{1}H NMR spectrum in D_2O of the product FNPE.2

In FT-IR spectrum of the products (FNPE.2 and FNPE.4) the same peaks of the products containing monomeric units deriving from dimethyl L-tartrate are present, but in this case the C-O stretching peaks characteristic of the trehaluronic units are visible at 1151, 1108, 1070, 1027 cm^{-1}. Also in this case, the amide bands I and II were not observed separately because of the presence of other overlapped bands such as H-OH bending, probably due to coordinated water that seems to be present for all FNPE products; moreover for FNPE.2 a band attributable to N-H amine bending is present.

6.4.1.4 Nanocomposite syntheses: oligoamide formation by polymerization of FNP or FNPE with dimethyl ester and diamine (FNPO or FNPEO)

Oligoamides were obtained by polymerization of FNP (or FNPE) with a dimethyl ester (dimethyl L-tartrate or dimethyl α,α'-trehaluronate) and the diamine (ethylenediamine) (Figure 125). Their respective products were named as shown in Table 20 and Table 21.

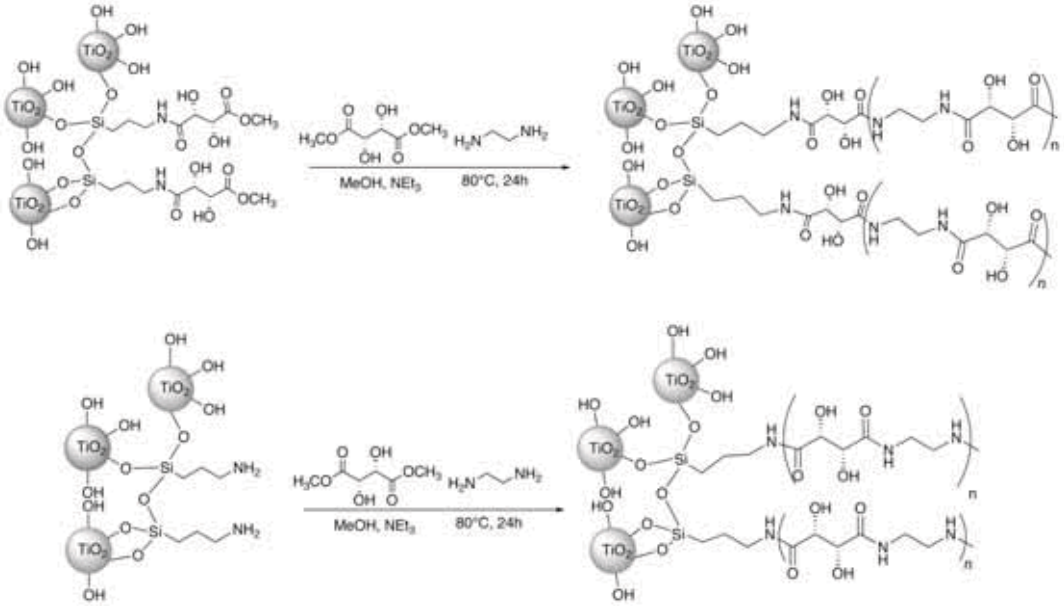

Figure 125: syntheses of FNPEO (above) and FNPO (below) based on dimethyl L-tartrate

The polycondensation reaction was carried out following the procedure previously reported for analogous oligoamides[34] but with shorter reaction times; the best conditions observed for this reaction include the use of methanol as a solvent, triethylamine as catalyst (27% m/m on the monomer used), at 80°C. Differently from the synthesis of the oligoamides, that were prolonged up to 7 days of reaction to favor the molecular weight growth, in the nanocomposite syntheses the times were reduced to 24 hours. This is due to the fact that, in order to make the application on a surface possible, higher molecular weights aren't required.
The reactions were carried out using different molar ratios (diester/diamine) compared to FNP (or FNPE), as reported in Table 21.

At the end of the reaction, solvent was removed from the product by distillation at reduced pressure and the solid obtained was washed with methanol and centrifuged (5 minutes at 2800 rpm) for three times. The product was dried under reduced pressure.

After the work-up, the solid obtained for each nanocomposite was extracted in water, in order to observe the presence of free or bonded oligoamide. The dispersion was stable, however after centrifugation for 1 hour at 2800 rpm, a soluble fraction (A≈ 50-60%) and an insoluble one (B≈ 40-50%) were separated.

Nanocomposites FNPO and FNPEO of the same type (FNPO.1 / FNPEO.1, FNPO.2 / FNPEO.2, FNPO.3 / FNPEO.3, FNPO.4 / FNPEO.4) have the same characteristic signals. Out of simplicity, the spectra of only one of the two samples will be discussed.

FNPO.1- FNPEO.1

These products were obtained through reaction between FNP.1 (or FNPE.1) with dimethyl L-tartrate and ethylenediamine, as reported in Table 20.

Soluble and insoluble fractions were compared through FT-IR spectroscopy (Figure 126): both fractions showed the same set of signals, but with different intensity. In fact, in FT-IR spectrum of the soluble fraction, amide signals (1660 cm^{-1} and 1537 cm^{-1}) were stronger respect to the characteristic band due to the TiO_2 nanoparticles (620 cm^{-1}), while the opposite was observed in the insoluble fraction. Therefore, the nanocomposite was found in both fractions; in the soluble fraction, nanocomposite with longer oligomeric chains is probably present along with free oligomeric chains. All samples showed in FT-IR spectra the same differences between the two fractions.

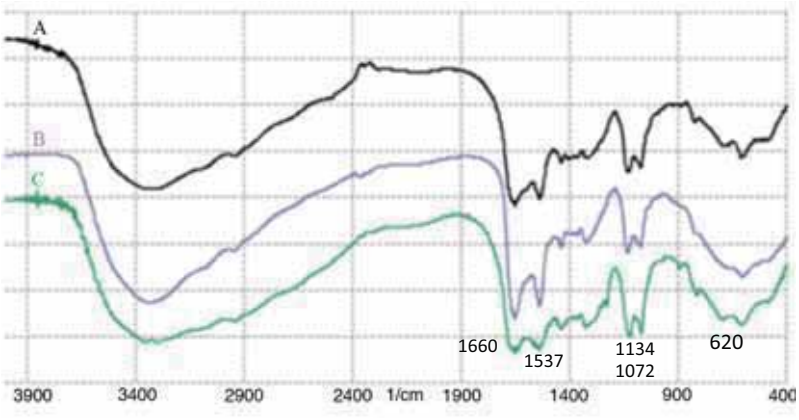

Figure 126: FT-IR spectra comparison between the soluble fraction (A), the insoluble one (B) and the not-separate fractions (C=A+B) of the product FNPO.1 (1:4:3).

The soluble fraction was also analyzed by NMR spectroscopy. ^{1}H NMR and ^{13}C NMR spectra (Figure 127) of the soluble fraction (FNPO.1 (1:4:3)) are reported.

^{1}H NMR spectrum confirms the formation of an amide compound thanks to the presence of the signal between 3.40-3.60 ppm (c'' + e) related to the CH_2 in α position to the amide; the signal at

4.57 ppm (d) attributable to the C**H**OH group is present and the signal between 2.90- 3.15 ppm, relative to the groups c, c', e' is also present. Confirm of the nanocomposite formation is also given by the presence of two signals at 0.70 ppm (a) and 1.73 ppm (b), related to the coupling agent.

In gCOSY spectrum (Figure 128), the attributions made for the signals in ^{1}H NMR spectrum can be confirmed. In fact a coupling between the hydrogens of the CH_2 group in α position to the terminal amino group (e') with the C**H**$_2$NHCO (e) and the couplings between the different hydrogens of the coupling agent are present.

^{13}C NMR spectrum (Figure 127) confirms the product formation by the signal at 38.5- 39.4 ppm (-**C**H$_2$NHCO, c''+ e) and from that to 174.0 ppm (**C**ONH, f). Moreover the signals relating to the **C**H-OH group (d) at 72.3- 73.8 ppm and those related to the coupling agent at 9.3 ppm (Si**C**H$_2$CH$_2$CH$_2$NH, a), 20.6 ppm (SiCH$_2$**C**H$_2$CH$_2$NH, b), 50.3 ppm (Si(CH$_2$)$_2$**C**H$_2$NH, c) and 46.9 ppm (Si(CH$_2$)$_3$NH**C**H$_2$CH$_2$NHCO, c') are present.

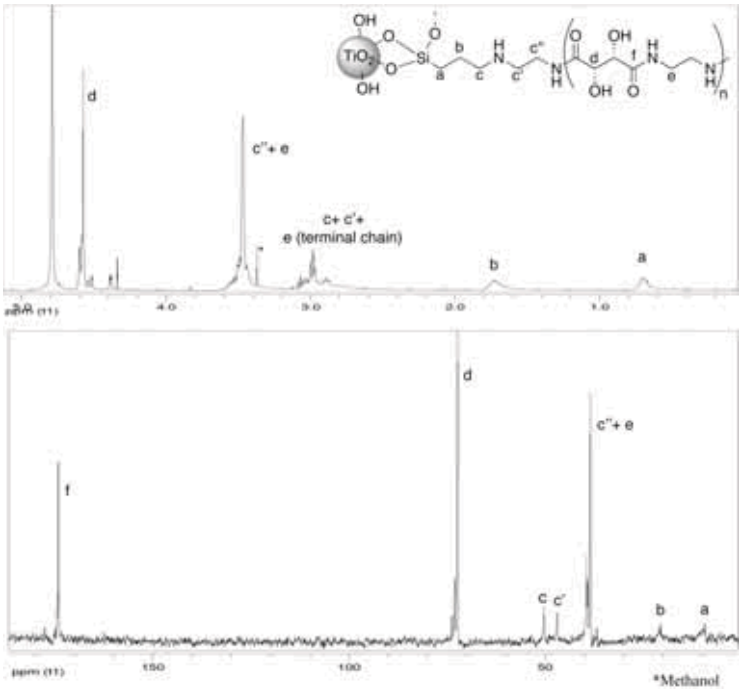

Figure 127: ^{1}H NMR and ^{13}C NMR spectra in D$_2$O of the product FNPO.1

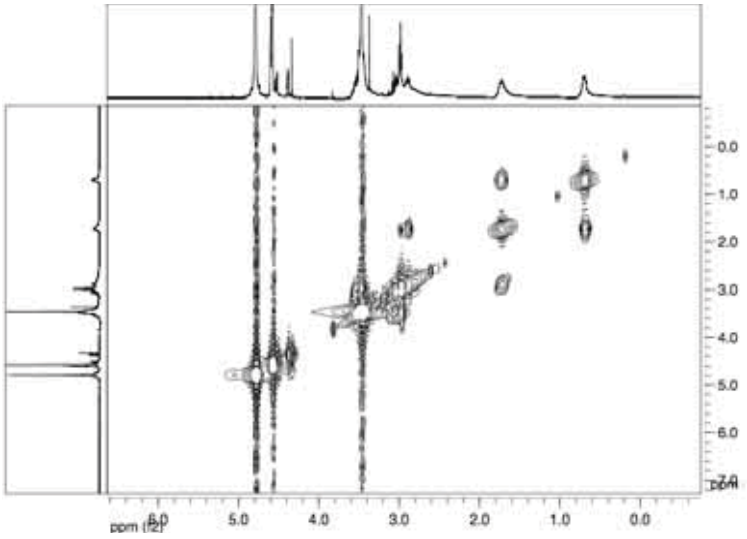

Figure 128: gCOSY spectrum in D_2O of the nanocomposite FNPO.1

Degree of polymerization (DP) of the oligomers present in the soluble fraction, both "free" and bonded to TiO_2, was determined from the integral of signals in ^{1}H NMR spectrum.

The signals related to the $SiC\mathbf{H}_2(CH_2)_2NH$ and $SiCH_2C\mathbf{H}_2CH_2NH$ groups are indicative of the presence of the nanocomposite in the soluble fraction and their integrals were used as the reference values to determinate the DP being set as equal to 2; other signals were evaluated with respect to these two values.

The calculations used to determine the DP are indicated below:

*integral of C**H**-OH signal = 2x*

integral of C$\mathbf{H}_2$NHCO signal (except terminal CH_2NH_2)= 4x

The signal related to $Si\text{-}CH_2CH_2C\mathbf{H}_2NHC\mathbf{H}_2CH_2NH$ (c+ c') and $C\mathbf{H}_2NH_2$ (e') should have integrals equal to 6 for AEAPTMS. These integrals, in some cases, result to be bigger than the theoretical values due to the presence of free oligomeric chains in agreement with the simultaneous presence in the soluble fraction of nanocomposite and free oligoamide.

From elaboration of the integrals of the signals present in the ^{1}H NMR of the product FNPO.1 (1:4:3) it was deduced that the soluble fraction consists of 3 repeating units with amino termination; DP of the other products is shown schematically in Table 21.

FNPO.2- FNPEO.2

These products were obtained through reaction between FNP.1 (or FNPE.2) with dimethyl α,α'-trehaluronate and ethylenediamine, as reported in Table 20.

As for the previous reaction, soluble and insoluble fractions were compared by FT IR spectroscopy (Figure 129), which shows that both fractions have the same set of signals but with different intensity. It is possible to observe the formation of the nanocomposite contining an amide bond by the presence of bands at 1649 cm^{-1} and 1554 cm^{-1} (amide I and II) and at about 630 cm^{-1} the peak relative to the Ti-O stretching. The first bands have a higher intensity in the soluble fraction (A), the second ones in the insoluble fraction (B). Moreover between 1149, 1107, 1066 and 1027 cm^{-1} the C-O stretching peaks are present, typical of the trehaluronic unit, overlapped to the Si-O stretching.

Consequently, it is possible to conclude that the nanocomposite is present in both fractions, but the soluble fraction is composed by longer oligomeric chains, probably also in presence of free oligomeric chains.

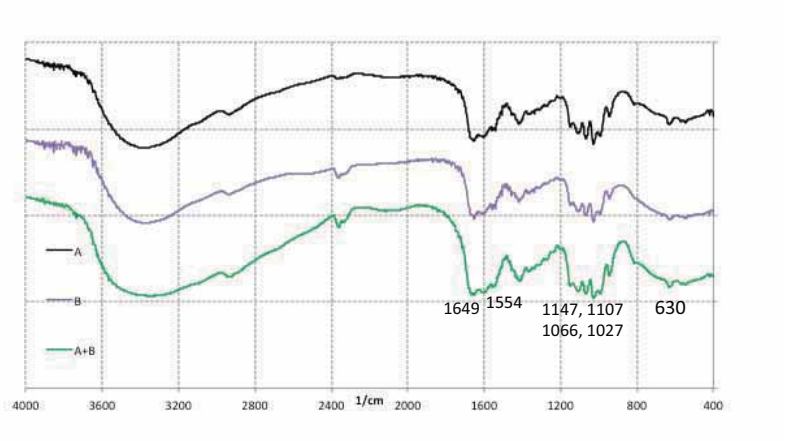

Figure 129: FT-IR spectra comparison between the soluble fraction (A), the insoluble one (B) and the not-separate fractions (C=A+B) of the product FNPO.2

The soluble fraction of products based on dimethyl α,α'-trehaluronate, was also analyzed by NMR spectroscopy.

^{1}H NMR spectrum (Figure 130) confirms the formation of an amide compound thanks to the presence of signal at 3.40- 3.60 ppm (c''+ e) relative to the CH_2 in α position to the amide; moreover the presence of the signals related to C-H of the trehaluronic backbone (H_1/H_1', H_2/H_2', H_3/H_3',/ H_4/H_4' and H_5/H_5' respectively to 5.18, 3.67, 3.84, 3.53 and 4.00- 4.25 ppm) and the signal at 3.00- 3.20 ppm related to the c, c' and e' ($C\mathbf{H}_2NH_2$ end chain) confirm the product formation.

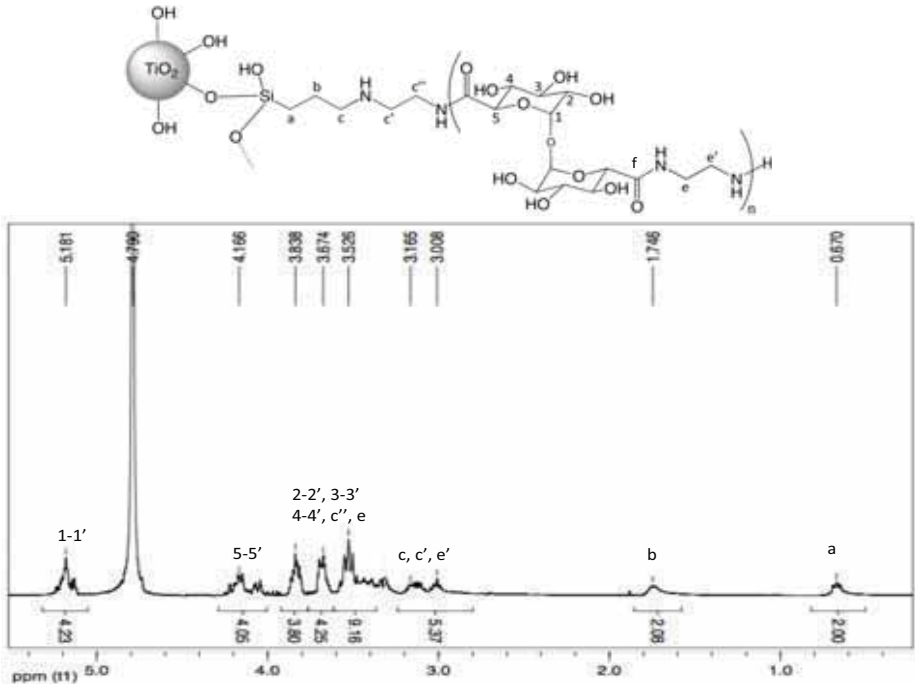

Figure 130: ^{1}H NMR spectrum in D_2O of the product FNPO.2

The correlations between hydrogen atoms visible in gCOSY spectrum (Figure 131), that allow distinguishing the couplings between the hydrogens of the coupling agent, between the one of CH_2 in α on the amino terminal group (e') with the C**H**$_2$NHCO (e) group and, lastly, between the hydrogens of the trehaluronic backbone (couplings between H_1 and H_2, H_5 and H_4 and H_4 and H_3) are visible.

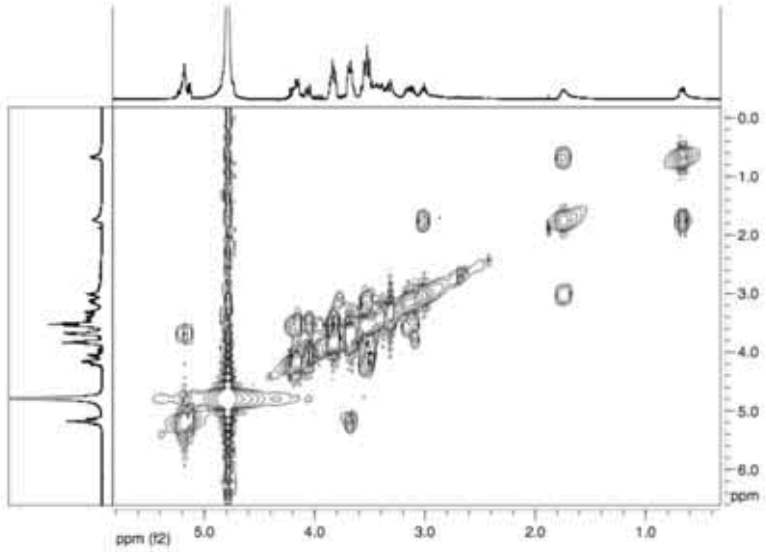

Figure 131: spettro gCOSY del nanocomposito FNPO.2

In ^{13}C NMR spectrum (Figure 132) the confirm of the product formation is given by the signal at 36.0- 39.0 ppm (-CH_2NH-, c''+ e) and at 171.2- 176.3 ppm (-CONH-, f). Signals related to the sugar backbone are present: C_1-C_1' at 93.4- 94.3 ppm, C_2-C_2' at 70.4 ppm, C_4-C_4' at 71.6 ppm, C_3-C_3' and C_5-C_5' at 71.9 ppm. Furthermore the presence of coupling agent signals is detectable at 8.7 ppm (Si**C**H_2, a), 19.6 ppm (SiCH_2**C**H_2, b), 49.9 ppm (Si$(CH_2)_2$**C**H_2NH, c) and 46.6 ppm (Si$(CH_2)_3$NH**C**H_2CH_2NH, c').

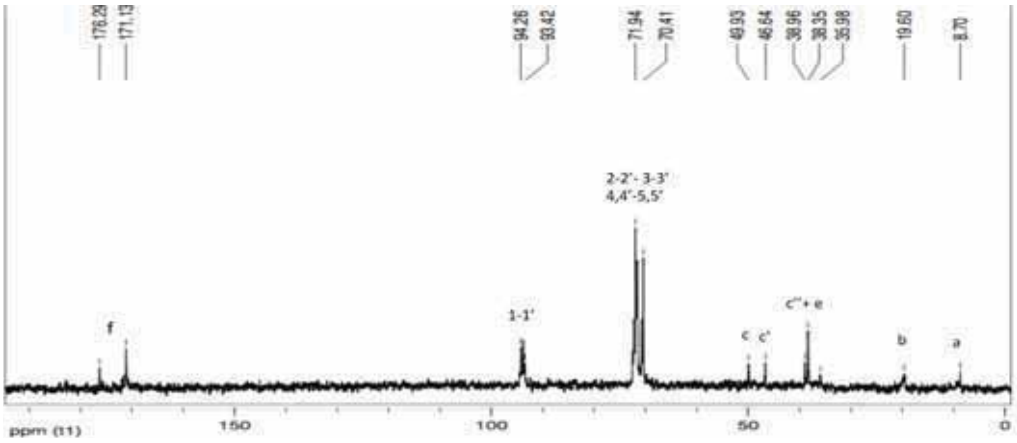

Figure 132: ^{13}C NMR spectrum of FNPO.2 e FNPEO.2

Degree of polymerization (DP) of the oligomers present in the soluble fraction, both free and bonded to TiO_2, was determined from the integral of signals in ^1H NMR spectrum.

Also in this case the signals related to the Si***H***$_2(CH_2)_2$NH and $SiCH_2C$***H***$_2CH_2$NH groups are indicative of the nanocomposite presence in the soluble fraction and their integrals were used as reference values to determinate the DP and set as equal to 2 each; other signals were evaluated with respect to these two values.

The calculations used to determine the DP are indicated below:

integral of H-1, H-1', H-5, H-5', H-2, H-2', H-3, H-3' or H-4, H-4' signal = 2x

*integral of C**H**$_2$NHCO signal (except terminal CH_2NH_2)= 4x*

The signal related to $SiCH_2CH_2C$**H**$_2$NHC**H**$_2CH_2$NH (c+ c') and C**H**$_2NH_2$ (e') should have integrals equal to 6 for AEAPTMS, as shown in the previous case (FNPO.1/FNPEO.1). These integrals, in some cases, result be larger than the theoretical values due to the presence of free oligomeric chains in agreement with the contemporary presence in the soluble fraction of nanocomposite and free oligoamide.

From elaboration of the integrals obtained by ^{1}H NMR of the product FNPO.1 (1:4:3) was deduced that the soluble fraction consists of 2 repeating units with amino termination; DP of the other products is shown schematically in Table 21.

FNPO.3- FNPEO.3

These product were obtained through reaction between FNP.2 (or FNPE.3) with dimethyl L-tartrate and ethylenediamine, as reported in Table 20.

As the previous reaction, after work-up the product was extracted in water, obtaining a soluble (A) and an insoluble fraction (B), compared using FT IR spectroscopy (Figure 133).

Spectra show that both fractions have the same set of signals but with different intensity. Consequently, in both fractions, bands relative to the amide bond (1660 cm^{-1} and 1537 cm^{-1}, amide I and II) are present, having higher intensity in the soluble fraction as well as the band relative to the stretching Ti-O to about 600 cm^{-1}, more intense in the insoluble fraction.

Consequently, it is possible to conclude that the nanocomposite is present in both fractions, but the soluble fraction is composed by longer oligomer chains, probably also in presence of free oligomer chains.

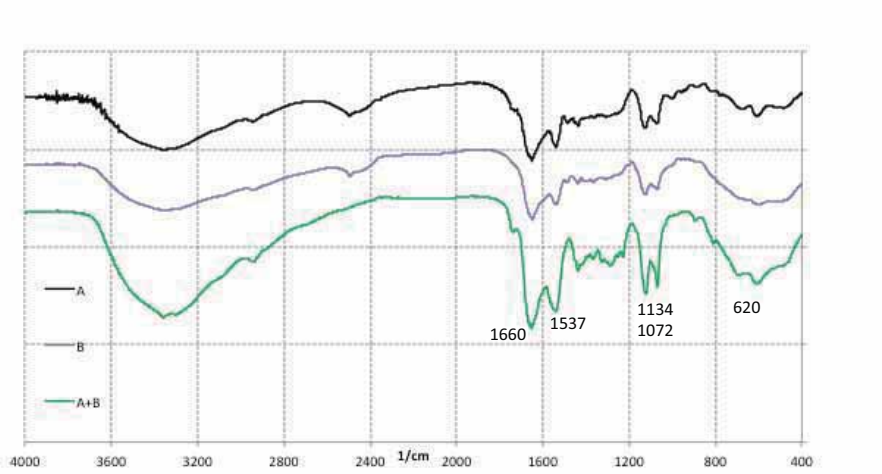

Figure 133: FT-IR spectra comparison between the soluble fraction (A), the insoluble one (B) and the not-separate fractions (C=A+B) of the product FNPO.3

Also in this case, as for the previous products, NMR characterization of the soluble fraction was performed; data are reported from

Table 23 to Table 26, and the determination of DP value is present in Table 21.

FNPO.4- FNPEO.4

These products were obtained through reaction between FNP.2 (or FNPE.4) with dimethyl α,α'-trehaluronate and ethylenediamine, as reported inTable 20.

After work-up, the product was extracted in water, as in previous cases, obtaining a soluble fraction and an insoluble one, which were compared by FT IR spectroscopy.

From the spectra (Figure 134), it appears that both fractions show the same set of signals but with different intensity. Consequently, in both fractions peaks relative to the amide bond (1660 cm^{-1} and 1540 cm^{-1}, amide I and II) are present, having higher intensity in the soluble fraction, as well as the band relative to the Ti-O stretching about at 630 cm^{-1}, more intense in the insoluble fraction.

It is possible to conclude that the nanocomposite is present in both fractions, but the soluble fraction is composed from longer oligomer chains, probably also with the presence of oligomer free chains.

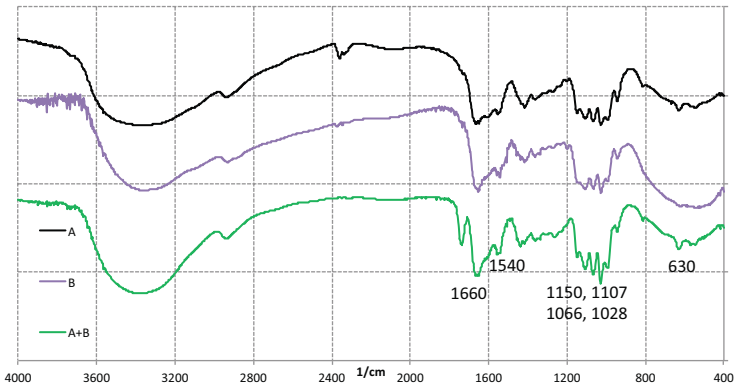

Figure 134: FT-IR spectra comparison between the soluble fraction (A), the insoluble one (B) and the not-saperate fractions (C=A+B) of the product FNPO.4

As in the previous cases, NMR characterization of the soluble fraction was performed, whose data are reported from Table 23 to Table 26, calculating the DP value as reported in Table 21.

Table 22: FT-IR spectral data (KBr pellet)

Product	N-H e O-H stretching	C-H stretching	C=O stretching (ester group)	C=O stretching (Amide I)	N-H bending (Amide II)	C-H bending	C-N stretching	Si-O stretching	C-O stretching	Ti-O-Si stretching	Ti-O stretching
FNPE.1 **FNPE.3**	3342 (vs[b], slargato)	2952 (w[b]) 2880 (w)	1738 (s)	N.D.[c]	N.D.[c]	1464 (w)	N.D.	1127 (vs) 1080 (vs)	1127 (vs) 1080 (vs)	904 (w)	620 (vs)
FNPE.2 **FNPE.4**	3343 (vs[b], broad)	2932 (w)	1730 (s)	N.D.[c]	N.D.[c]	1411 (w)	1353 (w)	1151 (vs) 1070 (vs)	1151 (vs) 1108 (vs) 1070 (vs) 1027 (vs)	912 (w)	620 (vs)
FNPO.1[a] **FNPEO.1**[a]	3348 (vs[b], broad)	2935 (w)	N.D.	1660 (vs)	1537 (s)	1385 (w)	N.D.	1134 (s) 1072 (s)	1134 (s) 1072 (s)	912 (w)	620 (vs)
FNPO.2[a] **FNPEO.2**[a]	3336 (vs[b], broad)	2935 (w)	N.D.	1649 (vs)	1554 (s)	1415 (w)	N.D.	1147 (s) 1066 (s)	1147 (s) 1107 (s) 1066 (s) 1027 (s)	943 (w)	630 (vs)
FNPO.3[a] **FNPEO.3**[a]	3348 (vs[b], broad)	2933 (w)	1730 (w)	1660 (vs)	1537 (s)	1436 (w)	1353 (w)	1134 (s) 1072 (s)	1134 (s) 1072 (s)	915 (w)	620 (vs)
FNPO.4[a] **FNPEO.4**[a]	3379 (vs[b], broad)	2935 (w)	1730 (w)	1660 (vs)	1540 (s)	1438 (w)	1353 (w)	1150 (s) 1066 (s)	1150 (s) 1107 (s) 1066 (s) 1028 (s)	943 (w)	630 (vs)

[a] spectrum recorded on the mixture of soluble (A) and insoluble (B) fractions; [b]vs: very strong; s: strong; w:weak; [c]N.D.: not observed separately for the presence of other overlapped bands (N-H amine bending and H-OH bending).

Table 23: ^{1}H NMR spectral data (400 MHz, δ, ppm, D_2O)

	Silyl derivate moiety				
Product	Si-C**H**$_2$	Si-CH$_2$-C**H**$_2$	Si-(CH$_2$)$_2$-C**H**$_2$-NH-C**H**$_2$	Si-(CH$_2$)-C**H**$_2$-NHCO	NH-CH$_2$-C**H**$_2$-NHCO
FNPE.1	0.73	1.81	3.00- 3.28	–	3.60
FNPE.2[a]	0.68	1.75	2.98	–	3.60
FNPE.3	0.77	1.81	–	3.05	–
FNPE.4[a]	0.77	1.83	–	3.10	–
FNPO.1[b]	0.70	1.73	2.90- 3.15	–	3.40- 3.60
FNPO.2[b]	0.67	1.75	3.00- 3.20	–	3.40- 3.60
FNPO.3[b]	0.70	1.79	–	3.00- 3.15	–
FNPO.4[b]	0.67	1.74	–	3.00	–
FNPEO.1[b]	0.72	1.77	3.00- 3.20	–	3.40- 3.60
FNPEO.2[b]	0.69	1.74	3.00- 3.15	–	3.40- 4.60
FNPEO.3[b]	0.71	1.79	–	3.00- 3.20	–
FNPEO.4[b]	0.76	1.81	–	3.00-3.20	–

[a]Spectra recorded at 200 MHz; [b]Spectra recorded on the soluble fraction of nanocomposite

Table 24: ^{1}H NMR spectral data (400 MHz, δ, ppm, D_2O)

	Diamine moiety		Dicarboxylic moiety								
Product	C**H**$_2$NHCO	C**H**$_2$NH$_2$	OCH$_3$	C**H**-OH near ester group	C**H**-OH near amide group	H-1	H-2	H-3	H-4	H-5	H-5 end chain
FNPE.1	–	–	3.82	4.66	4.40	–	–	–	–	–	–
FNPE.2[a]	–	–	3.80	–	–	5.19	3.69	3.84	3.60	4.07	4.40
FNPE.3	–	–	3.84	4.68	4.42	–	–	–	–	–	–
FNPE.4[a]	–	–	3.80	–	–	5.19	3.69	3.82	3.58	4.06	4.40
FNPO.1[b]	3.40- 3.60	2.90- 3.15	–	–	4.57	–	–	–	–	–	–
FNPO.2[b]	3.40-3.60	3.00- 3.20	–	–	–	5.18	3.67	3.84	3.53	4.00-4.25	–
FNPO.3[b]	3.40-3.60	3.00- 3.15	–	–	4.57	–	–	–	–	–	–
FNPO.4[b]	3.40- 3.60	3.16	3.80	–	–	5.18	3.68	3.85	3.54	3.90-4.20	4.38
FNPEO.1[b]	3.40-3.60	3.00- 3.20	–	–	4.58	–	–	–	–	–	–
FNPEO.2[b]	3.40-4.60	3.00- 3.15	–	–	–	5.23	3.70	3.86	3.58	4.07-4.27	–
FNPEO.3[b]	3.40-4.60	3.00-3.20	–	–	4.57	–	–	–	–	–	–
FNPEO.4[b]	3.54	3.00-3.20	–	–	–	5.23	3.73	3.89	3.59	4.10-4.30	–

[a]Spectra recorded at 200 MHz; [b]Spectra recorded on the soluble fraction of nanocomposite

Table 25: ^{13}C NMR spectral data (100 MHz, δ, ppm, D_2O)

	Silyl derivate moiety				
Product	Si-**C**H_2	Si-CH_2-**C**H_2	Si-$(CH_2)_2$-**C**H_2-NH	NH-**C**H_2-CH_2-NH	NH-CH_2-**C**H_2-NHCO Si-$(CH_2)_2$-**C**H_2-NHCO
FNPO.1 and FNPEO.1[a]	9.3	20.6	50.3	46.9	38.5- 39.4
FNPO.3 and FNPEO.3[a]	8.8	20.8	–	–	37.9- 39.4
FNPO.2 and FNPEO.2[a]	8.7	19.6	49.9	46.6	36.0- 39.0
FNPO.4 and FNPEO.4[a, b]	N.D.[c]	N.D.[c]	–	–	N.D.

[a]soluble fraction of nanocomposite; [b]Signal attributable to the coupling agent are not visible with increasing molecular weight of the polymers; [c]N.D.: not detrmined

Table 26: ^{13}C NMR spectral data (100 MHz, δ, ppm, D_2O)

	Diamine moiety		Dicarboxylic moiety							
Product	**C**H_2NHCO	**C**H_2NH_2	-OCH_3	**C**H-OH	C-1	C-2	C-3	C-4	C-5	C=O
FNPO.1 and FNPEO.1[a]	38.5- 39.4	N.D.[c]	–	72.3- 73.8	–	–	–	–	–	174.0
FNPO.3 and FNPEO.3[a]	37.9- 39.4	N.D.[c]	–	72.3- 73.8	–	–	–	–	–	174.0-174.4
FNPO.2 and FNPEO.2[a]	36.0- 39.0	N.D.[c]	–	–	93.4- 94.3	70.4	71.9	71.6	71.9	171.2- 176.3
FNPO.4 and FNPEO.4[a]	36.7- 39.0	41.6	53.0	–	93.5- 94.6	70.4	72.0	71.3	71.6	171.2- 176.3

[a]soluble fraction of nanocomposite; [b]Signal attributable to the coupling agent are not visible with increasing molecular weight of the polymers; [c]N.D.: not detrmined

6.4.1.5 Dynamic Light Scattering (DLS)

In order to characterize the stability of the water dispersion of TiO_2-polyethylenetartaramide FNPO.1 (1:4:3), dynamic light scattering measurements were performed. At the start (t = 0), after dispersion preparation, due to the high concentration of particles and the resulting opacity, the dispersion was analyzed using the FOQELS (Fiber Optic Quasi-Elastic Light Scattering) accessory for non-diluted dispersions. The DLS analysis showed a particle size distribution with the most abundant population ranging between 50 and 125 nm in terms of hydrodynamic diameter (i.e., the size of the diffusing particle, including the polymer coating and the solvation layer). A second distribution, related to a much smaller amount of particles, ranged approximately between 350 and 750 nm (Figure 135 left). During time, the sedimentation of a small part of the nanocomposite particles was observed, leading to the reduction of the opacity of the system. After 24 hours, the dispersion was investigated in the conventional geometry (scattering angle of 90°), resulting in a particle size distribution ranging between 65 and 100 nm (Figure 135 right). A very small amount of larger particles was detected, consistently with a progressive aggregation and sedimentation of particles.

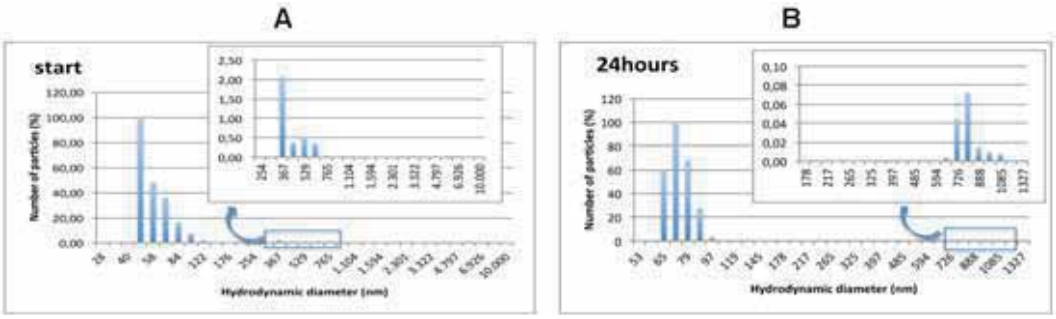

Figure 135 DLS of water dispersion of FNPO.1 (1: 4: 3). A: t = 0, B: t = 24 h.

6.4.1.6 Morphological analysis

Morphological analysis (TEM) was performed to verify the quality of the dispersion of the nanocomposites. TEM images of the nanocomposite were compared with those recorded on unmodified TiO_2 and on TiO_2 simply mixed with the free polyethylene-L-tartaramide (Figure 136)

The analyses were performed on grid carbon and holey carbon, to verify the homogeneity of the dispersion obtained.

Sample A is composed by TiO_2 powder nanoparticles.

Sample B is composed by TiO_2 nanoparticles dispersed in oligoethylene-L-tartaramide (molecular weight: 930 g/mol), namely 3.5 mg of nanoparticles in 25 mg of polymer. The dispersion was obtained by sonication in 1 ml of water: the concentration of the nanoparticles in the solvent was 3.5 mg/mL

Sample C is composed by functionalized nanoparticles, in situ polymerized and water dispersed. The dispersion was obtained with dispersion of 15 mg of the composite TiO_2-oligoamide (containing about 1.75 mg of nanoparticles) in 0.5 ml of water: the concentration of nanoparticles dispersed in the solvent is therefore 3.5 mg /mL, as for sample B.

Since the concentrations of samples B and C are the same, it is possible to compare the dispersions thanks to the images obtained.

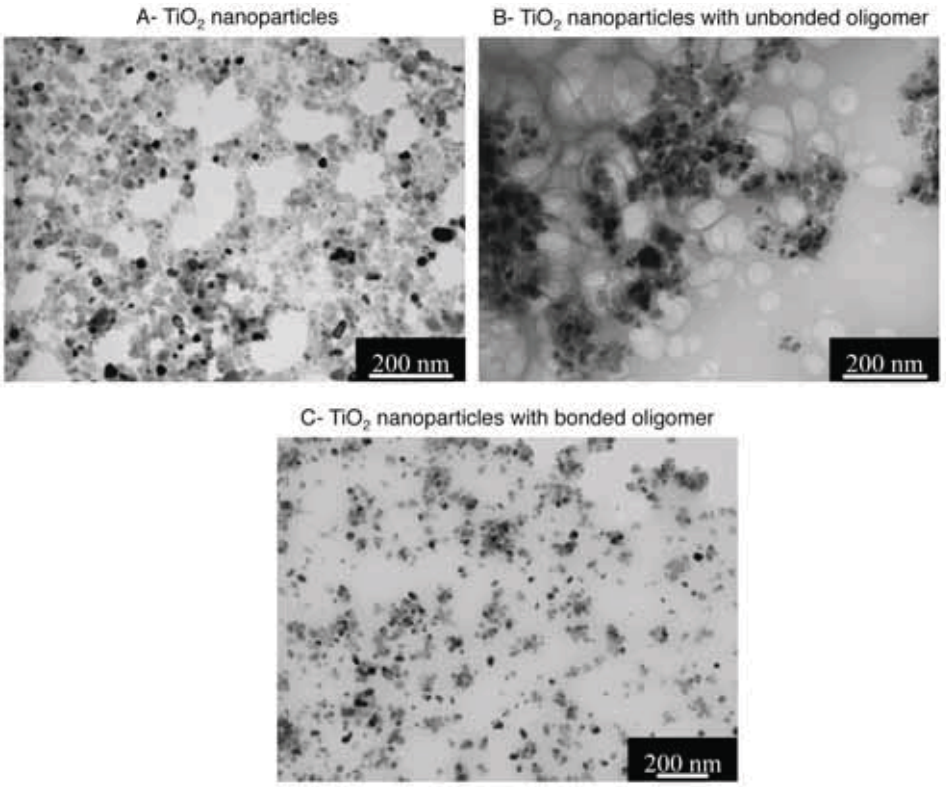

Figure 136: TEM images of TiO_2 nanoparticles (A), TiO_2 with unbonded oligomer (B), TiO_2 with bonded oligomer (C) on grid carbon.

The images appear significantly different: image B reveals the presence of two distinct areas, one constituted of nanoparticles aggregates, the other one with great amount of oligomer;

consequently the material does not appear homogeneous. In figures C a better dispersion of nanoparticles in the material is observed, in agreement with an improved homogeneity.

The nanocomposite was also observed on holey carbon to better evaluate the uniformity of dispersion (Figure 137).

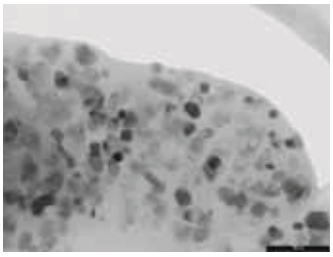

Figure 137: TEM image of nanocomposite on holey carbon

6.4.2 Antimicrobial activity of the synthesized nanocomposites

A water dispersion of TiO_2-polyethylene-L-tartaramide nanocomposite (FNPO.1_1:4:3) was used to evaluate its antimicrobial action of the specimens of beech (*Fagus sylvatica*), against the attack of a fungus (*Trametes versicolor*).

To use the nanocomposite in applicative field, preliminary tests on its photocatalytic activity were performed via the **test of methylene blue** and subsequently evaluating the **resistance to photodegradation** and possible **color changes** before and after exposure to UV radiation.

6.4.2.1 Test of methylene blue

As previously stated, in order to think about a possible use of the nanocomposites in this type of applications, it was necessary to evaluate the real catalytic activity of TiO_2 nanoparticles by means of test with a solution of methylene blue (0.15%) with and without nanocomposite, subjected to UV exposure for 5, 10, 20 minutes. Images in Figure 138 show the degradation of methylene blue in presence of the nanocomposite even only after 5 minutes of exposure, observed thanks to color disappearance in the solution. On the contrary, methylene blue without nanocomposite does not undergo any variation.

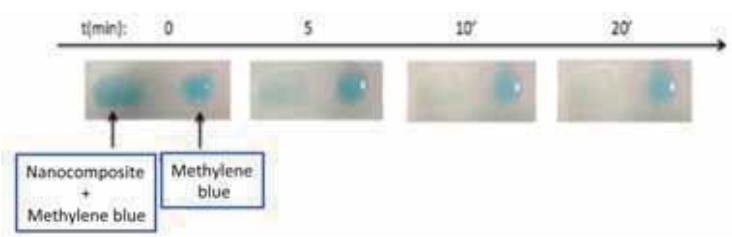

Figure 138: degradation test of methylene blue

6.4.2.2 Resistance to photodegradation and color effect

Resistance to photodegradation was evaluated on the nanocomposite as such, monitoring the possible structural changes following interaction with the UV radiation. The behavior of nanocomposites after UV irradiation was studied by determination of weight changes, FT IR analysis and colorimetric measurements.

A water solution of the product FNPO.1 (1:4:3) was deposited on a glass slide, allowed to dry at room temperature. Afterwards it was exposed to UV radiation for 10 hours/day for 3 weeks, at a wavelength of 365 nm (irradiation indoor) and 254 nm (irradiation outdoor).

Weight variation was evaluated through the weight measurements of the glass slide with the nanocomposite, before and after the irradiation however, changes in weight were not observed, index of a possible non-alteration of the product.

Subsequently, the product was analyzed with FT-IR (KBr pellet) (Figure 139) and its spectrum was comparable to those of the starting material recorded before UV exposure In fact, in both spectra the characteristic bands of the product at 1645, 1550 cm^{-1} (amide I and II), 1128, 1068 cm^{-1} (C-O stretching) are visible.

However, yellowing was observed in the nanocomposite, probably due to the presence of low amount of oxidation products which were not detectable in FT-IR spectrum and ^{1}H-NMR spectra.

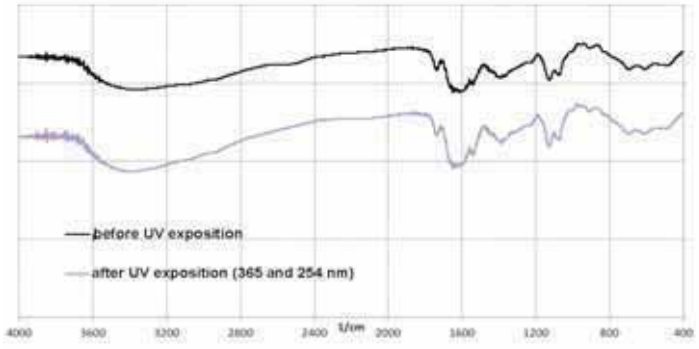

Figure 139: FT IR spectra of the product FNPO.1 (1:4:3) before and after three weeks of exposition at UV radiation

In order to observe the effect of the yellowing on wood surfaces, new tests were performed on wood specimens. As reference, samples of untreated beech (Fagus sylvatica) were used. The colorimetric measurements were made before and after treatment (three weeks of exposure at 254 and 365 nm), to evaluate the color effect induced from the product as such on the wood and to highlight color variations due to interaction with the UV radiation.

The color change as ΔE* was evaluated, according to the formula:

$$\Delta E^{*} = \sqrt{\Delta L^{*2} + \Delta a^{*2} + \Delta b^{*2}}$$

where ΔL* is the lightness variation, Δa* and Δb* are the chromaticity indices (Figure 140).

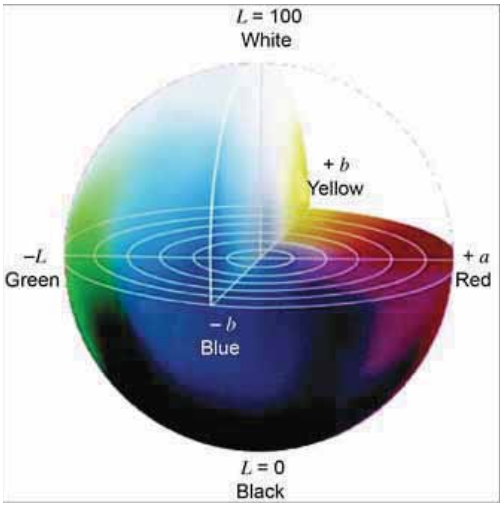

Figure 140: CIE Lab color space:

L is always positive and represents brightness;
a>0 represents red component, a<0 green component;
b>0 represents yellow component and b<0 blue component

The measurements were performed on the same samples before and after treatment: it is therefore fundamental, to achieve significant results that they are analyzed in the same spot. For this purpose, during the measurements a mask was used, allowing the correct positioning of the instrument.

Two wood samples (1 and 2) were treated with the nanocomposite dispersion as reported above and exposed at UV light (365 and 254 nm) for three weeks. Colorimetric measurements were performed according to the CIELab system. The color changes observed on the wood (ΔE = 4,6 after treatment at 254 nm and ΔE = 6,1 after treatment at 365 nm) were comparable to natural weathering of wood when exposed to ultra-violet light, water, oxygen or variations in temperature[135] and were hardly noticeable compared to those observed by the human eye due to the attack of microorganisms.

Table 27 Color changes after UV treatments

	After three weeks			
Sample	ΔL	Δa	Δb	ΔE
1(exposure at 254 nm)	-1.8	1.0	4.1	4.6
2(exposure at 365 nm)	-2.5	1.8	5.3	6.1

6.4.2.3 Application of the nanocomposite on recent wood specimens

After confirmation of the photocatalytic activity and stability of the nanocomposite, an applicative study on specimens of beech (Fagus sylvatica) was developed, to assess the nanocomposite activity against the white-rot decay fungus (*Trametes versicolor*).

The tests were carried out under different conditions: with and without UV exposure of the sample, on specimens as such and on specimens previously subjected to a consolidant treatment by immersion in an aqueous solution of oligoethylene-L-tartaramide. The nanocomposite was dispersed in water and applied on the surface of wood; its activity was studied comparing the sample with similar samples not treated superficially.

28 wood specimens, measuring 10 x 20 x 2 mm were dehydrated using a ventilated oven at 103°C (UNI EN 13183-1, *Moisture content of a piece of sawn timber - Part 1: Determination by oven dry method*). 12 wood specimens were subjected to a consolidation treatment for 2 weeks: 6 samples with a 3.3% solution of consolidant in water MilliQ (233 mg of consolidant in 7.0 mL of MilliQ water), and other 6 samples with a 3.3% solution of consolidant in water MilliQ and biocide (117 mg); the other 16 samples were not treated neither with the biocide nor with the consolidant. At the end of the two weeks of consolidant treatment, all wood samples were conditioned to constant mass at 20°C and 65% relative humidity (RH) in dryers containing xylene to prevent the growth of fungi.

Half of each sample family, conditioned to constant mass, was treated with the nanocomposite (Table 28), using a brush (three applications/day for 7 days) on all the faces applied.

The samples treated with the nanocomposite dispersion were observed with the microscope to check the uniformity of the film applied (Figure 141).

Figure 141: wood sample treated with nanocomposite (FNPO.1 (1:4:3)), observed at the microscope (magnification 200X)

The fungi treatment occurred at 65% RH and 20°C; samples were placed on a sterile small net on *T. versicolor* cultures in Petri dishes (four samples per dish). Half of the samples were exposed to UV light for three weeks while the other ones were kept in the dark (Table 28). For each sample three or four repetitions were tested.

Table 28: type of treatment of 28 samples

	Nanocomposite treatment	No nanocomposite treatment	UV light exposition
Consolidant treatment	2, 4, 6	1, 3, 5	yes
Consolidant and biocide treatment	7, 8, 9	10, 11, 12	yes
No consolidant treatment	17, 18, 19, 20	25, 26, 27, 28	yes
	21, 22, 23, 24	29, 30, 31, 32	no

All the equivalent samples (ex: samples 1-4) were placed on different Petri dishes to have a better reproducibility (Figure 142).

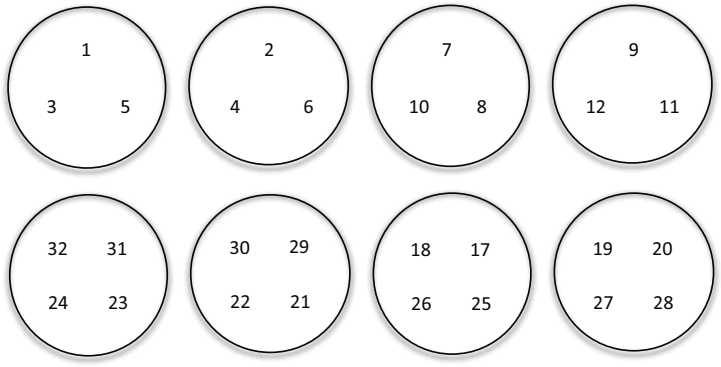

Figure 142: Scheme of the placement of the samples in petri dishes containing the fungus

After 3 weeks of treatment the following conclusions were drawn:

- Samples (1-6) treated **with consolidant, with and without nanocomposite** gave problems in initial treatment phase with the consolidant due to the spontaneous growth of an unidentified environmental fungus on the surface of the samples. The cause was attributed to the high temperature in the laboratory where the test was performed (> 30°C). The samples were anyway treated with the nanocomposite and exposed to UV radiation without nutrient medium, to measure the variation of the growth of this fungus. Immediately after the start of the exposure the fungus died due to lack of nutrient medium in petri dish, invalidating the test (Figure 143).

Figure 143: samples 1-6 with unidentified environmental fungus (left) and magnification of the micelium (200X)

- Samples (7-12) **with consolidant and biocide, with and without nanocomposite**, did not show the presence of fungal growth on any of the samples (Figure 144) thanks to the presence of biocide; given this reason it is not possible to evaluate the antimicrobial effect of the nanocomposite.

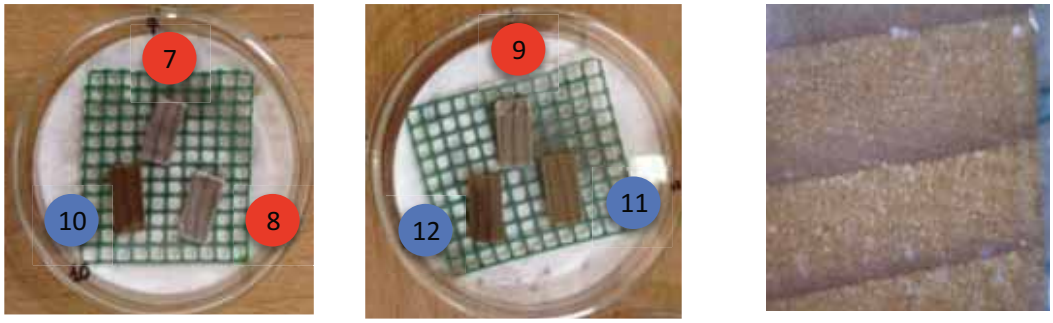

Figure 144: samples 7-12 (left and centre) and microscope image (200x), where the absence of fungus growth is evidenced.

- Samples (21-24, 29-32) incubated **in the dark, with and without nanocomposite** exhibited fungal growth on both samples, with or without nanocomposite (**Figure 145**), after one week. This result confirm the inactivity of nanoparticles in the dark.

- Samples (17-20, 25-28) incubated **in UV light, with and without nanocomposite** showed different behaviors; the samples treated with the nanocomposite did not show fungal growth, conversely to those without nanocomposite that have exhibited fungal growth (**Figure 145**). Accordingly, the activity of the nanocomposite was demonstrated when the sample was exposed at UV radiation.

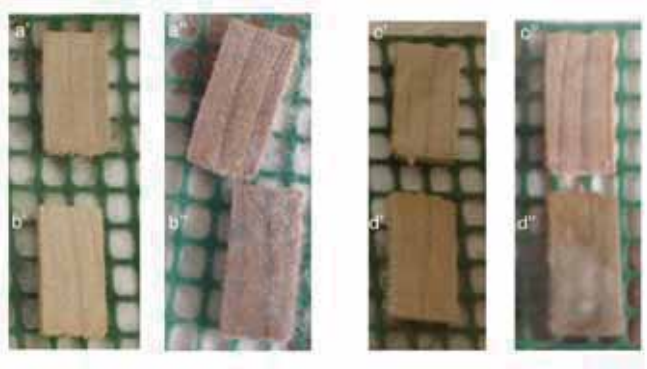

Figure 145: Wood samples with and without nanocomposite, kept in the dark or exposed to UV light after three weeks. a' (time 0) and a'' (time 3 weeks): sample with nanocomposite in the dark; b' (time 0) and b'' (time 3 weeks): sample without nanocomposite in the dark; c' (time 0) and c'' (time 3 weeks): sample with nanocomposite in the UV light; d' (time 0) and d'' (time 3 weeks): sample without nanocomposite in the UV light.

Optical microscope analysis confirmed fungal growth on the sample without nanocomposite (Figure 146) and the absence of any fungal growth in samples containing the nanocomposite (Figure 146).

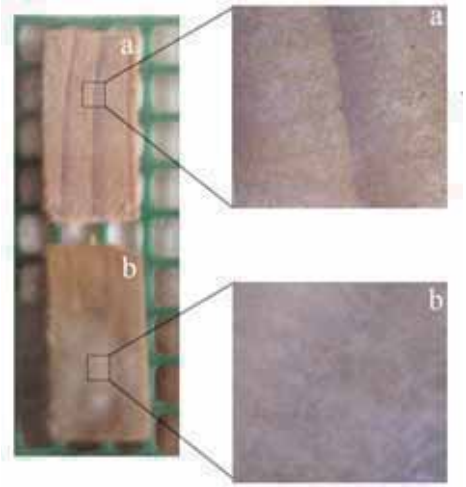

Figure 146: Microscope images (magnification 200x) of wood samples with nanocomposite (a) and without nanocomposite (b) after UV exposure of three weeks.

It is worth noting that NP-containing samples, on which fungi did not grow during the three weeks of UV exposure, showed appearance of fungal growth after nine more weeks of incubation

in the dark (Figure 147). This confirms the need for exposure to UV radiation in order to prevent fungal growth.

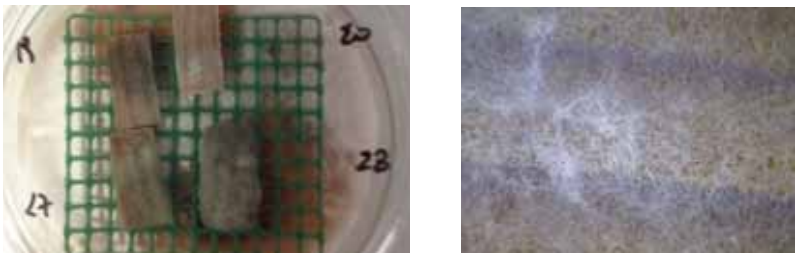

Figure 147: Sample with nanocomposite after 9 weeks more of incubation in the dark (c).

6.5 Conclusions

In this study several nanocomposites were synthesized based on functionalized oligoamides on TiO_2 nanoparticles, allowing oligoamide growth in controlled steps and obtaining very homogeneous core-shell systems.

The activated TiO_2 nanoparticles were functionalized using two different coupling agents (obtaining FNP). A preliminary reaction with the diester, dimethyl L-tartrate or dimethyl α,α'-trehaluronate (obtaining FNPE) was performed to verify the reactivity of functionalized nanoparticles, modifying the end group of the functionalized nanoparticles as ester group. Lastly, to verify the same behavior for functionalized nanoparticles containing amino or ester as end group, the oligoamide-nanocomposites were synthesized using two different procedures. Indeed, polycondensation reactions with diamines and dimethyl ester were performed using directly FNP derivatives or, after their preliminary reaction with dimethyl ester, using FNPE derivatives.

The chemical structure of the products synthesized was characterized by ^{1}H NMR, ^{13}C NMR and FT IR spectroscopies and by DLS and TEM analysis. Stable water dispersions were formed with all the nanocomposites synthesized. Soluble and water-insoluble fractions were separated by centrifugation for FT IR characterization and the soluble fraction was subjected to NMR analysis. Both fractions contained TiO_2 nanoparticles with oligoamides bonded on the surface but the presence of free oligoamide was also observed in water soluble fractions.

The synthetic procedure allowed to obtain more homogeneous composites in comparison to blends obtained simply mixing TiO_2 and "unbonded" oligomer. Morphological analysis showed a homogeneous dispersion when the nanoparticles are bonded with the polymer matrix: the nanoparticles are uniformly distributed, without formation of aggregates which may deteriorate the mechanical properties and reduce the optical transparency of polymer-based nanocomposites. The ability of the nanocomposite to degrade methylene blue when subjected to UV radiation, the resistance to photodegradation, and possible color variations due to interaction with the UV radiation were evaluated, using two different wavelengths: 365 nm (irradiation indoor) and 254 nm (irradiation outdoor).

Finally, the nanocomposite was used for the surface treatment of wood, with the aim of preserving them from biotic attack.

Applicative tests on wood samples showed the beneficial effect of the nanocomposite on wood preservation. Indeed, inhibition of fungal growth was obtained in samples treated with the nanocomposite when irradiated with UV light, as confirmed by microscopical analysis.

Moreover, it was shown that after the interruption of the irradiation, fungal growth occurs also on the samples treated with the nanocomposite, indicating that the samples are protected only when they are exposed to a UV radiation.

In the future, samples exposition to sunlight should be evaluated (without altering the conditions of temperature and RH% or, if not possible, altering them the least possible).

6.6 EXPERIMENTAL

6.6.1 Materials

6.6.1.1 Solvents

- MilliQ water
- 1,4-dioxane, product Aldrich, 99% pure
- Isopropanol, product Aldrich, 99,5% pure
- Methanol, product Normapur, 99.9% pure

6.6.1.2 Reagents

- L-tartaric acid, product Aldrich, 99% pure
- Boric acid, product Aldrich, 99,5% pure
- Amberlite IR-120H, product Aldrich
- [3-(2-aminoethylamino)propyl]trimethoxysilane, product Aldrich, 97% pure
- (3-aminopropyl)trimethoxysilane, product Aldrich, 97% pure
- (diacetoxyiodo)benzene (BAIB), product Aldrich, 98% pure
- 1,2- ethylenediamine, product Aldrich, 99% pure
- Titanium(IV) oxide (powder, d< 25nm, anatase), product Aldrich, 99.7% pure
- α,α'-trehalose dihydrate, product Aldrich, 99% pure
- 2,2,6,6-Tetramethylpiperidine-1-oxyl(TEMPO), product Aldrich, 98% pure
- Triethylamine, product Carlo Erba, 97% pure
- Acid solution of vanillin for TLC:
- 3 g of vanillin are dissolved in a solution of 4 ml of H_2SO_4 (conc) and 250 ml of ethanol.

6.6.2 Instruments

6.6.2.1 NMR spectroscopy

^{1}H NMR, ^{13}C NMR, gCOSY and gHSQC spectra were recorded with a Varian Mercury Plus 400 spectrometer and a Varian VXR 200 spectrometer, working at 399.921 MHz and 199.985 MHz, respectively. All spectra are reported in ppm and referred to TMS as internal standard. Spectra elaboration was performed with the software Mestre-C 4.3.2.0. Solvents used (D_2O, $CDCl_3$) are produced by Aldrich Co.

6.6.2.2 FT IR spectroscopy

FT IR spectra were recorded with a Shimadzu FT-IR-8400S model, and elaborated with the Spectrum v.3.0202. Solutions were analyzed using KBr or CaF_2 round cell windows, after deposition and evaporation of solvent. Spectra of solid samples were recorded as KBr pellets.

6.6.2.3 Dynamic light scattering measurements (DLS)

DLS analyses were carried out by means of a BI-90Plus light scattering apparatus from Brookhaven Instruments. The autocorrelation functions recorded for each sample are the result of an average of 10 individual measurements and the data were analyzed according to the CONTIN algorithm to provide the size distribution of scattering objects. Diluted dispersions were investigated in the conventional geometry (at a scattering angle of 90°). Non-diluted dispersions, due to their opacity, cannot be investigated in such geometry; therefore, they were investigated by means of a FOQELS (Fiber Optic Quasi-Elastic Light Scattering) accessory (at a scattering angle of 135°).

6.6.2.4 Transmission electron microscopy (TEM)

TEM analyses were performed on TEM Philips CM 12, equipped with an Olympus Megaview G2 camera and using an accelerating voltage of 100 kV. Samples were prepared by depositing a drop of dispersion of the sample on carbon film of 200 mesh Cu grid and on holey carbon.

6.6.2.5 Colorimeter

Colorimetric analyses were performed using a CM-2600d Konica-Minolta portable spectrophotometer equipped with the integrative sphere inside the apparatus and a Xenon lamp to pulse the light on the sample surface. The measurement aperture is 3 mm, and light is reflected

from surface with an angle of 8°. Color coordinates are based on CIEL*a*b* system using an illuminant D65 with an observer angle of 10.

6.6.2.6 Microscope

Sample surface was observed by a Dino-Lite Pro Portable Digital Microscope with 1.3 megapixel image sensor. The microscope is equipped with polarized light (useful with reflective objects) and magnification up to 200x.

6.6.2.7 UV lamp

Exposure to UV radiation was carried out using a Spectroline Lamp, Model ENF-260C/FE, with an emission in UV-A range at wavelength of 365 nm (tube of 6W).

6.6.2.8 Microorganism and growth conditions

Trametes versicolor strain MB52, obtained from the Austrian Center of Biological Resources and Applied Mycology, was used as test organism in this study. In order to test wood specimens susceptibility to fungal attack, a cells suspension of *T. versicolor* was spread on Malt Extract Agar (MEA, OXOID) plates and incubated at 30°C for four weeks to obtain a thick mycelium.

6.6.2.9 Wood specimens preparation

Sixteen samples were prepared from European beech (*Fagus sylvatica* L.) a wood type free of any previous biological alteration. European beech is well known for its low natural durability and high susceptibility to Fungi and Bacteria, which make it one of the most suitable species to test the performances of antimicrobial products. Wood specimens, measuring 10 × 20 × 2 mm, were cut keeping the longitudinal faces parallel to the grain. Prior to the treatment the wood samples were equilibrated at 20 ° C and 65% relative humidity (RH) inside dryers contained xylene as inhibitor of Fungal activity.

6.6.3 Syntheses of the precursors

6.6.3.1 Dimethyl L-tartrate

See synthesis discussed in chapter 3.

6.6.3.2 α,α'- trehaluronic acid.

Into a dry 100 mL flask, TEMPO (305 mg, 1.95 mmol) is added under continuous stirring to 45 mL of a 1,4-dioxane/water (2:1) solution of α,α'-trehalose (1.5 g, 4.4 mmol). BAIB (7.0 g, 21.9 mmol) is then added, and the mixture is allowed to react at room temperature. The reaction, monitored by thin layer chromatography (2-propanol/water, 3:1), is completed in 24h. After vacuum distillation at 60°C, a yellow solid is obtained (1.6 g, 97.4% yield).

^{1}H-NMR (D_2O, 400 MHz): 3.62 ppm (dd, $J_{4,5}$ 10.0 Hz, $J_{4,3}$ 9.2 Hz, 2H, H4, H4'); 3.72 ppm (dd, $J_{2,3}$ 9.6 Hz, $J_{2,1}$ 3.6 Hz, 2H, H_2, H_2'); 3.88 ppm (m, 2H, H_3, H_3'); 4.36 ppm (d, J 10.0 Hz, 2H, H_5, H_5'); 5.23 ppm (d, J 3.6 Hz, 2H, H_1, H_1').

^{13}C-NMR (D_2O, 100 MHz): 70.4 ppm (C_4, C_4'); 71.1 ppm (C_5, C_5'); 71.4 ppm (C_3, C_3'); 72.0 ppm (C_2, C_2'); 94.2–94.3 ppm (C_1, C_1'); 173.2 ppm (**C**OOH).

6.6.3.3 Dimethyl- α,α'-trehaluronate.

Into a 40-mL Sovirel® tube, Amberlite IR-120H (3.5 g) is added to 25 mL of a methanol solution of α,α'-trehaluronic acid (1.71 g, 4.62 mmol), and the mixture is heated at 80°C under gentle stirring. The reaction, monitored by thin layer chromatography (2-propanol/water, 3:1), is completed after 48h. The mixture is cooled to room temperature and filtered, then the solution is distilled under reduced pressure at 50°C. The solid obtained is dried in vacuum at room temperature (1.67 g, 91.0% yield).

^{1}H-NMR (D_2O, 400 MHz): 3.64 ppm (dd, $J_{4,5}$ 10.0 Hz, $J_{4,3}$ 9.2 Hz, 2H, H_4, H_4'); 3.73 ppm (dd, $J_{2,3}$ 9.6 Hz, $J_{2,1}$ 3.6 Hz, 2H, H_2, H_2'); 3.85 ppm (s, 6H, -COOC**H**$_3$); 3.88 ppm (m, 2H, H_3, H_3'); 4.44 ppm (d, J 10.0 Hz, 2H, H_5, H_5'); 5.22 ppm (d, J 3.6 Hz, 2H, H_1, H_1').

^{13}C-NMR (D_2O, 50 MHz): 53.1 ppm (-COO**C**H$_3$); 70.4 ppm (C_4, C_4'); 71.2–71.4 ppm (C_5, C_5', C_3, C_3'); 72.0 ppm (C_2, C_2'); 94.4 ppm (C_1, C_1'); 171.3 ppm (-**C**OOH).

6.6.4 Syntheses of the products

6.6.4.1 TiO_2 activation

TiO_2 (1.6 g, 0.02 mol) nanoparticles are dispersed in HNO_3 (2 M). The dispersion is placed in a 25 mL flask fitted with a reflux condenser and heated at 95°C for 8 h. The mixture is cooled and centrifuged, then the solid is dispersed in Milli-Q water (dispersion at 4.5% w/w).

FT IR (KBr pellet): peaks at 3396 (d, O-H stretching), 1635 (d, O-H bending), 1386 (m, N-O stretching) e a 450-800 (ff, broad, Ti-O stretching) cm^{-1}.

TEM: diameter of nanoparticles as about 10-20 nm

6.6.4.2 Functionalized nanoparticle (FNP) syntheses

The functionalized nanoparticles were synthesized using two different silylating agents, [3-(2-aminoethylamino)propyl]trimethoxysilane (AEAPTMS) and (3-aminopropyl)-trimethoxysilane (APTMS), obtaining respectively FNP.1 and FNP.2.

Synthetic procedure

Into a Sovirel® tube, silylating agent (1.6 mmol) is added under continuous stirring to 3.80 mL of methanol. Then, a water dispersion of TiO_2 nanoparticles at 4.5% w/w (3.75 mmol) is added and the blend is sonicated for 30 min. The mixture is heated at 40°C for 8h under dry nitrogen atmosphere. After cooling to room temperature, a sample of nanoparticles dispersion (0.5 mL) is recovered and solvent and volatile compounds are distilled at reduced pressure at 40°C. The white solid obtained is washed with chloroform, recovered by centrifugation (5 min at 2800 rpm), then dried in vacuum at room temperature (75% yield).

The reaction was repeated by increasing the reaction times up to 15 hours, keeping constant the other conditions and the work-up (90% yield).

The solid obtained is analysed by FT-IR spectroscopy and after dispersion in D_2O by ^{1}H NMR and ^{13}C NMR spectroscopies.

FNP.1: ^{1}H NMR (D_2O, 200 MHz): signals at δ 0.63 ppm (m, 2H, $SiC\mathbf{H}_2$), 1.67 ppm (m, 2H, $SiCH_2C\mathbf{H}_2$), 2.87 ppm (m, 6H, $Si(CH_2)_2C\mathbf{H}_2NH(C\mathbf{H}_2)_2NH_2$).

^{13}C NMR (D_2O, 50 MHz): signals at δ 9.8 ppm (Si-**C**H_2), 21.0 ppm ($SiCH_2$**C**H_2), 38.1 ppm ($Si(CH_2)_3NHCH_2$**C**H_2NH_2), 48.8 ppm ($Si(CH_2)_3NH$**C**H_2CH_2NH), 50.6 ppm ($Si(CH_2)_2$**C**H_2NH).

FTIR (KBr pellet): peaks at 3246 (s, broad, N-H and O-H stretching), 2924, 2870 (w, C-H stretching), 1596 (s, N-H bending), 1457 (w, C-H bending), 1353 (m, C-N stretching), 1115, 1032 (s, Si-O stretching), 912 (w, Ti-O-Si stretching), 630 (vs, Ti-O stretching) cm^{-1}.

FNP.2: ^{1}H NMR (D_2O, 200 MHz): signals at δ 0.62 ppm (m, 2H, SiC**H**$_2$), 1.70 ppm (m, 2H, $SiCH_2$C**H**$_2$), 2.90 ppm (m, 2H, $SiCH_2CH_2$C**H**$_2NH_2$).

^{13}C NMR (D_2O, 50 MHz): signals at δ 9.5 ppm (Si**C**H_2), 21.6 ppm ($SiCH_2$**C**H_2), 42.0 ppm (-Si-$(CH_2)_2$-**C**H_2-NH_2).

FTIR (KBr pellet): peaks at 3343 (s, broad, N-H and O-H stretching), 2924, 2880 (w, C-H stretching), 1595 (s, N-H bending), 1457 (w, C-H bending), 1353 (m, C-N stretching), 1120, 1033 (s, Si-O stretching), 920 (w, Ti-O-Si stretching), 620 (vs, Ti-O stretching) cm^{-1}.

6.6.4.3 Amide syntheses by reaction of FNP and dimethyl ester (FNPE)

The amides were obtained by reacting the functionalized nanoparticles (FNP.1 or FNP.2) with dimethyl ester (dimethyl l-tartrate or dimethyl α,α'-trehaluronate); the respective products were named as shown in Table 20.

Synthetic procedure

Into a Sovirel® tube, a methanol solution (2.5 mL) of dimethyl ester (1.06 mmol) is added under continuous stirring to a FNP.1 or FNP.2 dispersion (0.53 mmol). Then, triethylamine (0.14 mmol) is added and the mixture was heated at 80 °C for 24 h under dry nitrogen atmosphere. After cooling to room temperature, solvent and volatile compounds are distilled under reduced pressure at 40°C. The solid obtained (white for tartrate derivative or amber for trehaluronic derivative) is washed with methanol and centrifuged (5 min at 2800 rpm). The residual solid was dried in vacuum at room temperature (yield ≈ 85%), analyzed by FT-IR (Table 22) spectroscopy and after dispersion in D_2O by ^1H NMR (Table 23, Table 24) spectroscopy.

NPFE.1: ^{1}H-NMR (D_2O, 400 MHz): signals at δ 0.73 ppm (m, 2H, SiC**H**$_2$CH$_2$CH$_2$NH), 1.81 ppm (m, 2H, SiCH$_2$C**H**$_2$CH$_2$NH), 3.00- 3.28 ppm (m, 4H, SiCH$_2$CH$_2$C**H**$_2$NHC**H**$_2$CH$_2$NH), 3.60 ppm (2H, NHCH$_2$C**H**$_2$NH), 3.82 ppm (s, 3H, COOC**H**$_3$), 4.40 ppm (s, 1H, C**H**OH amide), 4.66 ppm (ds 1H, C**H**OH ester).

NPFE.3: ^{1}H-NMR (D_2O, 400 MHz): signals at δ 0.77 ppm (m, 2H, SiC**H**$_2$CH$_2$CH$_2$NH), 1.81 ppm (m, 2H SiCH$_2$C**H**$_2$CH$_2$NH), 3.05 ppm (m, 2H, SiCH$_2$CH$_2$C**H**$_2$NH), 3.84 ppm (s, 3H, COOC**H**$_3$), 4.42 ppm (m, 1H, C**H**OH amide), 4.68 ppm (m, 1H, CHOH ester).

NPFE.1- NPFE.3: FT-IR (KBr pellet): peaks at 3342 (vs, broad, N-H and O-H stretching), 2952, 2880 (w, C-H stretching), 1738 (s, C=O ester stretching), 1611 (vs, N-H and H-OH bending), 1464 (w, C-H bending), 1127, 1080 (vs, Si-O and C-O stretching), 904 (w, Ti-O-Si stretching), 620 (vs, Ti-O stretching) cm^{-1}.

NPFE.2: ^{1}H-NMR (D_2O, 200 MHz): signals at δ 0.68 ppm (m, 2H, SiC**H**$_2$CH$_2$CH$_2$NH), 1.75 ppm (m, 2H, SiCH$_2$C**H**$_2$CH$_2$NH), 2.98 ppm (m, 4H, SiCH$_2$CH$_2$C**H**$_2$NHC**H**$_2$CH$_2$NH), 3.60 ppm (m, 2H, NHCH$_2$C**H**$_2$NH), 3.60 (m, 2H, H_4, H_4'), 3.69 ppm (2H, H_2, H_2'), 3.80 ppm (s, 3H, COOC**H**$_3$), 3.84 ppm (m, 2H, H_3, H_3'), 4.07 ppm (m, 1H, H_5 near amide), 4.40 ppm (m, 1H, H_5' end chain), 5.19 ppm (m, 2H, H_1, H_1').

NPFE.4: ^{1}H-NMR (D_2O, 200 MHz): signals at δ 0.77 ppm (m, 2H, SiC**H**$_2$CH$_2$CH$_2$NH), 1.83 ppm (m, 2H, SiCH$_2$C**H**$_2$CH$_2$NH); 3.10 ppm (m, 2H, SiCH$_2$CH$_2$C**H**$_2$NH), 3.58 ppm (m, 2H, H_4, H_4'), 3.69 ppm (2H, H_2, H_2'), 3.80 ppm (s, 3H, COOC**H**$_3$), 3.82 ppm (m, 2H, H_3, H_3'), 4.06 ppm (m, 1H, H_5 near amide), 4.40 ppm (m, 1H, H_5' end chain), 5.19 ppm (m, 2H, H_1, H_1').

NPFE.2- NPFE.4: FT-IR (KBr pellet): peaks at 3343 (vs, broad, N-H and O-H stretching), 2932 (w, C-H stretching), 1730 (s, C=O ester stretching), 1600 (vs, N-H and H-OH bending), 1411 (w, C-H bending), 1353 (w, C-N stretching) 1151, 1070 (vs, Si-O and C-O stretching), 1108, 1027 (vs, Si-O and C-O stretching), 912 (w, Ti-O-Si stretching), 620 (vs, Ti-O stretching) cm^{-1}.

6.6.4.4 Oligoamide syntheses by polymerization of FNPE or FNP with dimethyl ester and diamine (FNPO or FNPEO)

Oligoamides were obtained by polymerization of FNP (or FNPE) with dimethyl ester (dimethyl l-tartrate or dimethyl α,α'-trehaluronate) and diamine (ethylenediamine), see Table 21. The respective products were denoted as shown in Table 20.

Synthetic procedure to obtain FNPO

In a Sovirel® tube, a methanol solution (1.8 mL) of dimethyl ester (1 mmol) is added under continuous stirring to FNP (0.3 mmol). Then, a methanol solution (1.25 mL) of 1,2- ethylendiamine (0.7 mmol) and triethylamine (0.27 mmol) are added and the mixture is heated at 80 °C for 24 h (Table 21) under dry nitrogen atmosphere. After cooling to room temperature, solvent and volatile compounds are distilled under reduced pressure at 40 °C. The solid is washed with methanol and centrifuged (5 min at 2800 rpm) and the resulting solid is dried at room temperature.

Solid product (50 mg) is suspended in D_2O (1 mL) in a vial. After centrifugation (1h at 2800 rpm), a soluble fraction (A≈ 50-60%) in D_2O and an insoluble one (B ≈ 40-50%) are obtained. The soluble fraction was analyzed by FT-IR (Table 22), ^{1}H NMR (Table 23, Table 24), and ^{13}C NMR (Table 25, Table 26) spectroscopies; the insoluble fraction is analyzed with FT-IR spectroscopy (Table 22).

FNPO.1

Soluble fraction in D_2O: ^{1}H-NMR (D_2O, 400 MHz): signals at δ 0.70 ppm (m, 2H, SiC**H**$_2$), 1.73 ppm (m, 2H SiCH$_2$C**H**$_2$), 2.90-3.15 ppm (m, 4H, SiCH$_2$CH$_2$C**H**$_2$NHC**H**$_2$CH$_2$NH, 2H, C**H**$_2$-NH$_2$), 3.40- 3.60 ppm (m, 2H, SiCH$_2$CH$_2$CH$_2$NHCH$_2$C**H**$_2$NHCO, 4H, C**H**$_2$NHCO), 4.57 ppm (m, 2H, C**H**OH).

^{13}C-NMR (D_2O, 100 MHz): signals at δ 9.3 ppm (Si**C**H$_2$), 20.6 ppm (SiCH$_2$**C**H$_2$), 38.5- 39.4 ppm (**C**H$_2$NHCO), 46.9 ppm (NH**C**H$_2$CH$_2$NH), 50.3 ppm (SiCH$_2$CH$_2$**C**H$_2$NHCH$_2$), 72.3- 73.8 ppm (**C**HOH), 174.0 ppm (**C**ONH).

Soluble and insoluble fractions: FT-IR (KBr pellet): peaks at 3348 (vs, broad, N-H and O-H stretching), 2935 (w, C-H stretching), 1660 (vs, C=O amide stretching), 1537 (s, N-H bending), 1385 (w, C-H bending), 1134, 1072 (s, Si-O and C-O stretching), 912 (w, Ti-O-Si stretching), 620 (vs, Ti-O stretching) cm^{-1}.

FNPO.2

Soluble fraction in D_2O: ^{1}H-NMR (D_2O, 400 MHz): signals at δ 0.67 ppm (m, 2H, $SiCH_2$), 1.75 ppm (m, 2H $SiCH_2CH_2$), 3.00- 3.20 ppm (m, 4H, $SiCH_2CH_2CH_2NHCH_2CH_2NH$, 2H, CH_2NH_2), 3.40- 3.60 ppm (m, 2H, $SiCH_2CH_2CH_2NHCH_2CH_2NH$, 4H, CH_2NH), 3.53 ppm (m, 2H, H_4, H_4'), 3.67 ppm (m, 2H, H_2, H_2'), 3.84 ppm (m, 2H, H_3, H_3'), 4.00- 4.25 ppm (m, 2H, H_5, H_5'), 5.18 ppm (m, 2H, H_1, H_1').

^{13}C-NMR (D_2O, 100 MHz):): signals at δ 8.7 ppm ($SiCH_2$), 19.6 ppm ($SiCH_2CH_2$), 36.0- 39.0 ppm (CH_2NHCO), 46.6 ppm ($NHCH_2CH_2NH$), 49.9 ppm ($SiCH_2CH_2CH_2NHCH_2$), 70.4 ppm (C_2, C_2'), 71.6 ppm (C_4, C_4'), 71.9 ppm (C_3, C_3', C_5, C_5'), 93.4- 94.3 ppm (C_1, C_1'), 171.2- 176.3 ppm (**C**ONH).

Soluble and insoluble fractions: FT-IR (KBr pellet): peaks at 3336 (vs, broad, N-H and O-H stretching), 2935 (w, C-H stretching), 1649 (vs, C=O amide stretching), 1554 (s, N-H bending), 1415 (w, C-H bending), 1147, 1066 (s, Si-O and C-O stretching), 1107, 1027 (s, C-O stretching), 943 (w, Si-O-Ti stretching), 630 (vs, Ti-O stretching) cm^{-1}.

FNPO.3

Soluble fraction: ^{1}H-NMR (D_2O, 400 MHz): signals at δ 0.70 ppm (m, 2H, $SiCH_2$), 1.79 ppm (m, 2H $SiCH_2CH_2$), 3.00- 3.15 ppm (m, 2H, $SiCH_2CH_2CH_2NHCO$, 2H, CH_2NH_2), 3.40- 3.60 ppm (m, 4H, CH_2NHCO), 4.57 ppm (m, 2H, CHOH).

^{13}C-NMR (D2O, 100 MHz): signals at δ 8.8 ppm ($SiCH_2$), 20.8 ppm ($SiCH_2CH_2$), 37.9- 39.4 ppm (CH_2NH), 72.3- 73.8 (CHOH), 174.0- 174.4 ppm (CONH).

Soluble and insoluble fractions: FT-IR (KBr pellet): 3348 (vs, broad, N-H and O-H stretching), 2933 (w, C-H stretching), 1730 (w, C=O ester stretching), 1660 (vs, C=O amide stretching), 1537 (s, N-H bending), 1436 (w, C-H bending), 1353 (w, C-N stretching), 1134, 1072 (s, Si-O and C-O stretching), 912 (w, Ti-O-Si stretching), 620 (vs, Ti-O stretching) cm^{-1}.

FNPO.4

Soluble fraction: ^{1}H-NMR (D_2O, 400 MHz): signals at δ 0.67 ppm (m, 2H, $SiCH_2$), 1.74 ppm (m, 2H $SiCH_2CH_2$), 3.00 ppm (m, 2H, $SiCH_2CH_2CH_2NH$), 3.16 ppm (m, 2H, CH_2NH_2), 3.40- 3.60 ppm (m, 4H, CH_2NH), 3.54 ppm (m, 2H, H_4, H_4'), 3.68 ppm (m, 2H, H_2, H_2'), 3.80 ppm (m, 3H, $COOCH_3$), 3.85 ppm (m, 2H, H_3, H_3'), 3.90- 4.20 ppm (m, 2H, H_5, H_5'), 4.38 ppm (m, 1H, H_5 end chain), 5.18 ppm (m, 2H, H_1, H_1').

^{13}C-NMR (D_2O, 100 MHz): signals at δ 36.7- 39.0 ppm (CH_2NH), 53.0 ppm (OCH_3), 70.4 ppm (C_2, C_2'), 71.3 ppm (C_4, C_4'), 71.6 ppm (C_5, C_5'), 72.0 ppm (C_3, C_3'), 93.5- 94.6 ppm (C_1, C_1'), 171.2- 176.3 ppm (CONH).

Soluble and insoluble fractions: FT-IR (KBr pellet): peaks at 3379 (vs, broad, N-H and O-H stretching), 2935 (w, C-H stretching), 1730 (w, C=O ester stretching), 1652 (vs, C=O amide stretching), 1540 (s, N-H bending), 1438 (w, C-H bending), 1353 (w, C-N stretching), 1150, 1066 (s, Si-O and C-O stretching), 1107, 1028 (s, C-O stretching), 943 (w, Si-O-Ti stretching), 630 (vs, Ti-O stretching) cm^{-1}.

Synthetic procedure to obtain FNPEO

In a Sovirel® tube, a methanol solution (1.25 mL) of dimethyl ester (0.7 mmol) is added under continuous stirring to FNPE (0.3 mmol). Then, a methanol solution (1.8 mL) of 1,2- ethylendiamine (1 mmol) and triethylamine (0.27 mmol) are added and the mixture is heated at 80 °C for 24 h (Table 4) under dry nitrogen atmosphere. The work-up is carried out operating as above.

Solid product (50 mg) is suspended in D_2O (1 mL) in a vial. After centrifugation (1h at 2800 rpm), a soluble fraction (A≈ 50-60%) in D_2O and an insoluble one (B ≈ 40-50%) are obtained. The soluble fraction was analyzed by FT-IR (Table 22), ^{1}H NMR (Table 23, Table 24), and ^{13}C NMR (Table 25, Table 26) spectroscopies; the insoluble fraction is analyzed with FT-IR spectroscopy (Table 22).

FNPEO.1

Soluble fraction: ^{1}H-NMR (D_2O, 400 MHz): signals at δ 0.72 ppm (m, 2H, SiC**H**$_2$), 1.77 ppm (m, 2H $SiCH_2C\mathbf{H}_2$), 3.00- 3.20 ppm (m, 4H, $SiCH_2CH_2C\mathbf{H}_2NHC\mathbf{H}_2CH_2NH$, 2H, C**H**$_2NH_2$), 3.40- 3.60 ppm (m, 2H, $SiCH_2CH_2CH_2NHCH_2C\mathbf{H}_2NHCO$, 4H, C**H**$_2$NHCO), 4.58 ppm (m, 2H, C**H**OH).

^{13}C NMR spectrum shows the same signals of the corresponding FNPO.1 but are not visible signals related to the coupling agent because the product has higher molecular weight.

Soluble and insoluble fractions: FT-IR (KBr pellet): peaks at 3348 (vs, broad, N-H and O-H stretching), 2935 (w, C-H stretching), 1660 (vs, C=O amide stretching), 1537 (s, N-H bending), 1385 (w, C-H bending), 1134, 1072 (s, Si-O and C-O stretching), 912 (w, Ti-O-Si stretching), 620 (vs, Ti-O stretching) cm^{-1}.

FNPEO.2

Soluble fraction: ^{1}H-NMR (D_2O, 400 MHz): 0.69 ppm (m, 2H, Si-C**H**$_2$), 1.74 ppm (m, 2H $SiCH_2C\mathbf{H}_2$), 3.00- 3.15 ppm (m, 4H, $SiCH_2CH_2C\mathbf{H}_2NHC\mathbf{H}_2CH_2NH$, 2H, C**H**$_2NH_2$), 3.40- 3.60 ppm (m, 2H, $SiCH_2CH_2CH_2NHCH_2C\mathbf{H}_2NHCO$, 4H, C**H**$_2$NHCO), 3.58 ppm (m, 2H, H_4, H_4'), 3.70 ppm (m, 2H, H_2, H_2') 3.86 ppm (m, 2H, H_3, H_3', 3H, -OC**H**$_3$); 4.07- 4.27 ppm (m, 2H, H_5, H_5'), 5.23 ppm (m, 2H, H_1, H_1').

^{13}C NMR spectrum shows the same signals of the corresponding FNPO.2 but signals related to the coupling agent are not visible because the product has higher molecular weight.

Soluble and insoluble fractions: FT-IR (KBr pellet): peaks at 3336 (vs, broad, N-H and O-H stretching), 2935 (w, C-H stretching), 1649 (vs, C=O amide stretching), 1554 (s, N-H bending), 1415 (w, C-H bending), 1147, 1066 (s, Si-O and C-O stretching), 1107, 1027 (s, C-O stretching), 943 (w, Si-O-Ti stretching), 630 (vs, Ti-O stretching) cm^{-1}.

FNPEO.3:

Soluble fraction: ^{1}H-NMR (D_2O, 400 MHz): signals at δ 0.71 ppm (m, 2H, SiC**H**$_2$), 1.79 ppm (m, 2H $SiCH_2C\mathbf{H}_2$), 3.00- 3.20 ppm (m, 2H, $SiCH_2CH_2C\mathbf{H}_2NHCO$, 2H, C**H**$_2NH_2$), 3.40- 3.60 ppm (m, 4H, C**H**$_2$NHCO), 4.57 ppm (m, 2H, C**H**OH).

^{13}C NMR spectrum shows the same signals of the corresponding FNPO.3 but signals related to the coupling agent are not visible because the product has higher molecular weight.

Soluble and insoluble fractions: FT-IR (KBr pellet): 3348 (vs, broad, N-H and O-H stretching), 2933 (w, C-H stretching), 1730 (w, C=O ester stretching), 1660 (vs, C=O amide stretching), 1537 (s, N-H bending), 1436 (w, C-H bending), 1353 (w, C-N stretching), 1134, 1072 (s, Si-O and C-O stretching), 912 (w, Ti-O-Si stretching), 620 (vs, Ti-O stretching) cm^{-1}.

FNPEO.4.

Soluble fraction: ^{1}H-NMR (D_2O, 400 MHz): signals at δ 0.76 ppm (m, 2H, SiC**H**$_2$), 1.81 ppm (m, 2H $SiCH_2C\mathbf{H}_2$); 3.00- 3.20 ppm (m, 2H, $SiCH_2CH_2C\mathbf{H}_2NHCO$, 2H, C**H**$_2NH_2$), 3.54 ppm (m, 4H, C**H**$_2$NHCO), 3.59 ppm (m, 2H, H_4, H_4'), 3.73 ppm (m, 2H, H_2, H_2'), 3.89 ppm (m, 2H, H_3, H_3'), 4.10- 4.30 ppm (m, 2H, H_5, H_5'), 5.23 ppm (m, 2H, H_1, H_1').

^{13}C NMR spectrum shows the same signals of the corresponding FNPO.4 but signals related to the coupling agent are not visible because the product has higher molecular weight.

Soluble and insoluble fractions: FT-IR (KBr pellet): peaks at 3379 (vs, broad, N-H and O-H stretching), 2935 (w, C-H stretching), 1730 (w, C=O ester stretching), 1652 (vs, C=O amide stretching), 1540 (s, N-H bending), 1438 (w, C-H bending), 1353 (w, C-N stretching), 1150, 1066 (s, Si-O and C-O stretching), 1107, 1028 (s, C-O stretching), 943 (w, Si-O-Ti stretching), 630 (vs, Ti-O stretching) cm^{-1}.

7 Bibliography

1. Anastas, P. T. & Warner, J. C. *Green Chemistry: Theory and Practice*. (Oxford University, 2000).
2. Reap, J., Roman, F., Duncan, S. & Bras, B. A survey of unresolved problems in life cycle assessment - Part I goals and scope and inventory analysis. *Int. J. Life Cycle Assess.* **13,** 290–300 (2008).
3. Kamm, B., Kamm, M., Gruber, P. R. & Kromus, S. in *Biorefineries- Industrial Processes and Products- Status Quo and Future Directions* 1–40 (WYLEY-VCH, 2010).
4. Raquez, J.-M. *et al.* Oxidative degradations of oxodegradable LDPE enhanced with thermoplastic pea starch: Thermo-mechanical properties, morphology, and UV-ageing studies. *J. Appl. Polym. Sci.* **122,** 489–496 (2011).
5. Lemieux, G. A. & Bertozzi, C. R. Chemoselective ligation reactions with proteins, oligosaccharides and cells. *Trends Biotechnol.* **16,** 506–513 (1998).
6. Parisi, F. & Centola, G. *Zuccheri, Cellulosa, Fermentazioni- Dal 'Trattato di chimica industriale e applicata' di Alberto Girelli, Leno Matteoli, Federico Parisi, 4*. (Zanichelli, 1974).
7. Klemm, D., Heublein, B., Fink, H.-P. & Bohn, A. Cellulose: Fascinating Biopolymer and Sustainable Raw Material. *Angew. Chem. Int. Ed.* **44,** 3358–3393 (2005).
8. Lancaster, M. *Green Chemistry: An Introductory Text*. (The Royal Society of Chemistry, 2002).
9. Brandt, L. *Ullmann's Encyclopedia of industrial chemistry, Cellulose Ethers*. **A5,** (VCH, 1986).
10. Christensen, M., Kutzke, H. & Hansen, F. K. New materials used for the consolidation of archaeological wood–past attempts, present struggles, and future requirements. *J. Cult. Herit.* **13,** S183–S190 (2012).
11. Cipriani, G., Salvini, A., Baglioni, P. & Bucciarelli, E. Cellulose as a renewable resource for the synthesis of wood consolidants. *J. Appl. Polym. Sci.* **118,** 2939–2950 (2010).
12. Rinaudo, M. Chitin and chitosan: Properties and applications. *Prog. Polym. Sci.* **31,** 603–632 (2006).
13. Khan, T. A., Peh, K. K. & Ch'ng, H. S. Reporting degree of deacetylation values of chitosan: the influence of analytical methods. *J Pharm Sci* **5,** 205–12 (2002).
14. Kurita, K. Controlled functionalization of the polysaccharide chitin. *Prog. Polym. Sci.* **26,** 1921–1971 (2001).
15. Carothers, W. H. Linear condensation 'superpolymers' suitable for production of pliable, strong, elastic fibers. US 2071250 (1937).
16. Schlack, P. Polyamides. US 2241321 (1941).

17. Berti, L., Calatozzolo, M. & Di Bartolo, R. *Processi di polimerizzazione*. (G. D'Anna, 1981).
18. Bou, J. J. & Mun˜oz-Guerra, S. Synthesis and characterization of a polytartaramide based on l-lysine. *Polymer* **36,** 181–186 (1995).
19. Okada, M. Chemical syntheses of biodegradable polymers. *Prog. Polym. Sci.* **27,** 87–133 (2002).
20. Kiely, D.E. & Lin, T.H. Polyhydroxypolyamides and process for making same. US4833230 (1989).
21. Feng, Q., Li, H., Lv, S. & Huang, Y. Preparation method of polyamide adhesive with improved bonding force for preparation of card. 7pp. CN103937440 (2014).
22. Ogata, N., Sanui, K., Hosoda, Y. & Nakamura, H. Active polycondensation of diethyl 2,3,4,5-tetrahydroxyadipate with diamines. *J. Polym. Sci. Polym. Chem. Ed.* **14,** 783–792 (1976).
23. Ogata, N., Sanui, K. & Kayama, Y. Copolycondensation of hydroxyl diesters and active diesters with hexamethylenediamine. *J. Polym. Sci. Polym. Chem. Ed.* **15,** 1523–1526 (1977).
24. Ogata, N. & Hosoda, Y. Synthesis of hydrophilic polyamide by active polycondensation. *J. Polym. Sci. Polym. Lett. Ed.* **12,** 355–358 (1974).
25. Ogata, N. & Hosoda, Y. Synthesis of hydrophilic polyamide from L-tartarate and diamines by active polycondensation. *J. Polym. Sci. Polym. Chem. Ed.* **13,** 1793–1801 (1975).
26. Hoagland, P. D. The formation of intermediate lactones during aminolysis of diethyl galactarate. *Carbohydr. Res.* **98,** 203–8 (1981).
27. Hoagland, P. D., Pessen, H. & McDonald, G. G. The formation of intermediate lactones during aminolysis of diethyl xylarate. *J. Carbohydr. Chem.* **6,** 495–9 (1987).
28. Chen, L. & Kiely, D. E. d-Glucaric Acid Esters/Lactones Used in Condensation Polymerization to Produce Hydroxylated Nylons—A Qualitative Equilibrium Study in Acidic and Basic Alcohol Solutions. *J. Carbohydr. Chem.* **13,** 585–601 (1994).
29. Kiely, D. E., Chen, L. & Lin, T. H. Hydroxylated nylons based on unprotected esterified D-glucaric acid by simple condensation reactions. *J. Am. Chem. Soc.* **116,** 571–578 (1994).
30. Kiely, D. E. & Chen, L. Glucaric acid monoamides and their use to prepare poly(glucaramides). US5329044 A (1994).
31. Minoura, Y., Urayama, S. & Noda, Y. Syntheses of optically active polymers by condensation polymerization of d-tartaric acid with some diamines. *J. Polym. Sci. [A1]* **5,** 2441–2451 (1967).
32. Bou, J. J., Rodriguez-Galan, A. & Munoz-Guerra, S. Optically active polyamides derived from L-tartaric acid. *Macromolecules* **26,** 5664–70 (1993).

33. Cipriani, G., Salvini, A., Fioravanti, M., Di Giulio, G. & Malavolti, M. Synthesis of hydroxylated oligoamides for their use in wood conservation. *J. Appl. Polym. Sci.* **127,** 420–431 (2013).
34. Oliva, R. *et al.* Water soluble trehalose-derived oligoamides. *J. Polym. Res.* **21,** 1–12 (2014).
35. Kamm, B., Kamm, M., Schimidt, M., Hirth, T. & Schulze, M. in *Biorefineries- Industrial Processes and Products- Status Quo and Future Directions* 97–149 (WYLEY-VCH, 2010).
36. Teramoto, N., Sachinvala, N. D. & Shibata, M. Trehalose and Trehalose-based Polymers for Environmentally Benign, Biocompatible and Bioactive Materials. *Molecules* **13,** 1773–1816 (2008).
37. Higashiyama, T. Novel functions and applications of trehalose. *Pure Appl Chem* **74,** 1263–1270 (2002).
38. Brazier, M. A. B. A new method for the separation of the products of protein hydrolysis. *Biochem. J.* **24,** 1188 (1930).
39. Pfefferle, W., Möckel, B., Bathe, B. & Marx, A. in *Microbial Production of l-Amino Acids* (eds. Faurie, R. et al.) **79,** 59–112 (Springer Berlin Heidelberg, 2003).
40. Cavani, F. & Alini, S. in *Sustainable Industrial Chemistry* 367–425 (Wiley-VCH Verlag GmbH & Co. KGaA, 2009).
41. Sapuan, S. M. & Bachtiar, D. Mechanical Properties of Sugar Palm Fibre Reinforced High Impact Polystyrene Composites. *Procedia Chem.* **4,** 101–106 (2012).
42. Aglietto, M. & Bongiovanni, R. *Sintesi di materiali polimerici. XXXIII Convegno- Scuola AIM 'Mario Farina'*. **2,** (Edizioni Nuova Cultura, 2012).
43. Ogata, N., Sanui, K., Ohtake, T. & Nakamura, H. Solution polycondensation of diesters and diamines having hetero atom groups in polar solvents. *Polym. J. Tokyo Jpn.* **11,** 827–33 (1979).
44. Houston, T. A., Wilkinson, B. L. & Blanchfield, J. T. Boric acid-catalyzed chemoselective esterification of α-hydroxycarboxylic acids. *Org. Lett.* **6,** 679–681 (2004).
45. Borghi, G. P. in *Enciclopedia degli idrocarburi* **III,** 85– 112
46. Kelland, M. A. Method of inhibiting the formation of gas hydrates using amine oxides. 31pp. WO2013053770 (2013).
47. Kelland, M. A. A review of kinetic hydrate inhibitors - tailor-made water-soluble polymers for oil and gas industry applications. *Adv. Mater. Sci. Res.* **8,** 121–209 (2012).
48. Norland, A. K. & Kelland, M. A. Crystal growth inhibition of tetrahydrofuran hydrate with bis- and polyquaternary ammonium salts. *Chem. Eng. Sci.* **69,** 483–491 (2012).

49. Li, S., Wang, Y., Lang, X. & Fan, S. Effects of cyclic structure inhibitors on the morphology and growth of tetrahydrofuran hydrate crystals. *J. Cryst. Growth* **377,** 101–106 (2013).
50. Del Villano, L. & Kelland, M. A. Tetrahydrofuran hydrate crystal growth inhibition by hyperbranched poly(ester amide)s. *Chem. Eng. Sci.* **64,** 3197–3200 (2009).
51. Blicke, F. F. & Monroe, E. Antispasmodics. I. *J. Am. Chem. Soc.* **61,** 91–3 (1939).
52. Kelland, M. A., Kvæstad, A. H. & Astad, E. L. Tetrahydrofuran Hydrate Crystal Growth Inhibition by Trialkylamine Oxides and Synergism with the Gas Kinetic Hydrate Inhibitor Poly(N-vinyl caprolactam). *Energy Fuels* **26,** 4454–4464 (2012).
53. Balagam, B. & Richardson, D. E. The Mechanism of Carbon Dioxide Catalysis in the Hydrogen Peroxide N-Oxidation of Amines. *Inorg. Chem.* **47,** 1173–1178 (2008).
54. Chen, L. & Kiely, D. E. Synthesis of Stereoregular Head,Tail Hydroxylated Nylons Derived from d-Glucose. *J. Org. Chem.* **61,** 5847–5851 (1996).
55. Adamson, D. W. 13. The anhydrides of basic amino-acids. *J Chem Soc* 39–40 (1943). doi:10.1039/JR9430000039
56. Katchalski, E., Grossfeld, I. & Frankel, M. synthesis of lysine anhydride. *Contrib. Lab. High Mol. Chem.* **68,** 879–880 (1946).
57. Ishibashi, N., Kouge, K., Shinoda, I., Kanehisa, H. & Okai, H. A Mechanism for Bitter Taste Sensibility in Peptides. *Agric. Biol. Chem.* **52,** 819–827 (1988).
58. Borthwick, A. D. 2,5-Diketopiperazines: Synthesis, Reactions, Medicinal Chemistry, and Bioactive Natural Products. *Chem. Rev.* **112,** 3641–3716 (2012).
59. Bohak, Z. & Katchalski, E. Synthesis, Characterization, and Racemization of Poly-L-serine*. *Biochemistry (Mosc.)* **2,** 228–237 (1963).
60. Jin, S., Mungara, P. M. & Gonsalves, K. E. Synthesis of polyamides and polyureas containing leucine-tyrosine linkages. *J. Polym. Sci. Part Polym. Chem.* **35,** 499–507 (1997).
61. El-Faham, A., Hassan, H. H. & Khattab, S. N. Synthesis and characterization of new polyamides derived from alanine and valine derivatives. *Chem. Cent. J.* **6,** 128 (2012).
62. Roy, S. G. & De, P. pH responsive polymers with amino acids in the side chains and their potential applications. *J. Appl. Polym. Sci.* **131,** (2014).
63. Majó, M. A., Bou, J. J., Herranz, C. & Muñoz-Guerra, S. Polycondensation ofL-Lysine Diketopiperazine with Tartaric Acid - Evidence on the Formation of Cyclic Oligomers. *Macromol. Chem. Phys.* **207,** 615–620 (2006).
64. Gachard, I., Coutin, B. & Sekiguchi, H. Synthesis and characterization of polyamides based on natural monomers: l-lysine and l-aspartic acid. *Polym. Bull.* **38,** 643–649 (1997).

65. Chu, C.-C. & Pang, X. Poly(ester amide)s and poly(ester ether amide)s with pendant crosslinkable functional groups. 101pp. WO2010/135739 A2 (2010).
66. Katsarava, R., Ochkhikidze, N., Tugushi, D. & Gomurashvili, Z. D. AABB-poly(depsipeptide) biodegradable polymers and methods of use in biomedical applications. 61pp. WO 2010/019716 A1 (2010).
67. Horwitz, J. A. *et al.* Biological performance of biodegradable amino acid-based poly(ester amide)s: endothelial cell adhesion and inflammation in vitro. *J. Biomed. Mater. Res. A* **95A,** 371–380 (2010).
68. Pang, X. & Chu, C.-C. Synthesis, characterization and biodegradation of functionalized amino acid-based poly(ester amide)s. *Biomaterials* **31,** 3745–3754 (2010).
69. Akerlund, J., Harmeier, S., Pumphrey, J., Timm, D. C. & Brand, J. I. Diketopiperazine-based polymers from common amino acids. *J. Appl. Polym. Sci.* **78,** 2213–2218 (2000).
70. Terada, K., Sanda, F. & Masuda, T. Polycondensation of Diketopiperazine-based Dicarboxylic Acids with Diamines and Dibromoxylenes. *J. Macromol. Sci. Part A* **44,** 789–794 (2007).
71. Alborzi, A. R., Zahmatkesh, S., Zare, K. & Sadeghi, J. Optically active: microwave-assisted synthesis and characterization of l-lysine-derived poly (amide-imide)s. *Amino Acids* **41,** 485–494 (2011).
72. Kunisaki, T., Kawai, K., Hirohata, K., Minami, K. & Kondo, K. Synthesis of polyethers containing cyclodipeptide moiety in the main chain. *J. Polym. Sci. Part Polym. Chem.* **39,** 927–933 (2001).
73. Rafiemanzelat, F., Fathollahi Zonouz, A. & Emtiazi, G. Synthesis and characterization of poly(ether-urethane)s derived from 3,6-diisobutyl-2,5-diketopiperazine and PTMG and study of their degradability in environment. *Polym. Degrad. Stab.* **97,** 72–80 (2012).
74. Crescenzi, V., Giancotti, V. & Quadrifoglio, F. Polyamides from diketopiperazines. I. Condensation of L-lysine diketopiperazine with adipyl cloride. *Makromol. Chem.* **120,** 220–224 (1968).
75. Ciana, A., Crescenzi, V., Giancotti, V., Russo, E. & Salvestrini, L. Diketopiperazine ring containing compounds and process for preparing same. US3763091 (1973).
76. Parrish, D. A. & Mathias, L. J. Synthesis and characterization of polymers containing diketopiperazine. *Polym. Prepr. Am. Chem. Soc. Div. Polym. Chem.* **41,** 1311–1312 (2000).
77. Bou, J. J. & Mun˜oz-Guerra, S. Synthesis and characterization of a polytartaramide based on l-lysine. *Polymer* **36,** 181 – 186 (1995).

78. Majó, M. A., Alla, A., Bou, J. J., Herranz, C. & Muñoz-Guerra, S. Synthesis and characterization of polyamides obtained from tartaric acid and l-lysine. *Eur. Polym. J.* **40,** 2699 – 2708 (2004).
79. Ho, K. M., Li, W. Y., Wong, C. H. & Li, P. Amphiphilic polymeric particles with core–shell nanostructures: emulsion-based syntheses and potential applications. *Colloid Polym. Sci.* **288,** 1503–1523 (2010).
80. Pu, Z., Mark, J. E., Jethmalani, J. M. & Ford, W. T. Effects of dispersion and aggregation of silica in the reinforcement of poly (methyl acrylate) elastomers. *Chem. Mater.* **9,** 2442–2447 (1997).
81. Kumar, A. P., Depan, D., Singh Tomer, N. & Singh, R. P. Nanoscale particles for polymer degradation and stabilization—Trends and future perspectives. *Prog. Polym. Sci.* **34,** 479–515 (2009).
82. Paul, D. R. & Robeson, L. M. Polymer nanotechnology: Nanocomposites. *Polymer* **49,** 3187–3204 (2008).
83. Zhang, Z., Yang, J.-L. & Friedrich, K. Creep resistant polymeric nanocomposites. *Polymer* **45,** 3481–3485 (2004).
84. Jia, X., Li, Y., Cheng, Q., Zhang, S. & Zhang, B. Preparation and properties of poly(vinyl alcohol)/silica nanocomposites derived from copolymerization of vinyl silica nanoparticles and vinyl acetate. *Eur. Polym. J.* **43,** 1123–1131 (2007).
85. Tang, E., Cheng, G. & Ma, X. Preparation of nano-ZnO/PMMA composite particles via grafting of the copolymer onto the surface of zinc oxide nanoparticles. *Powder Technol.* **161,** 209–214 (2006).
86. Patra, N., Salerno, M., Malerba, M., Cozzoli, P. D. & Athanassiou, A. Improvement of thermal stability of poly(methyl methacrylate) by incorporation of colloidal TiO2 nanorods. *Polym. Degrad. Stab.* **96,** 1377 – 1381 (2011).
87. Motaung, T. E. *et al.* PMMA–titania nanocomposites: Properties and thermal degradation behaviour. *Polym. Degrad. Stab.* **97,** 1325–1333 (2012).
88. Rittigstein, P. & Torkelson, J. M. Polymer–nanoparticle interfacial interactions in polymer nanocomposites: Confinement effects on glass transition temperature and suppression of physical aging. *J. Polym. Sci. Part B Polym. Phys.* **44,** 2935–2943 (2006).
89. Kango, S. *et al.* Surface modification of inorganic nanoparticles for development of organic–inorganic nanocomposites—A review. *Prog. Polym. Sci.* **38,** 1232–1261 (2013).
90. Schadler, L. S., Kumar, S. K., Benicewicz, B. C., Lewis, S. L. & Harton, S. E. Designed interfaces in polymer nanocomposites: A fundamental viewpoint. *MRS Bull.* **32,** 335–340 (2007).

91. Balazs, A. C., Emrick, T. & Russell, T. P. Nanoparticle Polymer Composites: Where Two Small Worlds Meet. *Science* **314,** 1107–1110 (2006).
92. Pukánszky, B. Interfaces and interphases in multicomponent materials: past, present, future. *Eur. Polym. J.* **41,** 645–662 (2005).
93. Lu, Z., Wang, J., Li, Q., Chen, L. & Chen, S. Controllable synthesis of nanosilica surface-grafted PMMA macromonomers via catalytic chain transfer polymerization. *Eur. Polym. J.* **45,** 1072–1079 (2009).
94. Zhang, S.-W., Zhou, S.-X., Weng, Y.-M. & Wu, L.-M. Synthesis of SiO2 /Polystyrene Nanocomposite Particles via Miniemulsion Polymerization. *Langmuir* **21,** 2124–2128 (2005).
95. Razmjou, A., Mansouri, J. & Chen, V. The effects of mechanical and chemical modification of TiO2 nanoparticles on the surface chemistry, structure and fouling performance of PES ultrafiltration membranes. *J. Membr. Sci.* **378,** 73–84 (2011).
96. Rong, M. Z. *et al.* Irradiation graft polymerization on nano-inorganic particles: An effective means to design polymer-based nanocomposites. *J. Mater. Sci. Lett.* **19,** 1159–1161 (2000).
97. Yoshida, W., Castro, R. P., Jou, J.-D. & Cohen, Y. Multilayer Alkoxysilane Silylation of Oxide Surfaces. *Langmuir* **17,** 5882–5888 (2001).
98. Siwińska-Stefańska, K., Krysztafkiewicz, A. & Jesionowski, T. Modification of hydrophilic/hydrophobic character of TiO2 surface using selected silane coupling agents. *Physicochem Probl Min. Process* **41,** 205–214 (2007).
99. Tsubokawa, N., Maruyama, K., Sone, Y. & Shimomura, M. Graft Polymerization of Acrylamide from Ultrafine Silica Particles by Use of a Redox System Consisting of Ceric Ion and Reducing Groups on the Surface. *Polym J* **21,** 475–481 (1989).
100. Von Werne, T. & Patten, T. E. Preparation of structurally well-defined polymer-nanoparticle hybrids with controlled/living radical polymerizations. *J. Am. Chem. Soc.* **121,** 7409–7410 (1999).
101. Bourgeat-Lami, E. & Lang, J. Encapsulation of inorganic particles by dispersion polymerization in polar media: 1. Silica nanoparticles encapsulated by polystyrene. *J. Colloid Interface Sci.* **197,** 293–308 (1998).
102. Džunuzović, E., Jeremić, K. & Nedeljković, J. M. In situ radical polymerization of methyl methacrylate in a solution of surface modified TiO2 and nanoparticles. *Eur. Polym. J.* **43,** 3719–3726 (2007).
103. Basilissi, L., Silvestro, G. D., Farina, H. & Ortenzi, M. A. Synthesis and characterization of PLA nanocomposites containing nanosilica modified with different organosilanes I. Effect of the

organosilanes on the properties of nanocomposites: Macromolecular, morphological, and rheologic characterization. *J. Appl. Polym. Sci.* (2012). doi:10.1002/app.38324

104. Li, S. *et al.* Preparation and characterization of porous titania-grafted poly(styrene-divinylbenzene)/maleic anhydride nanocomposite microspheres. *Sci. China Chem.* **53,** 605–611 (2010).
105. Yuvaraj, H., Park, E. J., Gal, Y.-S. & Lim, K. T. Synthesis and characterization of polypyrrole–TiO2 nanocomposites in supercritical CO2. *Colloids Surf. Physicochem. Eng. Asp.* **313-314,** 300–303 (2008).
106. Rong, Y., Chen, H.-Z., Wu, G. & Wang, M. Preparation and characterization of titanium dioxide nanoparticle/polystyrene composites via radical polymerization. *Mater. Chem. Phys.* **91,** 370–374 (2005).
107. Klaine, S. J. *et al.* Nanomaterials in the environment: behavior, fate, bioavailability, and effects. *Environ. Toxicol. Chem.* **27,** 1825–1851 (2008).
108. Kwon, S. *et al.* Nasal and Pulmonary Toxicity of Titanium Dioxide Nanoparticles in Rats. *Toxicol. Res.* **28,** 217–224 (2012).
109. Peng, X., Ding, E. & Xue, F. In situ synthesis of TiO2/polyethylene terephthalate hybrid nanocomposites at low temperature. *Appl. Surf. Sci.* **258,** 6564–6570 (2012).
110. Jordan, J., Jacob, K. I., Tannenbaum, R., Sharaf, M. A. & Jasiuk, I. Experimental trends in polymer nanocomposites—a review. *Mater. Sci. Eng. A* **393,** 1 – 11 (2005).
111. Cui, L. *et al.* Polyamide- and polycarbonate-based nanocomposites prepared from thermally stable imidazolium organoclay. *Polymer* **50,** 2492 – 2502 (2009).
112. Fornes, T. D., Yoon, P. J. & Paul, D. R. Polymer matrix degradation and color formation in melt processed nylon 6/clay nanocomposites. *Polymer* **44,** 7545 – 7556 (2003).
113. Mesnage, A. *et al.* Grafting polymers to titania nanoparticles by radical polymerization initiated by diazonium salt. *J. Mater. Sci.* **46,** 6332–6338 (2011).
114. Othman, S. H., Abdul Rashid, S., Mohd Ghazi, T. I. & Abdullah, N. Effect of Postdeposition Heat Treatment on the Crystallinity, Size, and Photocatalytic Activity of TiO 2 Nanoparticles Produced via Chemical Vapour Deposition. *J. Nanomater.* **2010,** 1–10 (2010).
115. Allen, N. S. *et al.* Photocatalytic titania based surfaces: Environmental benefits. *Polym. Degrad. Stab.* **93,** 1632–1646 (2008).
116. Fu, G., Vary, P. S. & Lin, C.-T. Anatase TiO $_2$$ Nanocomposites for Antimicrobial Coatings. *J. Phys. Chem. B* **109,** 8889–8898 (2005).

117. Karvinen, S. & Lamminmäki, R.-J. Preparation and characterization of mesoporous visible-light-active anatase. *Solid State Sci.* **5,** 1159–1166 (2003).
118. Sandrolini, F. & Giordano, D. Il Biossido di Titanio nei materiali da costruzione antinquinamento ed autopulenti.
119. Kato, S. *et al.* Photocatalytic degradation of gaseous sulfur compounds by silver-deposited titanium dioxide. *Appl. Catal. B Environ.* **57,** 109–115 (2005).
120. Gamage, J. & Zhang, Z. Applications of Photocatalytic Disinfection. *Int. J. Photoenergy* **2010,** 1–11 (2010).
121. Montazer, M. & Pakdel, E. Reducing photoyellowing of wool using nano TiO2. *Photochem. Photobiol.* **86,** 255–260 (2010).
122. Millington, K. R. Photoyellowing of wool. Part 1: Factors affecting photoyellowing and experimental techniques. *Color. Technol.* **122,** 169–186 (2006).
123. Millington, K. R. Photoyellowing of wool. Part 2: Photoyellowing mechanisms and methods of prevention. *Color. Technol.* **122,** 301–316 (2006).
124. Church, J. S. & Millington, K. R. Photodegradation of wool keratin: Part I. Vibrational spectroscopic studies. *Biospectroscopy* **2,** 249–258 (1996).
125. Nogueira, A. C. S., Richena, M., Dicelio, L. E. & Joekes, I. Photo yellowing of human hair. *J. Photochem. Photobiol. B* **88,** 119–125 (2007).
126. Parkin, I. P. & Palgrave, R. G. Self-cleaning coatings. *J. Mater. Chem.* **15,** 1689 (2005).
127. Erkan, A., Bakir, U. & Karakas, G. Photocatalytic microbial inactivation over Pd doped SnO2 and TiO2 thin films. *J. Photochem. Photobiol. Chem.* **184,** 313–321 (2006).
128. Foster, H. A., Ditta, I. B., Varghese, S. & Steele, A. Photocatalytic disinfection using titanium dioxide: spectrum and mechanism of antimicrobial activity. *Appl. Microbiol. Biotechnol.* **90,** 1847–1868 (2011).
129. Kubacka, A. *et al.* Boosting TiO2-anatase antimicrobial activity: Polymer-oxide thin films. *Appl. Catal. B Environ.* **89,** 441–447 (2009).
130. Wang, Z., Li, G., Peng, H., Zhang, Z. & Wang, X. Study on novel antibacterial high-impact polystyrene/TiO2 nanocomposites. *J. Mater. Sci.* **40,** 6433–6438 (2005).
131. Ou, B. & Li, D. Location of functionalized-TiO2 nanoparticle in an immiscible PP/PA6 blends and its effect on the compatibility of the components. *Polym. Bull.* **63,** 441–447 (2009).
132. Lei, Y., Zhang, C., Lei, H. & Huo, J. Visible light photocatalytic activity of aromatic polyamide dendrimer/TiO2 composites functionalized with spirolactam-based molecular switch. *J. Colloid Interface Sci.* **406,** 178–185 (2013).

133. Barnes, R. J., Molina, R., Xu, J., Dobson, P. J. & Thompson, I. P. Comparison of TiO2 and ZnO nanoparticles for photocatalytic degradation of methylene blue and the correlated inactivation of gram-positive and gram-negative bacteria. *J. Nanoparticle Res.* **15,** (2013).
134. Suma, K. K., Jacob, S. & Joseph, R. Studies on the effect of nano-TiO2 on vinyl acetate–butyl acrylate latex-based surface coating. *Mater. Sci. Eng. B* **168,** 254 – 258 (2010).
135. Todaro, L., D'Auria, M., Langerame, F., Salvi, A. M. & Scopa, A. Surface characterization of untreated and hydro-thermally pre-treated Turkey oak woods after UV-C irradiation. *Surf. Interface Anal.* Ahead of Print (2014). doi:10.1002/sia.5689